Controlling the Edges:

From Nanographenes Towards to Graphene Nanoribbons

Dissertation

zur Erlangung des Grades

„Doktor Der Naturwissenschaften"

im Fachbereich Chemie, Pharmazie, und Geowissenschaften der

Johannes Gutenberg---Universität Mainz und in Kooperation mit dem

Max-Planck-Institut für Polymerforschung Mainz

vorgelegt von

Junzhi Liu

geboren in Sichuan/China

Mainz, 2015

Dekan: Prof. Dr. ███████████

1. Berichterstatter: Prof. Dr. ███████████

2. Berichterstatter: Prof. Dr. ███████████

Tag der mündlichen Prüfung: 14.01.2016

My parents, wife and daughter

Table of Contents

Index of Abbreviations

CNT carbon nanotubes

COSY correlation spectroscopy

CPP cycloparaphenylene

CVD chemical vapor deposition

DLS dynamic light scattering

DDQ 2,3-dichlor-5,6-dicyano-1,4-benzoquinone

DMF dimethyl formamide

EMPA Eidgenössische Materialprüfungs- und Forschungsanstalt

FET field effect transistor

GNR Graphene Nanoribbons

HMBC heteronuclear single quantum coherence

HR-MS high resolution mass spectrometry

HPB hexaphenylbenzene

HBC hexa-*peri*-benzocoronone

HSQC heteronuclear single quantum coherence

LWH length, width, height

MALDI-MS matrix-assisted laser desorption ionization mass spectrometry

MS mass spectrometry

MeOH methanol

MP melting point

MS mass spectrometry

MWCNT multiwalled carbon nanotube

NIR near infrared

NMP N-methylpyrrolidone

NMR nuclear magnetic resonance

NOE nuclear *Overhauser* effect

NOESY nuclear *Overhauser* enhancement and exchange spectrocopy

PAH polycyclic aromatic hydrocarbon

PPC polyphenylene cylinder

PDI polydispersity index

PPP poly(para-phenylene)

PS poly(styrene)

rGO reduced graphene oxide

SEC size-exclusion chromatography

SEM scanning electron microscopy

SiC silicon carbide

SLS static light scattering

SPM scanning probe microscopy

STM scanning tunneling microscopy

STS scanning tunneling spectroscopy

TfOH trifluoromethanesulfonic acid

THF tetrahydrofuran

r.t. room temperature

TMS trimethylsilyl

TOF time of flight

TTF tetrathiafulvalene

TBAF tetra-n-butylammonium fluoride

TCB 1,2,4-trichlorobenzene

TCNQ 7,7,8,8-tetracyanoquinodimethane

TIPS triisopropylsilyl

TLC thin-layer chromatography

UHV ultrahigh vacuum

UV–vis ultraviolet–visible (absorption spectroscopy)

Chapter 1. Introduction

Graphene is a two-dimensional, atomically thick sheet composed of a hexagonal network of sp^2-hybridized carbon atoms. It has been intensively investigated since its first isolation in 2004, when Geim, Novoselov *et al*. reported a micromechanical cleavage method for the exfoliation of graphite, based on repeated peeling of highly oriented pyrolyzed graphite (HOPG). For their pioneering works revealing the unexceptional physical properties of graphene, they were awarded the 2010 Nobel Prize in physics. The extraordinary electronic, thermal, and mechanical properties of graphene make it a promising candidate for various future applications, for example, in electronics, sensing, catalysis, energy storage and conversion, and biological labeling. Nevertheless, the implementation of graphene in electronics still remains challenging. The greatest challenge at present is the lack of an efficient way to produce graphene both in large quantities and with high quality. Another difficulty issue is the lack of a controllable synthetic method to produce graphene with defined size, shape, and edge structure. To date, two distinct strategies have been established for graphene synthesis: exfoliation of graphite towards graphene (top-down method) and construction of graphene from molecular building blocks (bottom-up method). The top-down methods include the mechanical exfoliation of HOPG, solution-based exfoliation of graphite intercalation compounds (GICs), electrochemical exfoliation of graphite and chemical oxidation/exfoliation of graphite followed by reduction of the resulting graphene oxide (GO). The bottom-up approaches for graphene synthesis are based on the growth on metallic substrates by means of chemical vapor deposition (CVD), thermal decomposition of SiC, and organic synthesis based on precursor molecules. One can envisage three different types of edge structures for the periphery of graphene (Figure 1): armchair, cove, and zigzag edges.

Grapene is semimetallic with zero-band gap. However, when graphene is cut into narrow strips, namely graphene nanoribbons (GNRs), a bandgap can be opened, rendering it potentially applicable in future electronics. Depending on their edge structures, two different types of GNRs can be classified: zigzag-edged GNRs (ZGNRs) and armchair-edged GNRs (AGNRs), and these

have been extensively investigated both theoretically and experimentally. Over many decades, GNRs have been of theoretical interest, predicting their intriguing physical properties. In the last decade, great efforts have been devoted to fabricating high-quality GNRs with narrow widths and smooth edges. To date, two main strategies have been established to prepare GNRs, namely "top-down" and "bottom-up" approaches. The "top-down" approach, such as the cutting of graphene, sonochemical extraction from expanded graphite and unzipping of carbon nanotubes, has produced GNRs with sub-10 nm widths, revealing their semiconducting nature and excellent charge transport properties. Bottom-up chemical synthesis can provide structurally well-defined GNRs with uniform structures. The synthesis is based on solution-mediated or surface-assisted cyclodehydrogenation, namely "planarization" of three-dimensional polyphenylene precursors.
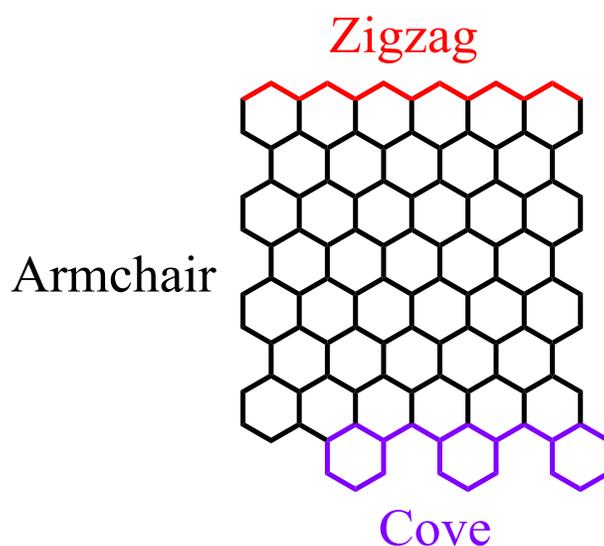
Figure 1. Edge structures of graphene.

Large polycyclic aromatic hydrocarbons (PAHs) can be regarded as finite graphene segments composed of all-sp^2 carbons that are termed nanographenes with an average diameter smaller than 10 nm. PAHs have attracted enormous interest due to their intriguing electronic and optoelectronic properties as well as the potential applications in organic electronics. Bottom-up organic synthesis has been developed which may serve as an indispensable tool to create structurally defined nanographenes. Fundamental contributions to the bottom-up synthesis and characterization of polycyclic aromatics were made by R. Scholl and E. Clar at the beginning of

20th century, who achieved the synthesis of numerous PAHs under drastic conditions, such as at high temperatures and using strong oxidants. A remarkable synthetic breakthrough was achieved with a help of the progress in the analytical techniques, which made it possible to selectively synthesize various PAHs under mild conditions. The systematic study of PAHs and their application as materials have stimulated scientists for several decades. The typical synthesis of extended PAHs is based on the intramolecular cyclodehydrogenation, i.e., planarization of 3D dendritic or hyperbranched polyphenylene precursors. By employing this synthetic strategy, various kinds of large PAHs with different molecular sizes, shapes, symmetries and peripheries have been obtained. Among them, hexa-*peri*-hexabenzocoronene (HBC), with 42 sp^2 carbons, is one of the most extensively studied PAH molecules. To date, the largest graphene-type molecule accessible with the bottom-up synthesis is a disk-shape nanographene consisting of 222 carbon atoms. Other large PAHs with, e.g., triangle-shape (C60), linear ribbon-shape (C72), cordate-shape (C96), square-shape (C132) are also attainable (Figure 2).


1(C18)   **2**(C42)   **3**(C60)   **4**(C72)   **5**(C78)   **6**(C96)   **7**(C132)   **8**(C222)
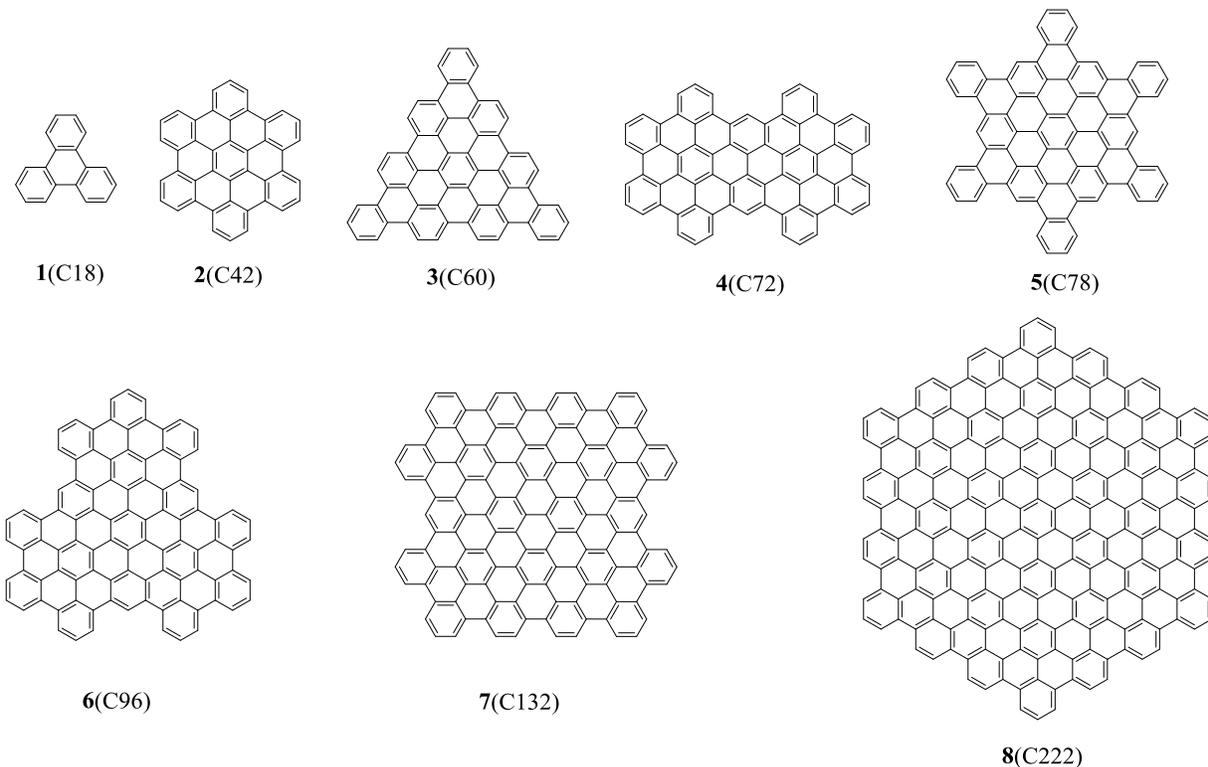
Figure 2. Structures of various large PAHs.

3

At first sight, one may think that PAHs constitute a single class of very similar molecules, all built up solely of sp^2 carbons. However, depending on the periphery structure, dramatically different optical and chemical properties are observed. For example, triphenylene with armchair edges is extremely stable against oxidation and possesses a relatively high optical energy gap. In contrast, the structural isomer tetracene with zigzag edges is easily oxidized and shows absorption at much longer wavelengths (Figure 3). As another example, there are two ways to fuse three benzene rings: fusing them in 1D gives anthracene, while fusing them into a triangle gives phenalene (Figure 4). The former is stable and chemically inactive as a Kekulé molecule having a closed-shell electronic structure, whereas the latter is unstable and chemically active as a non-Kekulé molecule having an open-shell electronic structure.

Triphenylene

Tetracene
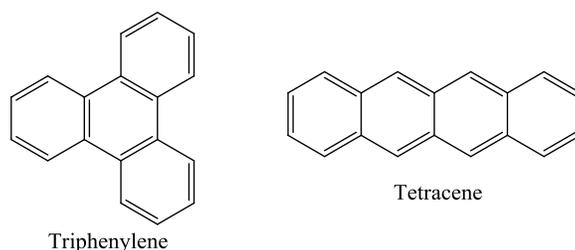
Figure 3. Two ways to fuse four benzene rings.


Anthracene

Phenalene
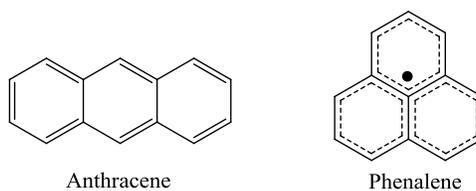
Figure 4. Two ways to fuse three benzene rings.
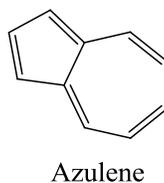

Azulene

Figure 5. Structure of non-benzenoid aromatic azulene.

Thereby, regarding the different type of molecules, define the aromaticity of these polycyclic hydrocarbons at the beginning is indispensable: compounds which exhibit significantly exalted

diamagnetic susceptibility are aromatic. Cyclic electron delocalization also may result in bond length equalization, abnormal chemical shifts and magnetic anisotropies, as well as chemical and physical properties which reflect energetic stabilization. Antiaromatic molecules are defined in terms of the existence of 4n π-electrons disposed in a planar cyclic arrangement. Those compounds with exalted paramagnetic susceptibility may be antiaromatic. All compounds that contain a benzene ring possess special stability and are classified as benzenoid aromatic compounds (such as benzene, HBC). In contrast, compounds that lack a benzene ring and yet satisfy the criterion of the aromatic stabilization are classified as non-benzenoid aromatic compounds (such as azulene shows in Figure 5).

As mentioned above, the optical properties, chemical activity and aromaticity of PAHs are totally different depending on their size and periphery structure. Furthermore, the electronic properties such as the corresponding energy gaps of PAHs are very important for the future applications, e.g., as organic semiconductors. Following the classification of graphene, three different classes of PAHs can be defined depending on their edge structures: armchair-edged PAHs (A-PAHs), cove-edged PAHs (C-PAHs), and zigzag-edged PAHs (Z-PAHs). Thereby, this critical introduction will summarize the progress in the relationship between the periphery structure and electronic properties of PAHs. Include conventional and unconventional PAHs: (1) armchair-edged PAHs, (2) cove-edged PAHs, (3) zigzag-edged PAHs, (4) open-shell polycyclic hydrocarbons and (5) antiaromatic indenofluorenes. The discussion will cover their synthetic strategies, characterizations, physical properties, structure-property relationships, and potential material applications. I will attempt to elucidate how the chemical (such as reactivity and stability) and electronic properties (such as the energy gap) depend on the edge structure and size of these PAHs. In the end, I will present the motivation of this thesis.

1.1 PAHs with armchair-edged structure.

First, we start our discussion on the conventional armchair-edged PAHs. Triphenylene (**1**) is the most studied and simplest fully benzenoid armchair-edged PAH. Its good synthetic accessibility and use as a discotic liquid crystal have made it very important for material science.[1,2] The α-band of triphenylene (**1**) is observed at ~320 nm as a very weak peak due to the high symmetry and thus low transition probabilities. Its strongest absorption peak is found at ~260 nm with an extinction coefficient of 17 000 m^2/mol, which is a relatively high value for PAHs.[3] The absorption does not reach the visible region, so the compound is colorless. Triphenylene shows essentially two fluorescence bands at 355 and 370 nm.[4,5]
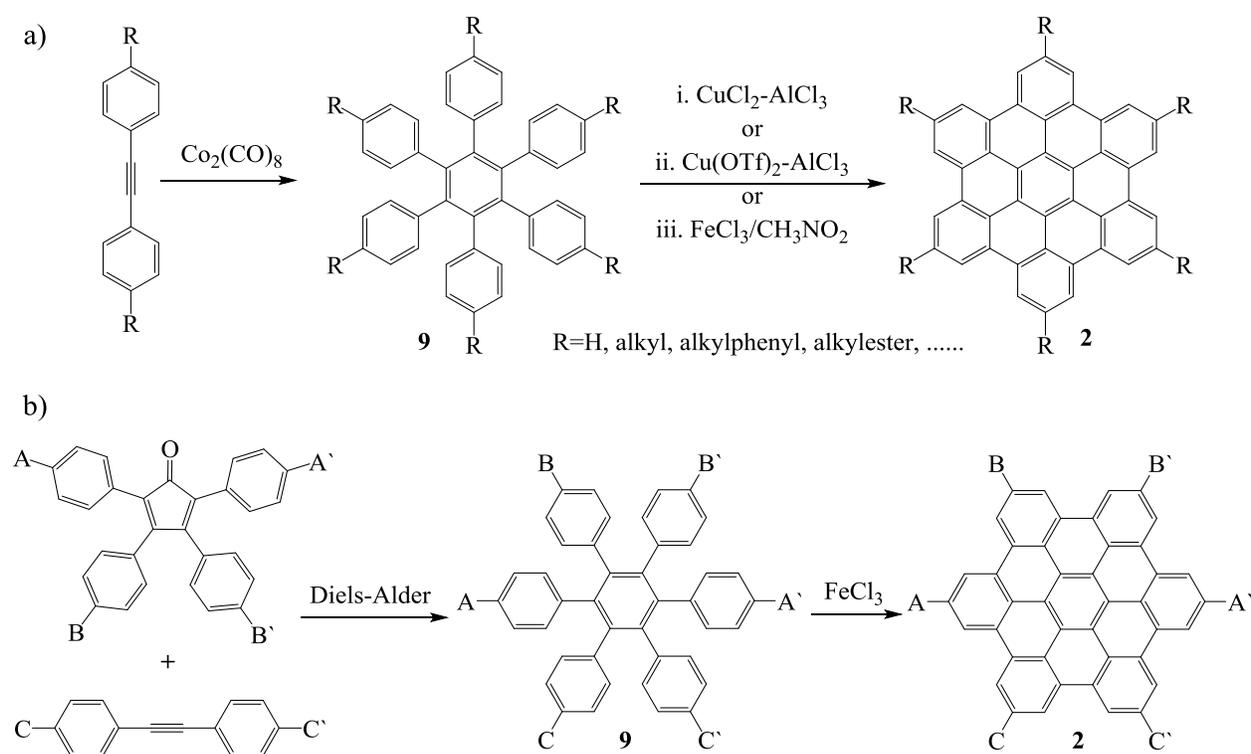
Figure 6. a) General synthetic route to six-fold symmetric HBCs **2**; b) General synthetic route to lower symmetric HBCs **2**.

Larger and the most intensively studied PAH with armchair periphery is hexa-*peri*-benzocoronene (**2**, HBC). Thanks to its easy accessibility from the hexaphenylbenzene precursor, a great variety of HBC derivatives have been prepared.[6-9] Typically, HBC **2** and their derivatives are derived from substituted hexaphenylbenzene (**9**) by an intramolecular oxidative

cyclodehydrogenation with iron (Ⅲ) chloride or $AlCl_3$-$Cu(OTf)_2$ as the Lewis acid/oxidant (Figure 6). HBCs with D_6 symmetry can be obtained in a facile manner through the $Co_2(CO)_8$ catalyzed cyclotrimerization of diphenylacetylenes to afford hexaphenylbenzene derivatives with six identical substituents (Figure 6a). An extraordinarily versatile route to prepare less symmetric or asymmetric hexaphenylbenzenes is the Diels-Alder reaction of tetraphenylcyclopentadienones (CPs) with diphenylacetylenes (Figure 6b). From the UV-vis absorption spectra, the α-band of HBC at 450 nm is found to be very weak, because this transition is forbidden in such symmetric molecules. The more intense p-band appears at 390 nm and the highest intensity is measured for the β-band at 360 nm with a very high molar extinction coefficient of 18 000 m^2/mol.[10] The fluorescence spectrum shows several peaks, the band of the shortest wavelength is measured at 464 nm, and the highest intensity is found at 484 nm.[11]
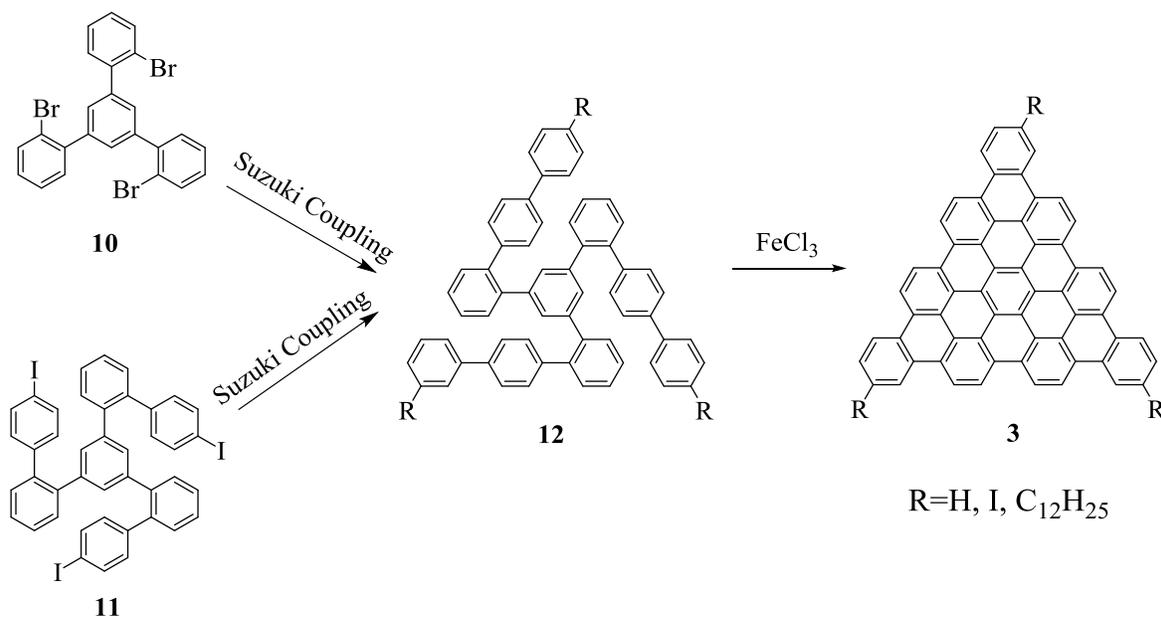
Figure 7. Synthesis route towards triangle PAHs **3**.

Triangular armchair-edged PAH **3** has been prepared and characterized as an extended homolog of HBC, containing ten electron sextets.[12] The synthesis of triangle-shaped molecules **3** is depicted in Figure 7. Precursor **12** was obtained through Suzuki coupling of 1,3,5-tris(2'-bromophenyl)benzene (**10**) and [1,1'-biphenyl]-4-ylboronic acid or 4,4''''-diiodo-5''-(4'-iodo-[1,1'-biphenyl]-2-yl)-1,1':2',1'':3'',1''':2''',1''''-quinquephenyl) (**11**) and phenylboronic acid. Intramolecular oxidative cyclodehydrogenation reactions were performed for the resulting

precursors **12** by using FeCl$_3$ as Lewis acid/oxidant until the quantitative removal of 18 hydrogen atoms gave triangle discs **3** as red powders. Solubilizing alkyl chains are necessary to dissolve the molecule in common organic solvents including THF, dichloromethane, and chloroform. The strong intermolecular interactions, however, lead to a line broadening of the absorption spectra. The spectrum is very similar to that of triphenylene **1**: weak bands around 500 nm are observed, and the strongest absorption is found at 405 nm.

Obviously, one of the major goals of large PAH synthesis is to produce structurally defined model compounds of graphene. By employing the Diels-Alder reaction or cyclotrimerization protocols, different sizes and shapes of armchair-edged PAHs have been designed and synthesized, such as "supernaphthalene" **4** (C72), **5** (C78), "superphenalene" **6** (C96), square-shape **7** (C132), and the largest armchair-edged PAH **8** (C222). [14, 16] The spectra of the two molecules **7** and **8** are substantially broadened due to the strong intermolecular π-π interactions induced aggregations. The compound **8** shows absorption over the complete visible range of the electronic spectrum, with a maximum of the band at approximately 765 nm.

The Clar structure of a given PAH is the resonance structure having the maximum number of isolated and localized aromatic-sextets, with a minimum number of localized double bonds. In general, a PAH with a given number of aromatic-sextets is kinetically more stable than its isomers with fewer aromatic-sextets. According to Clar's sextet rule (aromatic π-sextets are defined as six π-electrons localized in a single benzene-like ring separated from adjacent rings by forming C-C single bonds), particularly high stabilization energy and consequently low reactivity is observed if the π-electrons can all be grouped into sextets. One can consider these PAHs with armchair edges (such as HBC) as a set of benzene rings connected by six single bonds to neighboring rings or hydrogen atoms. Such PAHs are called fully benzenoid. The stabilization energy of the PAHs also correlates with their optical energy gaps. The size-dependent optical energy gap values for typical larger armchair-edged PAHs are depicted in Figure 8, in relation to the number of aromatic sextets. A decrease from 3.9 eV of triphenylene to a level at about 1.6 eV for the large disk C222 is found. Increasing the size of armchair-edged PAHs leads to greater delocalization of the π-electrons and to a decreased difference between the highest occupied molecular orbital (HOMO) and the lowest unoccupied molecular orbital (LUMO). From Figure

8, a semi-linear relationship was observed between the absorption and the number of 'full' aromatic rings in armchair-edged PAHs.
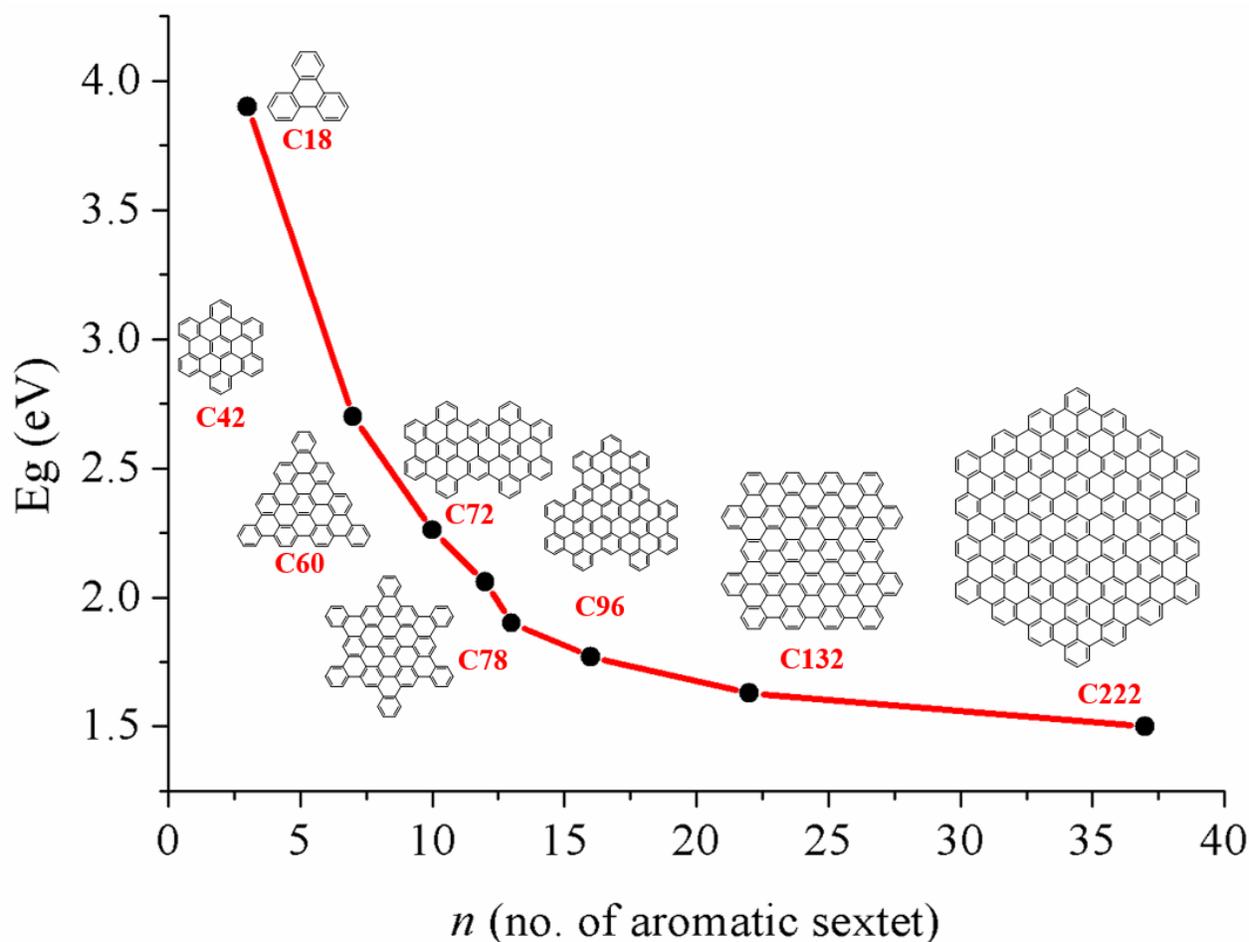
Figure 8. Correlation of the optical energy gap versus the number of aromatic sextets.

Among the larger fully benzenoid armchair-edged PAHs, structural isomers exist with the same number of electron sextets. The optical gap, however, is almost unaffected by the different shape of these isomers as long as they have fully armchair edge configurations. It can be clearly seen that the optical transitions in this class of armchair-edged PAHs are dominated by the size of the molecule rather than the shape of the disk. As will be discussed later, this rule does not apply for PAHs of other edge structures.

1.2 PAHs with cove edge structure.
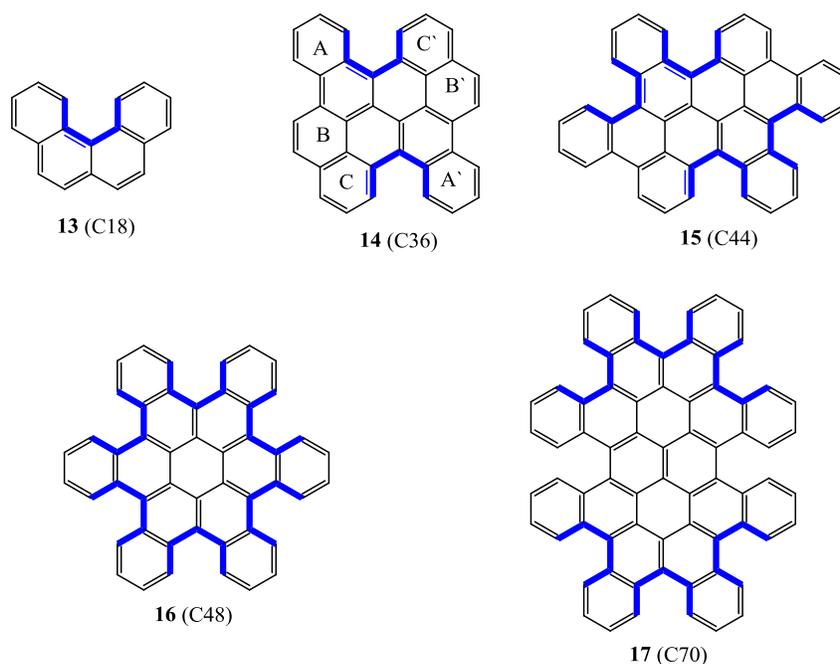
Figure 9. Various PAHs with cove periphery.

Different from the above-mentioned PAHs with armchair-edge peripheries that mostly have planar structures, the outstanding feature of cove-edged PAHs is a non-planar π-conjugated carbon skeleton, which results from the steric repulsion between the two C-H bonds at the inner cove position (Figure 9). Historically, the cove-edged [4]helicene **13** was reported in 1912 by R. Weitzenböck.[17] It was an early synthesis of a carbohelicene possessing an unambiguous distortion of the π-system. Recently, R. S. Liu and coworkers [18, 19] reported the synthesis of expanded cove-edged PAHs, namely benzo[*a*]dinaphtho[2,1,8-cde:1',2',3',4'-ghi]perylene (**14**) and benzo[ij]benzo[3,4]phenanthro[2,1,10,9-defg]naphtho[1,2,3,4-rst]pentaphene (**15**). From the crystal structure analysis, **14** reveals S_2-symmetry, resulting from the steric interaction between the two cove regions at the A- and C`-rings (or A`- and C-rings) (Figure 9). The central portion of the molecular geometry is highly distorted from planarity with a large dihedral angle (36.6°) between the A and C` rings. The resulting PAHs have aromatic characters on the outer benzenes but non-aromatic, polyene features on the central framework due to the non-planarity.

In 2005, a notable example of cove-edged PAH hexabenzo[*a,d,g,j,m,p*]coronene (Hexa-*cata*-HBC, **16**) was reported by C. Nuckolls and coworkers. [20, 21] HBC **16** is structurally related to HBC **2**: the benzo rings are connected at the *ortho*-positions of coronene in HBC **16** whereas the *peri*-positions are benzo-fused in armchair-edged HBC **2**. Figure 10 shows the structure of **16** deduced from single-crystal X-ray diffraction. The outstanding feature of this cove-edged **29** is its non-planar π-conjugated carbon skeleton, which results from the steric hindrance of its cove periphery. Notably, the benzene rings in the cove region of **16** adopt an alternating "up-down" conformation.

16a: R1=R2=H
16b: R1=H, R2=$OC_{12}H_{25}$
16c: R1=R2=$OC_{12}H_{25}$
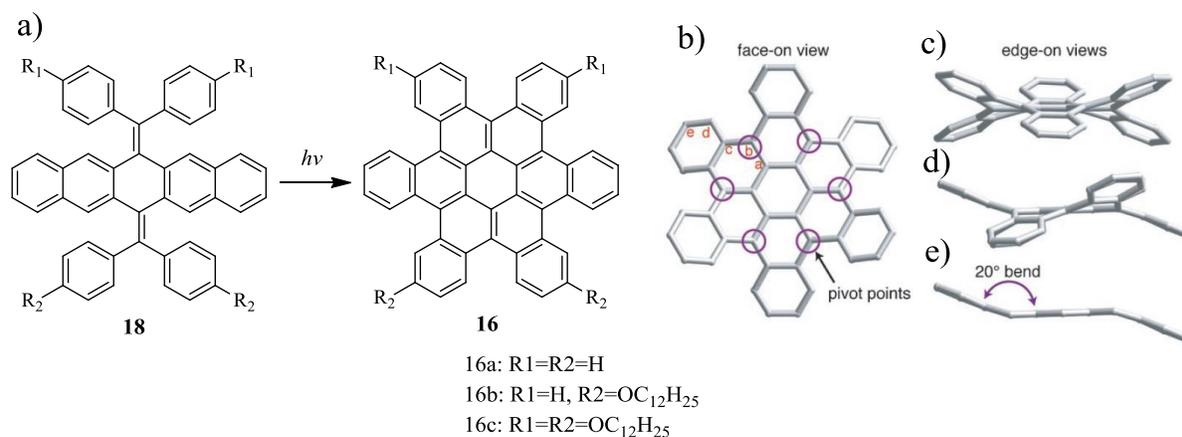
Figure 10. (a) Synthesis of **16**; (b-e) crystal structure of **16** grown from 1,2,4-trichlorobenzene: (b) Face-on view with marked pivot points (magenta circles). The C_a-C_b bond is relatively short and the C_b-C_c bond is relatively long. Side views are given in (c), (d) and (e). (d) and (e) Side view of one of the acene segments extracted from the crystal structure.

In contrast to the fully benzenoid PAHs, such as armchair-edged HBC **2**, compound **16** adopts a π-bond localized resonance structure in the solid state; the crystal structure demonstrates a strong contribution from the radialene resonance structure (Figure 11).
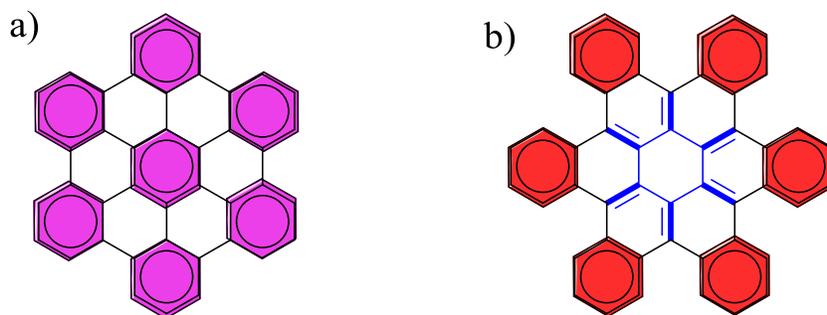
Figure 11. Resonance structure of armchair-edged HBC **2** (a) and cove-edged HBC **16** (b).
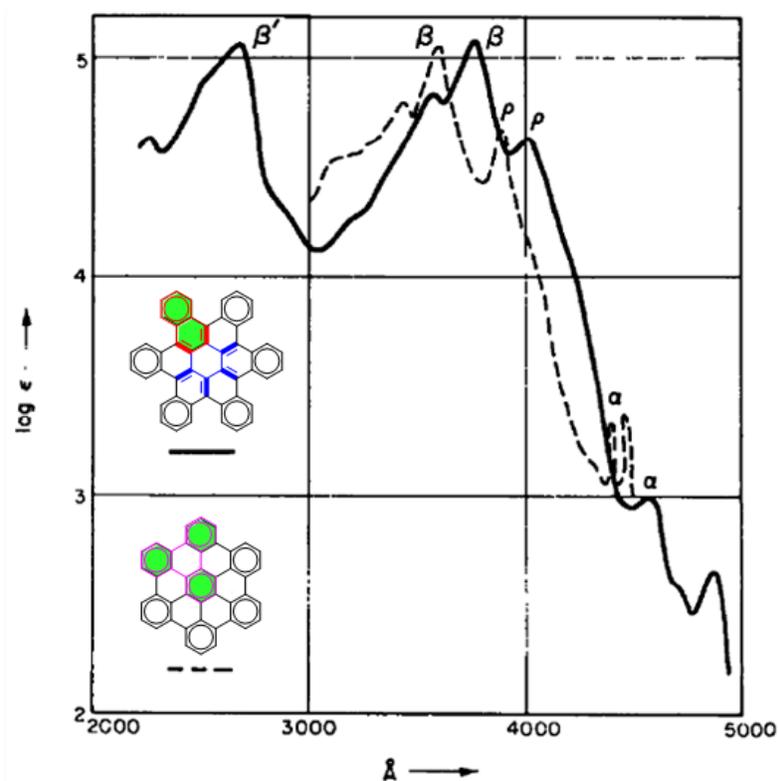
Figure 12. Absorption max (Å) and log ε of **16** in benzene and **2** in trichlorobenzene[20].

The absorption spectra of cove-edged HBC **16** and armchair-edged HBC **2** are compared in Figure 12. Compound **16** shows an absorption maximum bathochromically shifted (15 nm) relative to that of armchair-edged HBC **2**. The optical energy gaps of **2** and **16** are determined from the onsets of their UV-vis absorption spectra to be approximately 2.70 and 2.42 eV, respectively. These absorption spectra are located at relatively short wavelength when compared with the number of π-electrons in **16** and **2** which amount to 48 and 42 respectively. This can be

explained by assuming that only a fraction of the number of rings are in aromatic conjugation whilst some sextets are connected to the system by single bonds forming "empty" rings.[20] The aromatic conjugated system is that of naphthopentaphene (trinaphthylene) in **16** and is that of triphenylene in **2** (Figure 12).[22]

Moreover, C. Nuckolls *et al*. synthesized even larger cove-edged PAH (**17**),[23] which has eight aromatic rings appended around a circumbiphenyl core (Figure 13). The conformation of **17** is similar to that of the cove-edged HBC **16**. Compound **17** has a highly contorted exterior with six 4-helicenes and two 5-helicenes around the exterior of the expanded core of the aromatic. From the UV-vis absorption spectrum, **17** shows strong absorption peaks at 411, 433, and 493 nm. And the absorbance maxima for the **17** is red-shifted by 65 nm when compared to those of the smaller cove-edged HBC **16**.[24]
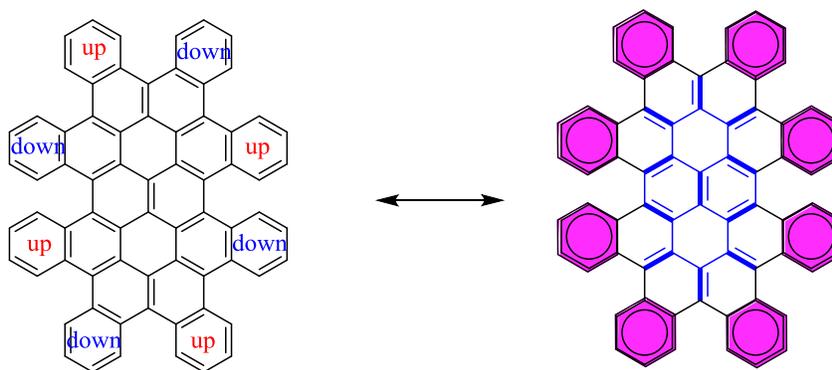
Figure 13. Cove-edged PAH **17** with alternating up and down benzo-rings and its resonance structure.

From mentioned above, in contrast to armchair-edged PAHs, cove-edged PAHs are not fully benzenoid, and possess a smaller optical energy gaps compared to the armchair-edged PAHs with the same carbons skeleton. Furthermore, the steric congestion of the hydrogen atoms in the cove regions gives rise to a non-planar disk shapes in contrast to planar structures of armchair-edged PAHs. By attaching alkyl chains, a liquid crystal has been prepared which shows remarkable charge-carrier mobilities, because the π surfaces of contorted molecules can approach each other and arrange themselves in very different ways, such as the π-π distance of the dimer cove-edged **16** is shorter than armchair-edge **2**. [21, 24, 25]

1.3 PAHs with zigzag edge structure.

19(C44)   **20**(C46)   **21**(C48)

22(C20)   **23**(C28)   **24**(C42)   **25**(C56)

26(C16)   **27**(C24)   **28**(C32)   **29**(C40)
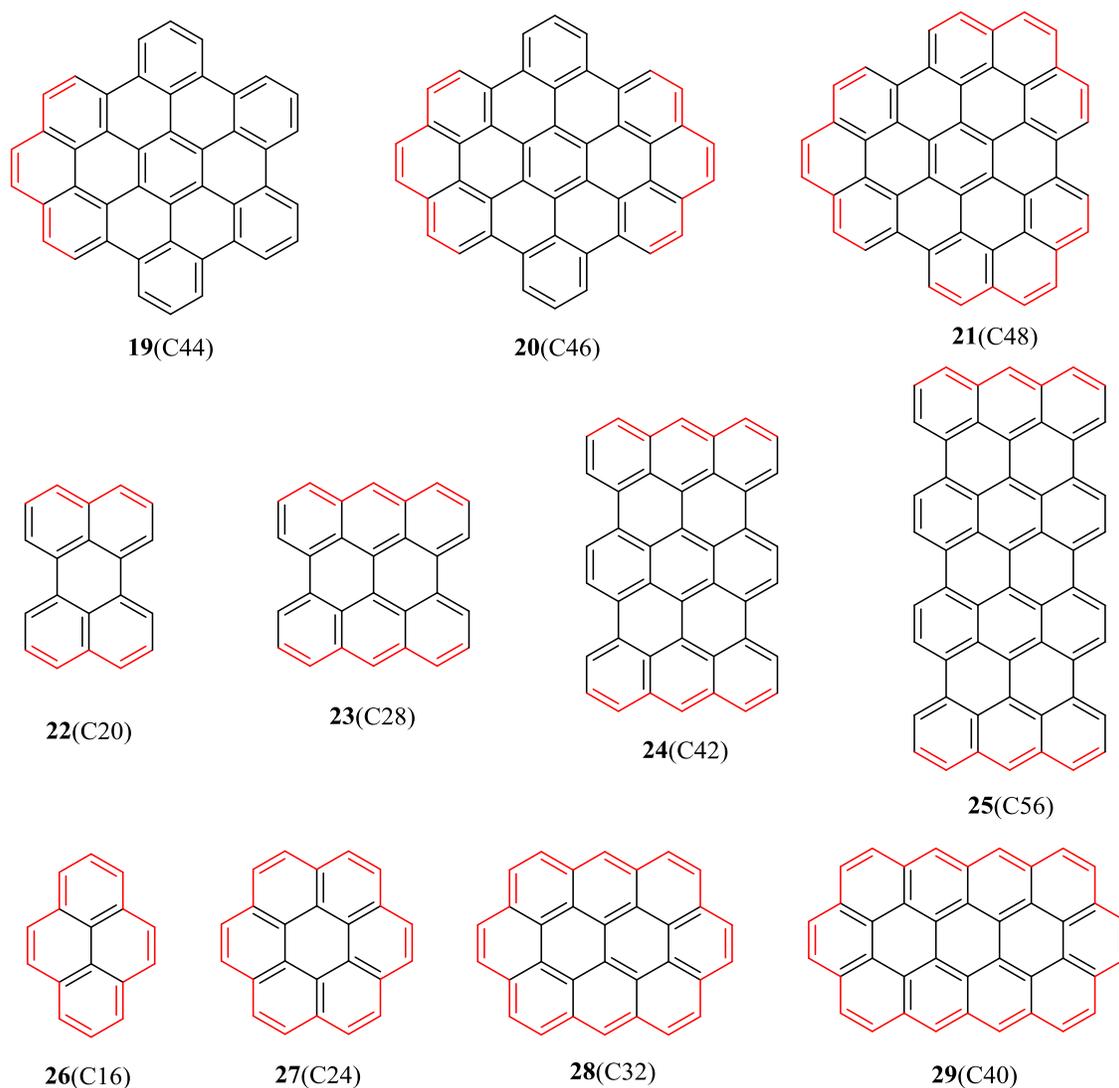
Figure 14. Various PAHs with zigzag periphery.

Compared to the fully benzenoid armchair-edged PAHs, the zigzag-edged PAHs are annulated with another ring in a bay region, where the added two π-electrons cannot be included in a sextet. For instance, if fully benzenoid HBC **2** (Figure 5) are annulated with one, two, and three additional rings in the bay regions, HBC with partial zigzag-edge or "reactive" double bonds can be obtained, namely mono-zigzag HBC **19**, bis-zigzag HBC **20**, and tri-zigzag HBC **21** (Figure 15), respectively.[26-28] The integration of zigzag edges influences dramatically not only its

electronic and optoelectronic properties but also its chemical reactivity as well as potentially two- and three-dimensional self-assembly behavior.
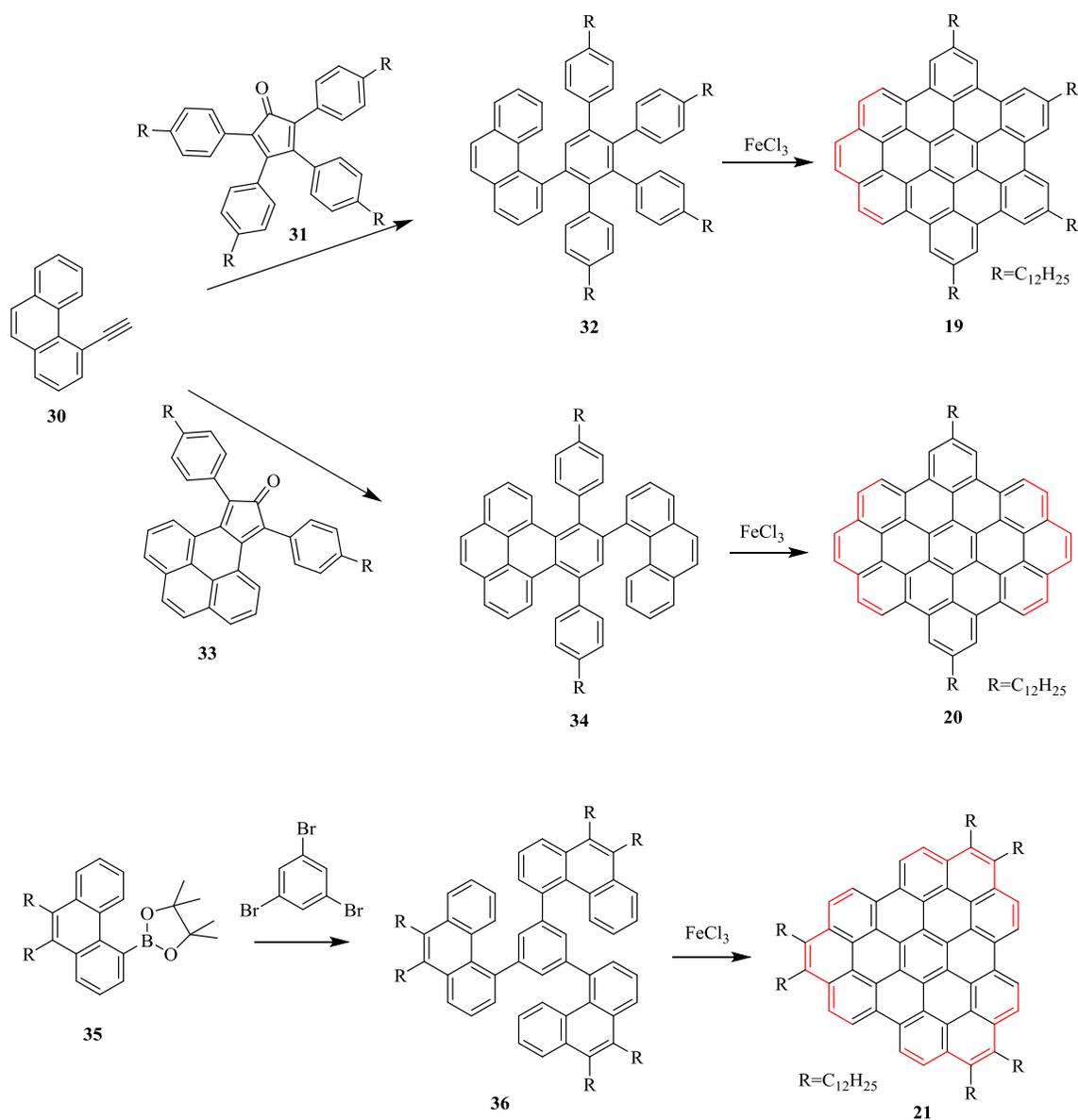
Figure 15. The synthesis route towards **19**, **20** and **21**.

The structural differences between these three molecules induce a strong effect on the absorption spectra. The α-bands and the β-bands follow a linear trend with the number of carbon atoms with the zigzag edges. The α-bands of **19** are determined to be 484 nm and that of **21** to be 530 nm. The β-bands go up from 380 nm for **19** to 400 nm for **21**. The p-bands, however, show a different

trend. Bis-zigzag HBC **20** (473 nm) shows *p*-bands at longer wavelengths than **21** (425 nm). The symmetry gives rise to this trend as revealed by quantum mechanical calculations. Tri-zigzag HBC **21** shows D_{3h} symmetry, and as a consequence the HOMO/HOMO-1 and the LUMO/LUMO-1 are degenerate leading to a transition at shorter wavelengths. The symmetry also has an influence on the fine structure of the spectrum. The higher the symmetry, the more symmetry-forbidden transitions exist, leading to a high degree of fine structure. Lower symmetry as for mono-zigzag **19** and bis-zigzag **20** (D_{2h}) broadens the peaks in the spectrum. The intensity of the *α*-bands in this series also depends on the symmetry: the higher the symmetry the lower the intensity. Thus the change of periphery and symmetry have a pronounced influence upon the electronic spectra, showing that the typical *α*- and *β*-bands of a PAH depended linearly upon the number of zigzag edges, while the *p*-band is mainly influenced by the symmetry.
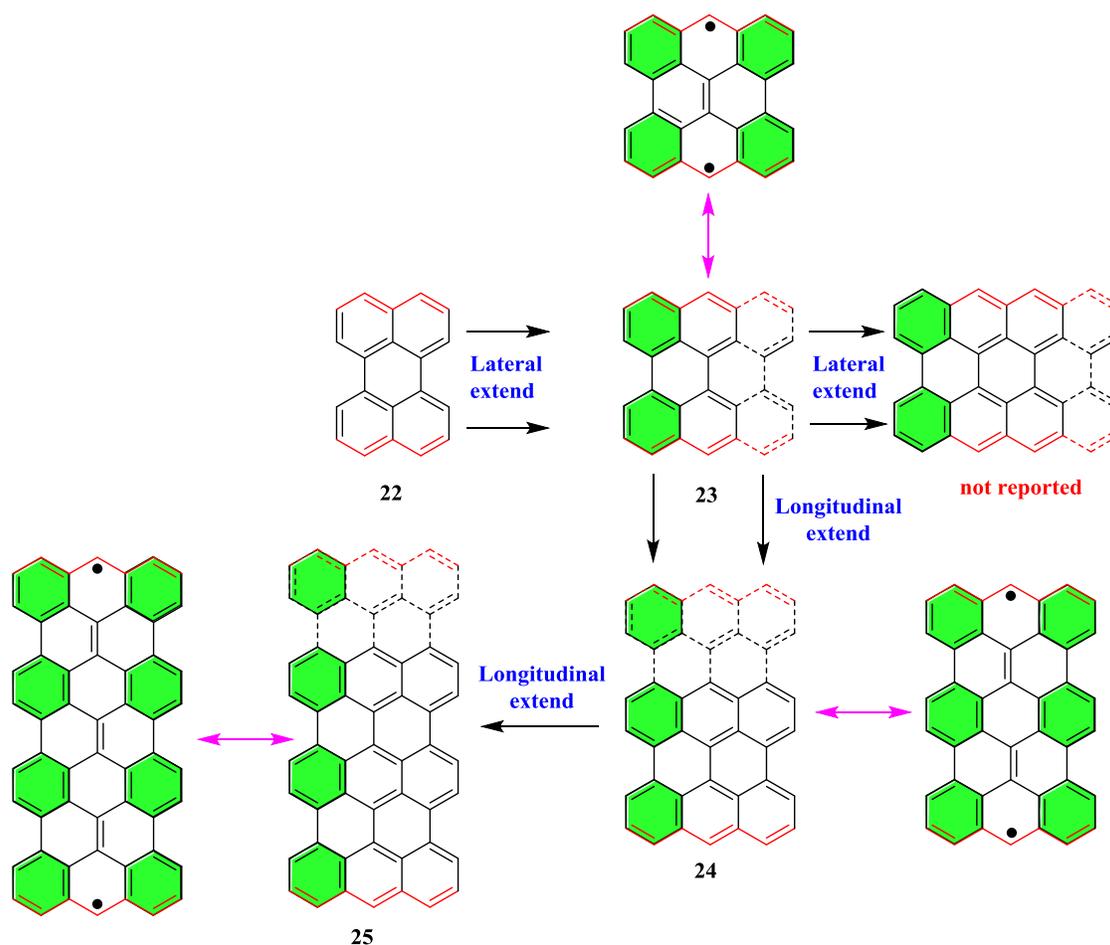

Figure 16. The structure and resonance structures of anthenes.

The other group of partial zigzag-edged PAHs, which are built up by *peri*-annulation of naphthalene, is called the rylene series. In naphthalene, one ring with an electron sextet can be formed, and the other ring remains with four π-electrons. The partial olefinic character of the π-electrons leads to an increased reactivity, especially for Diels-Alder reactions in the bay position of higher rylenes,[29] and the lower optical energy gap in comparison to the fully benzenoid PAHs. For example, perylene (**22**) shows absorption bands up to 440 nm,[30] having only two more π-electrons than triphenylene (**1**), which does not absorb at wavelengths longer than 300 nm.[31-34] Bisanthene **23**, which can also be viewed as laterally expanded perylene, has been known for many years. The synthesis of parent bisanthene **23** was first reported by Clar.[35, 36-38] Recently, Kubo *et al.* obtained the teranthene **24** and quateranthene **25** by expanding bisanthene at longitudinal direction (Figure 16).[39, 40] In order to obtain stable and soluble materials, they kinetically blocked the reactive sites with bulky mesityl and *tert*-butyl groups.

The crystal structures of **23**, **24**, and **25** are show in Figure 17a, and the corresponding bond lengths are summarized in Figure 17b.[41, 42] The single crystal structure of **25** strongly suggests the significant localization of electrons at the zigzag edges. Furthermore, the harmonic oscillator model of aromaticity (HOMA) values indicate large benzenoid character for peripheral six-membered rings (the green benzene rings in the biradical form in Figure 16), as shown in Figure 21b. For bisanthene **23**, the destabilization energy of the π-bond cleavage is not compensated by the formation of additional sextets since the additional sextets in the biradical form are only two, thus the Kekulé form has a dominant contribution to the ground state in **23**. For larger anthenes such as teranthene **24** and quateranthene **25**, the difference in the number of aromatic sextets between the biradical and the Kekulé forms increases with increasing molecular size, i.e., three for teranthene and four for quateranthene. More sextets in the biradical forms result in gaining more aromatic stabilization energies, and thus more dominant contribution of the biradical form to the ground state.
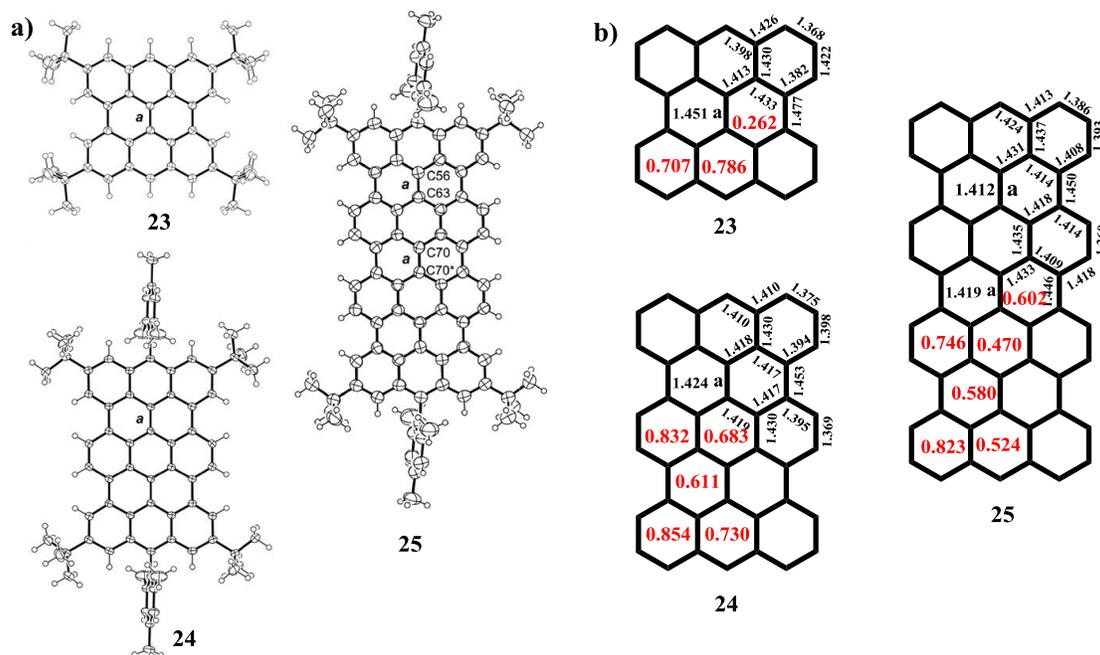
Figure 17. The crystal structures (a) and the mean bond lengths (b) of **23**, **24** and **25**. The numbers given in red denote the HOMA values.

The edge-localized electrons of **24** and **25** also induce unique optical properties. One signature of the biradicaloid character is the presence of a low-lying excited singlet state dominated by the doubly excited configuration.[43] Both compounds show a weak low-energy band centered at 1054 nm (**24**) and 1147 nm (**25**). Compared to bisanthene **23**, however, antiferromagnetic PAHs **24** and **25** give totally different band shapes and feature very weak low-energy bands, where the low-energy band absorption indicates a small HOMO-LUMO gap. From the theoretical (NEVPT2) calculation, the weak band at around 1150 nm of **25** is associated with the simultaneous excitation of the two edge-localized electrons.

The smallest PAH with full zigzag periphery is pyrene (**26**). The effect of the edges on the UV-vis absorption behavior can be well observed in this molecule.[44-47] The α-bands of pyrene are found at 372 nm, almost as long as that of the much bigger armchair-edged tribenzocoronene (pyrene consists of 16 carbon atoms, while armchair-edged tribenzocoronene has 36). Another unique feature is the large separation of the *p*-band (334 nm) and the β-band (272 nm), which is in contrast to the spectra of fully benzenoid armchair-edged PAHs. Coronene (**27**) is another full zigzag-edged PAH with three double bonds. Its α-bands at 375 nm are very weak due to the high

symmetry (D_{6h}).[48] This position is almost identical to the α-bands of pyrene, so the optical gap with increasing size does not follow a comparable trend as for the fully benzenoid armchair-edged PAHs; it also depends on the symmetry.[49-51] The synthesis of ovalene (**28**) was firstly reported by Clar through the Diels-Alder cycloaddition of bisanthene with several arynes in 1948.[52-54] Compound **28** can also be viewed as bisanthene (**23**) annulated with two additional rings at the bay regions, forming two double bonds to have a full zigzag-edged PAH structure. Compared to the pyrene (**26**) and coronene (**27**), ovalene (**28**) showed a red-shift in the absorption spectrum due to the effect of the extended π-conjugation.

Coronene (**27**) can be regarded as circumbenzene, and ovalene (**28**) as circumnaphthalene. Diederich *et al*. described an efficient synthetic route to the next generation circumarenes, namely circumanthracene (**29**) in 1991.[55] PAH **29** is a blue, and intensively red-fluorescing in 1,2,4-trichlorobenzene. From the UV-vis absorption spectrum of **29**, its α-bands are found at 609 nm, the *p*-bands at 582 nm, and the β-bands at 380 nm, which are in good agreement with the prediction by Clar and Schmidt *et al*.[56]

The UV-vis absorption spectrum of the full zigzag-edged PAHs **26-29** are compared in Figure 18. The α-, β-, and *p*-bands are gradually red-shifted upon extension of the conjugated circumarene systems. More interestingly, **28** have larger optical energy gap than that of the bisanthene **23**. This suggests that the circumarenes are more stable than the *peri*-acenes. In addition, the synthesis of circumanthracene **29** has been reported, while the similar-sized *peri*-tetracene has not been achieved yet. This fact is in line with the notion that circumanthracene **29** with the larger HOMO-LUMO energy gap is more stable than the *peri*-tetracene. There are two Clar's aromatic sextets in *peri*-tetracene, while circumanthracene **29** has four in the ground state (Figure 19). This also accounts for the lower stability of *peri*-tetracene.

Figure 18. UV-vis spetra of **26**, **27**, **28** and **29**.
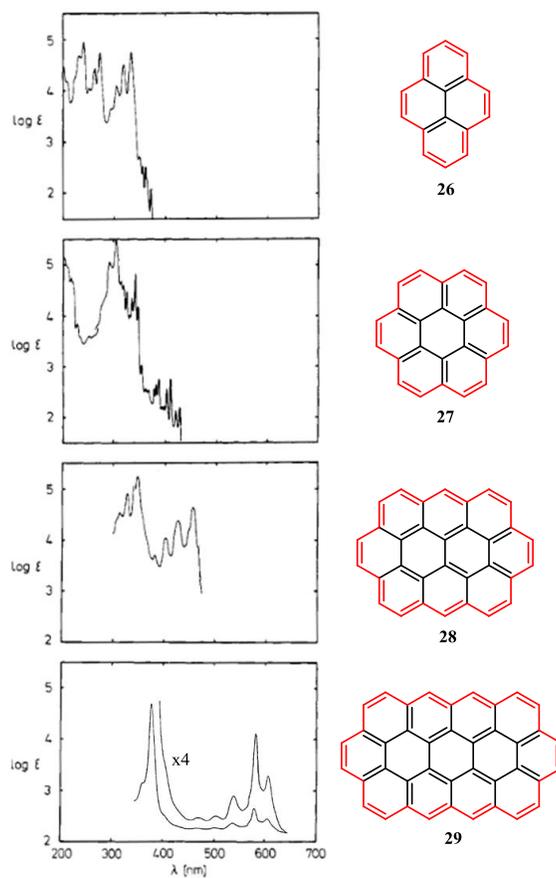
peri-Tetracene
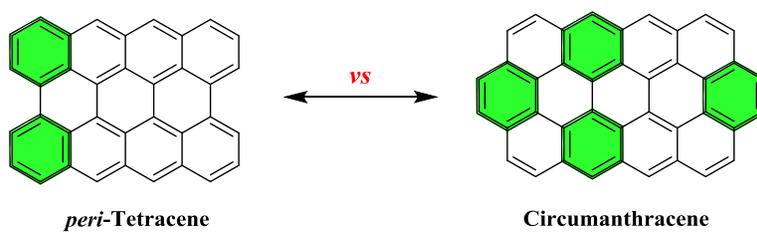
Circumanthracene

Figure 19. Clar's aromatic sextets in *peri*-tetracene and circumanthracene (**29)**.

1.4 Unconventional Polycyclic Aromatic Hydrocarbons

1.4.1 Open-shell Polycyclic Hydrocarbons

Most of the PAHs introduced in the previous sections have closed-shell electronic structures (all electrons in a molecule are paired) and are very stable. On the other hand, a few of them, such as higher anthenes **24** and **25**, have open-shell electronic structures (some electrons are unpaired), and show high reactivity, making their synthesis more challenging. The fundamental reason for their instability can be attributed to their intrinsic biradical character, which is induced by the topology of π-electron array, even if they have even number of carbon atoms. The electronic states of open-shell systems with two unpaired electrons can be either open-shell singlet (antiparallel) or open-shell triplet (parallel), depending on the spin directions of the electrons. PAHs with significant biradical characters exhibit unique electronic, magnetic, and optical properties. These open-shell compounds generally show a small energy gap, amphoteric redox behavior, and a moderate biradical character, which open the opportunities for applications in near-infrared (NIR) dyes, ambipolar organic field-effect transistors (OFETs), nonlinear optics (NLO), and energy storage devices. In addition, the unique magnetic response upon application of external stimuli (such as electric and magnetic field) qualifies them as multifunctional responsive materials and as spin injection/transporting materials in spintronic devices.


37
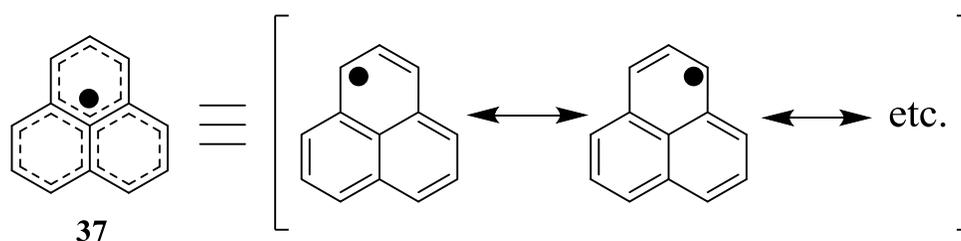
Figure 20. Phenalenyl radical **37** and its resonance forms.

Phenalenyl radical **37**, is a PAH radical, and has long attracted the attention of experimental and theoretical organic chemists for its delocalized spin structure (Figure 20). In the first study of **37** at 1950s, it was found to be reactive and could only survive in solution.[57-60] Later, by introducing three bulky *tert*-butyl groups, the phenalenyl radical could be sufficiently stabilized to allow for the isolation and characterization in its crystalline state.[61, 62] From then, phenalenyl-based radical became a useful and widely explored building block for preparing biradical

molecules, where a series of biphenalenyl derivatives have been the most intensively investigated. By connecting two phenalenyl radical units to π-conjugated systems, biradicals with Kekulé structures can be produced. Nakasuji and Kubo synthesized a series of biradical molecules based on the biphenalenyl.[63-65] In 2005, Kubo *et al.* reported a phenyl-bridged biphenalenyl **38**,[66, 67] which consists of *p*-quinodimethane and two phenalenyl units (Figure 21). From the resonance structure, its spins are delocalized over the whole phenalenyl moieties, due to the highly symmetric structure and the unpaired electron delocalize on the entire molecule. This resonance form **38-2** leads to the conclusion that **38** should be a stabilized singlet biradical as a result of gaining the aromatization energy of the central six-membered ring.
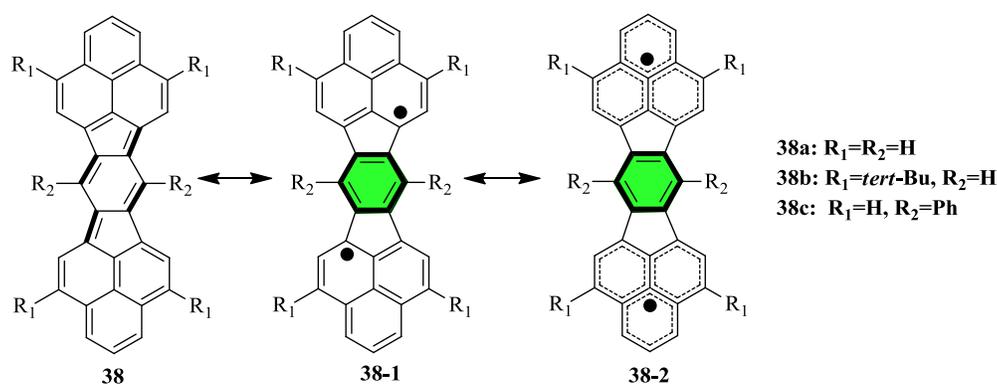

Figure 21. Resonance forms of **38**.

Naphthalene- and anthracene-bridged biphenalenyls **39** and **40**, respectively, were also synthesized by Kubo *et al.* through replacement of the central benzene ring.[68-70] Biphenalenyls **39** and **40** showed larger biradical characters (**40**: y=0.68, **39**: y=0.50, **38**: y=0.30), most probably because naphthalene and anthracene have much larger aromatic stabilization energies than benzene (Figure 22). Single crystal X-ray analysis unambiguous revealed that **39** and **40** formed 1D chains in a slipped stacking arrangement with the superimposed phenalenyl moieties overlapping, which were almost identical to that of **38**. Moreover, biphenalenyl **39** packed more tightly in the 1D chain with a π-π distance of 3.12 Å than benzene linked **38** with that of 3.23 Å. The very short π-π contacts indicated a prominent covalent bonding interactions between the molecules.[71]

39a: R$_1$=R$_2$=H
39b: R$_1$=Ph, R$_2$=*tert*-Bu
39c: R$_1$=Ph, R$_2$=H

40a: R$_1$=R$_2$=H
40b: R$_1$=Ph, R$_2$=*tert*-Bu
40c: R$_1$=Ph, R$_2$=H
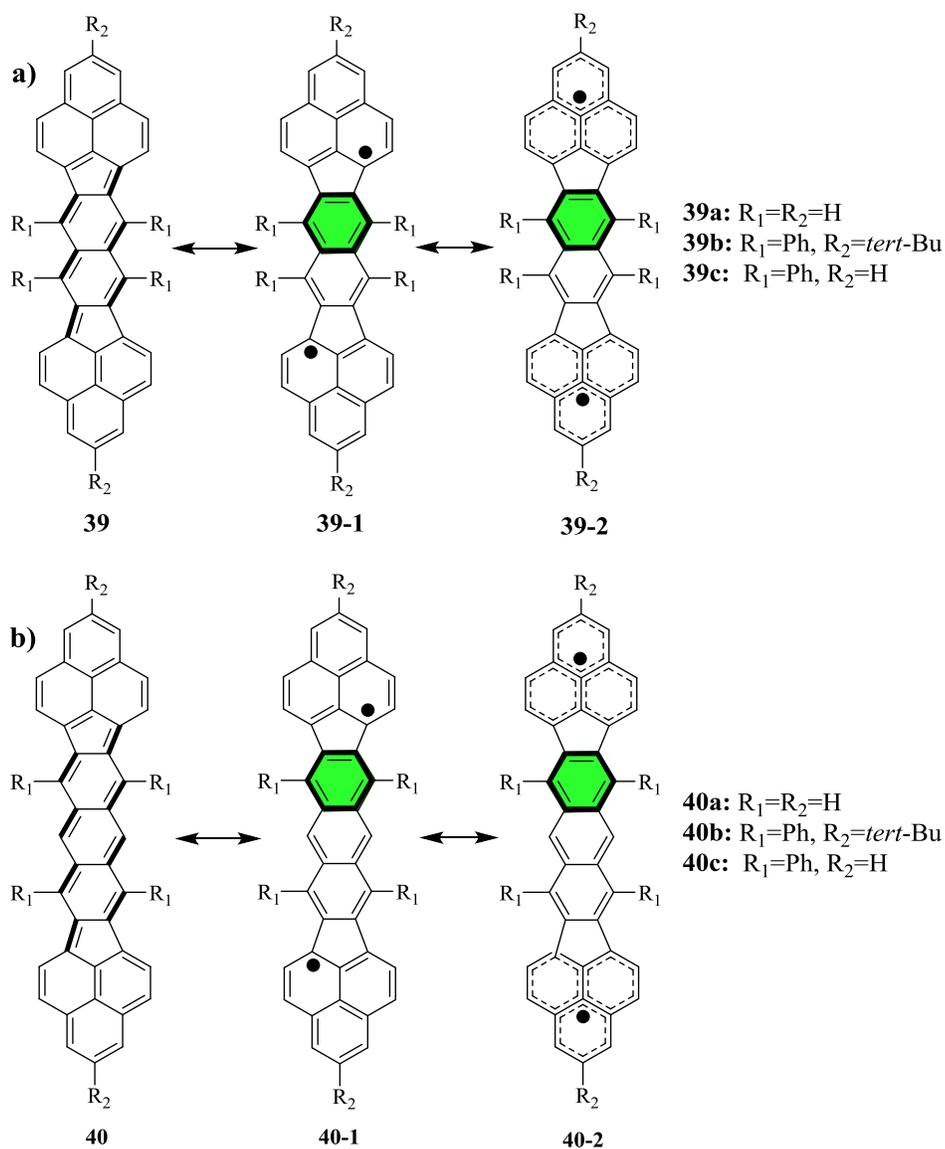
Figure 22. Resonance forms of (a) **39** and (b) **40**.

Kubo *et al*. also designed and synthesized an interesting PAH radical, containing three phenalenyl units (**41**, Figure 23), which was found to exhibit a highly delocalized monoradical.[72,73] Remarkably, **41** was stable enough to allow its purification by silica gel column chromatography under ambient conditions. The kinetic and thermodynamic stability of **41** results from the bulky *tert*-butyl groups and its highly delocalized structure.
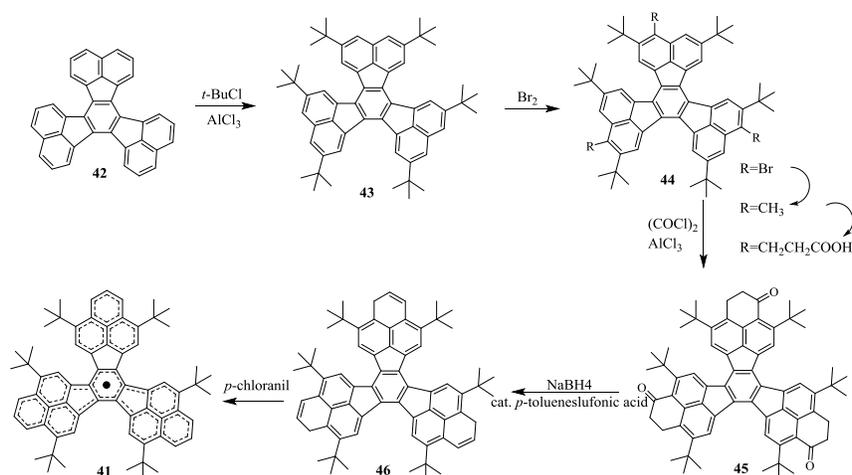
Figure 23. Synthetic route towards tri-phenalenyl **41**.

Another outstanding PAH molecule is zethrene **47**, a unique polycyclic aromatic hydrocarbon with formally fixed C-C double bonds, which can be viewed as a "head-to-head" fusion of two phenalenyl moieties (Figure 24). One characteristic feature of this molecule is the existence of two distinct resonance structures, a closed-shell quinoidal form and an open-shell biradical form, where there is a significant biradical contribution to the ground-state electronic configuration. It is predicted that zethrene **47** have interesting properties and potential applications as an optical, electronic and spintronic material. Zethrene **47** was first synthesized by E. Clar in 1955.[74] Later, Staab and Sondheimer *et al*. developed more straightforward synthesis methods in the 1960s.[75-77] So far, all of the reported zethrene derivatives adopted closed-shell properties, although their structures contain two phenalenyl rings connected head to head.[78-81] On the other hand, if the zethrene is longitudinally extend by introducing benzene or naphthalene between the two phenalenyl rings, the higher order analogues named heptazethrene and octazethrene, respectively, will be obtained. Recently, Wu and coworkers have paid particular attention to the zethrene and such higher analogues of it.[82-85]
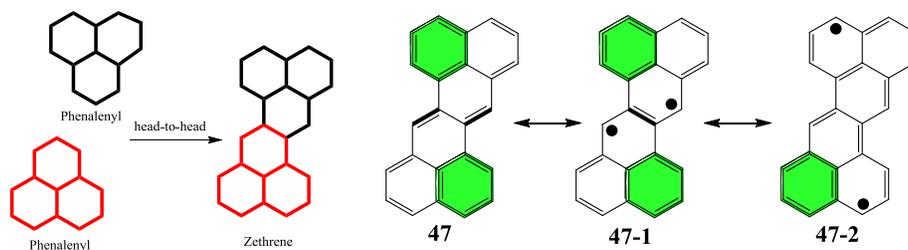

Figure 24. Resonance forms of zethrene **47**.

24

Wu and coworkers first reported an efficient synthetic route for a kinetically stabilized heptazethrene **48** and octazethrene **49** derivatives, in which the most reactive sites are protected by bulky groups (Figure 25).[86] From theoretical calculations, the biradical character (y) of zethrene **47**, heptazethrene **48**, and octazethrene **49** were 0.407, 0.537, and 0.628, respectively.[87] The higher biradical character of heptazethrene **48** and octazethrene **49** can be explained by the larger aromatic stabilization energies through the recovery of aromatic benzene and naphthalene rings, respectively, in their biradical resonance forms (Figure 25a). Interestingly, during the detailed experimental studies, Wu found that heptazethrene **48** featured a closed-shell ground state while octazethrene **49** exhibited a singlet biradical ground state. This can be explained by the relatively large energy gap of the heptazethrene **48**, indicating that a small energy gap is crucial for an open-shell ground state structure. In its UV-vis absorption spectrum, heptazethrene **48** shows a well-resolved *p*-band at 634 nm, which is typical for many closed-shell PAHs.[88, 89] On the other hand, the absorption spectrum of octazethrene **49** displays a well-resolved band in the near-infrared region with maxima at 795, 719, 668, and 613 nm. Importantly, octazethrene **49** exhibits a weak peak at 795 nm that is not observed for heptazethrene **48**, which is a characteristic feature of singlet biradical molecules (Figure 25b).
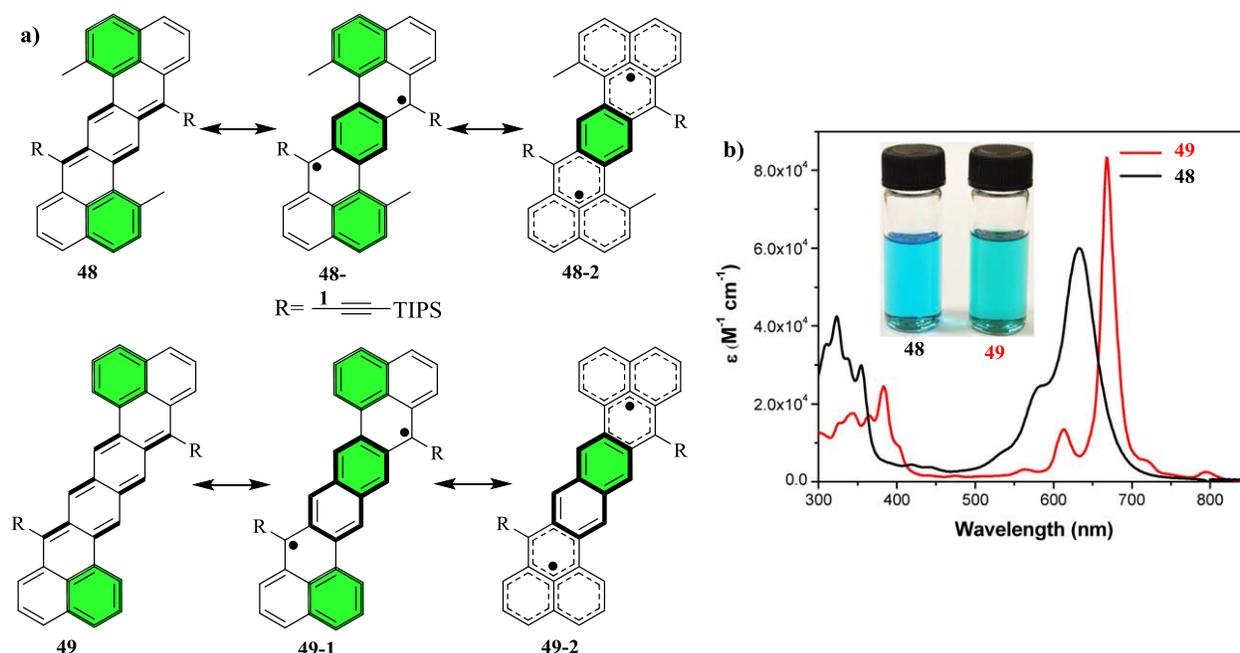

Figure 25. a) Resonance forms of **48** and **49**. b) UV-vis absorption spectra of **48** and **49**.

In order to understand the role of the aromatic sextet ring on a singlet biradical system, Wu and coworkers synthesized two dibenzoheptazethrene isomers, which have the same chemical skeleton ($C_{36}H_{20}$): 1,2:9,10-dibenzoheptazethrene (**50**) and 5,6:13,14-dibenzoheptazethrene (**51**) (Figure 26a).[90, 91] For obtaining stable and soluble materials, **50** and **51** were designed with bulky groups, such as mesityl and triisopropylsilylacetylene, to kinetically block the reactive sites. From resonance structures, isomer **50** has two aromatic sextets in the closed shell form and a maximum of three aromatic sextets in the biradical form; in contrast, isomer **51** has five aromatic sextets when the two radicals are located at the terminal anthracene units (**51-2**). Isomer **50** is blue in chloroform solution, and its absorption spectrum shows a *p*-band with a maximum peak at 687 nm and a shoulder peak at 628 nm. In contrast, compound **51** in chloroform displays an intense absorption at 804 nm and several small bands in the lower energy region, which is a typical absorption feature for singlet biradicaloid molecules (Figure 36b). The weak absorption bands in the low-energy region likely originate from admixing of the doubly excited electronic configuration ($H,H \rightarrow L,L$) into the ground state.[92]
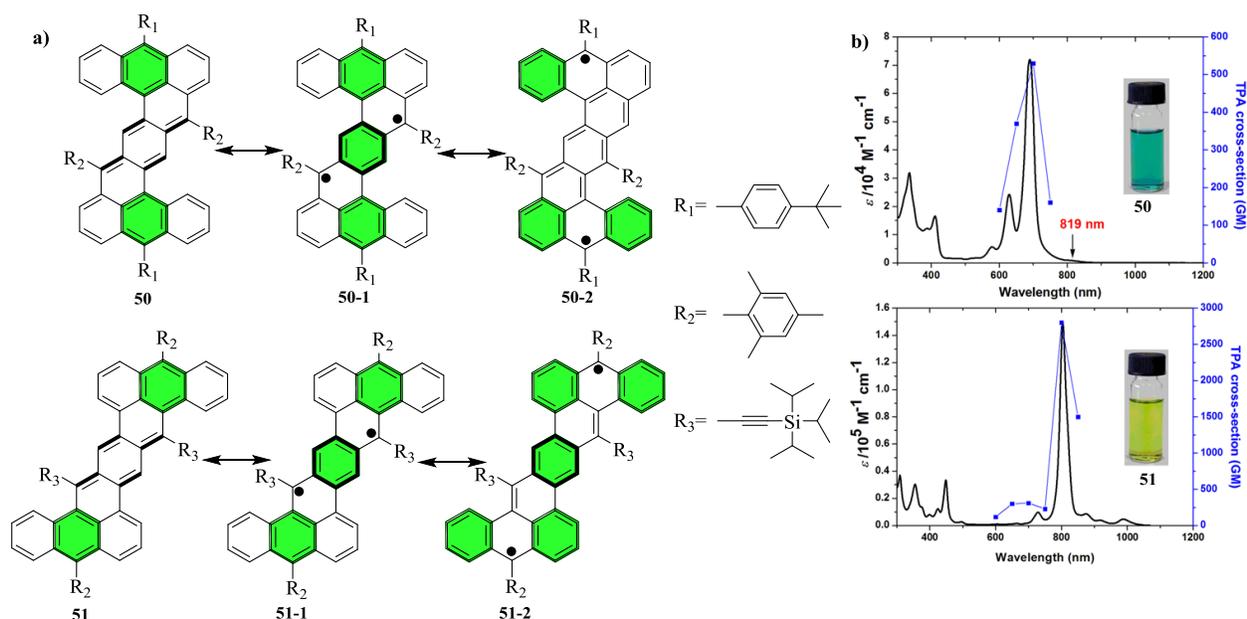

Figure 26. a) Resonance forms of **50** and **51**. b) UV-vis absorption spectra of **50** and **51**.

1.4.2 Antiaromatic Indenofluorenes

indeno[1,2-*a*]fluorene **52**   indeno[1,2-*b*]fluorene **53**

indeno[2,1-*a*]fluorene **54**   indeno[2,1-*b*]fluorene **55**   indeno[2,1-*c*]fluorine **56**
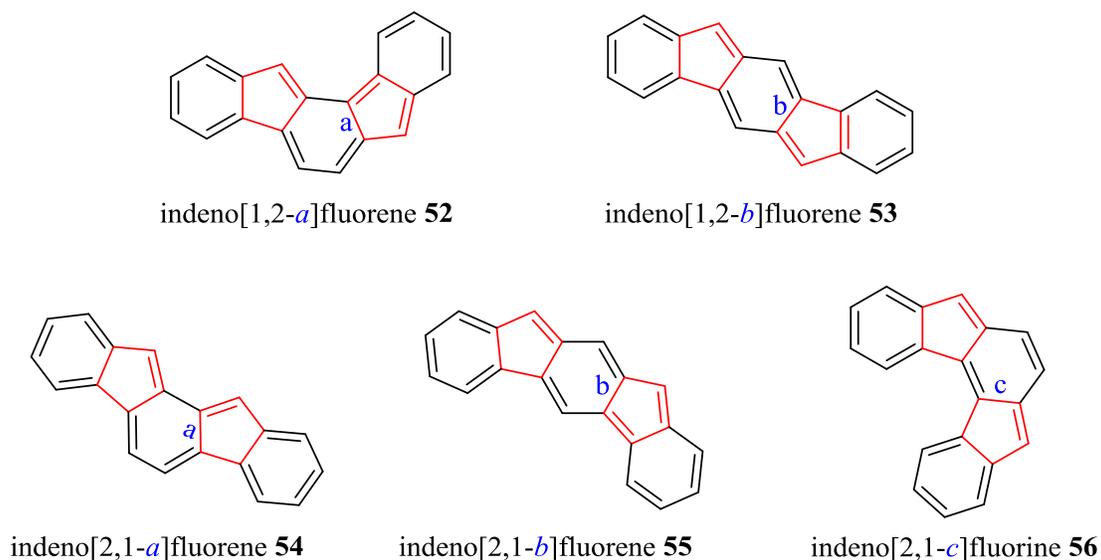
Figure 27. The five isomer structures of indenofluorene molecules.

Antiaromatic molecules are defined in terms of the existence of 4n π-electrons disposed in a planar cyclic arrangement. Indenofluorenes are prominent 20-π-electron, fully conjugated antiaromatic analogues of acenes with 6-5-6-5-6 fused ring systems. Compared to the acene-type aromatic compounds, the fused polycyclic antiaromatic systems are considered to have high HOMO levels and low LUMO levels, leading to narrower HOMO-LUMO energy gaps. Although antiaromatic systems are generally very reactive and unstable, the introduction of the bulky group at the active sites would enhance the kinetic and thermodynamic stability and allow for the solution processing. There are five distinct structural regioisomers in the indenofluorene family: indeno[1,2-*a*]fluorine (**52**), indeno[1,2-*b*]fluorine (**53**), indeno[2,1-*a*]fluorine (**54**), indeno[2,1-*c*]fluorine (**55**), and indeno[2,1-*b*]fluorine (**56**) (Figure 27).

The first synthesis of indenofluorenes was pursued in the late nineteenth century by Gabriel.[93] For a long time (more than 100 years), indenofluorenes and their derivatives were a scattered topic in the literature.[94-104] More recently, Haley and Tobe groups have made a significant progress in this field. In 2011, synthesis of a fully conjugated indeno[1,2-*b*]fluorene **53** and its derivatives were reported by Haley's group.[105-107] The molecular single crystal structure of **53** reveals that the fused ring system is essentially planar. Examination of the bond lengths in the

single crystal structure showed that there were alternating long and short bonds in the central *p*-xylylene core, but the peripheral benzene have homogeneous bonds. Both the experimental and computational data suggest that **53** should be described as a fully conjugated 20-π-electron hydrocarbon with fused *s-trans* 1,3-diene linkages across both the top and bottom portions of the carbon skeleton. The optical absorption spectra of **53a** and **b** are shown along with pentacene in Figure 28c. Similar to pentacene, indeno[1,2-*b*]fluorenes **53a** and **b** exhibit three low-energy absorptions (λ_{max}: 594 and 614 nm, respectively) but are blue-shifted by approximately 50 and 30 nm, respectively. Notably, no open-shell biradical ground state was observed for this system due to the relatively large HOMO-LUMO energy gap.
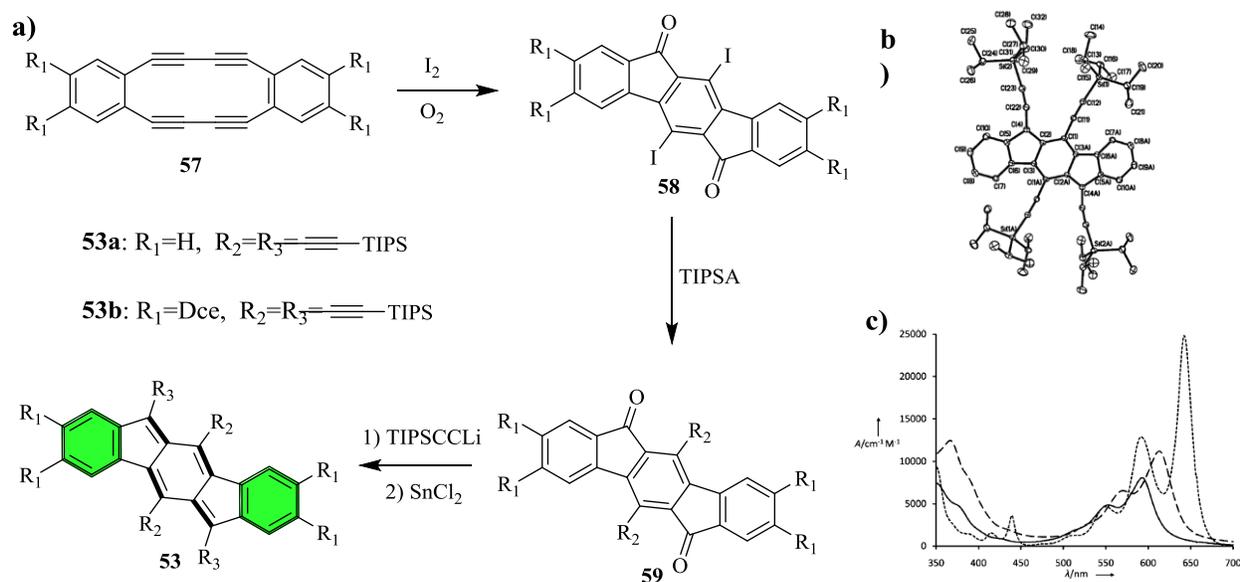

Figure 28. a) Syntheses of **53**. b) Molecular crystal structure of indenofluorene **53a**. c) Electronic absorption spectra of pentacene (dotted), **53a** (dashed), and **53b** (solid) in CH₂Cl₂.

At the same time, Tobe and coworkers synthesized and isolated air stable 11,12-dimesitylindeno[2,1-*a*]fluorene **54** with *o*-quinodimethane instead of the *p*-quinodimethane moiety (Figure 29).[108] From the X-ray crystallographic analysis, the bond lengths of **54** were also found to show alternation in the central *o*-quinodimethane core and to be homogeneous in the peripheral benzenes. The Nucleus-independent chemical shift (NICS) calculation and chemical shifts in the ¹H NMR spectrum suggest that **54** is weakly antiaromatic as a result of the

cis-indacene moiety, and possesses a closed-shell ground state, although **54** seems to have a biradical contribution in its resonance forms.
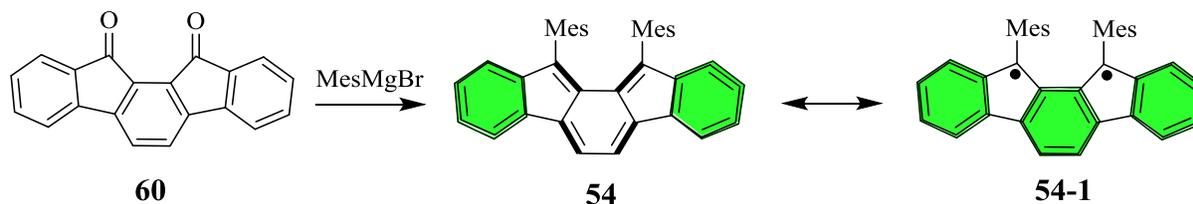

Figure 29. Synthesis and resonance forms of **54**.

Recently, a new class of fully conjugated indenoflurorenes, i.e., indeno[2,1-*c*]fluorenes **55** have been synthesized and characterized by Haley group (Figure 30).[109] These indeno[2,1-*c*]fluorene molecules, containing an antiaromatic *as*-indacene core, possess high electron affinities and show a broad absorption that extends into the near-IR region (550-800 nm) of the electromagnetic spectrum. Based on the single-crystal X-ray analysis, the bond lengths of **55** also showed alternation in the central *p*-quinodimethane core and a uniform value in the peripheral benzenes, suggesting a closed-shell ground state.
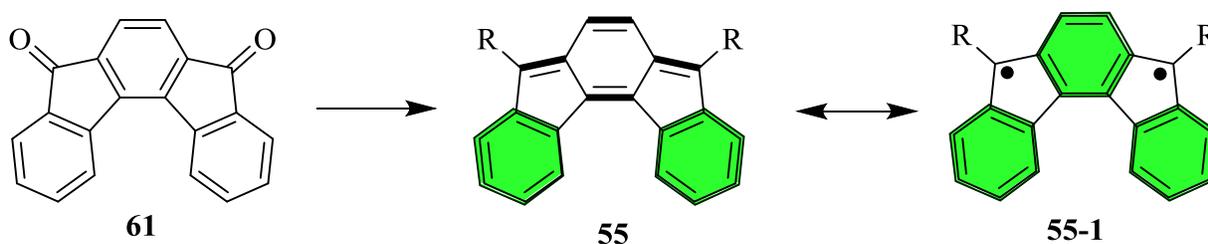

Figure 30. Synthesis and resonance forms of **55**.

An indeno[2,1-*b*]fluorine derivative **56** substituted by mesityl groups was reported by Tobe recently (Figure 31).[111] Indeno[2,1-*b*]fluorine **56** reveals a non-alternant hydrocarbon with a moderate singlet biradical character while other indenofluorene isomers usually feature a closed-shell ground state. Moderate singlet biradical character contributes to the ground state as indicated by NMR and X-ray single crystal structures. In the UV-vis absorption spectrum, **56** exhibits an extremely low-energy light absorption band, which extends to 2000 nm, despite its small conjugation space (Figure 32c).
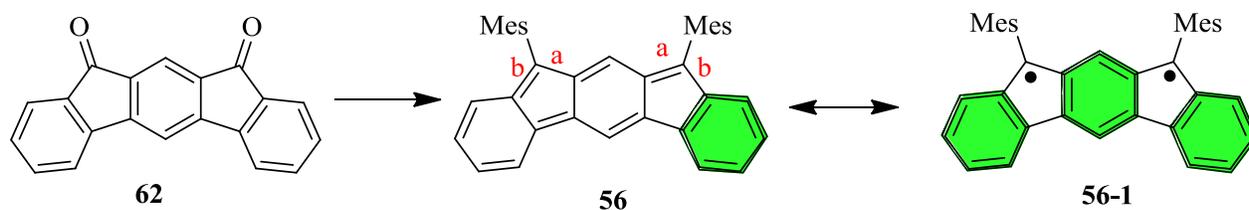
Figure 31. Synthesis and resonance forms of **56**.
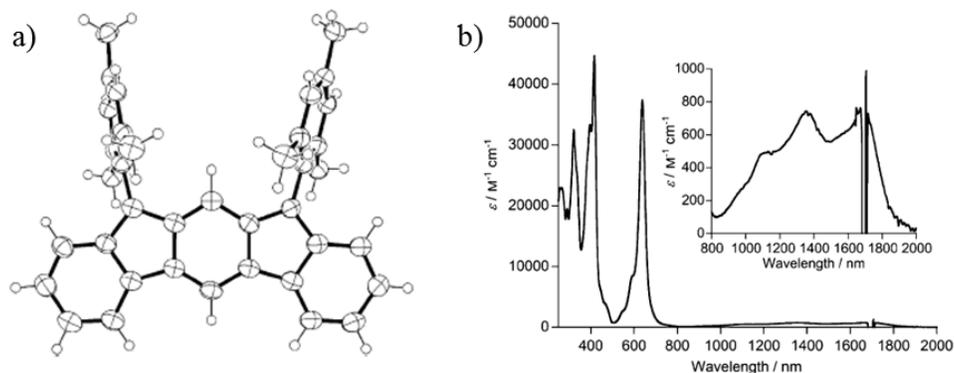
Figure 32. A) X-ray single crystal structure and b) UV-vis absorption spectrum of **56**.

Notably, indeno[2,1-*b*]fluorene **56** has a larger singlet biradical character than other three isomers (indeno[1,2-*b*]fluorene **53**, indeno[2,1-*a*]fluorene **54**, and indeno[2,1-*c*]fluorene **55**) because of its *meta*-quinodimethane subunit, in contrast to the *ortho*- and *para*-quinodimethane structures of the other isomers. Interestingly, there are two more Clar sextet rings in the biradical form of indeno[2,1-*b*]fluorene **56** compared to that of its form Kekulé form, while the difference in the number of Clar sextet rings is only one between the Kekulé and the biradical forms of other indenofluorenes. This observation suggests that the energy levels are very similar between two resonance forms if the difference in the number of Clar sextets is only one: however when the difference is more than two the additional aromatic stabilization energy will be sufficient for the contribution of the biradical character to the ground state. Thereby, following this principle, one can design new polycyclic hydrocarbons with singlet biradical character based on the *meta*-quinodimethane structure.

1.5 Motivation
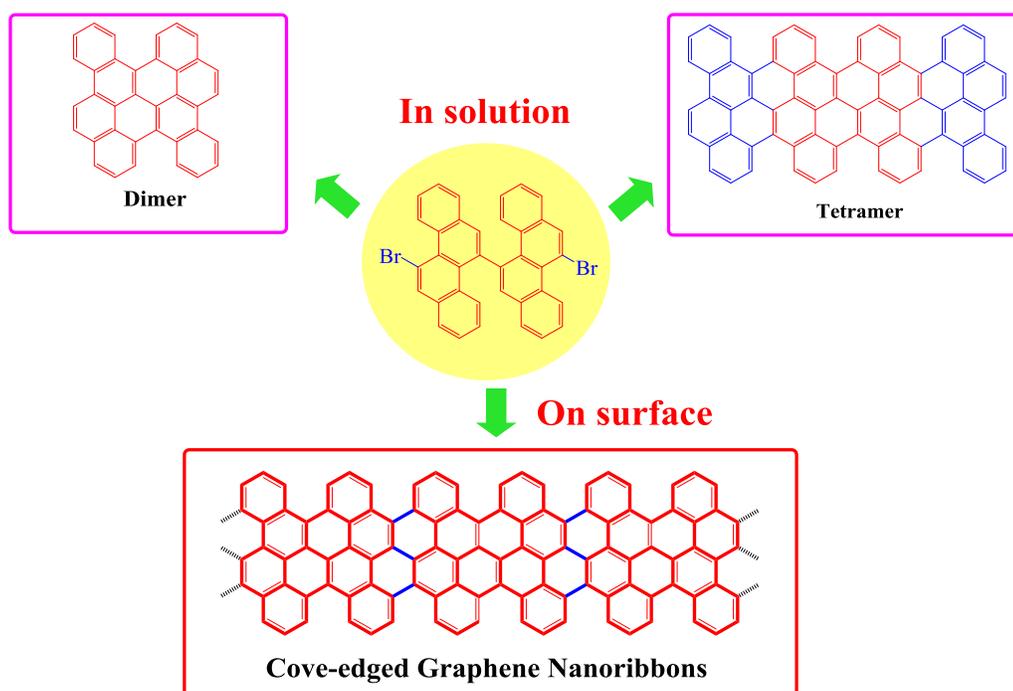
Figure 33. Cove-edged PAHs and GNRs synthesized based on 11,11'-dibromo-5,5'-bischrysene.

As reviewed above, "bottom-up" synthesis has been mainly focused on armchair-edged PAHs, whereas PAHs with cove- or zigzag- edges remained elusive. Interestingly, cove-edged PAHs are not fully benzenoid, which are expected to have smaller optical energy gaps compared to those of armchair-edged PAHs with similar sizes. In addition, in contrast to the PAHs with armchair peripheries that mostly have planar structures, the outstanding feature of cove-edged PAHs is non-planar π-conjugated carbon skeletons, which result from the steric repulsion between the two C-H bonds at the inner cove position. Furthermore, cove-edged PAHs are reported to show remarkable charge-carrier mobilities because the π surfaces of contorted molecules can approach each other and arrange in very different ways.[21] However, to date, only limited examples of this type of molecules have been reported, due to the lack of proper synthetic protocols. Thereby, in Chapter 2, a series of novel cove-type PAHs were designed and synthesized for the first time to investigate their electronic and optoelectronic properties (Figure 33). In order to fabricate structurally well-defined cove-edged PAHs, the key building block 11,11'-dibromo-5,5'-bischrysene was prepared (Figure 33). As model subunits of the infinite cove-edged GNRs, fused

chrysene-based oligomers or PAHs, namely dimer (two units of fused chrysene) and tetramer (four units of fused chrysene), were synthesized via the Ullmann coupling reaction of 11,11'-dibromo-5,5'-bischrysene followed by intramolecular oxidative cyclodehydrogenation in solution.

As described in the previous sections, the "top-down" approach, such as the cutting of graphene, sonochemical extraction from expanded graphite, and unzipping of carbon nanotubes, has produced GNRs with sub-10 nm widths, revealing their semiconducting nature and excellent charge transport properties. However, "top-down" methods generally suffer from low yields and non-uniform widths, as well as ill-defined edge structures. In contrast, fabrication of structurally well-defined GNRs has been realized by bottom-up synthetic approaches based on solution-mediated as well as surface-assisted cyclodehydrogenation of tailor-made polyphenylene precursors. The surface-assisted method enabled the direct growth of atomically precise GNRs on metal surfaces, which could be unambiguously demonstrated by the in-situ STM visualizations. However, to date, the bottom-up surface-assisted method has mainly focused on armchair-edged GNRs. Thereby, in Chapter 2, cove-edged GNRs were synthesized via on-surface synthesis for the first time by using 11,11'-dibromo-5,5'-bischrysene as the building block (Figure 33).

Compared to armchair- and cove-edged PAHs, PAHs with zigzag periphery display unique electronic and optoelectronic properties resulting from the spin-polarized state at the zigzag edges. More interestingly, some of them possess a prominent biradical character in the ground state. The smaller examples of zigzag-edged PAHs, such as perylene and bisanthene, have been known for a long time. Recently, the larger PAHs with zigzag periphery, such as teranthene and quateranthene, were obtained by extending the bisanthene structure along the longitudinal direction. However, the attempts to synthesis the next generation of *peri*-fused acenes, such as *peri*-tetracene, by expanding bisanthene along the lateral direction have not been successful yet, probably due to the extremely high reactivity as well as the lack of proper synthetic protocols. In Chapter 3, a novel tetrabenzo[*a,f,j,o*]perylene, namely "bistetracene" in which two tetracenes are connected side by side with two bonds, was synthesized and characterized for the first time (Figure 34). Such zigzag-edged PAH can be considered as a short segment of infinite graphene nanoribbons with zigzag edges. Therefore, our studies contribute to an understanding of the edge

states of expanded PAH homologues and graphene nanoribbons, which may possess a localized nonbonding π-state around the zigzag edges.
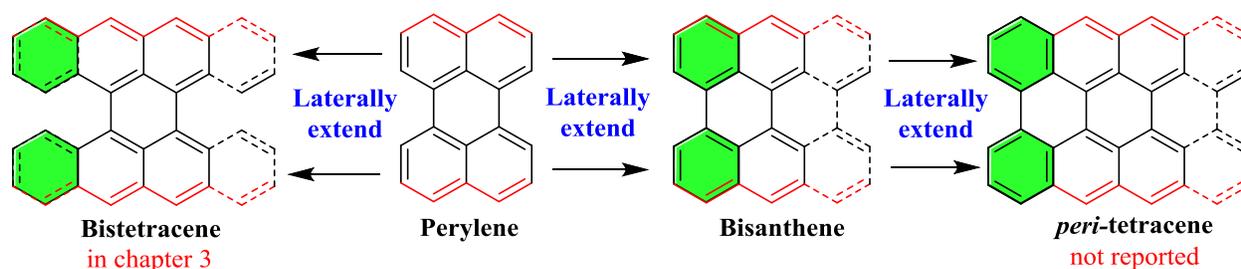

Figure 34. Synthesis of the bistetracene by extending the perylene along the longitudinal direction.

6,7,13,14-tetraphenylbenzo[*k*]tetraphene   5,14-diphenyldibenzo[*a,m*]rubicene
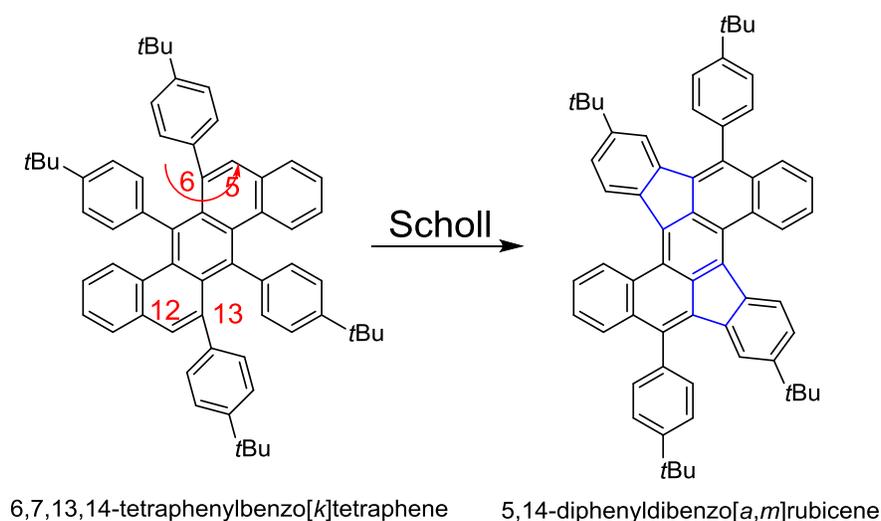
Figure 35. The structure of pentagon-embendded bistetracene and bistetracene.

The synthesis of tetrabenzo[*a,f,j,o*]perylene, namely "bistetracene", is demonstrated. However, theoretical calculations and physical property investigations manifest that such bistetracene possesses a prominent biradical character in the ground state. Accordingly, this bistetracene can easily undergo oxidation into tetrabenzo[*a,f,j,o*]perylene-9,19-dione (diketone) under ambient conditions. Thereby, the stabilization is the critical issue for such PAHs. In Chapter 4, a novel dibenzo[*a,m*]rubicene, pentagon-embedded bistetracene, was synthesized and characterized, and is more stable compared to the traditional bistetracene only with six-membered rings. This pentagon-embedded molecule was obtained through the migration of the phenyl group during the

Scholl reaction (Figure 35). The geometric and optoelectronic nature of these compounds were investigated by UV-vis absorption and single crystal structure analysis. Furthermore, the mechanism for the phenyl migration is proposed, providing a unique and unprecedented entry to extended and stable *peri*-tetracene or *peri*-pentacene like analogues with five-membered rings, and possibly even seven-membered rings in the future. This new synthetic pathway will give an access to promising materials, for example, for organic field-effect transistor applications.
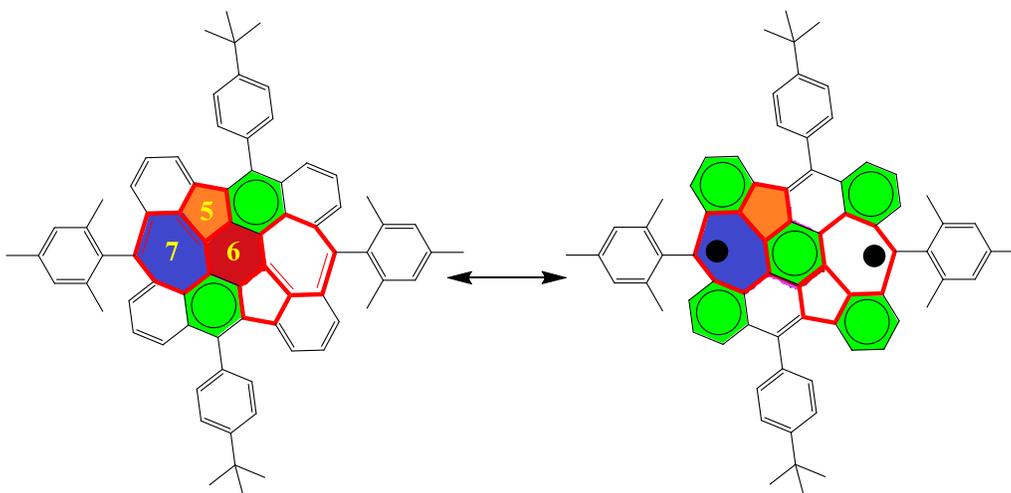

Figure 36. Structure of PAHs with odd-rings.

In chapter 4, we have demonstrated a series of novel PAHs incorporating five- or eight-membered rings from the precursor 6,7,13,14-tetraphenylbenzo[*k*]tetraphene, as a result of the "unexpected" phenyl migration during the Scholl reaction. Thus, we consider whether such "unexpected" synthetic protocol can be extended to other systems. In chapter 5, we will show that this "unexpected" migration protocol can serve as a universal approach to prepare structurally well-defined five- and seven-membered-ring embedding nanographene (Figure 36). As a typical example, azuene-embedding nanographene, with five- and seven-membered rings, can be synthesized rapidly from our previous phenyl migration of the precursor 6,7,13,14-tetraphenylbenzo[*k*]tetraphene during the cyclodehydrogenation process. Remarkably, this odd-ring-embedded graphene subunit has a low optical energy gap (1.24 eV) and exhibits a remarkable singlet biradical character in the ground state.

As discussed above, the zigzag-edged bistetracene possesses a prominent biradical character in the ground state due to the formation of aromatic sextets that overwhelms the penalty for breaking the π-bond and pushes the resulting unpaired electrons out to the zigzag edges. These molecules also belong to the *pro*-aromatic compounds. In the *pro*-aromatic concept for the formation of diradicals, the driving force for such solution is the aromaticity gaining of consecutive non-aromatic rings, i.e., a net energy minimization that can eventually surpass the energy required to break a double bond, thus giving a way to the generation of a diradical. In addition, the other Kekulé diradicals have *anti*-aromatic cores instead of the *pro*-aromatic structures. *Anti*-aromatic molecules are defined in terms of the existence of 4n π-electrons disposed in a planar cyclic arrangement. Indenofluorenes are prominent 20-π-electron fully conjugated antiaromatic analogues of acenes with a 6-5-6-5-6 skeleton. In Chapter 5, the first example of air-stable 24-π-electron fully conjugated antiaromatic acene analogue was synthesized and characterized, by including additional two double-bonds at the periphery of indeno[1,2-*b*]fluorene, leading to dibenzene-indeno[1,2-*b*]fluorene core (Figure 37). This compound can give us a rare glimpse into the 24-π-electron antiaromatic system. The physical and chemical properties were systematically studied by various experimental methods and DFT calculations. The results unambiguously demonstrated that this compound were new type air stable and fully conjugated antiaromatic system.


indeno[1,2-*b*]fluorene   dibenzene-indeno[1,2-*b*]fluorene
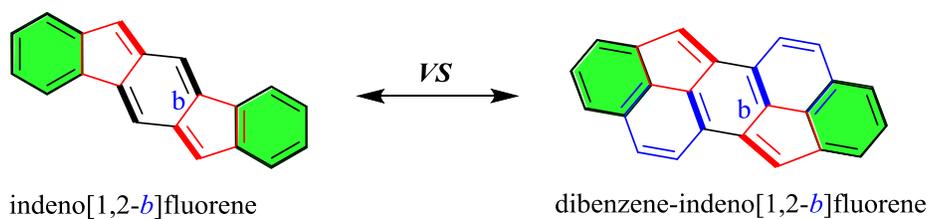
Figure 37. Structure of the dibenzene-indeno[1,2-*b*]fluorene.

References:

[1] S. Kumar. *Liq. Cryst.* **2005**, 32, 1089-1113.

[2] D. Adam, P. Schuhmacher, J. Simmerer, L. Haussling, K. Siemensmeyer, K. H. Etzbach, H. Ringsdorf, D. Haarer. *Nature* **1994**, 371, 141-143.

[3] E. Condon. *Phys. Rev.* **1926**, 28, 1182-1201.

[4] S. M. Meyerhoffer, L. B. McGown. *Anal. Chem.* **1991**, 63, 2082-2086.

[5] J. B. Birks. Photophysics of Aromatic Molecules, Wiley and Sons, Hoboken, 1970.

[6] A. Stabel, P. Herwig, K. Müllen, J. P. Rabe. *Angew. Chem. Int. Ed.* **1995**, 34, 1609-1611.

[7] L. Schmidt-Mende, A. Fechtenkötter, K. Müllen, E. Moons, R. H. Friend, J. D. MacKenzie. *Science* **2001**, 293, 1119-1122.

[8] J. P. Hill, W. S. Jin, A. Kosaka, T. Fukushima, H. Ichihara, T. Shimomura, K. Ito, T. Hashizume, N. Ishii, T. Aida. *Science* **2004**, 304, 1481-1483.

[9] F. Jäckel, M. D. Watson, K. Müllen, J. P. Rabe. *Phys. Rev. Lett.* **2004**, 92, 188303.

[10] W. Hendel, Z. H. Khan, W. Schmidt. *Tetrahedron* **1986**, 42, 1127-1134.

[11] Z. H. Wang, Z. Tomovic, M. Kastler, R. Pretsch, F. Negri, V. Enkelmann, K. Müllen. *J. Am. Chem. Soc.* **2004**, 126, 7794-7795.

[12] X. L. Feng, J. S. Wu, M. Ai, W. Pisula, L. J. Zhi, J. P. Rabe, K. Müllen. *Angew. Chem. Int. Ed.* **2007**, 46, 3033-3036.

[13] D.Wasserfallen, M. Kastler,W. Pisula,W. A. Hofer, Y. Fogel, Z. H.Wang, K. Müllen. *J. Am. Chem. Soc.* **2006**, 128, 1334-1139.

[14] F. Dö tz, J. D. Brand, S. Ito, L. Gherghel, K. Müllen. *J. Am. Chem. Soc.* **2000**, 122, 7707-7717.

[15] Z. Tomovic, M. D. Watson, K. Müllen. *Angew. Chem. Int. Ed.* **2004**, 43, 755-758.

[16] C. D. Simpson, J. D. Brand, A. J. Berresheim, L. Przybilla, H. J. Rader, K. Müllen. *Chem. Eur. J.* **2002**, 8, 1424-1429.

[17] R. Weitzenböck, H. Lieb. *Monatsh. Chem.* **1912**, 33, 549-565.

[18] T. A. Chen, R. S. Liu. *Chem. Eur. J.* **2011**, 17, 8023-8027.

[19] T. A. Chen, R. S. Liu. *Org. Lett.* **2011**, 13, 4644-4647.

[20] E. Clar, J. F. Stephen, *Tetrahedron* **1965**, 21, 467-470.

[21] S. Xiao, M. Myers, Q. Miao, S. Sanaur, K. Pang, M. L. Steigerwald, C. Nuckolls. *Angew. Chem., Int. Ed.* **2005**, 44, 7390-7394.

[22] E. Clar. Polycyclic Hydrocarbons 1964, Academic Press, p. 80.

[23] S. Xiao, S. J. Kang, Y. Wu, S. Ahn, J. B. Kim, Y. L. Loo, T. Siegrist, M. L. Steigerwald, H. X. Li, C. Nuckolls. *Chem. Sci.* **2013**, 4, 2018-2023.

[24] Y. S. Cohen, S. Xiao, M. L. Steigerwald, C. Nuckolls, C. R. Kagan. *Nano Lett.* **2006**, 6, 2838-2841.

[25] A. C. Whalley, K. N. Plunkett, A. A. Gorodetsky, C. L. Schenck, C. Y. Chiu, M. L. Steigerwald, C. Nuckolls. *Chem. Sci.* **2011**, 2, 132-135.

[26] S. E. Stein, R. L. Brown. *J. Am. Chem. Soc.* **1987**, 109, 3721-3729.

[27] Z. Wang, Ź. Tomović, M. Kastler, R. Pretsch, F. Negri, V. Enkelmann, K. Müllen. *J. Am. Chem. Soc.* **2004**, 126, 7794-7795.

[28] M. Kastler, J. Schmidt, W. Pisula, D. Sebastiani, K. Müllen. *J. Am. Chem. Soc.* **2006**, 128, 9526-9534.

[29] S. Alibert-Fouet, I. Seguy, J. F. Bobo, P. Destruel, H. Bock. *Chem. Eur. J.* **2007**, 13, 1746-1753.

[30] D. Rädulescu, G. Ostrogovich, F. Bärbulescu. *Chem. Ber.* **1931**, 64, 2240-2242.

[31] Y. Kono, H. Miyamoto, Y. Aso, T. Otsubo, F. Ogura, T. Tanaka, M. Sawada. *Angew. Chem. Int. Ed.* **1989**, 28, 1222-1223.

[32] R. Schoental, E. J. Y. Scott. *J. Chem. Soc.* **1949**, 1683-1696.

[33] I. B. Berlman. Energy Transfer Parameters of Aromatic Compounds, Academic Press, London, 1973.

[34] B. X. Mi, Z. Q. Gao, C. S. Lee, S. T. Lee, H. L. Kwong, N. B. Wong. *Appl. Phys. Lett.* **1999**, 75, 4055-4057.

[35] E. Clar. *Chem. Ber.* **1948**, 81, 62.

[36] S. M. Arabei, T. A. Pavich. *J. Appl. Spectrosc.* **2000**, 67, 236-244.

[37] Y. Hirao, A. Konishi, K. Matsumoto, H. Kurata, T. Kubo. *AIP Conf. Proc.* **2012**, 1504, 863-866.

[38] J. Li, K. Zhang, X. Zhang, K. W. Huang, C. Chi, J. Wu. *J. Org. Chem.* **2010**, 75, 856-863.

[39] A. Konishi, Y. Hirao, M. Nakano, A. Shimizu, E. Botek, B. Champagne, D. Shiomi, K. Sato, T. Takui, K. Matsumoto, H. Kurata, T. Kubo. *J. Am. Chem. Soc.* **2010**, 132, 11021-11023.

[40] A. Konishi, Y. Hirao, K. Matsumoto, H. Kurata, R. Kishi, Y. Shigeta, M. Nakano, K. Tokunaga, K. Kamada, T. Kubo. *J. Am. Chem. Soc.* **2013**, 135, 1430-1437.

[41] J. Kruszewski, T. M. Krygowski. *Tetrahedron Lett.* **1972**, 13, 3839-3842.

[42] T. M. Krygowski. *J. Chem. Inf. Comput. Sci.* **1993**, 33, 70-78.

[43] S. D. Motta, F. Negri, D. Fazzi, C. Castiglioni, E. V. Canesi. *J. Phys. Chem. Lett.* **2010**, 1, 3334-3339.

[44] P. P. Fu, H. M. Lee, R. G. Harvey. *J. Org. Chem.* **1980**, 45, 2797-2803.

[45] J. Hu, D. Zhang, F. W. Harris. *J. Org. Chem.* **2005**, 70, 707-708.

[46] R. Rieger, M. Kastler, V. Enkelmann, K. Müllen. *Chem. Eur. J.* **2008**, 14, 6322-6325.

[47] E. Clar, W. Schmidt. *Tetrahedron* **1979**, 35, 1027-1032.

[48] J. W. Patterson. *J. Am. Chem. Soc.* **1942**, 64, 1485-1486.

[49] E. J. Bowen, B. Brocklehurst. *J. Chem. Soc.* **1955**, 4320-4331.

[50] M. Mitsui, Y. Kobori, A. Kawai, K. Obi. *J. Phys. Chem. A* **2004**, 108, 524-531.

[51] B. T. Jones, N. J. Mullins, J. D. Winefordner. *Anal. Chem.* **1989**, 61, 1182-1185.

[52] E. Clar, *Nature* **1948**, 161, 238-239.

[53] E. Clar, *Chem. Ber.* **1949**, 82, 55.

[54] S. Saïdi-Besbes, É. Grelet, H. Bock. *Angew. Chem., Int. Ed.* **2006**, 45, 1783-1786.

[55] R. D. Bronene, F. Diederich. *Tetrahedron Lett.* **1991**, 32, 5227-5230

[56] E. Clar, J. M. Robertson, R. Schlogl, W. Schmidt. *J. Am Chem. Soc.* **1981**,103, 1320-1328.

[57] D. H. Reid. *Chem. Ind.* **1956**, 1504.

[58] D. H. Reid. *Tetrahedron* **1958**, 3, 339-352.

[59] P. B. Sogo, M. Nakazaki, M. Calvin. *J. Chem. Phys.* **1957**, 26, 1343-1345.

[60] D. H. Reid, M. Fraser, B. B. Molloy, H. A. S. Payne, R. G. Sutherland. *Tetrahedron Lett.* **1961**, 15, 530-535.

[61] K. Goto, T. Kubo, K. Yamamoto, K. Nakasuji, K. Sato, D. Shiomi, T. Takui, M. Kubota, T. Kobayashi, K. Yakusi, J. Y. Ouyang. *J. Am. Chem. Soc.* **1999**, 121, 1619-1620.

[62] V. Zaitsev, S. V. Rosokha, M. Head-Gordon, J. K. Kochi. *J. Org. Chem.* **2006**, 71, 520-526.

[63] K. Nakasuji, K. Yoshida, I. Murata. *J. Am. Chem. Soc.* **1983**, 105, 5136-5137.

[64] I. Murata, S. Sasaki, K. U. Klabunde, J. Toyoda, K. Nakasuji. *Angew. Chem. Int. Ed.* **1991**, 30, 172-173.

[65] K. Ohashi, T. Kubo, T. Masui, K. Yamamoto, K. Nakasuji, T. Takui, Y. Kai, I. Murata. *J. Am. Chem. Soc.* **1998**, 120, 2018-2027.

[66] T. Kubo, A. Shimizu, M. Sakamoto, M. Uruichi, K. Yakushi, M. Nakano, D. Shiomi, K. Sato, T. Takui, Y. Morita, K. Nakasuji. *Angew. Chem. Int. Ed.* **2005**, 44, 6564-6568.

[67] A. Shimizu, M. Uruichi, K. Yakushi, H. Matsuzaki, H. Okamoto, M. Nakano, Y. Hirao, K. Matsumoto, H. Kurata, T. Kubo. *Angew. Chem. Int. Ed.* **2009**, 48, 5482-5486.

[68] T. Kubo, A. Shimizu, M. Uruichi, K. Yakushi, M. Nakano, D. Shiomi, K. Sato, T. Takui, Y. Morita, K. Nakasuji. *Org. Lett.* **2007**, 9, 81-84.

[69] A. Shimizu, Y. Hirao, K. Matsumoto, H. Kurata, T. Kubo, M. Uruichi, K. Yakushi. *Chem. Commun.* **2012**, 48, 5629-5631.

[70] A. Shimizu, T. Kubo, M. Uruichi, K. Yakushi, M. Nakano, D. Shiomi, K. Sato, T. Takui, Y. Hirao, K.Matsumoto, H. Kurata, Y. Morita, K. Nakasuji. *J. Am. Chem. Soc.* **2010**, 132, 14421-14428.

[71] T. Kubo. *Chem. Rec.* **2015**, 15, 218-232.

[72] T. Kubo, K. Yamamoto, K. Nakasuji, T. Takui, I. Murata. *Angew. Chem. Int. Ed.* **1996**, 35, 439-441.

[73] T. Kubo, K. Yamamoto, K. Nakasuji, T. Takui, I. Murata. *Bull. Chem. Soc. Jpn.* **2001**, 74, 1999-2009.

[74] E. Clar, K. F. Lang, H. Schulz-Kiesow. *Chem. Ber.* **1955**, 88, 1520-1527.

[75] H. A. Staab, A. Nissen, J. Ipaktschi. *Angew. Chem. Int. Ed.* **1968**, 7, 226-226.

[76] R. H. Mitchell, F. Sondheimer. *Tetrahedron.* **1970**, 26, 2141-2150.

[77] H. A. Staab, J. Ipaktschi, A. Nissen. *Chem. Ber.* **1971**, 104, 1182-1186.

[78] R. Umeda, D. Hibi, K. Miki, Y. Tobe. *Org. Lett.* **2009**, 11, 4104-4106.

[79] R. Umeda, D. Hibi, K. Miki, Y. Tobe. *Pure Appl. Chem.* **2010**, 82, 871-878.

[80] T. C. Wu, C. H. Chen, D. Hibi, A. Shimizu, Y. Tobe, Y. T. Wu. *Angew. Chem. Int. Ed.* **2010**, 49, 7059-7062.

[81] L. Shan, Z. Liang, X. Xu, Q. Tang, Q. Miao. *Chem. Sci.* **2013**, 4, 3294-3297.

[82] Z. Sun, J. Wu. *J. Mater. Chem.* **2012**, 22, 4151-4160.

[83] Z. Sun, Q. Ye, C. Chi, J. Wu. *Chem. Soc. Rev.* **2012**, 41, 7857-7889.

[84] Z. Sun, Z. Zeng, J. Wu. *Chem. Asian J.* **2013**, 8, 2894-2904.

[85] Z. Sun, Z. Zeng, J. Wu. *Acc. Chem. Res.* **2014**, 47, 2582-2591.

[86] Y. Li, W. K. Heng, B. S. Lee, N. Aratani, J. L. Zafra, N. Bao, R. Lee, Y. M. Sung, Z. Sun, K. W. Huang, R. D. Webster, J. T. López Navarrete, D. H. Kim, A. Osuka, J. Casado, J. Ding, J. Wu. *J. Am. Chem. Soc.* **2012**, 134, 14913-14922.

[87] M. Nakano, R. Kishi, A. Takebe, M. Nate, H. Takahashi, T. Kubo, K. Kamada, K. Ohta, B. Champagne, E. Botek. *Comput. Lett.* **2007**, 3, 333-338.

[88] T. Weil, T. Vosch, J. Hofkens, K. Peneva, K. Müllen. *Angew. Chem. Int. Ed.* **2010**, 49, 9068-9093.

[89] J. Anthony. *Angew. Chem. Int. Ed.* **2008**, 47, 452-483.

[90] E. Clar. The Aromatic Sextet, Wiley: London, 1972.

[91] Z. Sun, S. Lee, K. Park, X. Zhu, W. Zhang, B. Zheng, P. Hu, Z. Zeng, S. Das, Y. Li, C. Chi, R. Li, K. Huang, J. Ding, D. Kim, J. Wu. *J. Am. Chem. Soc.* **2013**, 135, 18229-18236.

[92] S. D. Motta, F. Negri, D. Fazzi, C. Castiglioni, E. V. Canesi. *J. Phys. Chem. Lett.* **2010**, 1, 3334-3339.

[93] S. Gabriel. *Ber. Dt. Chem. Ges.* **1884**, 17, 1389-1396.

[94] G. Errera. *Gazz. Chim. Ital.* **1907**, 37, 624.

[95] G. Errera. *Gazz. Chim. Ital.* **1908**, 38, 588.

[96] G. Errera, G. Vaccarino. *Gazz. Chim. Ital.* **1909**, 39, 1.

[97] D. Marotta. *Gazz. Chim. Ital.* **1911**, 41, 59.

[98] D. Radulesc, V. Georgescu. *Bull. Soc. Chim. Fr.* **1925**, 37, 1187.

[99] F. Strauss, R. Kühnel, R. Hansel. *Ber. Dt. Chem. Ges.* **1933**, 66, 1847-1862.

[100] C. Weizmann, E. Bergmann, L. Haskelberg. *J. Chem. Soc.* **1939**, 391-397.

[101] D. Radulescu, M. Alexa. *Chem. Zentralbl.* **1943**, 622.

[102] W. Deuschel. *Helv. Chim. Acta.* **1951**, 34, 168-185.

[103] W. Deuschel. *Helv. Chim. Acta.* **1951**, 34, 2403-2416.

[104] L. Chardonnens, R. Ritter. *Helv. Chim. Acta.* **1955**, 38, 393-396.

[105] D. T. Chase, B. D. Rose, S. P. McClintock, L. N. Zakharov, M. M. Haley. *Angew. Chem. Int. Ed.* **2011**, 50, 1127-1130.

[106] D. T. Chase, A. G. Fix, B. D. Rose, C. D. Weber, S. Nobusue, C. E. Stockwell, L. N. Zakharov, M. C. Lonergan, M. M. Haley. *Angew. Chem. Int. Ed.* **2011**, 50, 11103-11106.

[107] D. T. Chase, A. G. Fix, S. J. Kang, B. D. Rose, C. D. Weber, Y. Zhong, L. N. Zakharov, M. C. Lonergan, C. Nuckolls, M. M. Haley. *J. Am. Chem. Soc.* **2012**, 134, 10349-10352.

[108] A. Shimizu, Y. Tobe. *Angew. Chem. Int. Ed.* **2011**, 50, 6906-6910.

[109] A. G. Fix, P. E. Deal, C. L. Vonnegut, C. L. Rose, L. N. Zakharov, M. M. Haley. *Org. Lett.* **2013**, 15, 1362-1365.

[110] B. D. Rose, C. L. Vonnegut, L. N. Zakharov, M. M. Haley. *Org. Lett.* **2012**, 14, 2426-2429.

[111] A. Shimizu, R. Kishi, M. Nakano, D. Shiomi, K. Sato, T. Takui, I. Hisaki, M. Miyata, Y. Tobe. *Angew. Chem. Int. Ed.* **2013**, 125, 6192-6195.

Chapter 2. Synthesis of Cove-Type Polycyclic Aromatic Hydrocarbons and Corresponding Cove-Edged Graphene Nanoribbons

In this chapter, we synthesis of a series of novel cove-edged polycyclic aromatic hydrocarbons (PAHs) and approaches towards cove-edged graphene nanoribbons (GNRs) will be presented. As model subunits of the infinite cove-edged GNRs, fused chrysene-based PAHs, namely a dimer (two units of fused chrysene) and a tetramer (four units of fused chrysene), will be investigated to obtain an insight into the corresponding cove-edged GNRs. These oligomers (or PAHs) are characterized by single crystal X-ray analysis, UV-vis absorption spectroscopy, and NMR spectroscopy, which are assisted by density functional theory (DFT) calculation. Furthermore, surface-assisted synthesis on an Au (111) substrate yields corresponding cove-edged GNRs with lengths up to 20 nm.

2.1 Introduction

Graphene nanoribbons (GNRs) have attracted a great interest in recent years.[1-5] In contrast to graphene, which is semimetallic with zero-band gap, GNRs are semiconductors with tunable band gaps and thus attractive materials for nanoscale electronic devices.[6-9] The width and edge structure of GNRs essentially determine their electronic features such as the band gap and spintronic properties.[10-15] One can envisage two different classes of GNRs depending on their edge structures, i.e., zigzag-GNRs (ZGNRs) and armchair-GNRs (AGNRs), and these have been extensively investigated both theoretically and experimentally. Two main strategies have been recently established to prepare GNRs, namely "top-down" and "bottom-up" approaches. The "top-down" approach, such as the cutting of graphene, sonochemical extraction from expanded graphite, and unzipping of carbon nanotubes, has produced GNRs with sub-10 nm widths,[16-22] revealing their semiconducting nature and excellent charge transport properties. However, "top-down" methods generally suffer from low yields and non-uniform widths, as well as ill-defined edge structures. Moreover, to achieve sufficient band gap control, GNRs should be narrowed to

sub-5 nm, at which width scale current lithography methods meet limitations. Thereby, it is highly desirable to produce GNRs with a precise periphery structure and controllable width.

In contrast, "bottom-up" chemical synthesis provides structurally well-defined GNRs with uniform structures.[5, 23-34] The synthesis is based on solution-mediated or surface-assisted cyclodehydrogenation, namely "planarization" of three-dimensional polyphenylene precursors. The polyphenylene precursors are designed and synthesized from small organic molecules, providing an access to GNRs with different widths and edge structures. Up to now, "bottom-up" synthesis has been mainly focused on AGNRs, whereas GNRs with zigzag or cove edges have remained elusive. [35-39]

Dimer 2-**1**: n=0, R=*t*-butyl
Tetramer 2-**2**: n=2, R=*t*-butyl
Hexamer 2-**3**: n=4, R=*t*-butyl
Octamer 2-**4**: n=6, R=*t*-butyl

2-5a:R=H
2-5b:R=*t*-butyl
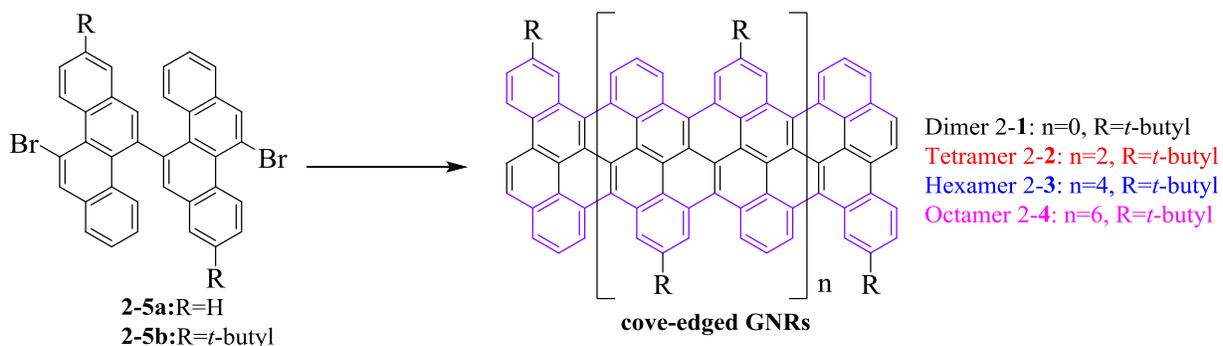
cove-edged GNRs

Scheme **2-1**. The design principle towards the cove-type PAH oligomers and the target **cove-edged GNRs** based on the building block **2-5**.

In this chapter, we demonstrate a novel type of GNR featuring a unique cove-edge periphery, based on 11,11'-dibromo-5,5'-bischrysene (**2-5**) as the key monomer (Scheme **2-1**). As model subunits of the infinite **cove-edged GNRs**, fused chrysene-based oligomers or polycyclic aromatic hydrocarbons (PAHs), namely dimer **2-1** (two units of fused chrysene) and tetramer **2-2** (four units of fused chrysene), are synthesized via the Ullmann coupling reaction of 11,11'-dibromo-5,5'-bischrysene (**2-5b**) followed by intramolecular oxidative cyclodehydrogenation in solution. The structure of dimer **2-1** and tetramer **2-2** are unambiguously proven by X-ray single crystal analysis. These PAHs are characterized by UV-vis absorption spectroscopy, matrix-assisted laser desorption/ionization time-of-flight (MALDI-TOF) mass spectrometry (MS), and cyclic voltammetry (CV). In contrast to planar PAHs with armchair or zigzag edges, the cove-edged analogues manifest characteristic non-planar structures with alternate "up-down"

conformations. We further demonstrate the surface-assisted synthesis of **cove-edged GNRs** based on monomer **2-5a**, thereby achieving the formation of GNRs with lengths up to 20 nm and a width of 0.9 nm. From spectroscopic data and DFT calculations, **cove-edged GNRs** are shown to possess a smaller band-gap than those of AGNRs with similar width[29] and excellent charge transport properties.

## 2.2 Synthesis and structure verification of the building block 2-5
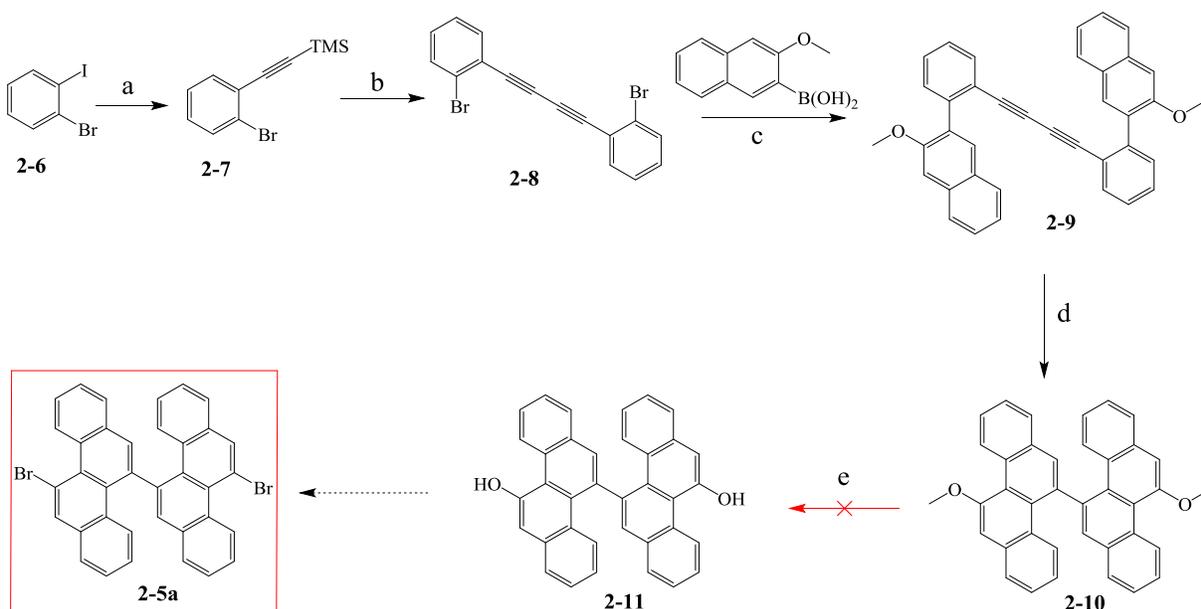
Scheme **2-2**. Unsuccessful synthetic route towards the building block **2-5a**. a) TMS-acetylene, $PdCl_2(PPh_3)_2$, CuI, Et_3N, THF, r.t, 24 h, 90%. b) CuCl, DMF, Air, 80 °C, 6 h, 81%. c) $Pd(PPh_3)_4/Na_2CO_3$, THF/H_2O/EtOH, 60 °C, 24 h, 70%. d) $PtCl_2$, Toluene, 85 °C, 24 h, 42%.

At the beginning, a synthetic route towards the building block **2-5a** was designed as depicted in Scheme **2-2**. By Sonogashira coupling of 1-bromo-2-iodobenzene (**2-6**) with trimethylsilyl-acetylene, 1-bromo-2-(trimethylsilylethynyl)benzene (**2-7**) was obtained in 95% yield. Next, 1,4-bis(*o*-bromophenyl)-diacetylene (**2-8**) was prepared through self-coupling of compound **2-7** with CuCl as a catalyst under air atmosphere in 80% yield. Compound **2-9** was obtained through Suzuki coupling of compound **2-8** and 2-methoxy-3-naphthaleneboronic acid in 56% yield, and compound **2-10** was produced by cyclization of compound **2-9** with $PtCl_2$ as a catalyst under

argon atmosphere (yield 42%). Unfortunately, the conversion of the methoxy group (**2-10**) to a hydroxy group (**2-11**) failed due to the steric hindrance at the bay position.

Therefore, the synthetic route toward compound **2-5a** was optimized as depicted in Scheme **2-3**. The bromo group in compound **2-8** was transformed to an iodo moiety by treatment with 1,2-diiodoethane, affording 1,4-bis(2-iodophenyl)buta-1,3-diyne (**2-12**) in 88% yield. Subsequently, the key precursor 1,4-bis(2-(3-bromonaphthalen-2-yl)phenyl)buta-1,3-diyne (**2-14**) was furnished through the Suzuki coupling of **2-12** and 2-bromo-3-naphthaleneboronic acid (**2-13**) in 52% yield. A final cyclization of compound **2-14** with PtCl$_2$ as a catalyst under argon atmosphere at 85 °C for 24 hours afforded the desired compound **2-5a** in 70% yield. The structure of **2-5a** was confirmed by mass spectrometry, NMR (Figures **2-1** and **2-2**), and single crystal analysis (Figure **2-3**).
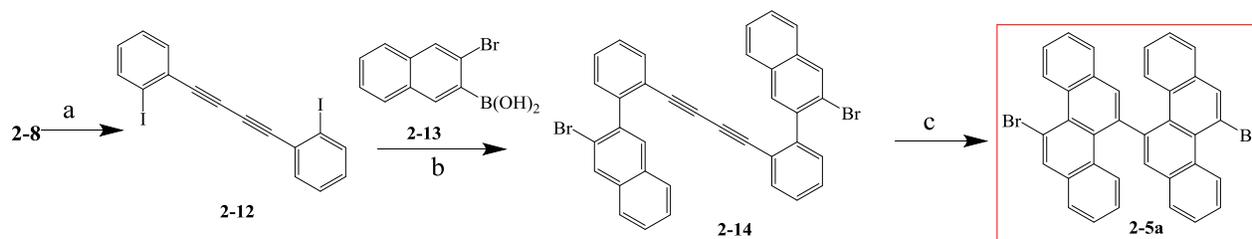
Scheme **2-3**. Modified synthetic route towards the building block 2-5a. a) *n*-BuLi, THF, ICH$_2$CH$_2$I, -78 °C to r.m, 88%. b) Pd(PPh$_3$)$_4$/Na$_2$CO$_3$, THF/H$_2$O/EtOH, 60 °C, 24 h, 52%. c) PtCl$_2$, Toluene, 85 °C, 24 h, 70%.
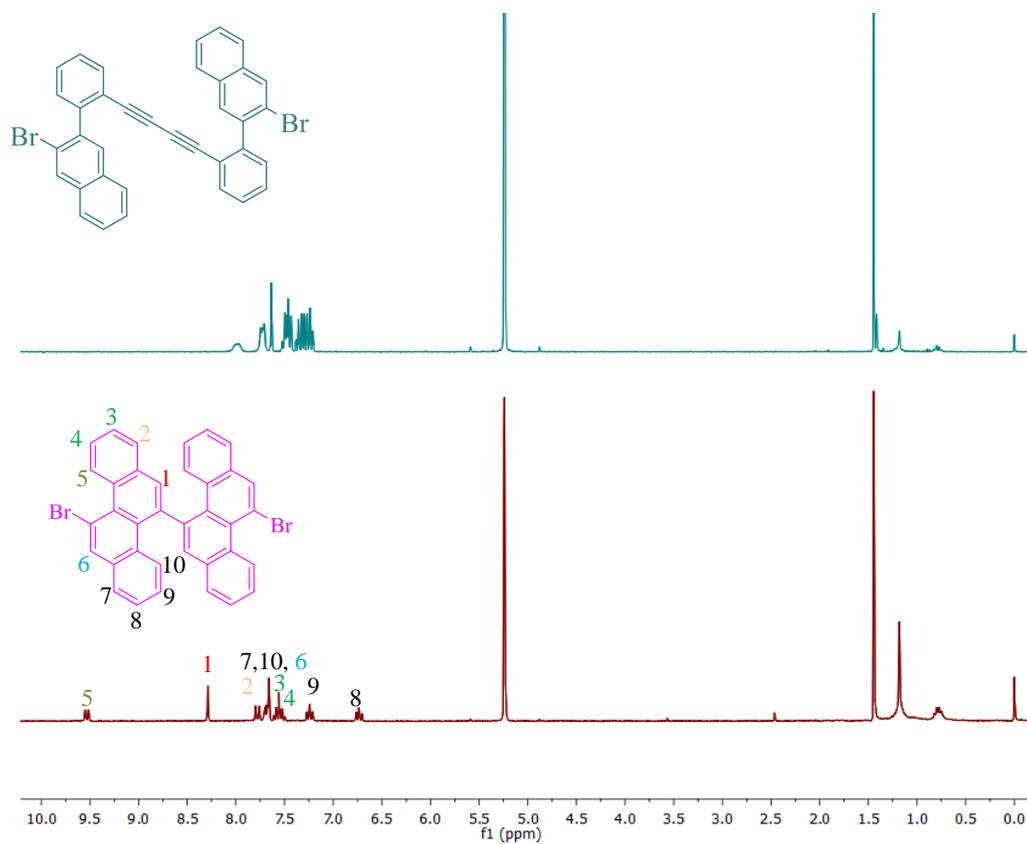
Figure **2-1**. ^{1}H-NMR spectra of compounds **2-14** and **2-5a** in CD$_2$Cl$_2$.
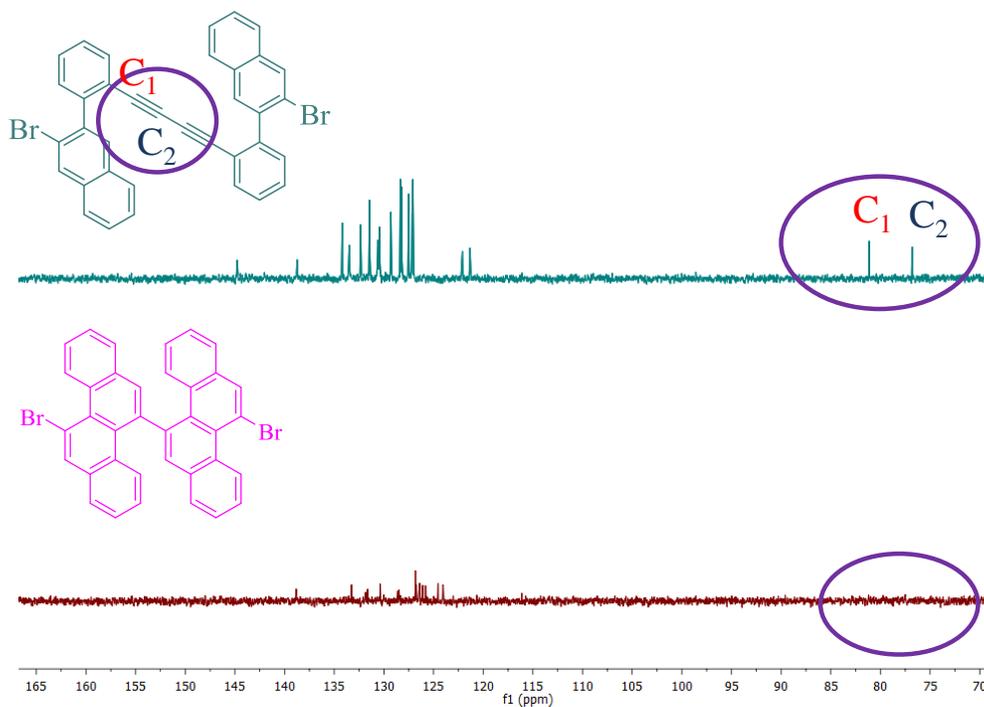
Figure **2-2**. ^{13}C-NMR spectra of compounds **2-14** and **2-5a** in CD$_2$Cl$_2$.
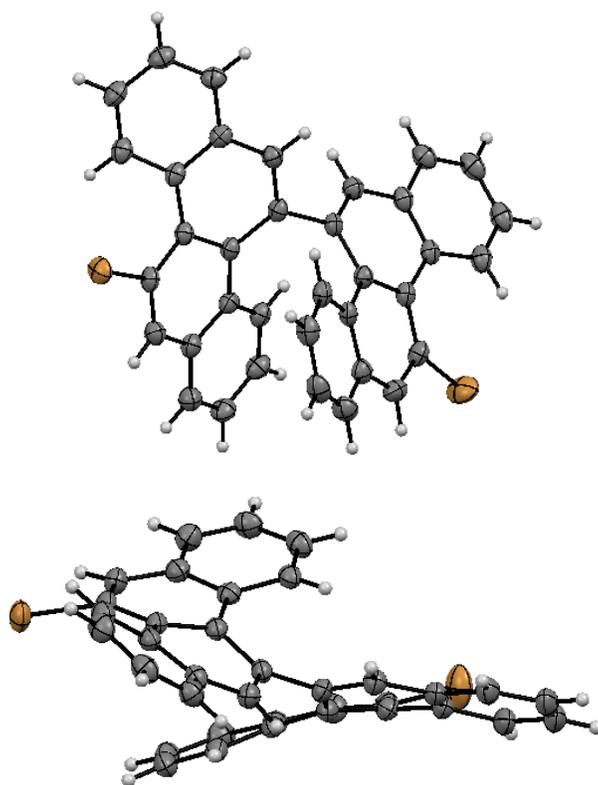
Figure **2-3**. Crystal structure of **2-5a**.

Following our previous work, *t*-butyl group was introduced into this system to improve the solubility of the monomer and the resulting GNRs. Thereby, the key molecule 1-bromo-4-(*tert*-butyl)-2-iodobenzene (**2-18)** was synthesized through three steps. 1-Bromo-4-(*tert*-butyl)-2-nitrobenzene (**2-16**) was obtained by nitration of 1-bromo-4-(*tert*-butyl)benzene with HNO_3 in H_2SO_4. Then, 2-bromo-5-(*tert*-butyl)aniline (**2-17**) was afforded by reduction of the nitro group. Finally, **2-18** was furnished through the Sandmeyer reaction. A final product 11,11'-dibromo-8,8'-di-*tert*-butyl-5,5'-bichrysene (**2-5b**) was synthesized with the same method as **2-5a** following the sequence of Sonogashira coupling, Glaser Coupling, iodization**,** Suzuki coupling, and Pt-catalyzed cyclization (Scheme **2-4**). The structure of **2-5b** was characterized by MALDI-TOF mass and NMR analysis, as depicted in Figures **2-4** and **2-5**.
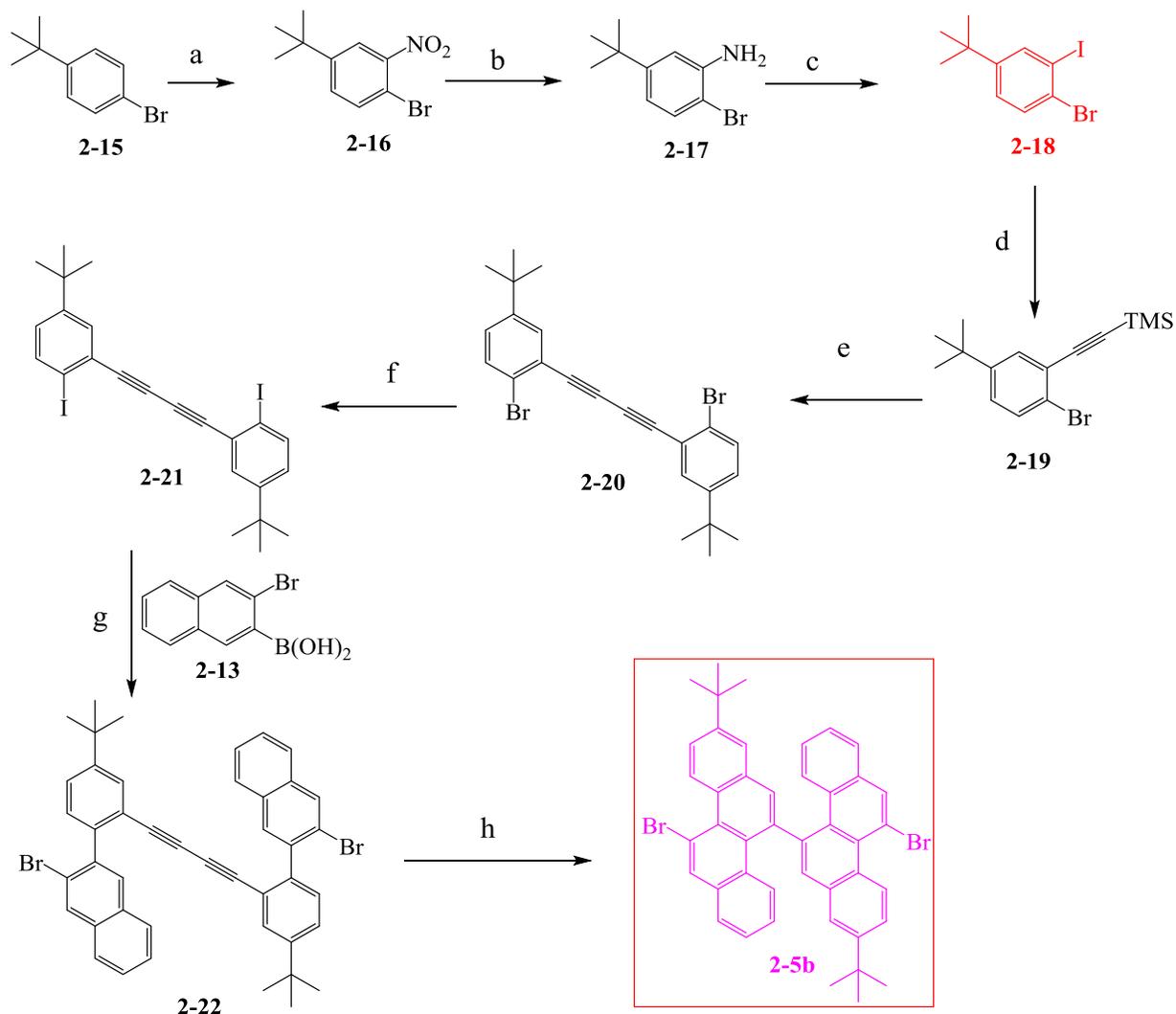
Scheme **2-4**. The synthetic route toward the key building block 11,11'-dibromo-5,5'-bischrysene (**2-5b**). Reagents and conditions: a) H_2SO_4, HNO_3, 6h, 92%. b) $Na_2S_2O_4$, HCl, 18h, 81%. c) HCl, $NaNO_2$, KI, 6h, 80%. d) TMS-acetylene, $PdCl_2(PPh_3)_2$, CuI, Et_3N, THF, r.t, 24 h, 85%. e) CuCl, DMF, Air, 80 ^{0}C, 6 h, 83%. f) *n*-BuLi, THF, ICH_2CH_2I, -78 ^{0}C to r.t, 90%. g) $Pd(PPh_3)_4$/Na_2CO_3, THF/H_2O/EtOH, 60 ^{0}C, 24 h, 56%. h) $PtCl_2$, Toluene, 85 ^{0}C, 24 h, 78%.
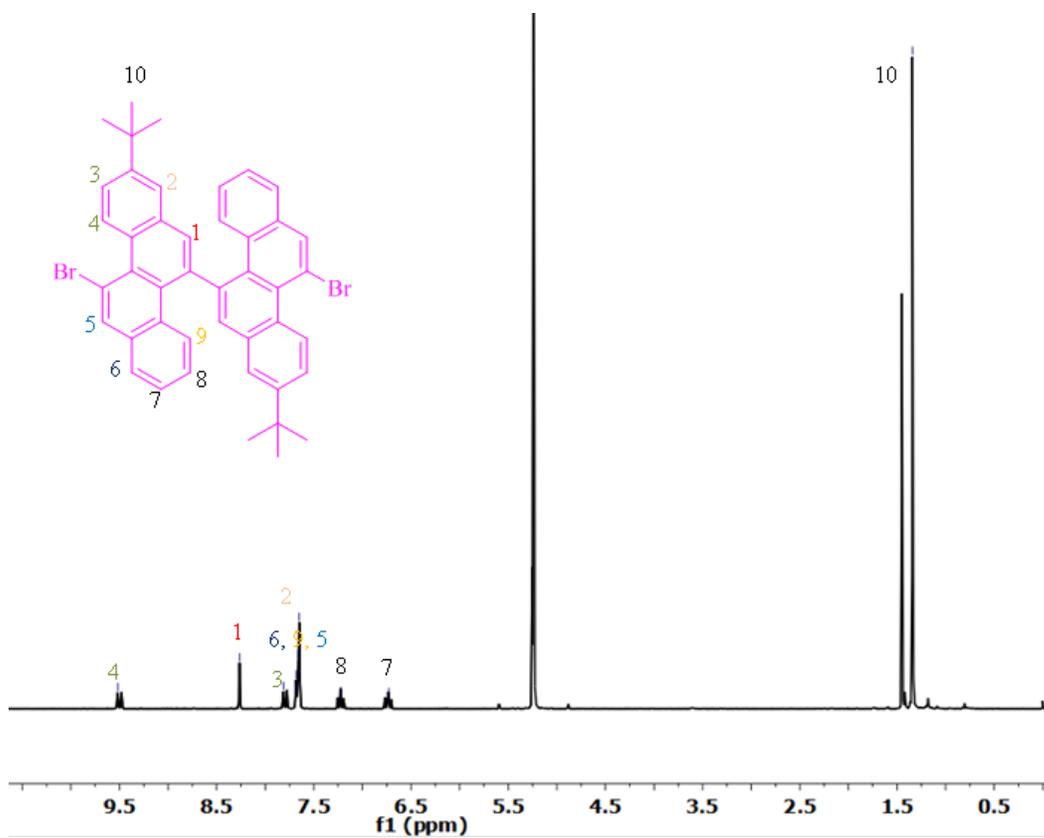
Figure **2-4**. The ^{1}H-NMR spectrum of compound **2-5b** in CD$_2$Cl$_2$.
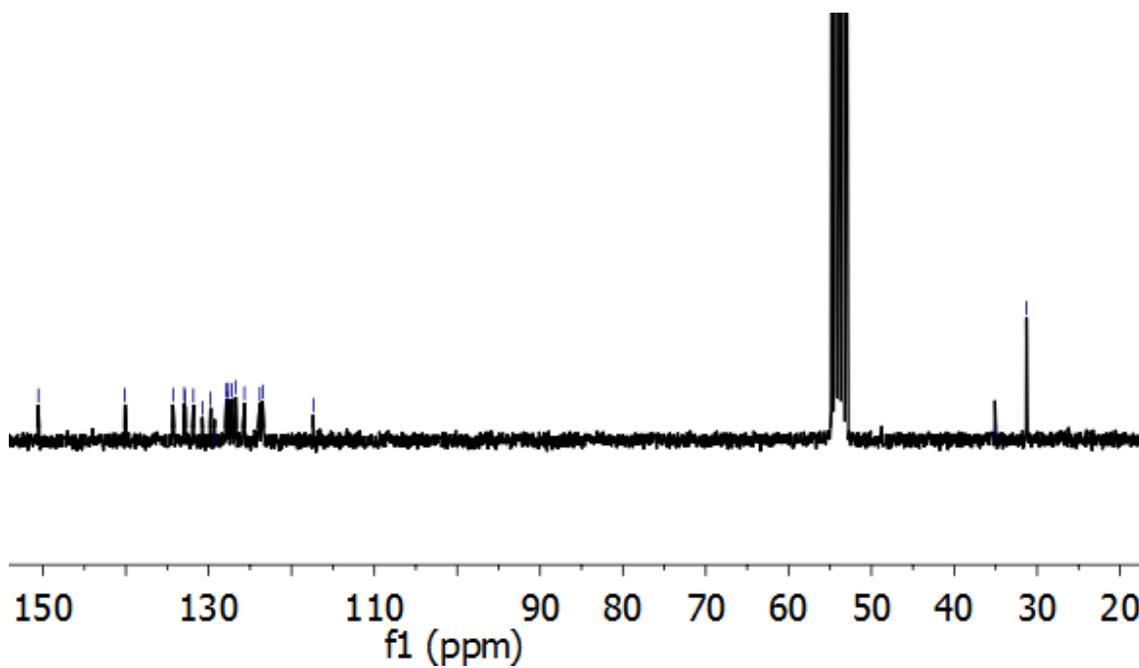
Figure **2-5**. The ^{13}C-NMR spectrum of compound **2-5b** in CD$_2$Cl$_2$.

2.3 Synthesis and structure verification of oligomers (cove-type PAHs) in solution
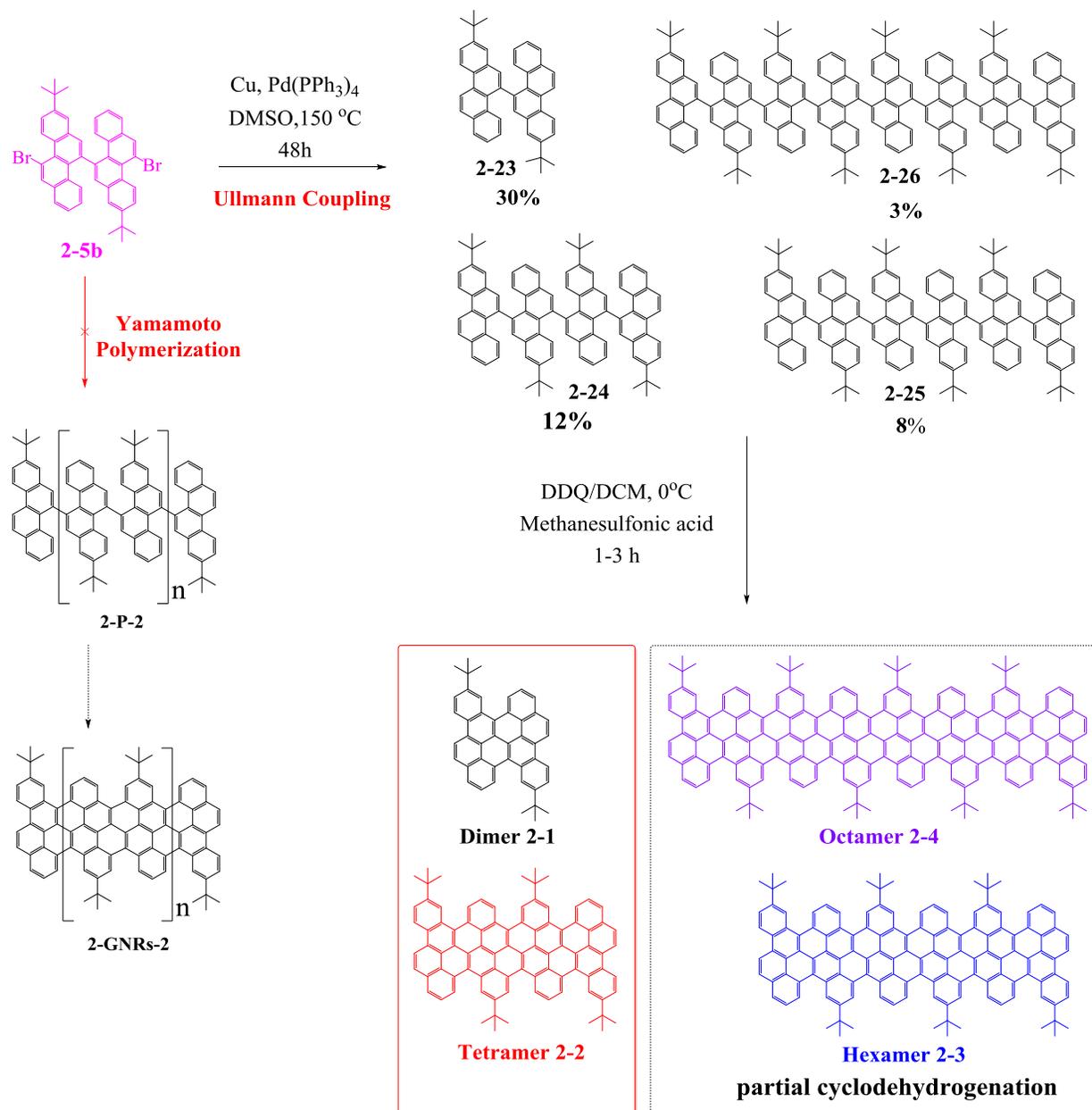
Scheme **2-5**. Synthetic route toward the oligomers and fused dimer **2-1** and tetramer **2-2**.

Next, the corresponding chrysene oligomers were synthesized by Ullmann coupling at 150 °C in dimethyl sulfoxide (DMSO) based on the core building block **2-5b**, as depicted in Scheme **2-5**. Initially, a Yamamoto coupling of compound **2-5b** was attempted at 80 °C and 100 °C in toluene

and dimethylformamide (DMF) solutions, respectively. The reaction failed even under microwave-assistance, most likely due to the high steric repulsion between the two C-H bonds at the bay-positions of chrysene. Therefore, we turned our attention to the Ullmann coupling at high temperature. Ullmann coupling, when tried at higher temperatures, did not yield the corresponding polymers, but produced some oligomers, which can be seen in the MALDI-TOF MS spectrum of the crude products after the Ullmann coupling as depicted in Figure **2-6**. Nevertheless, the crude oligomeric mixtures were first separated by silica gel column chromatography, and the pure homologues **2-23**, **2-24**, **2-25**, and **2-26** were obtained by recycling GPC. Afterwards, their cyclodehydrogenation was carried out by using iron (III) chloride (FeCl$_3$) or 2,3-dichloro-5,6-dicyano-1,4-benzoquinone (DDQ)/ trifluoromethanesulfonic acid (CF$_3$SO$_3$H) as the Lewis acid/oxidant. The former conditions produced some chlorinated products and partial cyclodehydrogenation, as confirmed by MALDI-TOF MS (Figure **2-7**). In contrast, cyclodehydrogenation with DDQ and CF$_3$SO$_3$H successfully afforded the desired fused dimer **2-1** and tetramer **2-2** without any chlorination. PAHs **2-1** and **2-2** were unambiguously characterized by MALDI-TOF MS, as depicted in Figure **2-8**. There is only one dominant peak in the respective mass spectra of **2-1** and **2-2**, revealing its defined molecular composition; the isotopic distribution patterns of the mass peaks are in good agreement with the calculated patterns.
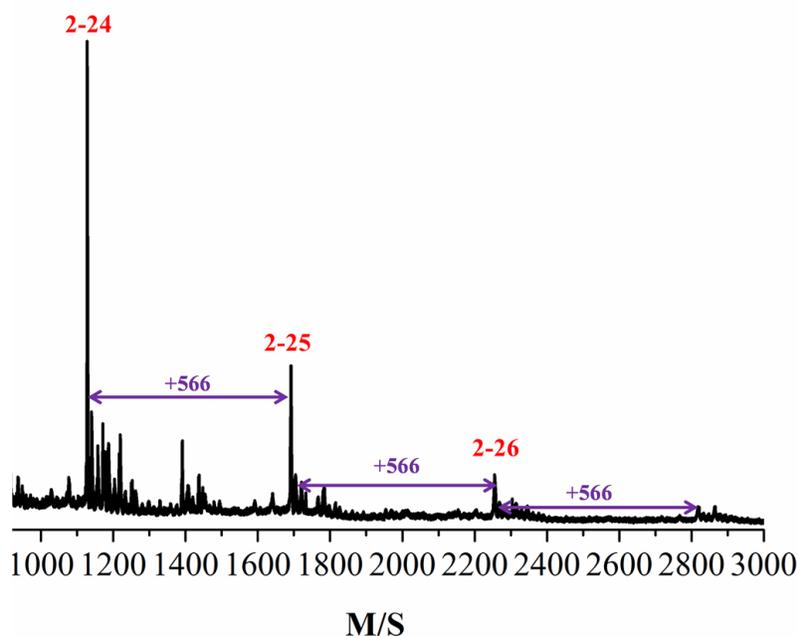

Figure **2-6**. MALDI-TOF MS spectrum of the crude products after the Ullmann coupling.
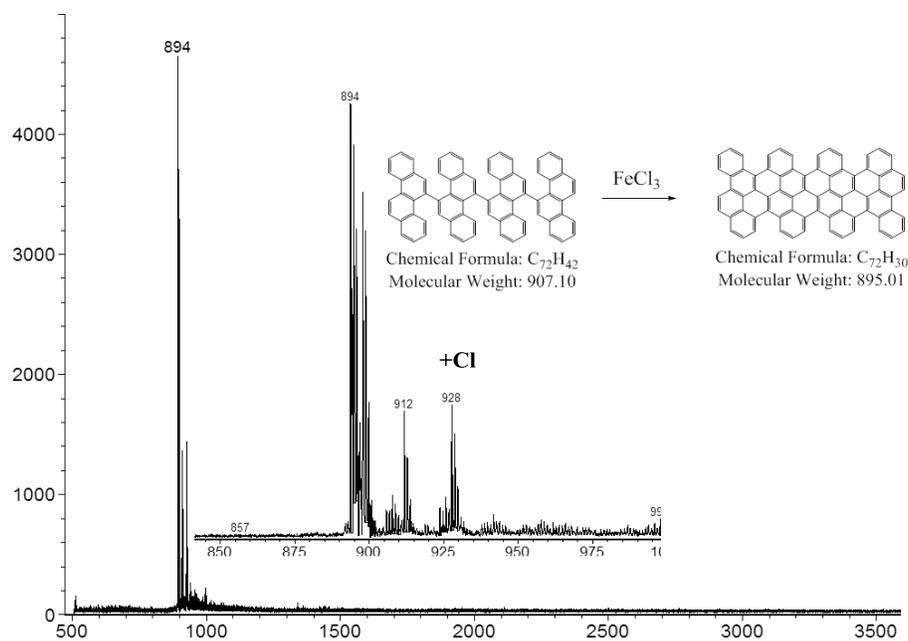
Figure **2-7**. Cyclodehydrogenation of the tetramer **2-2** by using the FeCl₃ methods.
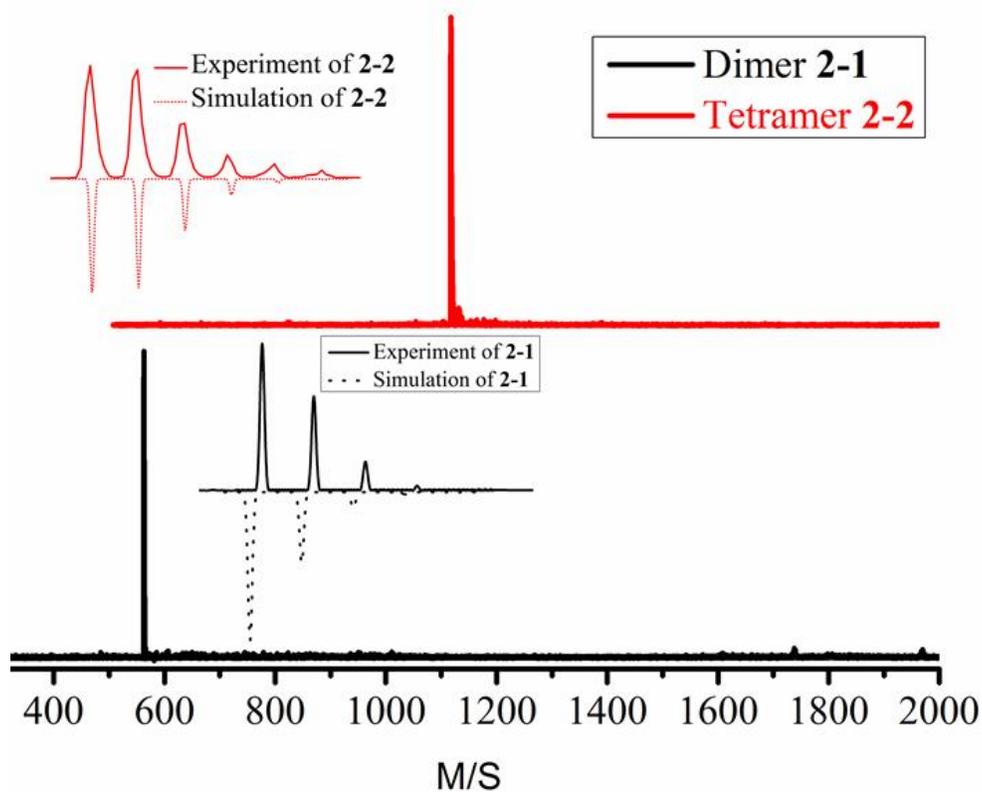

Figure **2-8**. MALDI-TOF MS results of dimer **2-1** and tetramer **2-2**.

To unambiguously characterize the structures of obtained dimer and tetramer, we succeeded in growing the single crystals of dimer **2-1** by slow solvent evaporation from dichloromethane. The crystal structure of dimer **2-1** is depicted in Figure **2-10** and detailed bond parameters of **2-1** are given in Figure **2-9**. Remarkably, we could also get the single crystals of tetramer **2-2** by slow solvent evaporation from carbon disulfide solution. As shown in Figure **2-11**, the detailed molecular structure of **2-2** was revealed. Compound **2-2** is a ribbon-shaped molecule, with the length and width of 1.8 nm and 0.9 nm, respectively, which could serve as a molecular model to understand the structure of the corresponding **cove-edged GNRs**. In contrast to the reported graphene molecules with zigzag or armchair periphery, which mostly have planar structure, the outstanding feature of **2-2** is the non-planar π-conjugated carbon skeleton, which results from the steric repulsion at the cove periphery. Notably, the benzenoid rings at cove region in **2-2** adopt an alternating "up-down" conformation with a mean torsion angle of 38.2 °, which suggests that the cove-edged GNRs could also adopt the similar alternating "up-down' conformation at the periphery.

The distorted carbon framework makes **2-2** chiral, as shown in Figure **2-11a**. Remarkably, one enantiomer forms a dimer by intermolecular π-π interactions with an interlayer distance as short as 3.22 Å (Figure **2-11b**), whereas such a dimer assembles with its corresponding enantiomeric isomer by face-to-edge CH-π interactions (Figure **2-11c**). Further attempts to separate the enantiomer pair of **2-2** in solution by chiral HPLC were unfortunately not successful. This is most likely due to the low activation barrier of racemization, as suggested by DFT calculations (vide infra).
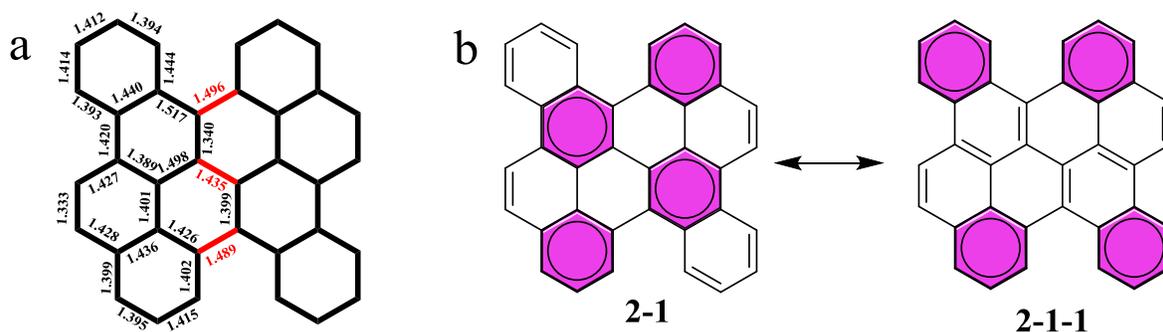

Figure **2-9.** Detailed bond parameters of **2-1**. (**a**) Bond lengths of **2-1**. (**b**) Proposed resonance structures of **2-1**.
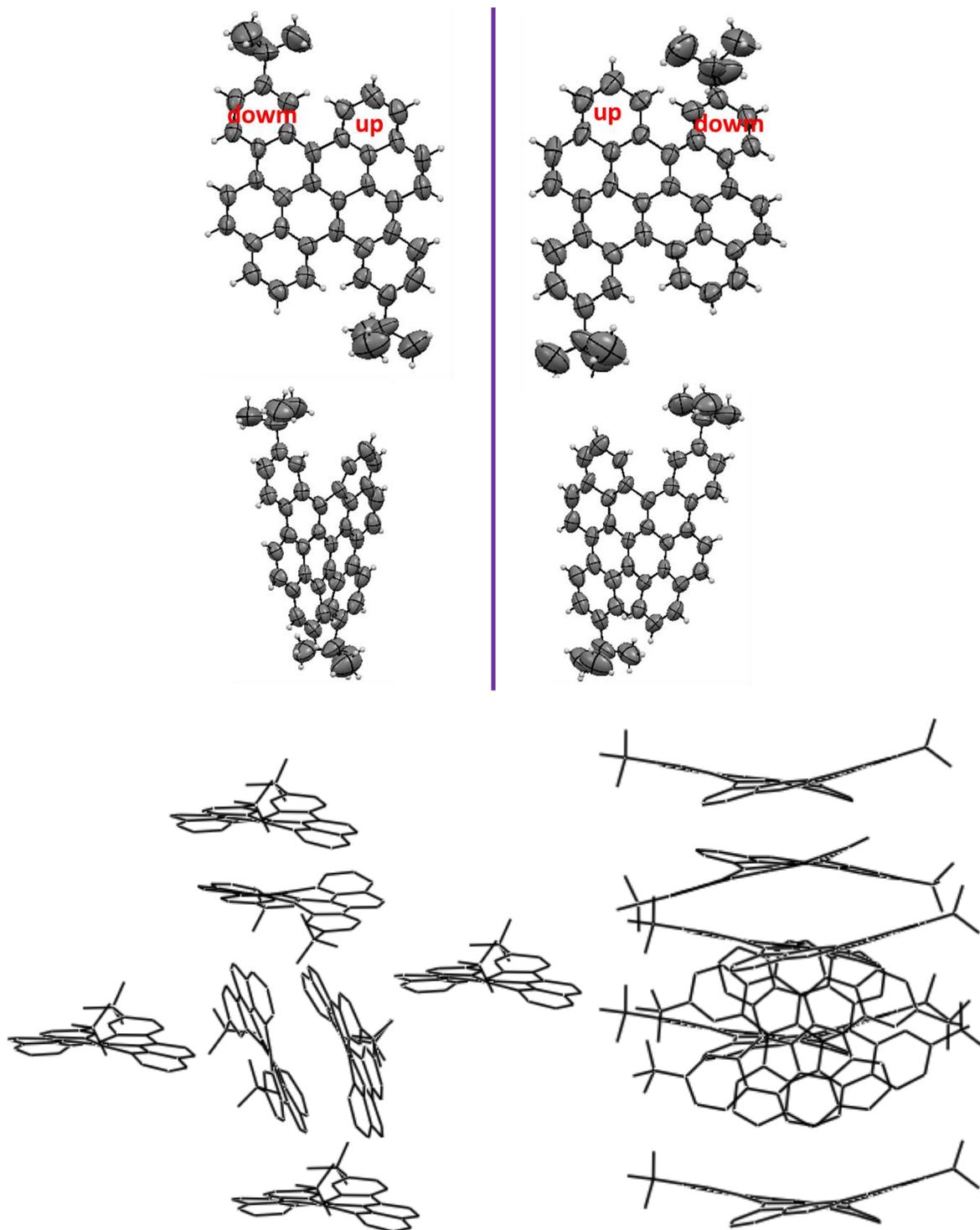
Figure **2-10.** Crystal structure (ORTEP drawing) and crystal packing of dimer **2-1**.
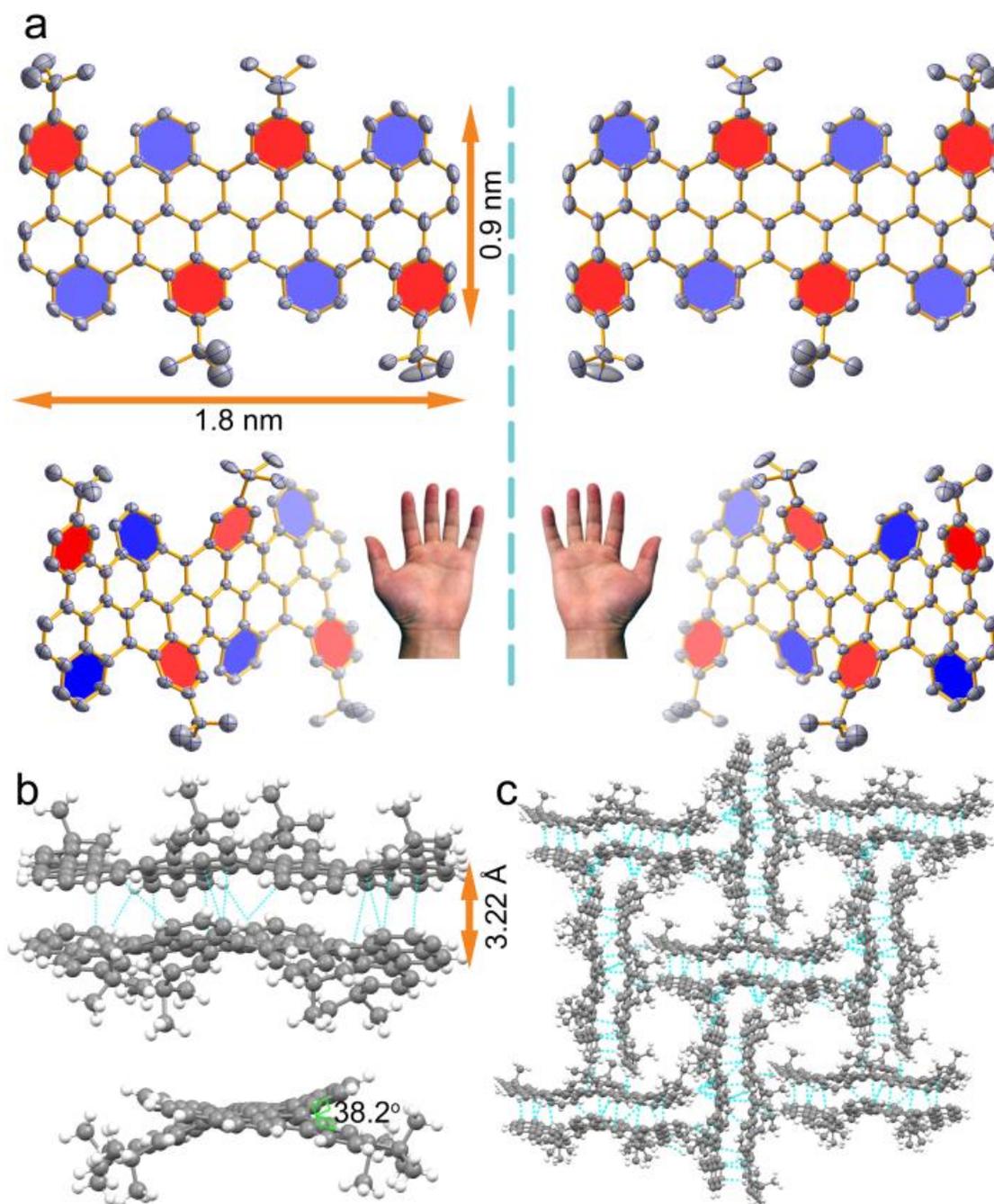
Figure **2-11**. Crystal structure of tetramer **2-2**. (a) Top view of enantiomer pair of **2-2**. (b) Crystal packing of dimer from side view. (c) Crystal packing of face-to-face (ð-ð) and face-to-edge (CH-ð).
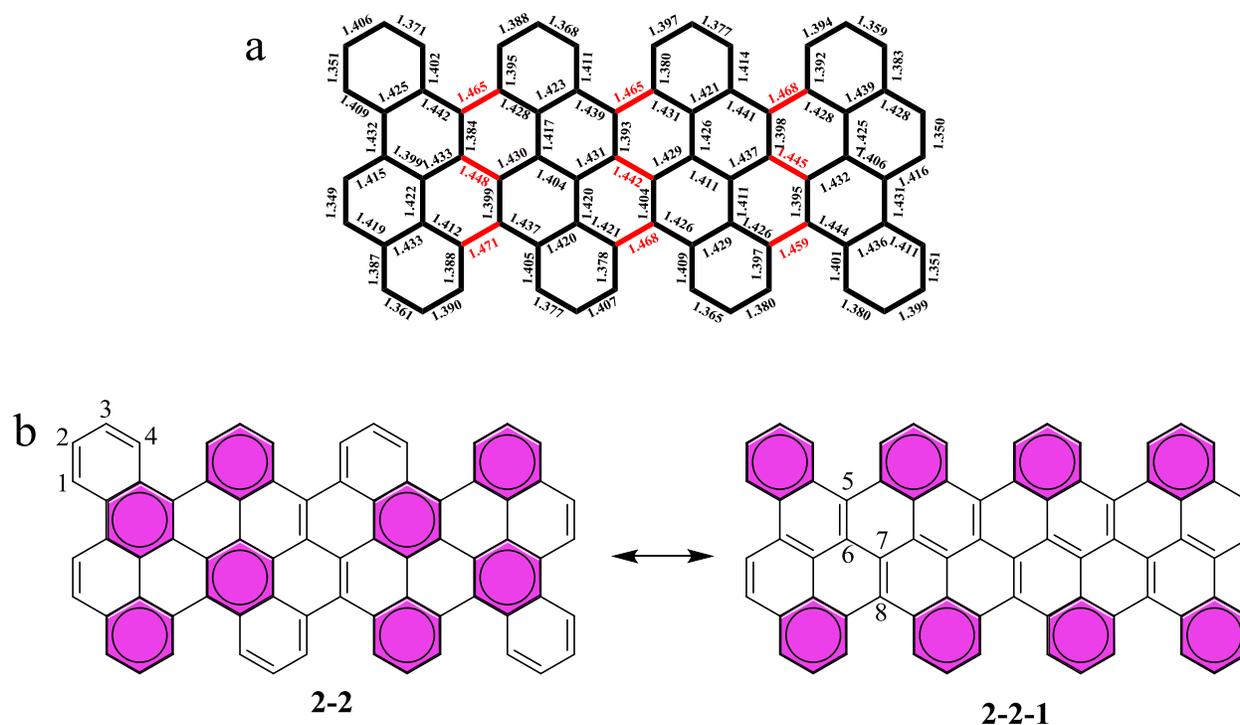
Figure **2-12.** Detailed bond parameters of **2-2**. (**a**) Bond lengths of **2-2**. (**b**) Proposed resonance structures of **2-2**: Clar formula is represented by two resonance structures comprising eight aromatic sextets.

The X-ray diffraction data also disclose the detailed bond parameters of **2-2** (Figure **2-12a**). The C-C bonds at the cove region are obviously longer (1.46 Å), most likely due to the repulsive forces of congested hydrogen atoms. In **2-2**, the chrysene units connect to each other by a single C-C bond, and the distribution of the bond lengths in the chrysene unit is consistent with the resonance structures shown in Figure **2-12b**. The short bond lengths of C(1)-C(2) and C(3)-C(4) support resonance structure **2-2**, whereas the short bond lengths of C(5)-C(6) and C(7)-C(8) imply structure **2-2-1**. Compound **2-2** thus adopts a π-bond localized resonance structure in the solid state, which is different from that prevailing in fully benzenoid PAHs. Moreover, the bonding-antibonding pattern calculated at the DFT level for the HOMO (HOCO) of the oligomers (ribbons) strongly supports **2-2-1** as the dominant Clar formula (Figure **2-13**).
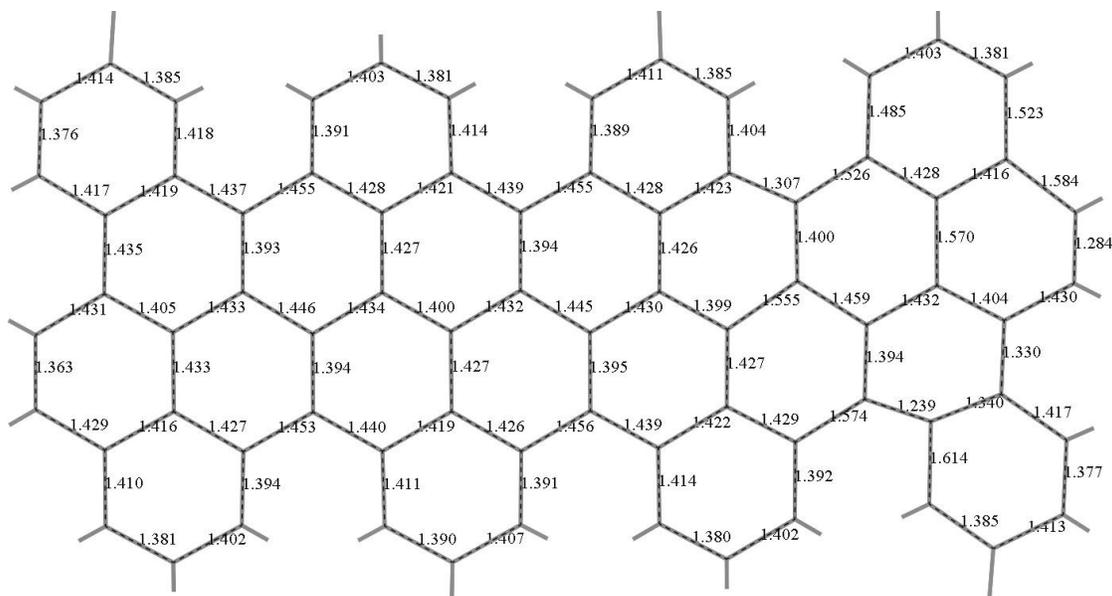
Figure **2-13**. Bond lengths of **2-2** predicted by DFT calculations.

We could also isolate precursors **2-25** and **2-26** for hexamer **2-3** and octamer **2-4**, respectively, from the Ullmann-reaction mixtures. Nevertheless, unfortunately, only partially fused compounds of hexamer **2-3** and octamer **2-4** could be obtained after cyclodehydrogenation, and further separation was impossible. It is difficult to judge the exact structure and purity from the MALDI-TOF MS spectra. It seems that hexamer **2-3** was fully fused after the cyclodehydrogenation based on the MS result (Figure **2-14**), but the UV-vis absorption spectrum after cyclodehydrogenation showed a broadening of the bands without pronounced bathochromic shift of corresponding bands compared with the spectrum of pure tetramer **2-2** (Figure **2-15**). This suggested that hexamer **2-3** observed in the MS spectrum was a minor product, and the major, partially fused products were underestimated by the MALDI-TOF MS. Therefore, we assume that hexamer precursor **2-25** was incompletely cyclized and formed products with the tetramer core, and that the further cyclodehydrogenation was prohibited by the steric hindrance of the twisted structure as indicated by DFT modeling. The possible structure and DFT calculation details are depicted in Figure **2-16**. We met the same problem when trying the cyclodehydrogenation of the octamer precursor **2-26**, as depicted in Figure **2-17** and **2-18**. Accordingly, for the further discussion, we only focus on the completely fused dimer **2-1** and tetramer **2-2**.
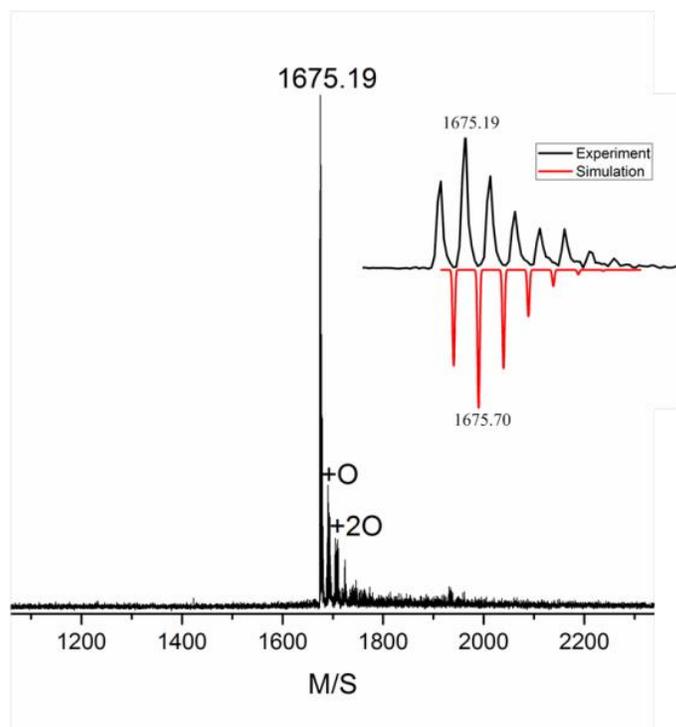
Figure **2-14**. MALDI-TOF MS spectrum of hexamer **2-3**.
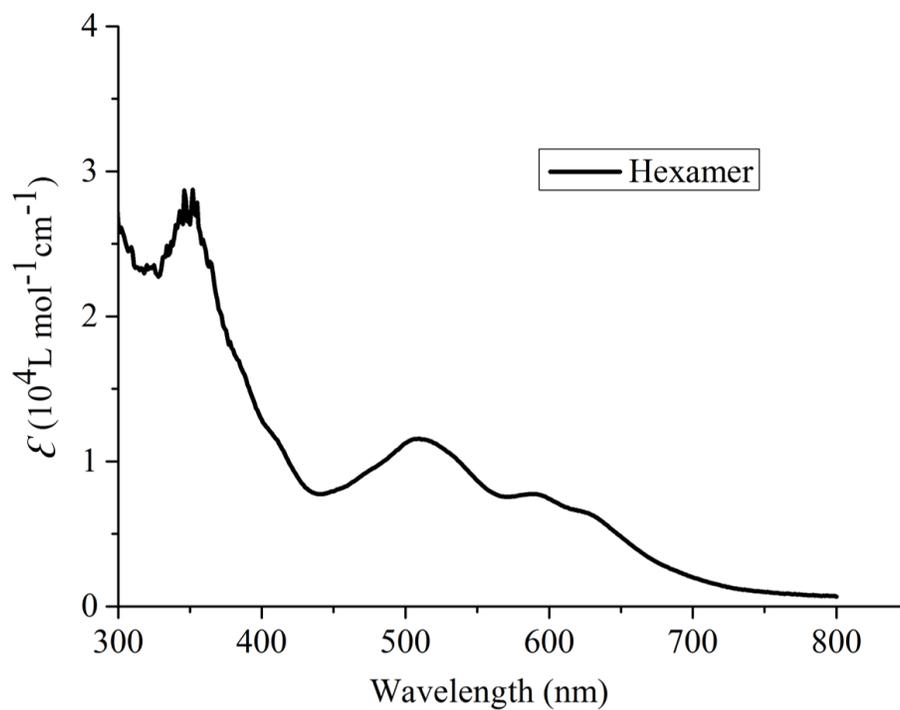
Figure **2-15**. UV-vis absorption spectrum of hexamer **2-3**.
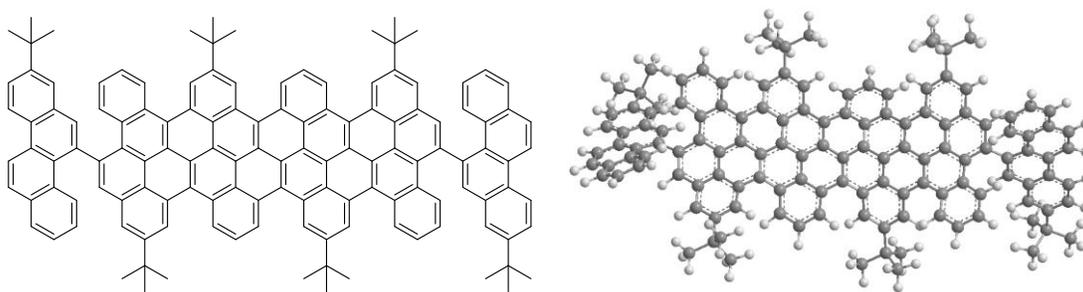
Figure **2-16**. Possible structure of hexamer **2-3** from the DFT simulation at the B3LYP/6-31G(d,p) level.
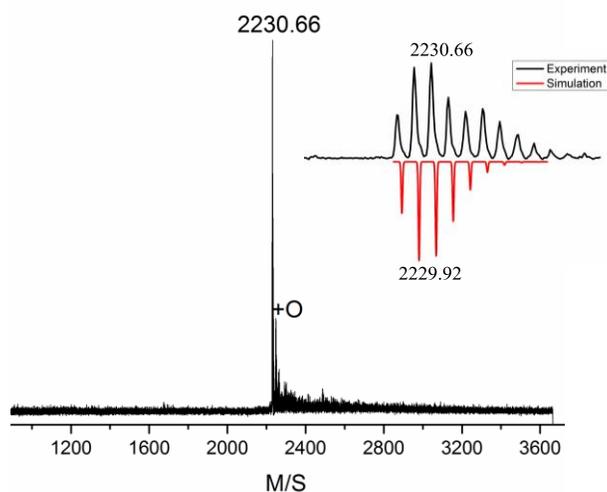

Figure **2-17**. MALDI-TOF MS spectrum of octamer mixture **2-4**.
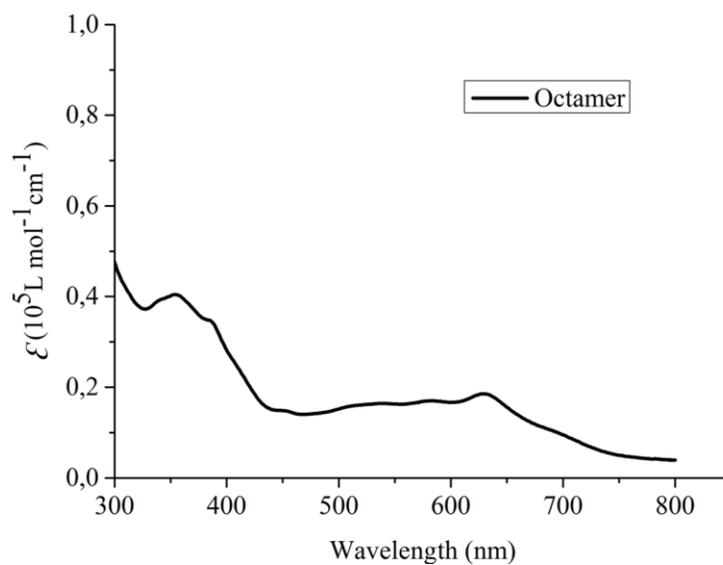
Figure **2-18**. UV-vis absorption spectrum of octamer mixture **2-4**.

2.4 Optical and Electrochemical Properties of 2-1 and 2-2

Optical Properties. The colors of the fused dimer **2-1** and tetramer **2-2** were light brown and violet in THF solutions, and changed to green and red, respectively, under UV lamps at 365 nm (Figure **2-19**). The UV-vis absorption spectra of precursors **2-23** and **2-24**, as well as the cyclodehydrogenation products **2-1** and **2-2** in THF solutions are compared in Figure **2-20a**. This becomes possible for the fused dimer **2-1** and tetramer **2-2**, since they have sufficient solubility in common organic solvents such as THF, toluene and trichlorobenzene, as a result of the non-planar cove structure at the periphery and the presence of *t*-butyl substituents. From the UV-vis spectra, we can see that PAHs **2-1** and **2-2** were significantly red shifted compared with their precursors **2-23** and **2-24**, respectively. Notably, compounds **2-1** and **2-2** exhibit similar shapes of UV-vis absorption patterns: **2-1** displays one major maximum between 300-400 nm, one major maximum at the 502 nm and two shoulder peaks at 469, 439 nm. Compound **2-2** shows a major absorption maximum at 623 nm with significant bathochromic shift of 121 nm relative to that of **2-1**, and two shoulder peaks at 574 and 532 nm. The optical energy gaps of **2-1** and **2-2** are determined from the onsets of the UV-vis absorption spectra to be 2.36 and 1.90 eV, respectively. These results suggest that the energy gap drastically decreased by increasing the conjugation length of such cove-type molecule. In comparison, the optical band gap of previously reported armchair-type GNRs with similar width but much extended length is about 1.88 eV.[26] Therefore, these oligomers were found to have rather low band gaps, which is in agreement with the DFT calculations (see below). The emission spectra of the precursors **2-23** and **2-24** and fused products **2-1** and **2-2** are demonstrated in Figure **2-20b**. Precursors **2-23** and **2-24** show fluorescence in THF solution with a maximum at 416 and 459 nm, respectively, while compounds **2-1** and **2-2** display the peaks at 546 and 638 nm, respectively.
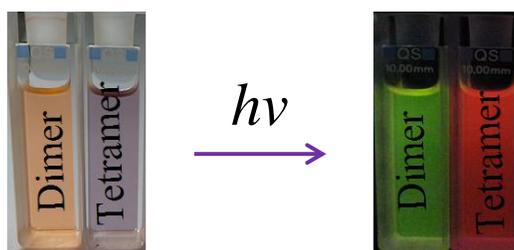

Figure **2-19.** Photographs of solutions of the dimer **2-1** and tetramer **2-2** in THF solution.
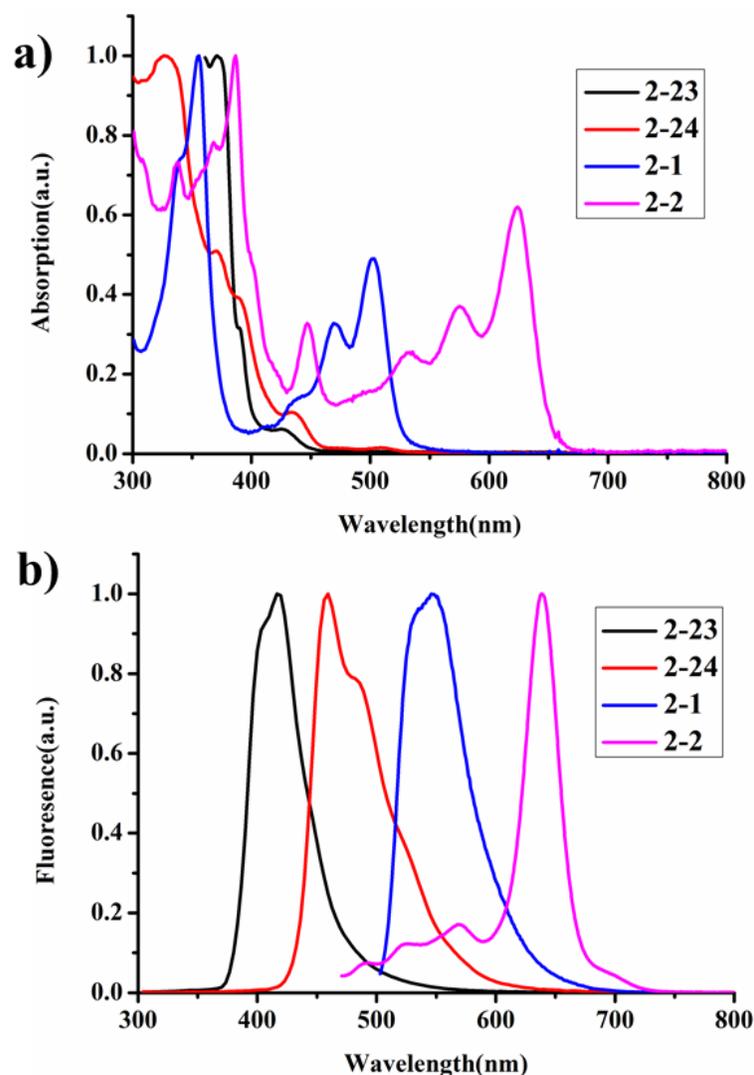
Figure **2-20**. (a) UV-vis absorption spectra and (b) Fluorescence spectra of precursors **12** and **13** and fused products **1** and **2** (for all spectra: 10^{-5} M in THF).

Electrochemical Properties. The electrochemical properties of **2-1** and **2-2** were investigated by means of cyclic voltammetry (CV) in THF solutions. Ferrocene/ferrocenium (Fc/Fc+) was used for the calibration. The redox potential of Fc/Fc+ was located at 4.37 eV relative to Ag/AgCl reference electrode under the same condition. Then the energy levels of the lowest unoccupied molecular orbitals (LUMO) were calculated according to the following equation: $E_{LUMO} = -e$ ($E_{red} + 4.37$) (eV). According to the CV analysis, compounds **2-1** and **2-2** show two reversible oxidation and one irreversible reduction (Figure **2-21**). The HOMO energy levels are estimated from the onsets of the reversible oxidation peaks to be –5.12 and –4.98 eV for **2-1** and **2-2**,

respectively. The LUMO energy levels are estimated using the optical gaps determined from the onsets of the absorption spectra, and the extracted values are listed in Table **1**. These results are fully consistent with the DFT calculations (see below).
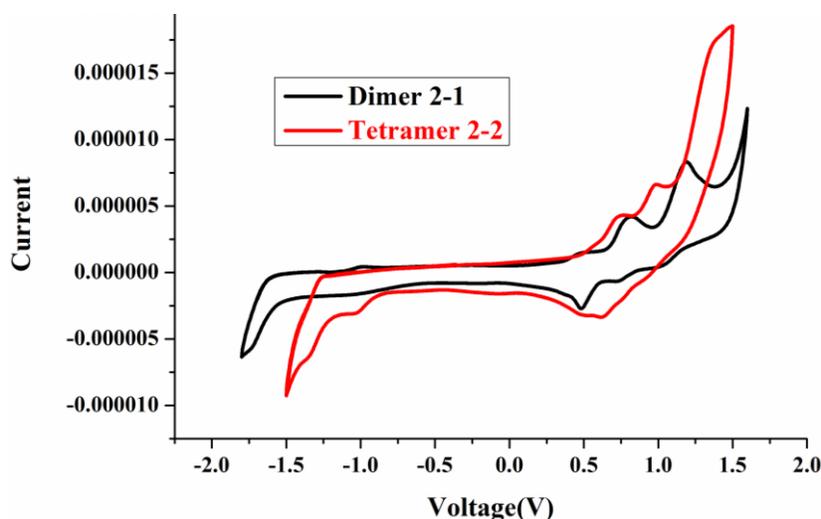

Figure **2-21**. Cyclic voltammograms of dimer **2-1** and tetramer **2-2** vs Fc/Fc+ (0.1 M nBu₄NPF₆ in CH₃CN), scan rate: 100 mVs⁻¹.

Table **2-1** Optical and electrochemical property data for the oligomers and its corresponding GNRs.

compd	λmax (nm)	λem (nm)	λedge (nm)	HOMO (eV)[a]	LUMO (eV)[a]	HOMO (eV)[b]	LUMO (eV)[c]	Eg(opt) (eV)[d]	Eg(cal) (eV)[a]
2-1	503	546	526	-4.67	-2.06	-4.99	-2.68	2.36	2.61
2-2	593	605	621	-4.38	-2.37	-5.33	-3.37	1.90	2.01
2-3	---	---	---	-4.33	-2.47	---	---	---	1.85
2-4	---	---	---	-4.31	-2.50	---	---	---	1.81
GNRs	---	---	---	-4.22	-2.52	---	---	---	1.70

(a) Calculations were performed at the B3LYP/6-31G (d,p) level; (b) HOMO levels were calculated from the measured first oxidation potential of CV; (c) LUMO levels were calculated from the optical band gap Eg(opt) and the respective HOMO levels; (d) optical band gaps were estimated from the wavelength of the absorption edge.

2.5 Surface synthesis of GNRs based on the building block 2-5a.
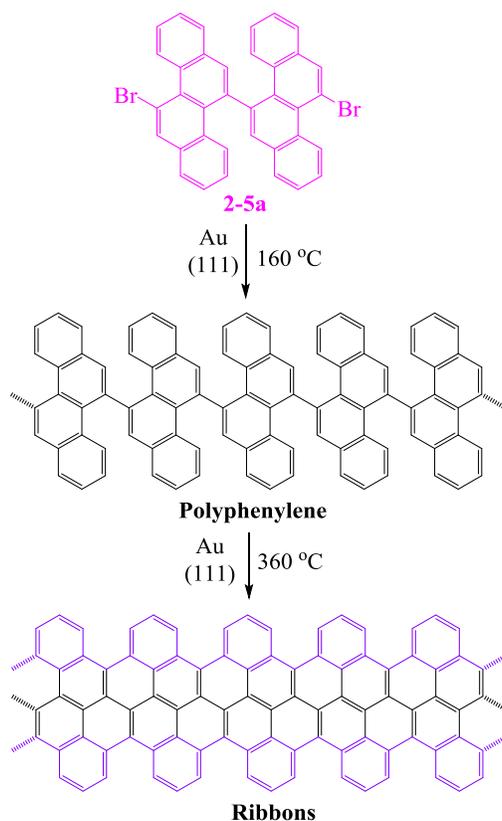
Scheme **2-6**. Synthesis of **cove-edged GNR** on surface.

As the solution approach suffers from the steric hindrance when trying to achieve high molecular weight, chrysene-based precursor polymers, we turned our attention to the surface-assisted synthesis employing **2-5a** (Cooperation with Prof. ████████). The on-surface approach is in principle based on the same two steps as used in solution: precursor monomers are introduced in supporting media (in this case the solid Au (111) surface), where they are driven to react to first form polyphenylene oligomers via dehalogenation and subsequent radical addition, and subsequently, provide the GNR by surface-assisted cyclodehydrogenation (Scheme **2-6**). Both steps are triggered by temperature, as described below. The resulting **cove-edge GNRs** grown under ultra-high vacuum conditions are shown in the STM images in Figure **2-22**, in which the lengths of the GNRs are up to 20 nm. Deposition of monomer **2-5a** on a clean Au (111) surface held at 160 °C and post-annealing of the system at 360 °C yields the GNRs with lengths ranging from tetramers to hexadecamers (sixteen chrysene repeating units). There is, however, a clear

tendency for interribbon cross-coupling. This can be rationalized in terms of on-surface diffusion and reaction during the cyclodehydrogenation step. The barriers to cyclodehydrogenation and to dehydrogenation at the edge are too close, edge radicals will be formed, which attack the C-H from neighboring ribbons and cross-couple in this way, hindering the formation of longer ribbons (Figure **2-22a**). When on a surface, oligomers adopt a flat geometry due to the tendency of aromatic structures to maximize the van der Waals interaction with the surface, in contrast to the non-planarity observed in solution. The apparent height of the GNRs is around 1.7Å, in good agreement with the value reported for other planar aromatic species on metallic surfaces. Despite their tendency to cross-couple, it is possible to find isolated oligomers such as the ones shown in Figure **2-22b** and **c**. In both cases, the cove-edge structure is discerned, in good agreement with the superimposed schematic model of the ribbon. The formation of longer GNRs under UHV conditions on metallic surfaces in comparison to solution can be rationalized in terms of monomer confinement and enhanced catalytic properties of metallic surfaces: monomers deposited on a surface are confined to a 2D geometry, in contrast to solution-based methods, thus increasing the probability of monomers to find each other and react, which gives rise to longer oligomers. Additionally, metallic surfaces are known to have catalytic properties, further increasing the polymerization efficiency.
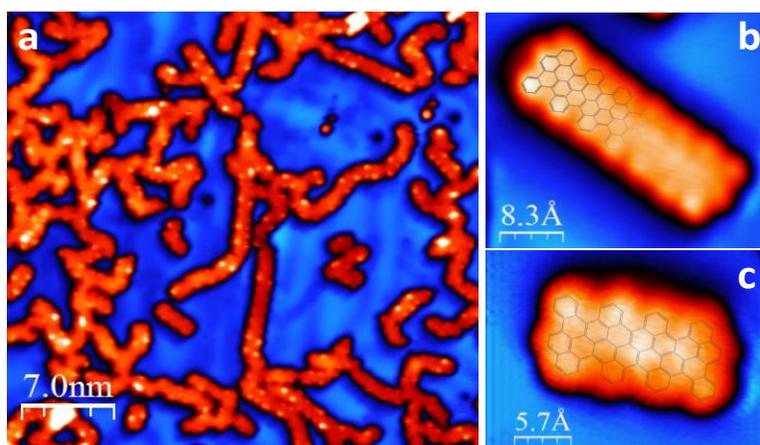

Figure **2-22**. Set of STM images showing **cove-edged GNRs** grown via on-surface bottom-up reaction of monomer **2-5a** under ultra-high vacuum conditions. (a) Long range STM image of the oligomers after cyclodehydrogenation. $I = 100$ pA, $V = -1.20$ V. (b) and (c) High-resolution STM images of two isolated short GNRs with schematic models superimposed. (b) $I = 400$ pA, $V = -0.90$ V. (c) $I = 200$ pA, $V = -0.70$ V.

Theoretical studies have addressed the electronic structure of ZGNRs, revealing an antiferromagnetic ground state with spin-polarized state, which lead to a well-defined spatial separation of the two spin components. Based on this, a number of intriguing applications have been predicted, such as spintronics. So far, however, a direct observation of the spin-polarized edge states for specifically designed and controlled zigzag edge topologies has not been achieved. As discussed above, we have successfully synthesized the cove-edge GNRs on the surface, based on our building block dibromo-bischrysene **2-5a**, with the lengths up to 20 nm. Accordingly, it makes sense and is interesting to design the compound **2-5c** with four methyl groups toward the full zigzag GNRs via the same method on the surface (Scheme **2-7**).
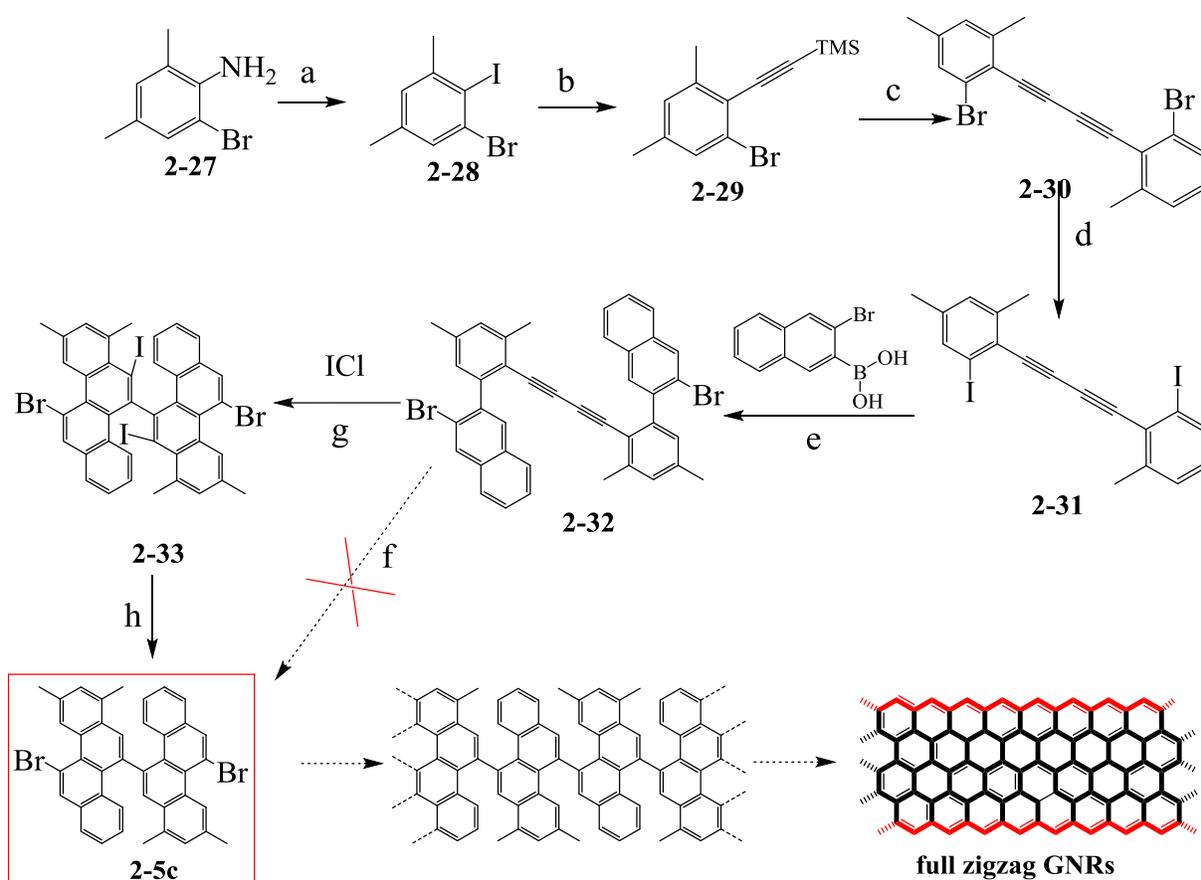
Scheme **2-7**. The synthetic route toward monomer **2-5c**. a) Sandmeyer reaction, 60%. b) TMS-acetylene, PdCl$_2$(PPh$_3$)$_2$, CuI, Et$_3$N, THF, r.t, 24 h, 82%. c) CuCl, DMF, Air, 80 °C, 6h, 78%. d) n-BuLi, THF, ICH$_2$CH$_2$I, −78 °C to r.t, 80%. e) Pd(PPh$_3$)$_4$/Na$_2$CO$_3$, THF/H$_2$O/EtOH, 60 °C, 24 h, 56%. f) PdCl$_2$, Toluene, 85 °C, 24 h. g) ICl, DCM, −78 °C, 3 h, 87%. h) hv, THF, 2 h, r.t, 50%.

To obtain the target monomer **2-5c,** compound **2-32** was first synthesized, following the previous synthesis of monomer **2-5b** by Sandmeyer, Sonogashira, Glasser and Suzuki coupling. Then **2-32** was treated with $PtCl_2$ in order to fuse the triple bond. Unfortunately, this reaction failed most probably due to the steric hindrance caused by the additional methyl groups. Increasing the temperature by refluxing in toluene, and then in *o*-xylene at 150 °C, however, did not improve the results. Nevertheless, the cyclization of **2-32** could be achieved by employing ICl to afford **2-33**, which could be subsequently converted to monomer **2-5c** by photodeiodination. Here, we have tried several methods to optimize the synthetic condition and got the pure target compound **2-5c**, as depicted in the table **2-2**. The crude product of **2-5c** was purified by flash chromatography on silica gel, recrystallization, and then recycling GPC to obtain the pure monomer **2-5c**. Characterizations by the FD-MS and ^{1}H-NMR validated the formation of **2-5c** and confirmed the high purity (Figure **2-23**, **2-24** and **2-25**).

	Light(365nm) number	Time （min）	Quench	Result	
1	4	30	H2O	incomplete	☹
2	4	60	Methanol	incomplete	☹
3	4	120	Methanol	incomplete	☹
4	6	60	Methanol	incomplete	☹
5	6	120	Methanol	best	☺

Table **2-2**. Synthesis of **2-5c** at different photodeiodination condition.
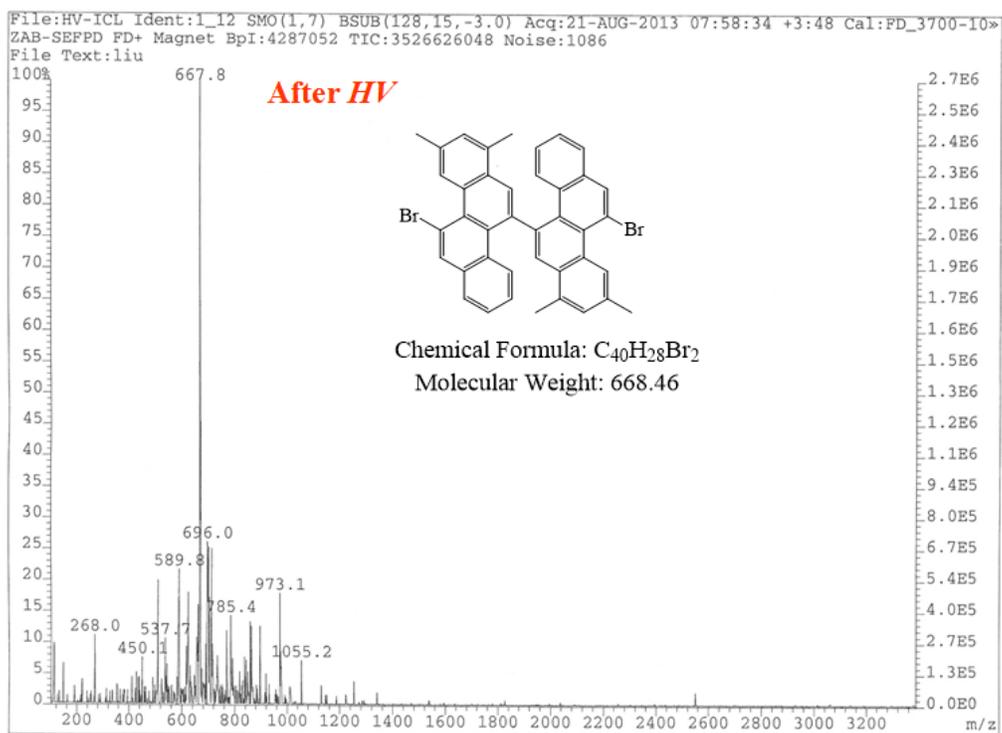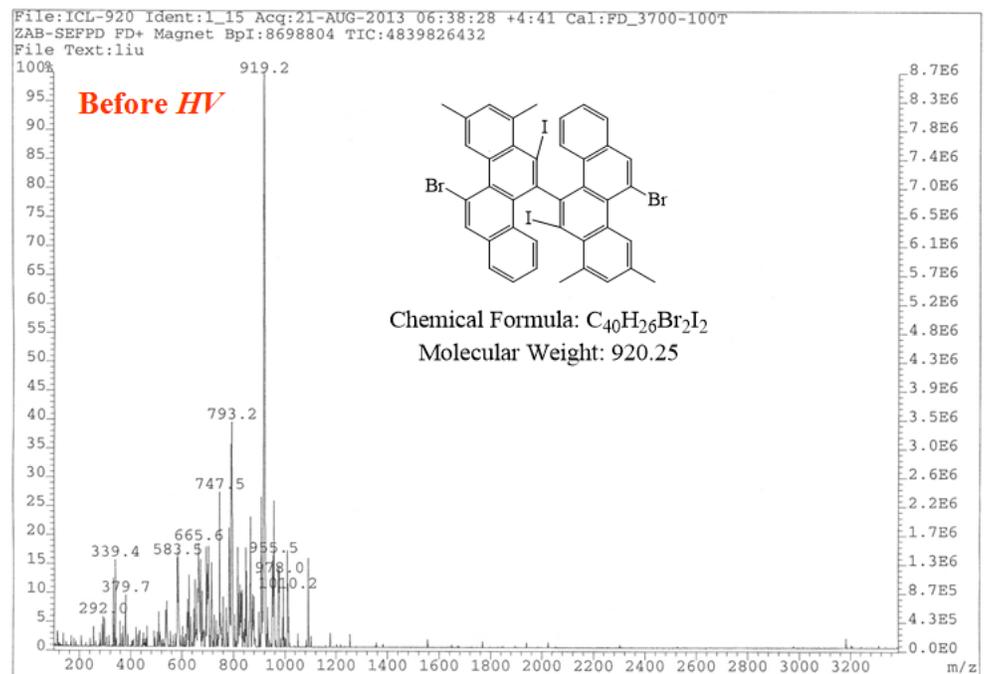
Figure **2-23**. The FD-MS spectra of **2-33** and **2-5c** at before and after UV-irradiation, respectively.
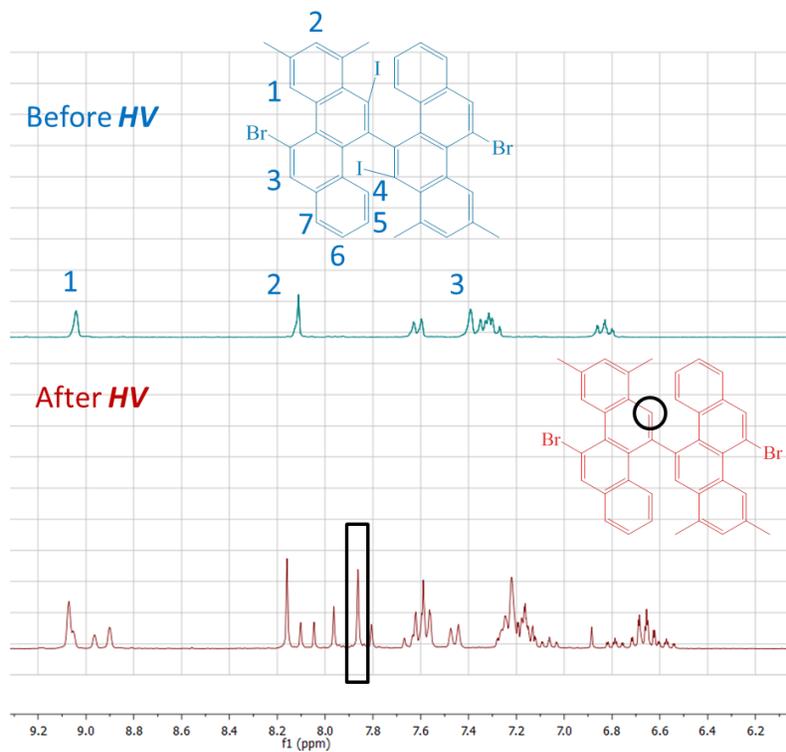
Figure **2-24**.The ^{1}H-NMR spectra of **2-33** and **2-5c** at before and after UV-irradiation.
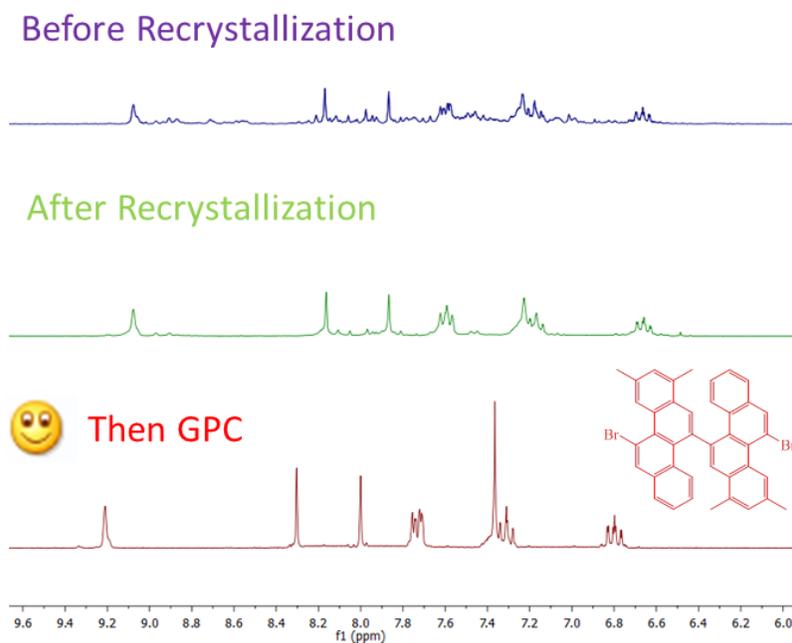

Figure **2-25**. The ^{1}H-NMR spectra of compound **2-5c** before and after purification by different methods.

Dibromo-bischrysene **2-5c** with tetra-methyl groups, however, failed to form the desired ZGNRs on the Au (111) surface, probably due to the steric hindrance induced by the methyl groups. From Figure **2-25**, we can see that there are some dendritic structures and a few very short straight segments, and further attempts are necessary for the surface reaction to obtain much better results.
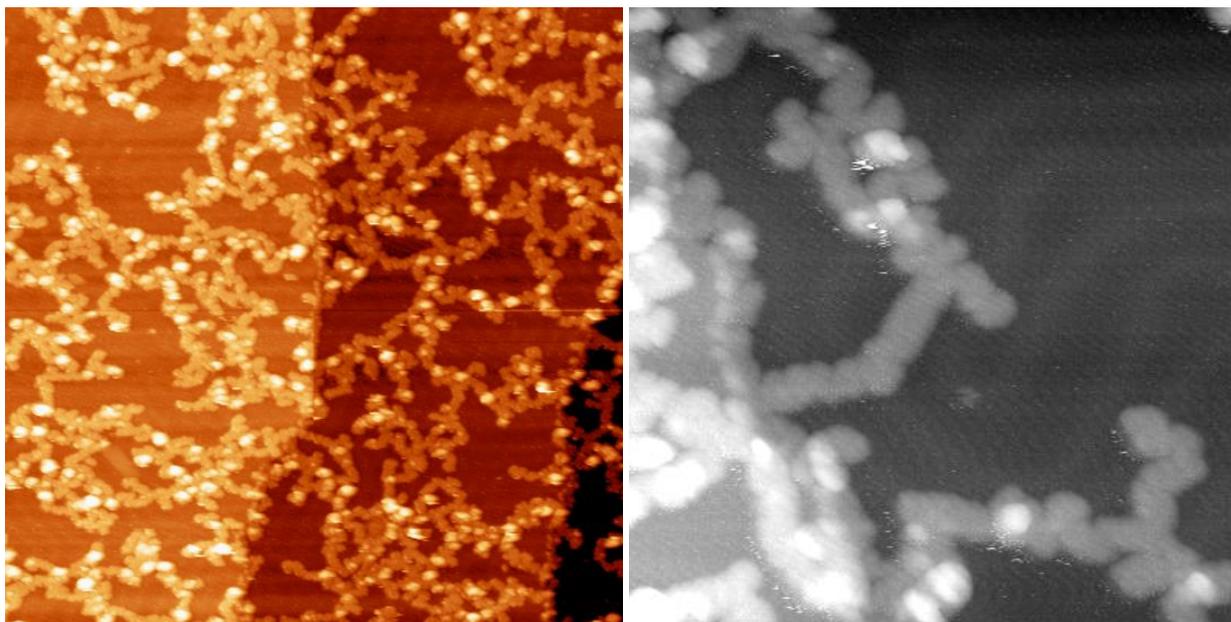

Figure **2-25**. STM images showing dendritic structures and short GNRs via on-surface bottom-up reaction of monomer **2-5c** under ultra-high vacuum conditions.

2.6 DFT Calculations (cooperation with Prof. ████████████)

First principle calculations were carried out in order to gain further insight into the electronic structures and optical properties of the oligomers and its corresponding GNRs. Geometry optimization was performed at the B3LYP level of theory with the 6-31G (d,p) basis set, using the Gaussian09 simulation package. Firstly, Ultraviolet-Visible spectroscopic calculations were performed for the fused oligomers (dimer to hexamer of chrysene) at the AM1/CIS (Figure **2-26**), and TD-DFT (Figure **2-27**) levels of theory. Calculations with the semi-empirical AM1 method performed with the Gaussian09 and AMPAC software (https://www.semichem.com/ampac/default.php) for comparison; however the results presented here are from Gaussian09 only. Both methods indicate two main absorption bands in the low-energy (high-wavelength) spectral domain, with the lowest electronic transition carrying much smaller oscillator strength (extinction coefficient).
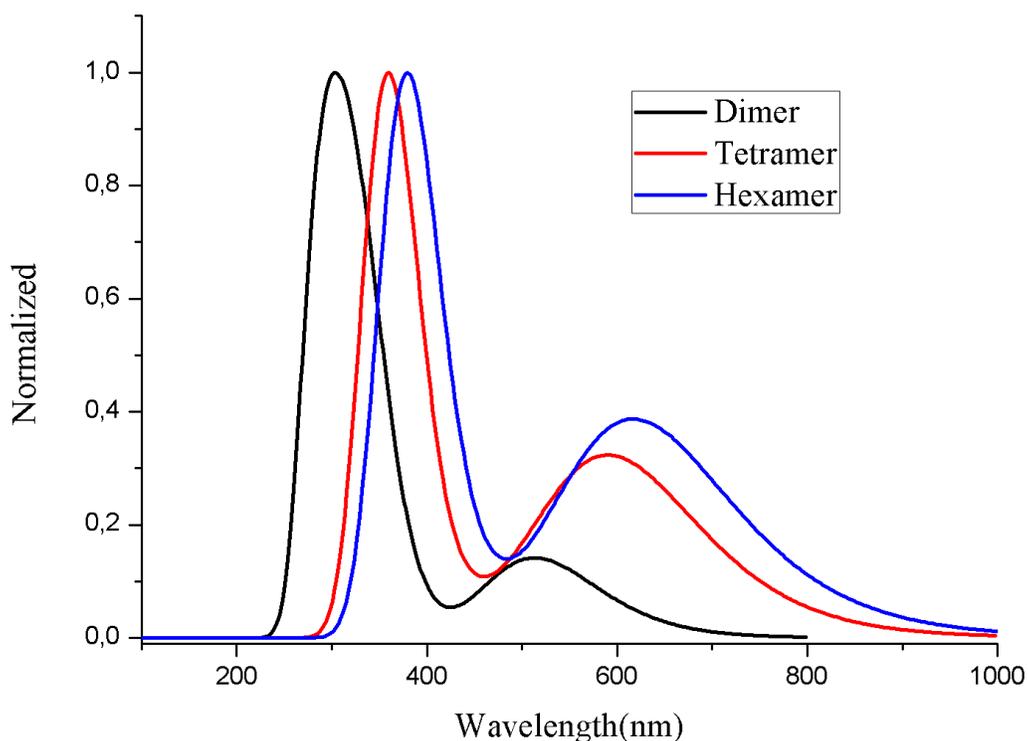

Figure **2-26.** Simulated UV-Vis spectra of the **oligomers** by AM1/CIS methods.
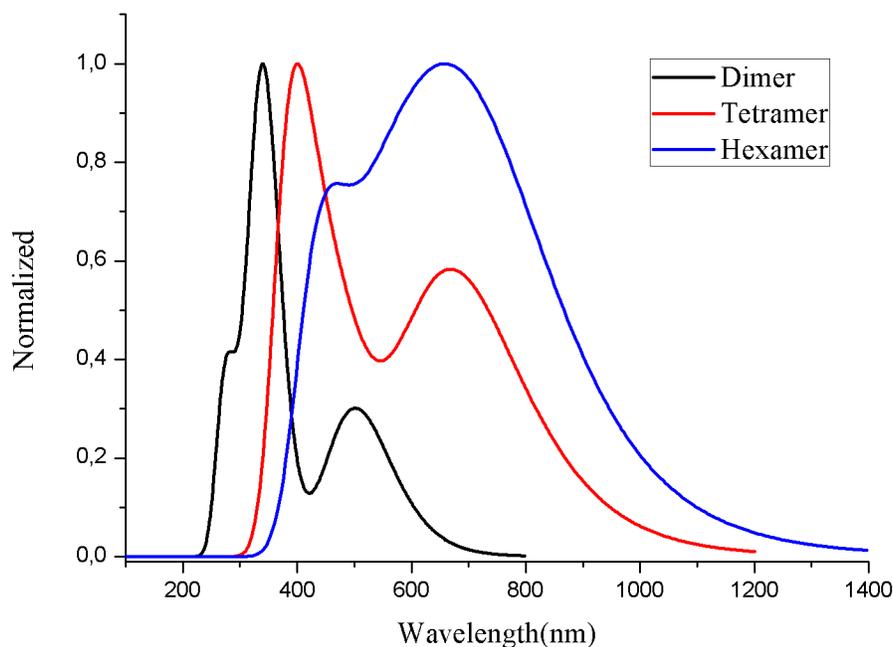
Figure **2-27.** Simulated UV-Vis spectra of the **oligomers** by TD-DFT methods.

Next, we found that these fused chrysene oligomers adopt a non-planar conformation due to the steric repulsion between the two C-H bonds on the inner cove position, in line with our crystal structure. Interestingly, multiple conformers that differ by the relative torsion angles along the ribbon (alternated 'top-down' or 'helical') and have slightly different optical fingerprints are predicted to co-exist. The geometry can be seen unambiguously for the model of the tetramer **2-2** shown in Figure **2-28**. The calculation reveal that there are three possible isomers for the tetramer: the alternating "down-up" model due to the repulsion of C-H atoms at the cove edge (**T-isomer-1**), the second is like the mixed "down-up" conformer (**T-isomer-2**), the third has a helical twist at each of the cove position, and is called the "helical" conformation (**T-isomer-3**). We calculated the relative energies of each isomer of the tetramer. The theory predicts that the alternating "down-up" **T-isomer-1** has the lowest energy level, and difference energy of 2.19 and 4.63 kcal/mol , respectively, for the mixed **T-isomer-2** and the helical **T-isomer-3** (Figure **2-29**). Furthermore, from the HOMO-LUMO calculation of these isomers of **2-2**, the "down-up" conformer **T-isomer-1** has the lowest energy band gap (Figure **2-30**). And the UV-Vis spectroscopic calculations of these isomers of tetramer **2-2** were performed at the AM1/CIS (Figure **2-31**), and TD-DFT (Figure **2-32**) levels of theory.
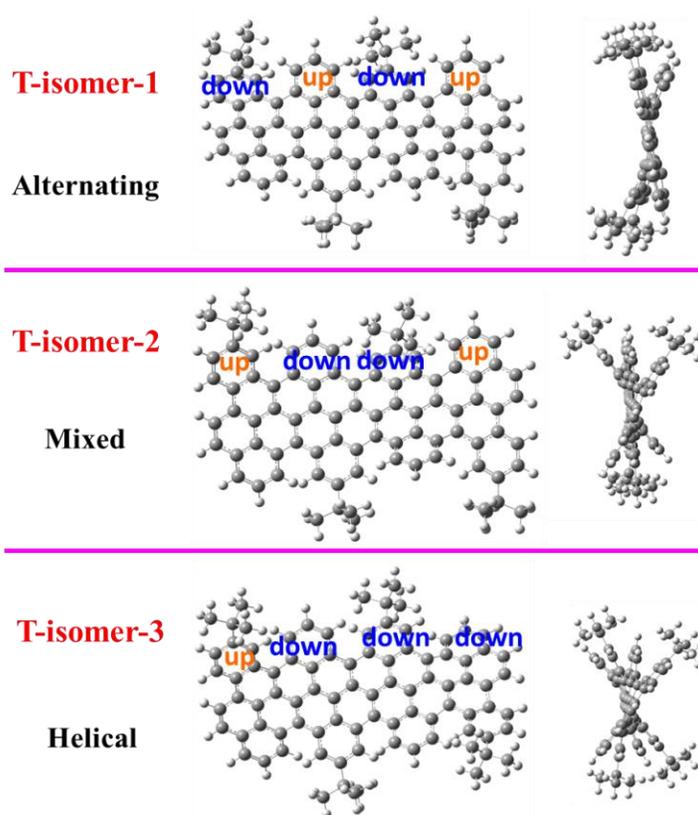
Figure **2-28**. DFT models of tetramer **2-2**.
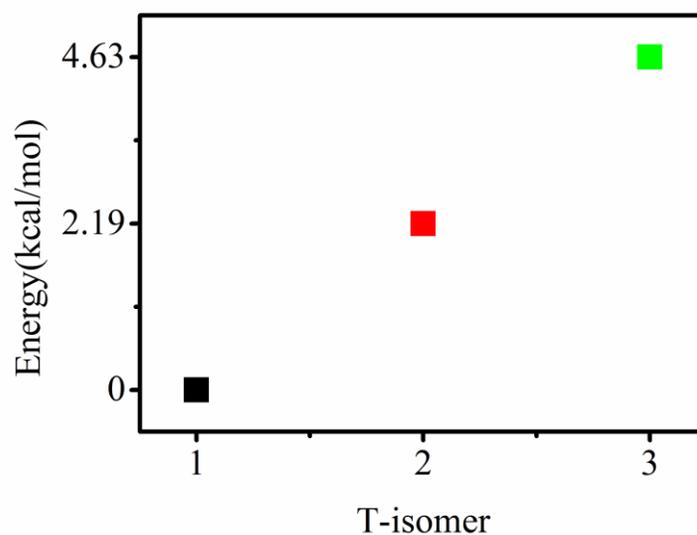
Figure **2-29**. Energy level of the conformers from tetramer **2-2**. The structure **T-isomer 1** (the more stable) is set as refer energy (0 kcal/mol); as a consequence the more stable the structure, the smaller the energy.

T-isomer-1

LUMO = -2.3526

HOMO = -4.4255

ΔEg = 2.07eV

T-isomer-2

LUMO = -2.3726

HOMO = -4.3680

ΔEg = 2.01eV

T-isomer-3

LUMO = -2.4285

HOMO = -4.2641

ΔEg = 1.83eV
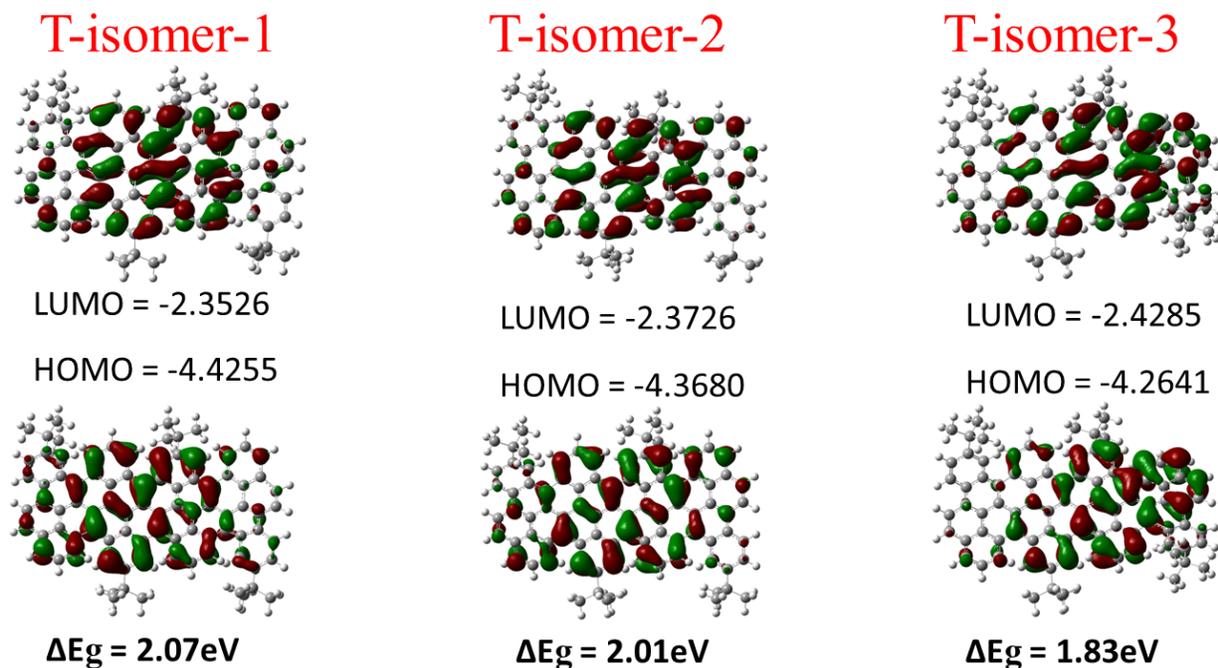
Figure **2-30**. HOMO-LUMO of the conformers from tetramer **2-2**.
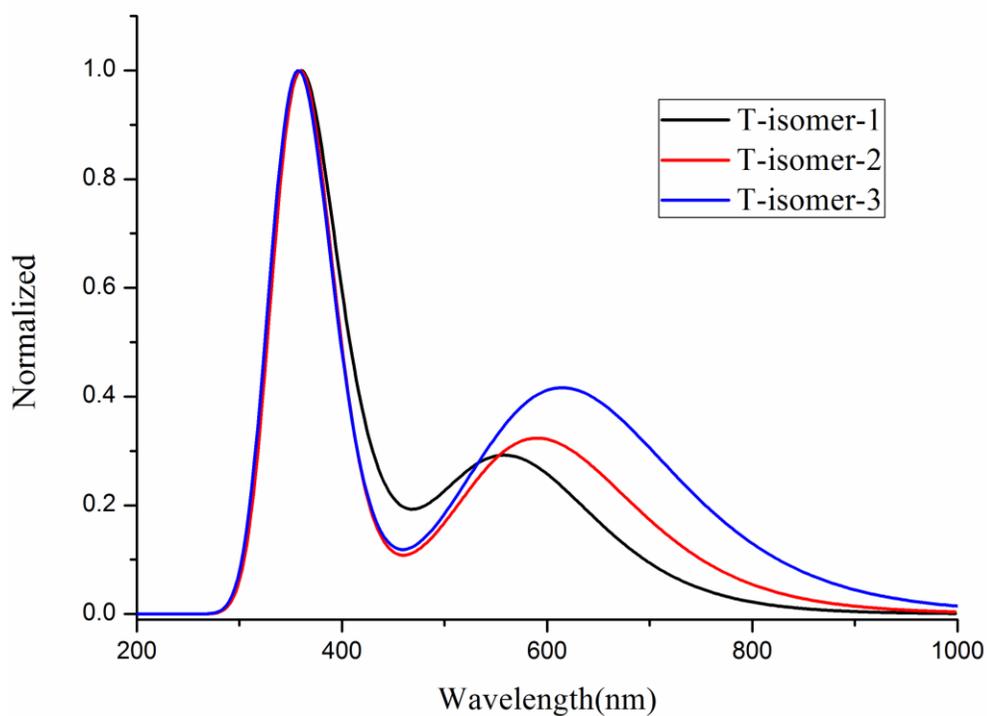
Figure **2-31**. Simulated UV-Vis spectra of the conformers of tetramer **2-2** by AM1/CIS methods.
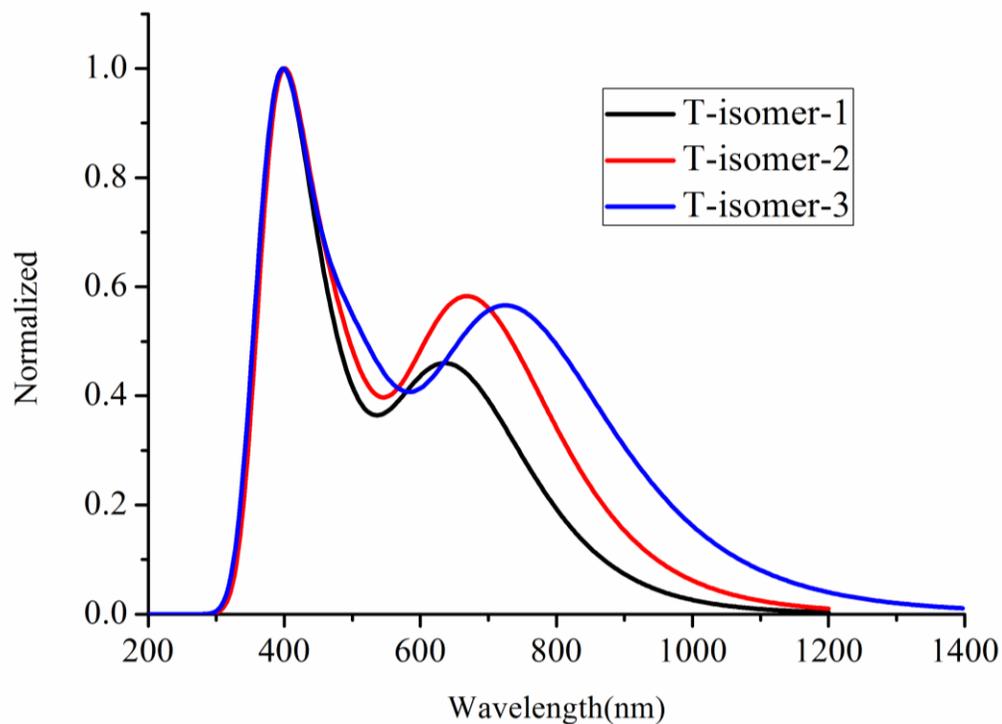
Figure **2-32**. Simulated UV-Vis spectra of the conformers of tetramer **2-2** by TD-DFT methods.

Furthermore, the DFT calculations reveal that hexamer **2-3** has six possible conformers. Similar to the tetramer, hexamer **2-3** was shown to have alternating "down-up" (**H-isomer-1**) and "helical" (**H-isomer-6**) conformers, and four more "mixed" conformers (**H-isomer-2**, **3**, **4** and **5**) (Figure **2-33**). We also calculated the relative energies of each conformer. We found that the alternating **H-isomer-1** have the lowest energy level, and the differences in the energy levels of these conformers from the mixed **H-isomer-2** to the helical **H-isomer-6** were predicted 2.42, 4.61, 4.67, 7.36 and 9.92 kcal/mol, respectively (Figure **2-34**).
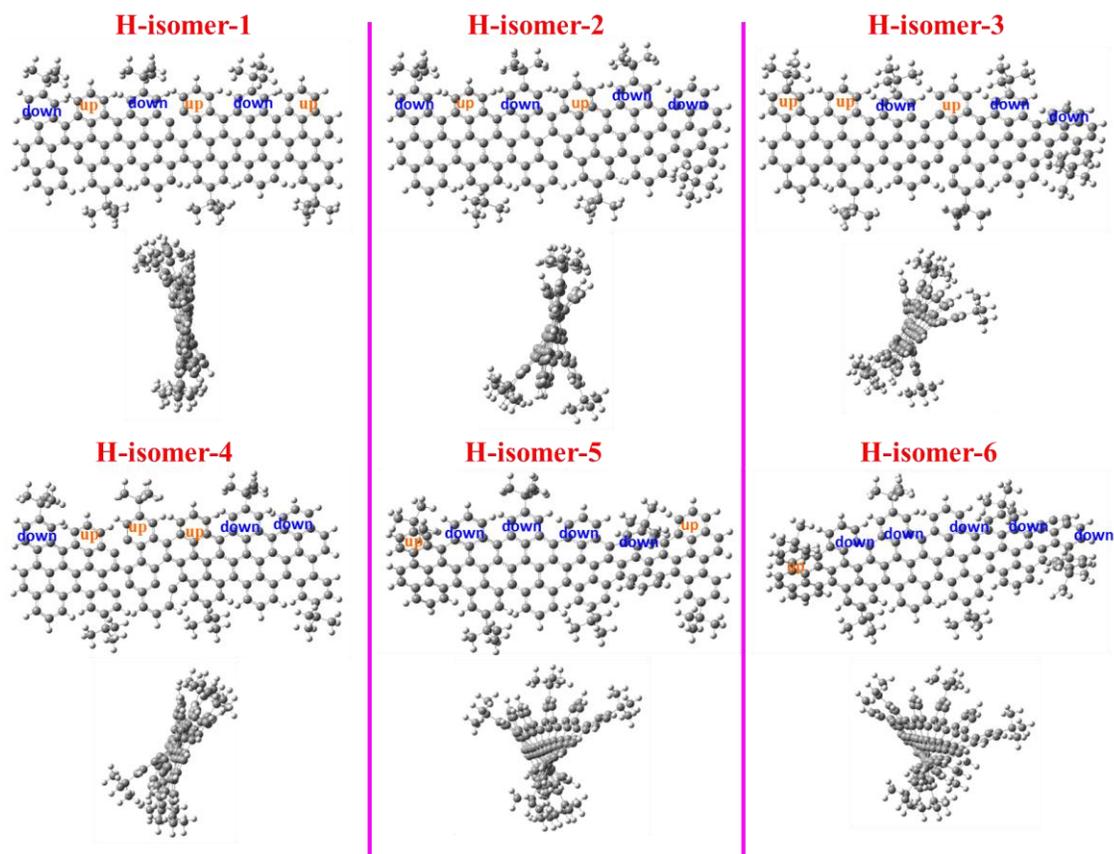
Figure **2-33**. DFT models of hexamer **2-3**.
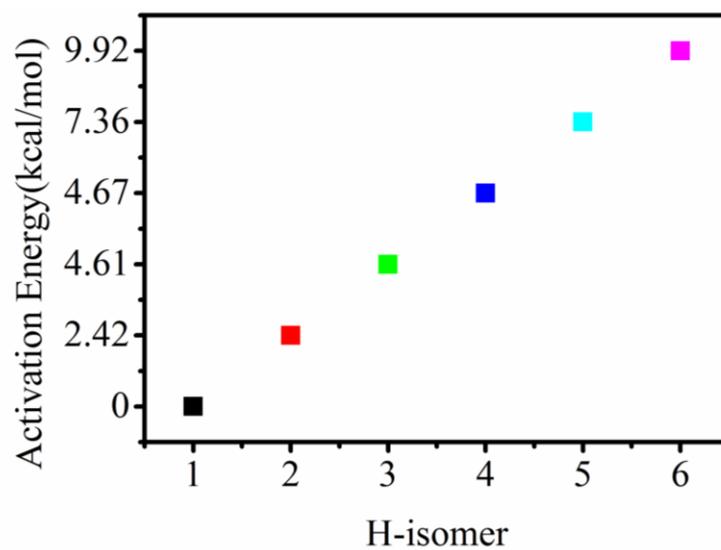
Figure **2-34**. Energy levels of conformers of hexamer **2-3**. The structure **H-isomer 1** (the more stable) is set as refer energy (0 kcal/mol); as a consequence the more stable the structure, the smaller the energy.

For both oligomers, the alternating "down-up" conformers (**T-isomer-1** and **H-isomer-1**) are energetically the most favorable ones. The HOMO and the LUMO orbitals of the oligomers are shown in Figure **2-35** with their corresponding energies. As one can see (Table **2-1**), the energy gap is reducing with increasing size of the oligomer, which explains the bathochromic shift observed in the UV-vis spectra of **2-1** and **2-2** (Figure **2-20a**) with very good agreement. Thereafter, the corresponding infinite graphene nanoribbon (GNR) was studied. As one would expect, the ribbon is not planar as well, featuring the alternating "down-up" conformation. The band structure and the HOMO-LUMO orbitals at *k*-point *k=2π/α* of the ribbon are displayed in Figure **2-36**. The orbitals show a bonding-antibonding pattern that is reminiscent of that obtained for the oligomers and are fully delocalized across the ribbon width, in contrast to zigzag graphene ribbons (with localized states at the ribbon edges). The corresponding GNR is predicted to have a low band gap of 1.70 eV. The length of the unit cell of the ribbon is 9.92Å.

Dimer	Tetramer	Hexamer	Corresponding GNRs

LUMO= -2.06 eV	LUMO= -2.37 eV	LUMO= -2.47 eV	LUMO= -2.52 eV

| HOMO= -4.67 eV	HOMO= -4.38 eV	HOMO= -4.33 eV	HOMO= -4.22 eV
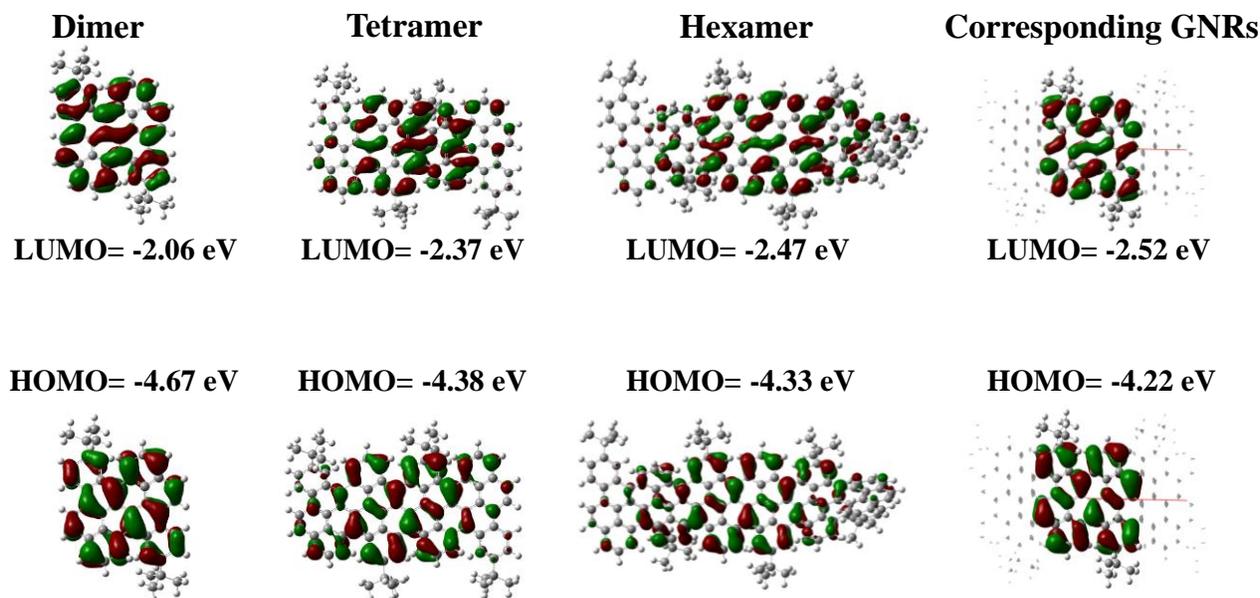
Figure **2-35**. HOMO-LUMO for **2-1**, **2-2**, **2-3** and the corresponding GNRs.
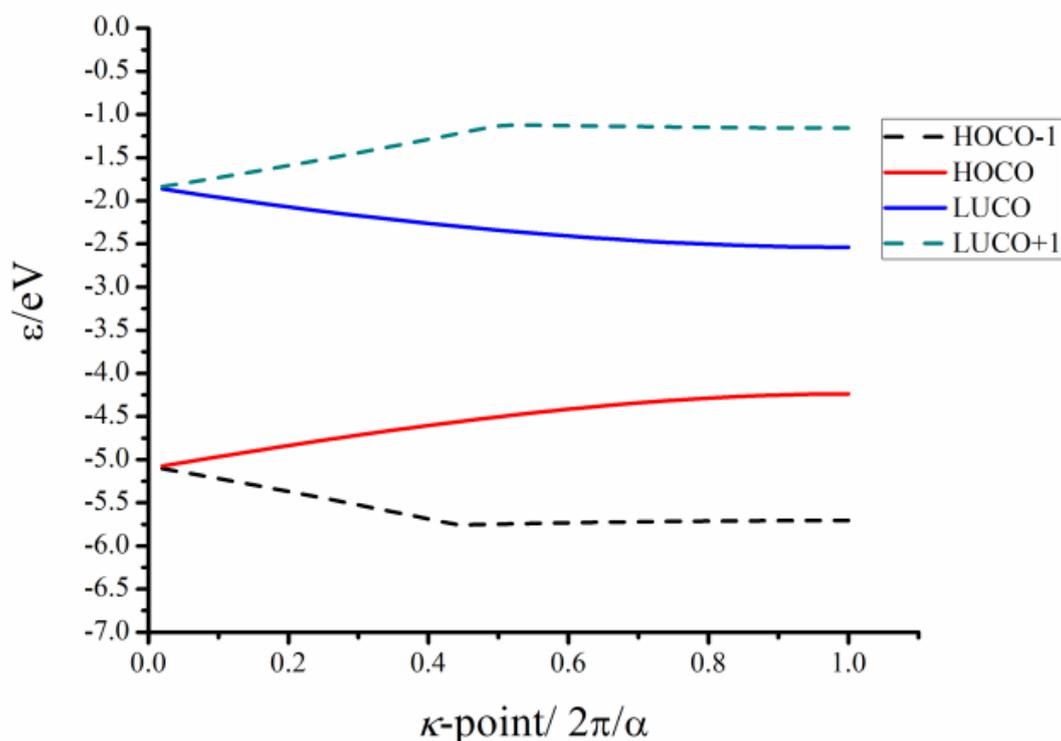
Figure **2-36**. Band structure of corresponding GNRs. Frontier bands are shown: Highest Occupied Crystallic Orbital (HOCO)-1 (dotted black), HOCO (red), Lowest Unoccupied Crystallic Orbital (LUCO) (blue), and LUCO + 1 (dotted green).

Mobility calculations were also carried out using the Boltzmann transport equation coupled with the deformation potential theory, as implemented in the BoltzTrapP software. In order to obtain the elastic constant (C) and the deformation potential constant for electrons and holes (E1h, E1e) needed for the mobility calculation, the lattice vector of the GNRs was stretched and compressed. C can be derived by $\Delta E/l0 = C(\Delta l/l0)2/2$, after fitting the total energy with respect to the lattice change, and was found to be 120 eV/Å. The deformation potential constant is defined as $E1 = \Delta\varepsilon/(\Delta l/l0)$, where $\Delta\varepsilon$ is the energy change of the corresponding band near the Fermi energy due to Δl (at valence band maximum – VBM – for holes and at conduction band minimum – CBM – for electrons). The deformation potential constants for holes and electrons were found to be $E1h = 3.13$ eV and $E1e = 1.61$ eV respectively. Finally, the mobility for holes is estimated to be 1009.8 cm^2/Vs and for electrons 2102.3 cm^2/Vs, in consistency with previous work done in GNRs[32]. According to their classification (nCNR-m-p, where n is the width of the ribbon, m is the ratio between the hydrogen atoms and benzene rings at the edge, and p the relative position of the phenyl rings on either side of the ribbon),

our nanoribbon corresponds to the 3CNR-0-1. Although the current cove-edged GNR is not reported in their work, the values obtained here are in very good agreement with the previous results from other CNRs (Table **2-3**).[32]

Table **2-3** Elastic constant and charge mobilities of CNRs under Boltzmann transport equation

	Elastic const. (eV/Å)	Hole DP const. (eV)	Electron DP const. (eV)	Hole mobility (cm^2/Vs)	Electron mobility (cm^2/Vs)
3CNR-0-1	120.33	3.13	1.61	1009.8	2102.3
4CNR-1-1	202.0	3.22	2.70	7730	10200
6CNR-1-1	299.3	3.29	2.98	19800	23200
4CNR-1-0	202.1	5.60	0.84	873	34600
6CNR-1-0	299.6	6.28	0.91	1770	76700

2.7 Conclusion

In summary, we have demonstrated a bottom-up synthetic approach toward unprecedented low band gap GNRs featuring a cove-edge periphery. Corresponding cyclized chrysene-based oligomers, i.e., dimer and tetramer, have been synthesized in solution, and the surface-assisted synthesis on an Au (111) yielded the cove-edged GNRs with lengths of up to 20 nm. The unambiguous crystallographic characterization of tetramer **2-2** reveals that the cove-edge structure causes the edges to deviate from planarity due to steric repulsion and that it possesses an alternative "up-down" geometry. DFT calculations further demonstrate that the "up-down" geometry of the tetramer has lower energy than the "mix" and "helix" conformers. One would safely conclude that the corresponding infinite GNRs also adopt the alternating "up-down" rolling hill. The DFT calculations predict that such cove-edged GNRs possess low band-gaps (Eg = 1.70 eV) and high charge carrier mobility for both holes and electrons. Moreover, the electronic properties of the GNRs are expected to be tuned through controlling the width with such cove-type periphery via the bottom-up synthesis. Furthermore, the attempt using chrysene motif to prepare the full zigzag-GNRs, which was unfortunately failed for the surface synthesis. Further optimization required in order to yield the target GNRs.

References:

[1] Y. W. Son, M. L. Cohen, S. G. Louie, *Nature* **2006**, 444, 347-349.

[2] X. Li, X. Wang, L. Zhang, S. Lee, H. Dai, *Science* **2008**, 319, 1229-1232.

[3] L. Jiao, L. Zhang, X. Wang, G. Diankov, H. Dai, *Nature*, **2009** 458, 877–880.

[4] D. Kosynkin, A. Higginbotham, A. Sinitskii, J. Lomeda, A. Dimiev, K. Price, J. Tour, *Nature* **2009**, 458, 872-876.

[5] J. Cai, P. Ruffieux, R. Jaafar, M. Bieri, T. Braun, S. Blankenburg, M. Muoth, P. Seitsonen, M. Saleh, X. Feng, K. Müllen, R. Fasel, *Nature* **2010**, 466, 470-473.

[6] A. H. Castro-Neto, F. Guinea, N. M. R. Peres, K. S. Novoselov, A. K. Geim, *Rev. Mod. Phys.* **2009**, 81, 109-162.

[7] M. E. Gemayel, A. Narita, L. F. Dössel, R. S. Sundaram, A. Kiersnowski, W. Pisula, M. R. Hansen, A. C. Ferrari, E. Orgiu, X. Feng, K. Müllen, P. Samori, *Nanoscale* **2014**, 6, 6301-6314.

[8] X. Wang, Y. Ouyang, X. Li, H. Wang, J. Guo, H. Dai, *Phys.Rew.Lett.* **2008**, 100, 206803

[9] K. A. Ritter, J. W. Lyding, *Nat. Mater.* **2009**, 8, 235-242.

[10] M. Han, B. Özyilmaz, Y. Zhang, P. Kim, *Phys. Rev. Lett.* **2007**, 98, 206805.

[11] O. Yazyev, *Acc. Chem. Res.* **2013**, *46*, 2319-2328.

[12] S. S. Datta, D. R. Strachan, S. M. Khamis, A. T. C. Johnson, *Nano Lett.* **2008**, 8, 1912-1915.

[13] J. Campos-Delgado, J. Romo-Herrera, X. Jia, D. Cullen, H. Muramatsu, Y. Kim, T. Hayashi, Z. Ren, D. Smith, Y. Okuno, T. Ohba, H. Kanoh, K. Kaneko, M. Endo, H. Terrones, M. Dresselhaus, M. Terrones, *Nano Lett.* **2008**, 8, 2773-2778.

[14] Z. H. Chen, Y. M. Lin, M. J. Rooks, P. Avouris, *Physica E* **2007**, 40, 228-232.

[15] M. Y. Han, B. Ozyilmaz, Y. B. Zhang, P. Kim, *Phys. Rev. Lett.* **2007**, 98, 206805.

[16] A. Elías, A. Botello-Méndez, D. Meneses-Rodríguez, V. González, D. Ramírez-González, L. Ci, E. Muñoz-Sandoval, M. Ajayan, H. Terrones, M. Terrones, *Nano Lett.* **2010**, 10, 366-372.

[17] L. Jiao, X. Wang, G. Diankov, H. Wang, H. Dai, *Nat. Nano.* **2010**, 5, 321-325.

[18] H. Sakaguchi, Y. Kawagoe, Y. Hirano, T. Iruka, M. Yano, T. Nakae, *Adv. Mater.* **2014**, 26, 4134-4138.

[19] Z. Pan, N. Liu, L. Fu, Z. Liu, *J. Am. Chem. Soc.* **2011**, 133, 17578-17581.

[20] J. Wu, L. Gherghel, M. Watson, J. Li, Z. Wang, C. Simpson, U. Kolb, K. Müllen, *Macromolecules* **2003**, *36*, 7082-7089.

[21] X. Yang, X. Dou, A. Rouhanipour, L. Zhi, H. Räder, K. Müllen, *J. Am. Chem. Soc.* **2008**, 130, 4216-4217.

[22] Y. Fogel, L. Zhi, A. Rouhanipour, D. Andrienko, H. Räder, K. Müllen, *Macromolecules* **2009**, 42, 6878-6884.

[23] M. G. Schwab, N. Narita, Y. Hernandez, Y. Balandina, K. S. Mali, S. D. Feyter, X. Feng, K. Müllen, *J. Am. Chem. Soc.* **2012**, 134, 18169-18172.

[24] L. Dössel, L. Gherghel, X. Feng, K. Müllen, *Angew. Chem. Int. Ed.* **2011**, 50, 2540-2543.

[25] L. Chen, Y. Hernandez, X. Feng, K. Müllen, *Angew. Chem. Int. Ed.* **2012**, 51, 7640-7654.

[26] A. Narita, X. Feng, Y. Hernandez, S. A. Jensen, M. Bonn, H. Yang, I. A. Verzhbitskiy, C. Casiraghi, M.R. Hansen, A. H. R. Koch, G. Fytas, O. Ivasenko, B. Li, K. S. Mali, B. Tatyana, S. Mahesh, S. D. Feyter, K. Müllen, *Nat. Chem.* **2014**, 6, 126-132.

[27] j. Cai, C. A. Pignedoli1, L. Talirz, P. Ruffieux, H. Söde, L. Liang, V. Meunier, R. Berger, R. Li, X. Feng, K. Müllen, R. Fasel1, *Nat. Nano* **2014**, 9, 896-900.

[28] A. Narita, I. A. Verzhbitskiy, W. Frederickx, K. S. Mali, S. N. Jensen, M. R. Hansen M. Bonn, S. D. Feyter, C. Casiragh, X. Feng, K. Müllen, *ACS Nano* **2014**, 8, 11622-11630.

[29] F. Plasser, H. Pašalić, M. H. Gerzabek, F. Libisch, R. Reiter, J. Burgdörfer, T. Müller, R. Shepard, H. Lischka, *Angew. Chem. Int. Ed.* **2013**, 52, 2581-2584.

[30] A. Konishi, Y. Hirao, K. Matsumoto, H. Kurata, R. Kishi, Y. Shigeta, M. Nakano, K. Tokunaga, K. Kamada, T. Kubo, *J*. Am. Chem. Soc. **2013**, *135*, 1430-1437

[31] Y. Zhong, B. Kumar, S. Oh, M. T. Trinh, Y. Wu, K. Elbert, P. Li, X. Zhu, S. Xiao, F. Ng, M. L. Steigerwald, C. Nuckolls, *J. Am. Chem. Soc.* **2014**, 136, 8122-8130.

[32] L. Chen, L. Wang, D. Beljonne, *Carbon* **2014**, 77, 868-879.

Chapter 3. Tetrabenzo[*a*,*f*,*j*,*o*]perylene: A Polycyclic Aromatic Hydrocarbon With An Open-Shell Singlet Biradical Ground State

Up to now, "bottom-up" synthesis of polycyclic aromatic hydrocarbons (PAHs) has mainly been focused on armchair-edged PAHs, whereas PAHs with cove or zigzag edges have remained elusive. In the last chapter, we have demonstrated the synthesis of several cove-type PAHs and the corresponding cove-edged graphene nanoribbons (GNRs) based on chrysene both in solution and on surface. However, the attempt full zigzagGNRs using chrysene was not successful so far. Here, an example of PAHs with zigzag periphery will be demonstrated, which possesses totally different properties from those of armchair-edged PAHs. In this chapter, a novel tetrabenzo[a,f,j,o]perylene, namely "bistetracene", in which two tetracenes are connected side by side with two bonds, was synthesized and characterized. An optical energy gap of about 1.56 eV is derived from the UV-vis absorption spectrum, showing the low optical gap feature of such zigzag-edged PAHs. Theoretical calculations and physical property investigations manifest that such a PAH possesses a prominent biradical character in the ground state, which is the first example among bistetracene derivatives. However, the bistetracene can easily undergo oxidation into tetrabenzo[a,f,j,o]perylene-9,19-dione (diketone) under ambient conditions. Thereby, such zigzag-edged PAH provides insight into the edge state of other expanded homologues, such as *peri*-tetracenes or *peri*-pentacenes.

3.1 Introduction
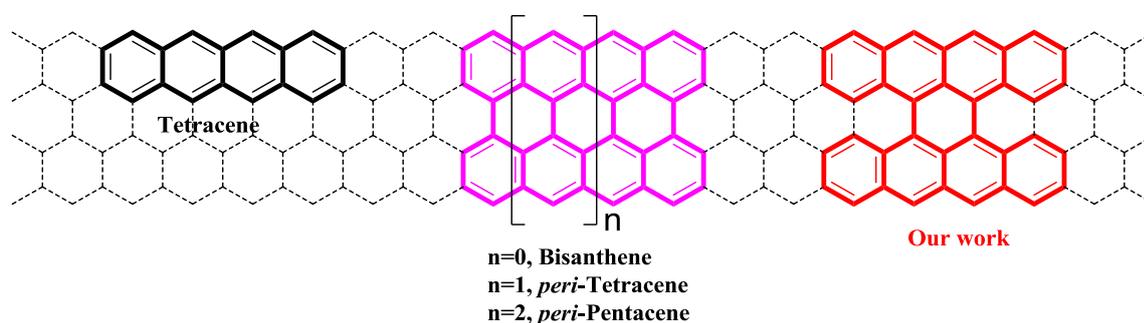
Scheme **3-1**. Structures of typical *peri*-fused acenes.

Polyacenes display fascinating electronic and optoelectronic properties resulting from the spin-polarized state at the zigzag edges.[1-3] To date, a number of reports have been published

on organic field-effect transistors (OFETs) or organic light-emitting diodes (OLEDs) that use tetracene, pentacene, and their derivatives.[2-8] However, the longer acenes, such as hexacene, and higher homologues, are susceptible to oxidation under ambient conditions and photolytic degradation, which causes difficulties in their synthesis.[9,10] On our way to pursue the synthesis of *peri*-fused acene molecules (Scheme **3-1**), which represent a series of conjugated systems with two rows of acenes *peri*-fused together, we face similar challenges. Theoretical calculations predict that the energy gap drastically decreases upon increasing the length of the *peri*-fused acenes.[11,12] The synthesis of higher homologous, such *as peri*-tetracene (Scheme 1), is expected to face low solubility, a small energy gap and high reactivity under ambient condition. Up to now, the largest reported *peri*-fused acene with experimental evidence is *peri*-pentacene, which just could be detected by mass spectrometry in the residue after sublimation of pentacene.[13,14] The smaller analogues, perylene and bisanthene, have been known for a long time. However, the attempts to synthesize the next generation of *peri*-fused acene, namely *peri*-tetracene, have not been successful yet, probably due to the extremely high reactivity as well as the lack of proper synthetic protocols.[15-18]
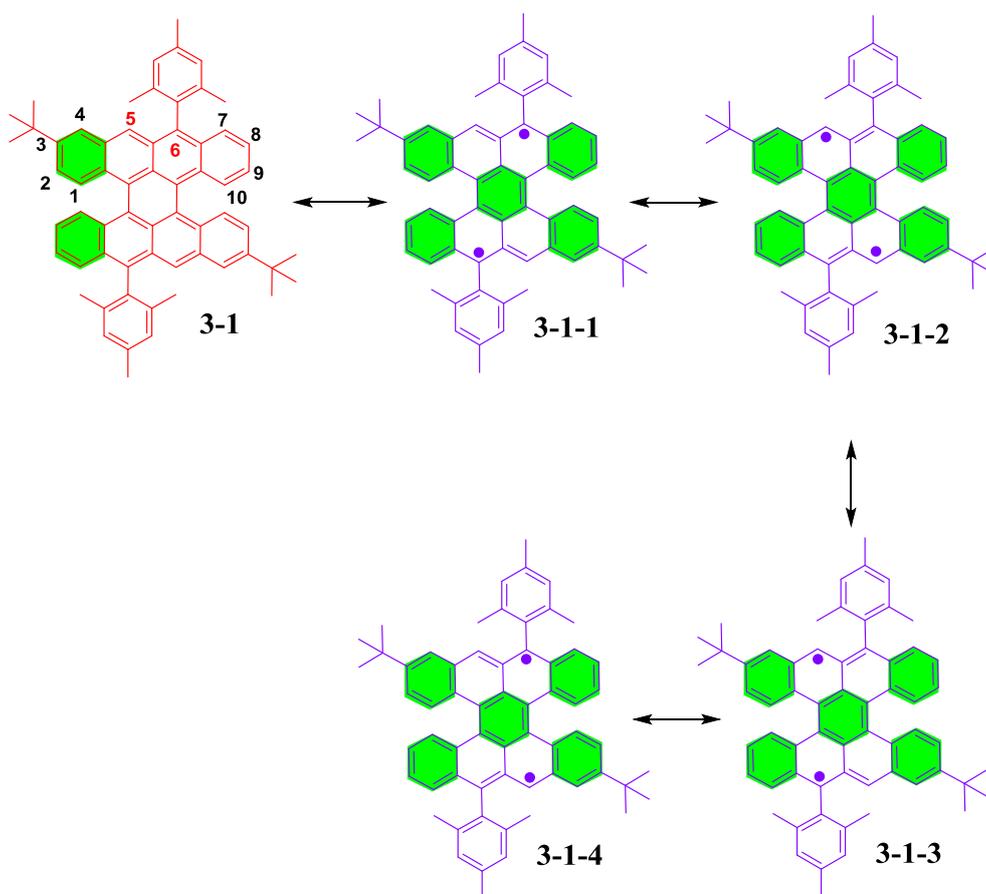

Figure **3-1**. Resonance structures of **TBP 3-1**.

Recently, polycyclic aromatic hydrocarbons (PAHs) with singlet biradical feature have been intensively explored.[19-23] Thus far, several representative types of stable open-shell PAHs have been reported, including bisphenalenyls,[24-29] indenofluorenes,[30-35] anthenes,[36,37] and zethrenes,[38-42] which allow a glimpse of their peculiar properties arising from the singlet biradical character. Theoretical and experimental results have demonstrated that the major driving force for a singlet biradical ground state is the gain of additional Clar sextet rings in the biradical resonance form in comparison to the closed-shell resonance form.[40,43] In this regard, the tetrabenzo[a,f,j,o]perylene (**TBP 3-1**), namely "bistetracene" in which two tetracenes are connected side by side with two bonds, has two aromatic sextets in the closed shell form and a maximum of five aromatic sextets in the biradical forms (Figure **3-1**), regardless of the positions of the radicals. From the resonance structures, we can see that the most reactive sites (C5 and C6) are located at zigzag edges within the two central benzene rings. In order to obtain stable and soluble materials, our design is to kinetically block the reactive sites with bulky mesityl groups (such as **3-1-1**). On the basis of the resonance structures, more aromatic sextets for the bistetracene **TBP 3-1-1** or **3-1-2** will help to stabilize the biradical resonance form as a result of gaining the aromatic stabilization energies, and thus it is expected to show more biradical character in the ground state.

3.2 Synthesis and structure verification of bistetracene TBP 3-1

Firstly, we design a novel synthetic strategy toward the key compound **3-11** (Scheme **3-2**). 1-Bromo-4-(*tert*-butyl)-2-iodobenzene (**3-5**) was synthesized through nitration, reduction, and Sandmeyer reaction starting from 1-bromo-4-(*tert*-butyl)benzene (**3-2**). Then (4-(*tert*-butyl)-2-((triisopropylsilyl)ethynyl)phenyl)boronic acid (**3-7**) was obtained via Sonogashira coupling and boration. ((4,4''-Di-*tert*-butyl-2',5'-di-*o*-tolyl-[1,1':4',1''-terphenyl]-2,2''-diyl)bis(ethyne-2,1-diyl))bis(triisopropylsilane) (**3-9**) was synthesized through selective Suzuki coupling of 1,4-dibromo-2,5-diiodobenzene with *o*-tolylboronic acid, and then with **3-7**.. 4-(*tert*-Butyl)-4'-(4-(*tert*-butyl)-2-ethynylphenyl)-2-ethynyl-2''-methyl-5'-(*o*-tolyl)-1,1':2',1''-terphenyl (**3-10**) was subsequently furnished through deprotection of the TIPS group. A final intramolecular cyclization of compound **3-10** with $PtCl_2$ as a catalyst afforded the desired compound 3,10-di-*tert*-butyl-7,14-di-*o*-tolylbenzo[k]tetraphene (**3-11**) in 30% yield after heating at 110 °C for 24 hours under argon atmosphere. Compound **3-11** was characterized by FD-MS, ^{1}H-NMR (Figure **3-2**), ^{13}C-NMR (Figure **3-3**), and single-crystal analysis (Figure **3-4**). When we enlarge the peaks of the ^{1}H-NMR and ^{13}C-NMR of compound **3-11**, there are two peaks of the

methyl groups, as the result of the rotation of the phenyl rings are restricted by the steric hindrance and co-existence of *cis-* and *anti*-isomers. Accordingly, we have rechecked the crystal structure of compound **3-11** to see if we also observed two conformers separately of the *o*-tolyl group (see Figure **3-5**). However, only the *anti*-isomer was observed by X-ray crystal structure of this compound, indicating that the *anti*-isomer crystalized more quickly, and the *cis*-isomer might have been slowly converted to the *anti*-isomer in the crystallization process.
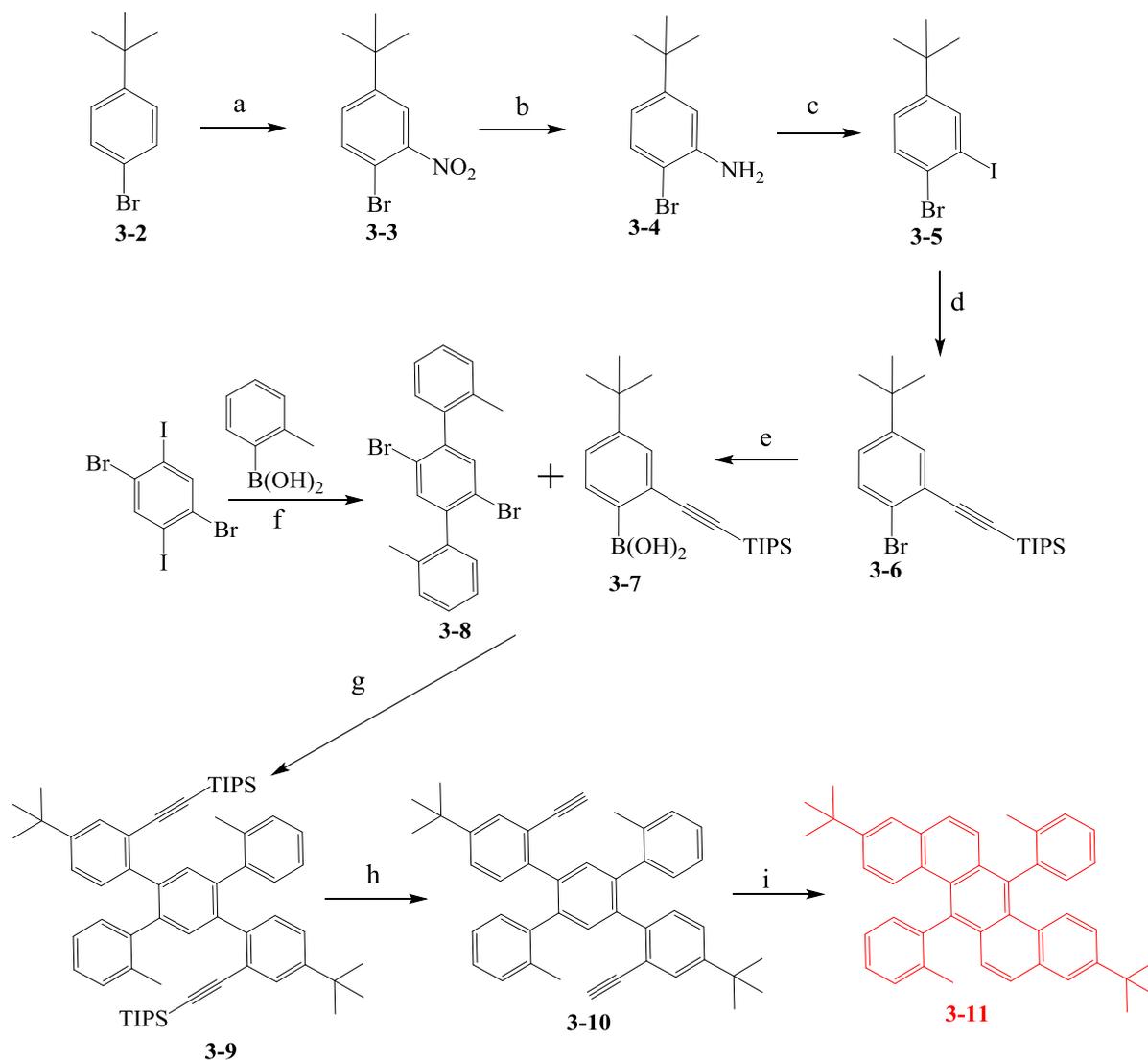
Scheme **3-2**. Synthetic route toward to compound **3-11**. a) H_2SO_4, HNO_3, 92%. b) $Na_2S_2O_4$, HCl, 81%. c) HCl/ $NaNO_2$, KI, 80%. d) TIPS-acetylene, $PdCl_2(PPh_3)_2$, CuI, Et_3N, THF, r.t, 24 h, 90%. e) *n*-BuLi, THF, -78 °C to r.t, 88%. f) $Pd(PPh_3)_4$/K_2CO_3, dioxane/H_2O, 90 °C, 24 h, 80%. g) $Pd(PPh_3)_4$/K_2CO_3, dioxane/H_2O, 95 °C, 24 h, 75%. h) TBAF, THF, r.t, 30 min, 90%. i) $PtCl_2$, Toluene, 110 °C, 24 h, 30%.
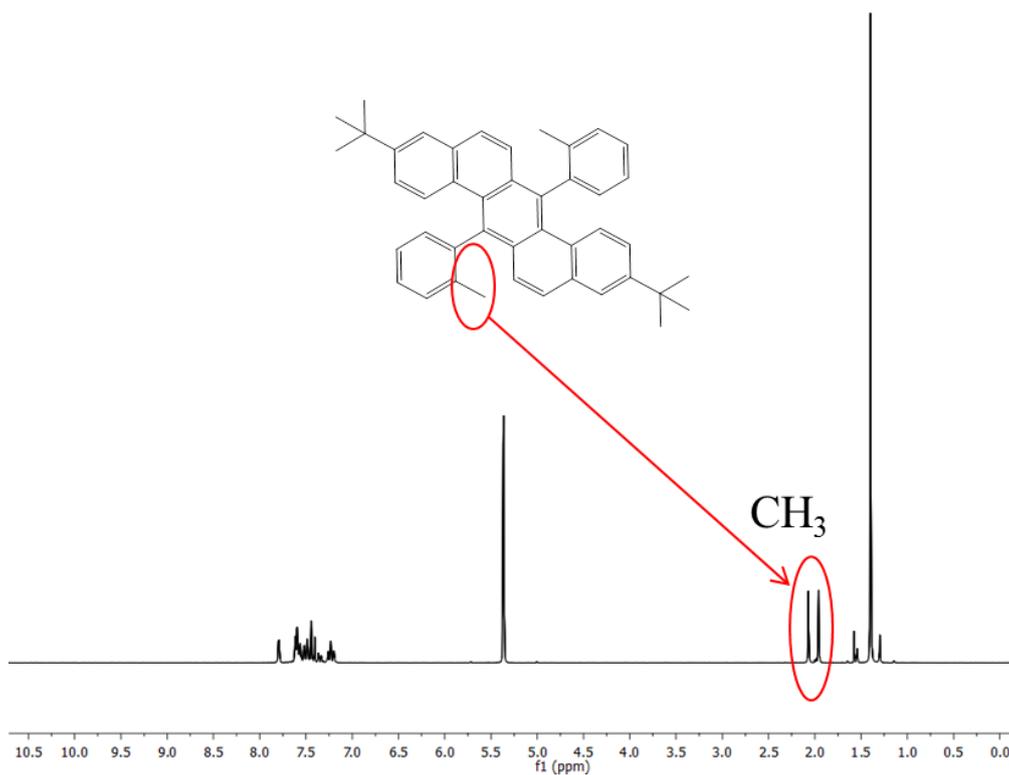
Figure **3-2**. ¹H-NMR spectrum of **3-11** (250 MHz, CD₂Cl₂) at r.t.
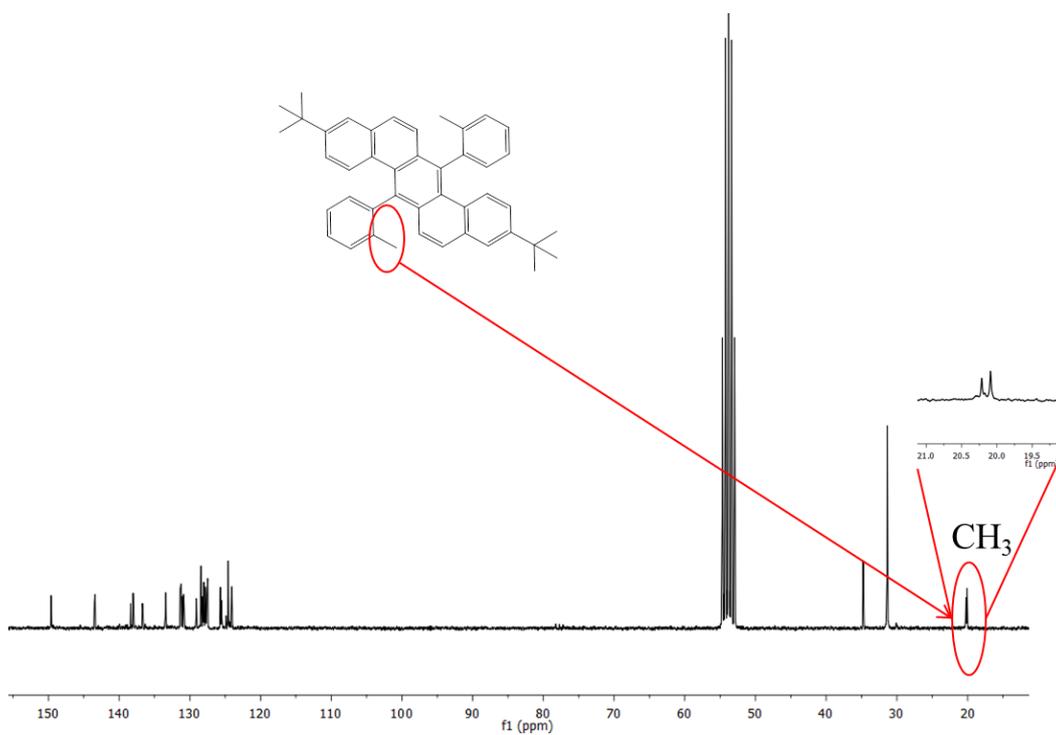
Figure **3-3**. ¹³C-NMR spectrum of **3-11** (250 MHz, CD₂Cl₂) at r.t.
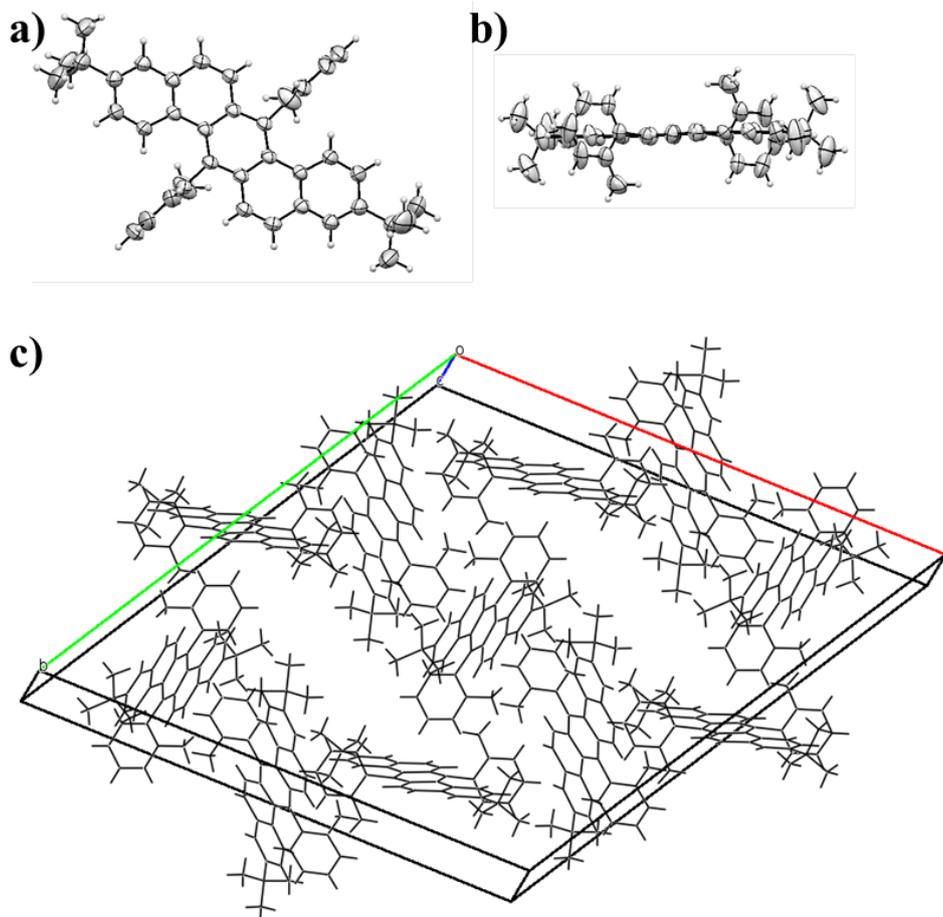
Figure **3-4**. Crystal structure of **3-11**. a) top view, b) side view, c) the packing of the **3-11**.
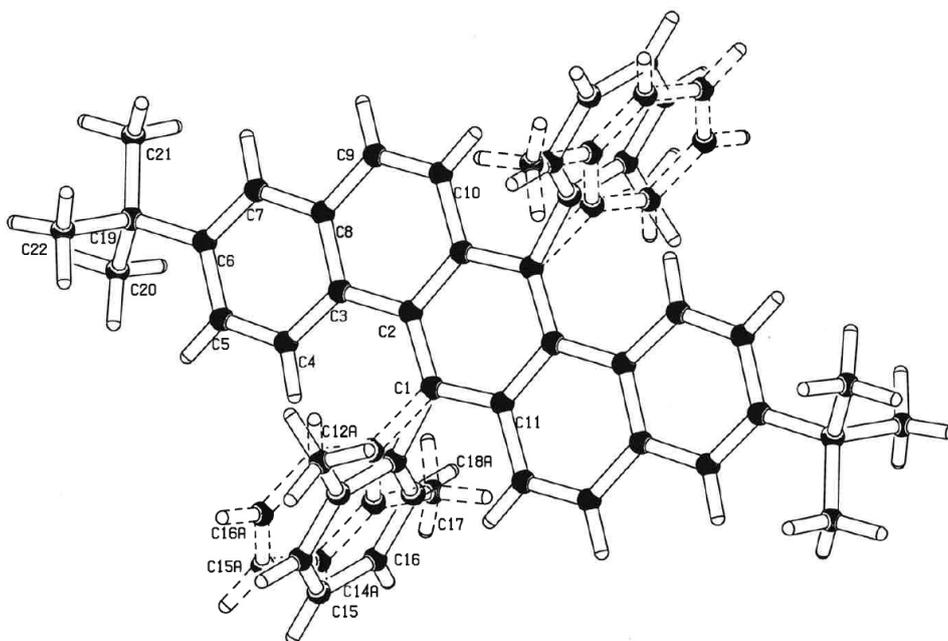

Figure **3-5**. Two conformers was observed with the methyl of compound **3-11**.

Secondly, the two methyl groups in compound **3-11** were transformed into dialdehyde **3-15** via a bromination-esterification-hydrolysis-oxidation sequence. Then, **3-15** was treated with mesitylmagnesium bromide to give diol compound **3-16**, which was subjected to a Friedel-Crafts alkylation promoted by BF$_3$•OEt$_2$ to afford compound **3-17**. Subsequently, compound **3-17** was oxidized by treatment with *p*-chloranil in dry toluene under argon, and after stirring at the room temperature for 12 hours, the final product **3-1** was obtained as a green solid through a silica gel column chromatography under argon (Scheme **3-3**). The chemical identity of **TBP 3-1** was unambiguously confirmed by MALDI-TOF MS analysis with solid-state sample preparation, as depicted in Figure **3-6**. There is only one dominant peak in the respective mass spectra of **TBP 3-1**, revealing its defined molecular composition. The isotopic distribution pattern of the mass peak is in good agreement with the calculated one.
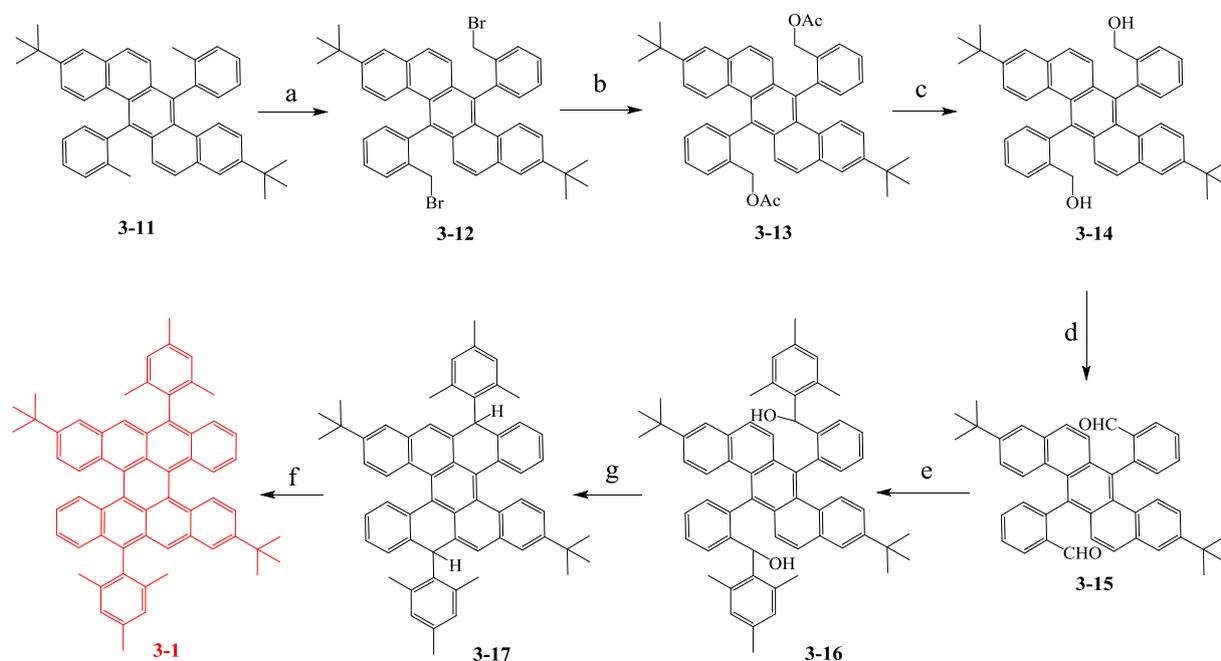
Scheme **3-3**. Synthetic route toward compound **TBP 3-1**. a) NBS, BPO, CCl$_4$, reflux. b) KOAc, Bu$_4$NBr, DMF, 100 °C, 57% in two steps from **3-11**. c) KOH (aq), THF/ethanol, reflux. d) PCC, DCM, r.t., 50% in two steps from **3-13**. e) mesitylmagnesium bromide, THF, r.t. f) BF$_3$·OEt$_2$, CH$_2$Cl$_2$, r.t. g) *p*-chloranil, toluene, r.t., 40% in three steps from **3-15**.
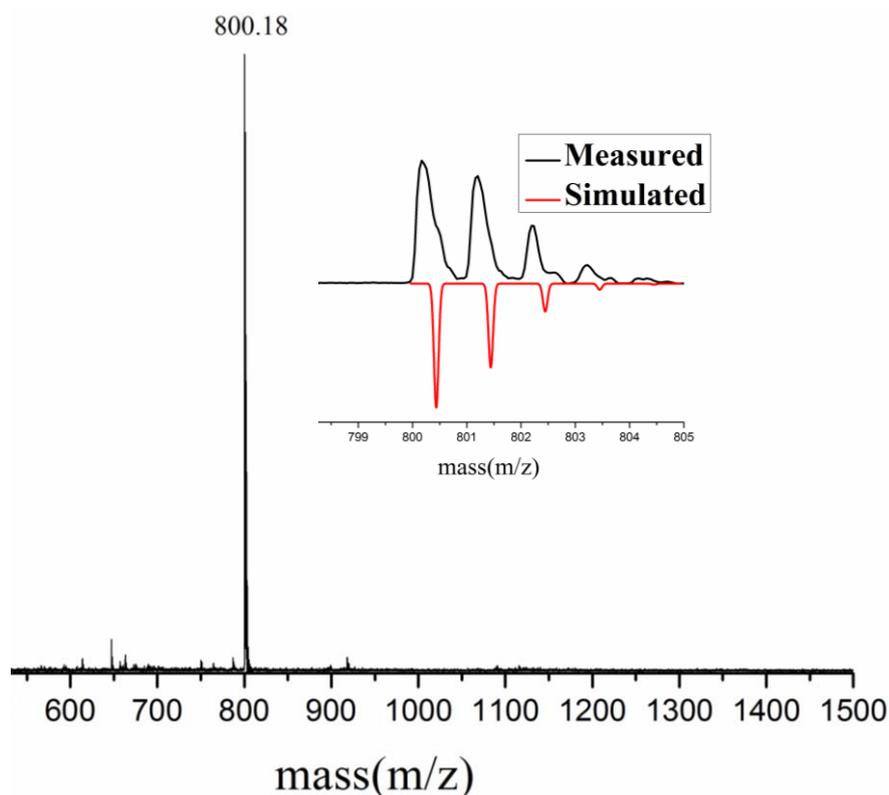
Figure **3-6**. MALDI-TOF spectra of **TBP 3-1** at solid state. Inset: MALDI-TOF MS of **TBP 3-1** with the calculated and measured isotopic pattern.
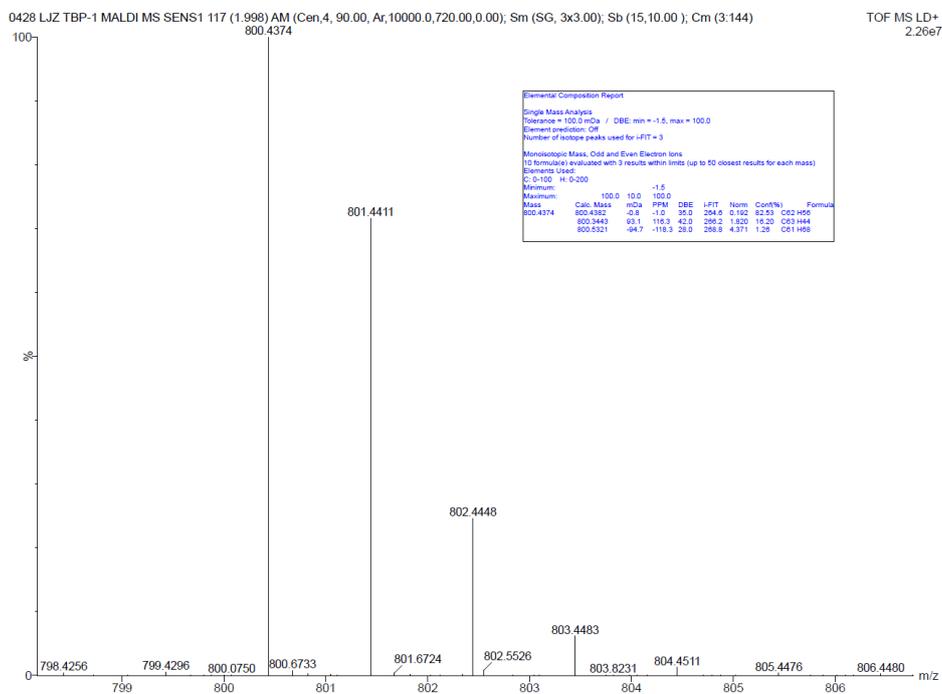

Figure **3-7**. HR-MS (MALDI) spectrum of compound **TBP 3-1**.
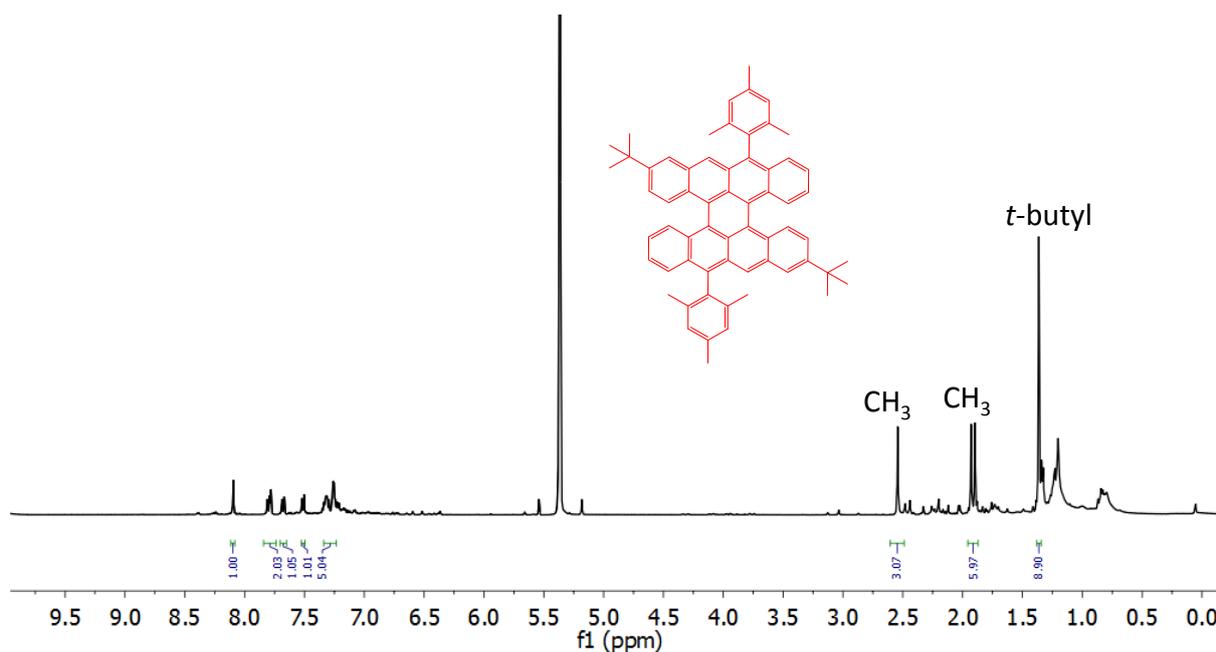
Figure **3-8**. ¹H-NMR spectrum of **TBP 3-1** (500 MHz, CD₂Cl₂) at -60 °**C**.
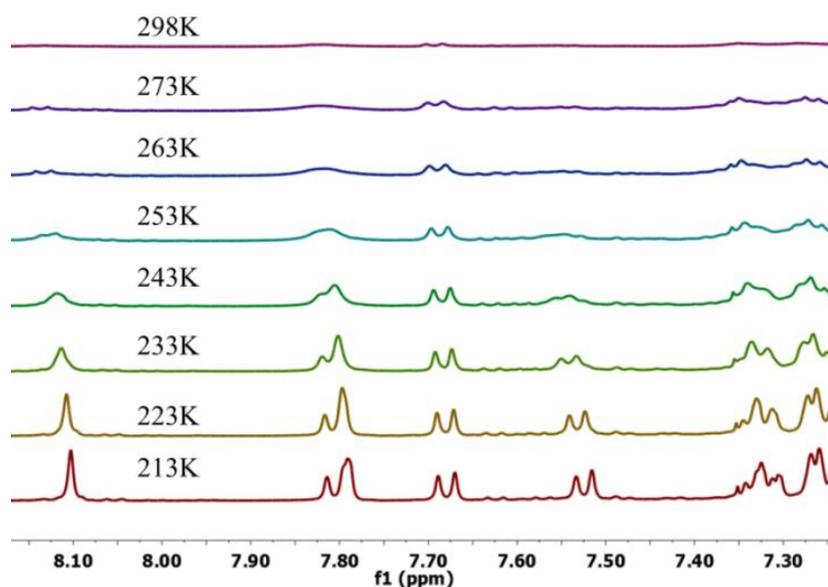

Figure **3-9**. Variable-temperature ¹H NMR spectra of **TBP 3-1** in CD₂Cl₂ in the aromatic region.

Then, **TBP 3-1** was further investigated by variable temperature ¹H-NMR spectra. A well-resolved ¹H-NMR spectrum in CD₂Cl₂ solution was obtained at 213 K (Figure **3-8**). Interestingly, when the temperature was increased, the peaks became weaker and disappeared at room temperature. The ¹H-NMR spectra of the aromatic region of **TBP 3-1** are depicted in Figure **3-9**. The NMR peaks could be assigned to the structure of **TBP 3-1** with the help of 2D-COSY NMR spectroscopy (Figure **3-11** and **3-12**). This process was reversible as cooling

back the sample to 213 K gave the same spectrum (Figure **3-10**). This result suggests a possible radical feature of **TBP 3-1** at room temperature. A similar phenomenon has been observed in biradicals based on phenalenyl,[24-29] zethrene[38-42] and teranthene[36,37], resulting from a thermally excited triplet specie which is slightly higher in energy than the singlet biradical state.
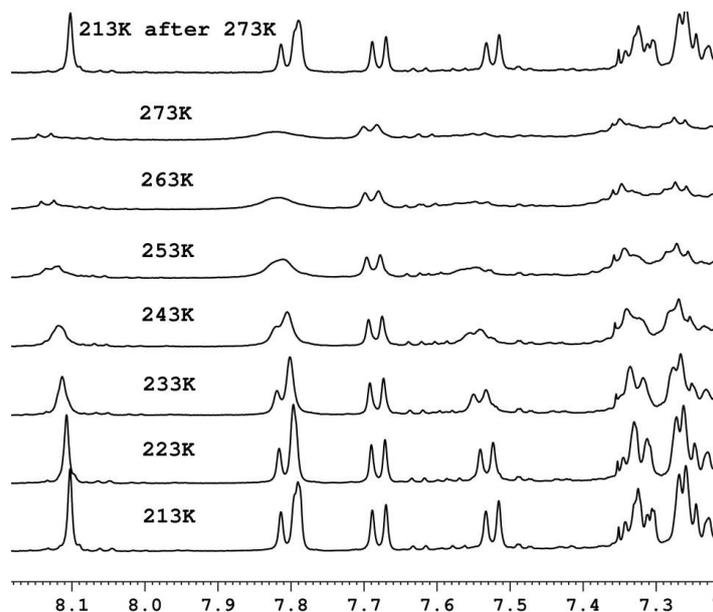


Figure **3-10**. Reversible ^{1}H NMR of compound **TBP 3-1** as cooling back the sample to 213 K yielding the same spectrum.
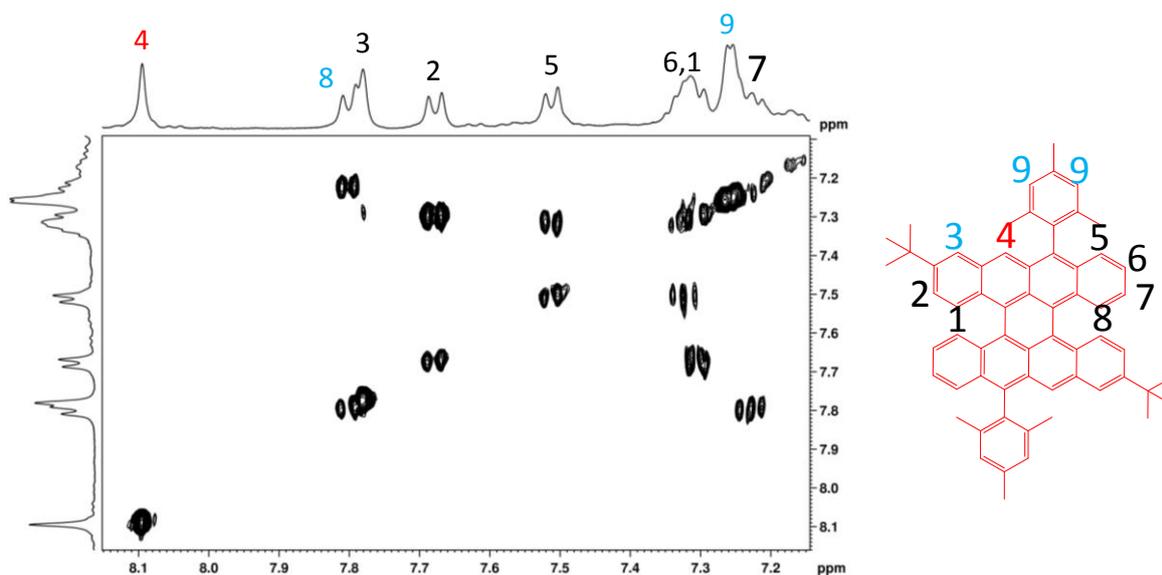

Figure **3-11**. 2D COSY NMR spectrum of **TBP 3-1** (500 MHz, CD$_2$Cl$_2$) at -60 °C.
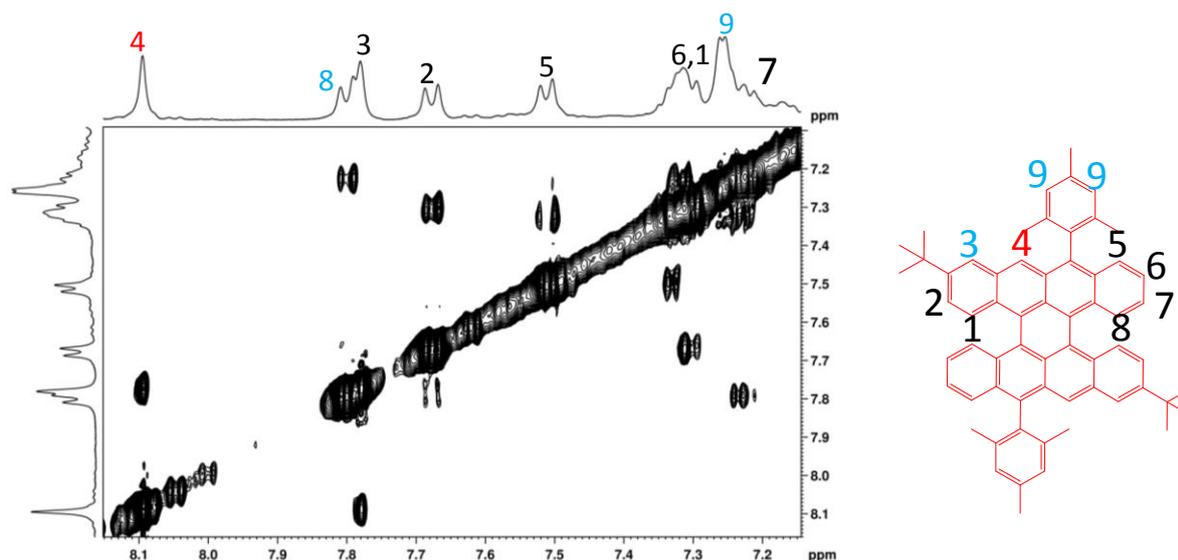
Figure **3-12**. 2D NOESY NMR spectrum of **TBP 3-1** (500 MHz, CD$_2$Cl$_2$) at -60 °C.

3.3 EPR analysis of bistetracene TBP 3-1

An electron paramagnetic resonance (EPR) measurement was carried out both in solution and in solid state to further confirm the biradical nature of **TBP 3-1** (Collaboration with Prof. ████████████████████). A freshly prepared solution of **TBP 3-1** in toluene gave unresolved EPR spectra for a biradical with a broad peak at *g*-value 2.0035 (Figure **3-13**). At the center of the broad peak a tiny low intensity peak was also observed which was attributed to a monoradical impurity. The powder sample of **TBP 3-1** was also EPR active indicating its biradical feature (Figure **3-14**). Upon increasing the temperature, the EPR signal intensity increased which is in agreement with the variable temperature ^{1}H-NMR measurements. The Bleaney Bower's fit of the intensity change in EPR signals with temperature in the solid state gave a singlet-triplet energy gap of 3.4 kcal/mol (Figure **3-16**). This result again supports the borderline character of **TBP 3-1** between a Kekulé structure and a biradical structure. Based on the NMR and EPR results we can safely conclude the biradical feature of compound **TBP 3-1**. The biradical structure of **TBP 3-1** can be described by four resonance forms, **3-1-1**, **3-1-2**, **3-1-3**, and **3-1-4** (Figure **3-1**). While the two radical centers are protected by bulky mesityl group in **3-1-1**, these two sites are unprotected in **3-1-2**. Thus, **TBP 3-1** was found to be unstable under ambient conditions. The time-dependent EPR measurement in toluene solution at room temperature indicated that the peak intensity decreased with the time, and that the signal almost disappeared after 72 hours (Figure **3-13**).
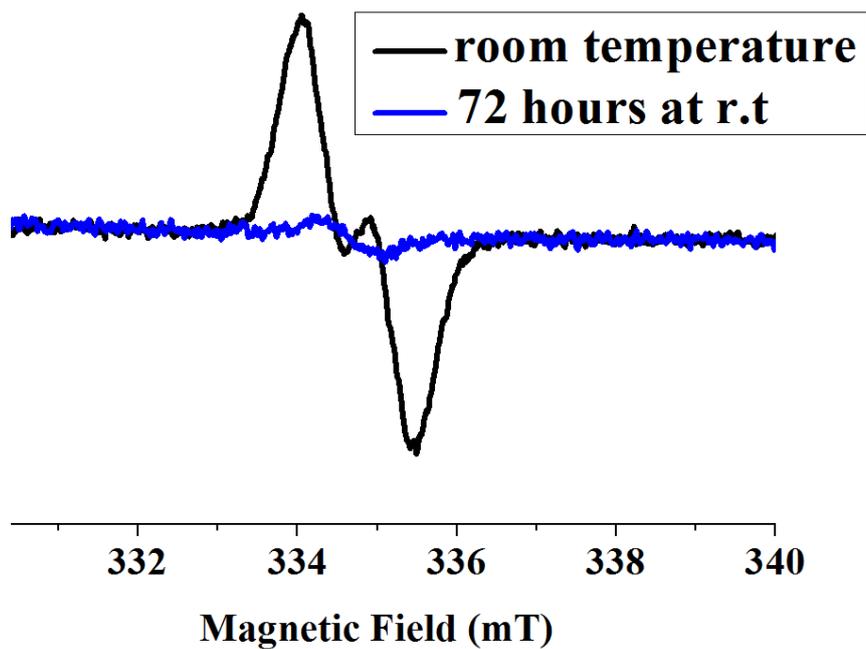
Figure **3-13**. EPR spectra of **TBP 3-1** in toluene solution at room temperature and after 72 hours.
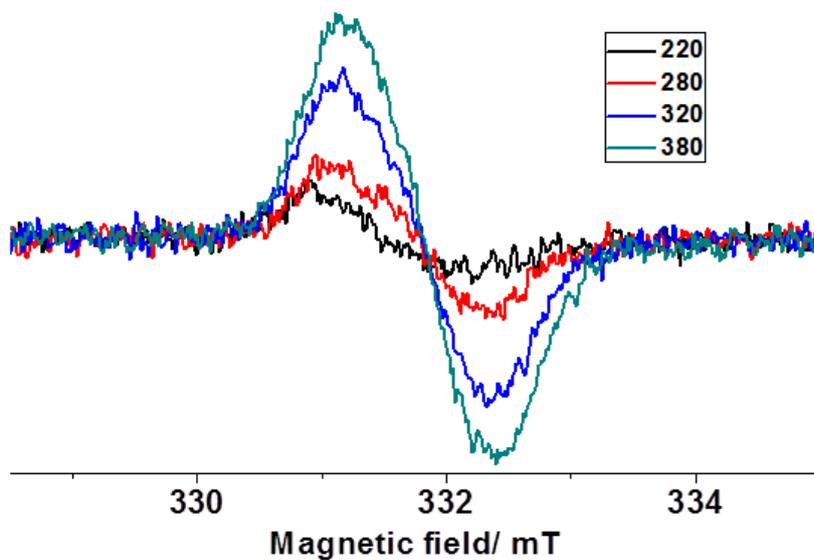
Figure **3-14**. EPR spectra of **TBP 3-1** in solid state at different temperatures.
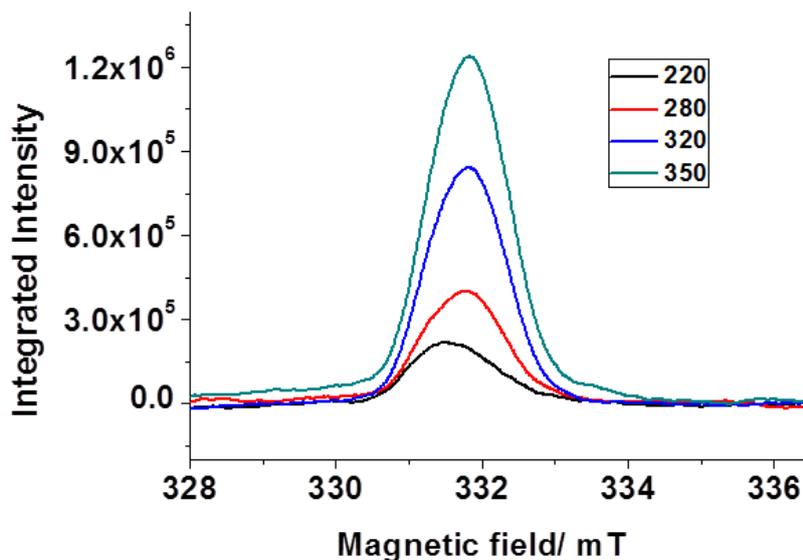
Figure **3-15**. The simulation of EPR spectra of **TBP 3-1** at solid state.
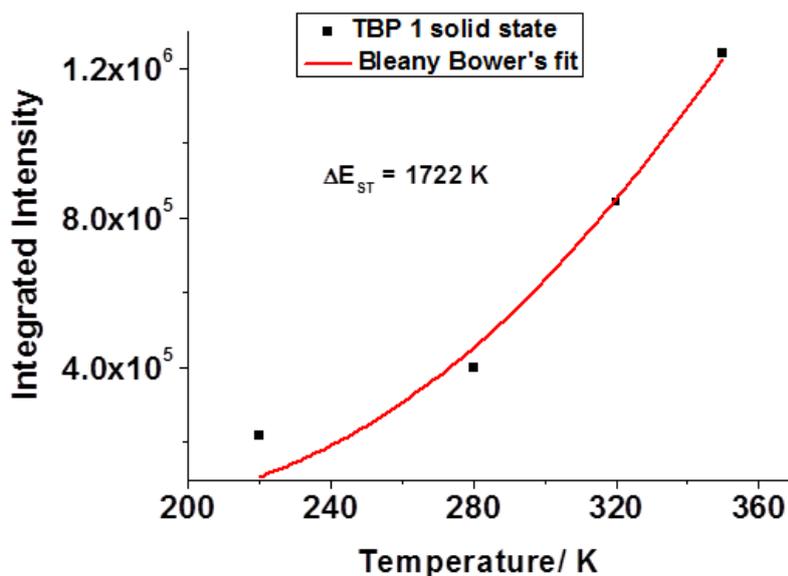
Figure **3-16**. The change in EPR signal intensity with temperature (black dot) and the Bleaney–Bower's fit (red line).

3.4 Optical Properties and oxidation process of TBP 3-1

Next, the UV-Vis absorption of precursor **3-17** and **TBP 3-1** were characterized. The absorption spectra of **3-17** and **TBP 3-1** in degassed and dry dichloromethane (DCM) solution are compared in Figure **3-17a**. Compound **3-17** exhibits a well-resolved absorption maximum

at 423 nm along with a small shoulder band peaking at 492 nm. Interestingly, the solution of **TBP 3-1** in DCM shows a green color and the absorption spectra yield a maximum in the near-infrared region (NIR) at 727 nm. From the onsets of its UV-vis absorption spectra, a low optical energy gap of 1.56 eV is derived for **TBP 3-1**. Moreover, **TBP 3-1** does not show any photoluminescence, which is a common behavior of biradicaloids.[37,40] This result again supports that both the Kekulé and biradical forms contribute similarly to the ground state. Notably, the color of **TBP 3-1** changed quickly when exposed to air, suggesting that oxidation took place at the zigzag edge of **TBP 3-1** as the reactive site. Thus, the time-dependent UV-Vis measurement was further performed under ambient condition to examine the stability of **TBP 3-1**. While the intensity of the absorption maximum in the NIR region (727 nm) decreased, the absorption peak at higher energy (295 nm) increased with time (Figure **3-17b**). The decay time (t) was obtained from the least square fitting by using the following equations; [44]

$$A(t)/A(0)=exp(-t\,/\tau) \text{ or} \tag{1}$$

$$A(t)/A(0)=\alpha\,exp(-t\,/\tau1) + (1-\alpha\,)\,exp(-t\,/\tau2) \tag{2}$$

where $A(t)$ is the absorbance of the low-energy λ_{max} at time t and τ is the lifetime, α is the purity of the radical and the contribution of $(1-\alpha)$ comes probably from the precursor. Then the calculated lifetime (τ) of **TBP 3-1** is approximately 35 min based on this equation. Finally, a red color was achieved for the oxidized product, which was identified as tetrabenzo[a,f,j,o]perylene-9,19-dione (**3-18**) (Figure **3-18**), as confirmed by NMR and MALDI-TOF MS analysis (Figures **3-19**, **3-20**, **3-21**, and **3-22**). With the help of 2D COSY NMR, the structure of compound **3-18** can be assigned as presented in Figure **3-22**. The UV-Vis absorption of **3-18** is compared with **TBP 3-1** in Figure **3-17a**. Apparently, compound **3-18** shows a significant blue shift (by 156 nm) for the visible-light absorption band relative to that of **TBP 3-1**, resulting in a relatively large optical energy gap of 2.04 eV compared to that of **TBP 3-1**. Furthermore, the cyclic voltammetry (CV) spectrum of the fresh compound **TBP 3-1** was conducted in degassed and dry dichloromethane solution (Figure **3-23**). From the CV spectrum, **TBP 3-1** shows one irreversible oxidation at -0.99 eV and two irreversible reductions at -1.40 and -1.78 eV. Apparently, the CV analysis suggests that **TBP 3-1** is electrochemically unstable, which is in agreement with our NMR, EPR, and optical results. In addition, we also try to introduce some bulky groups to stabilize **TBP 3-1** for further

examination (such as to grow the single crystal of **TBP 3-1**), but it unfortunately failed due to the steric hindrance (Scheme **3-4**).
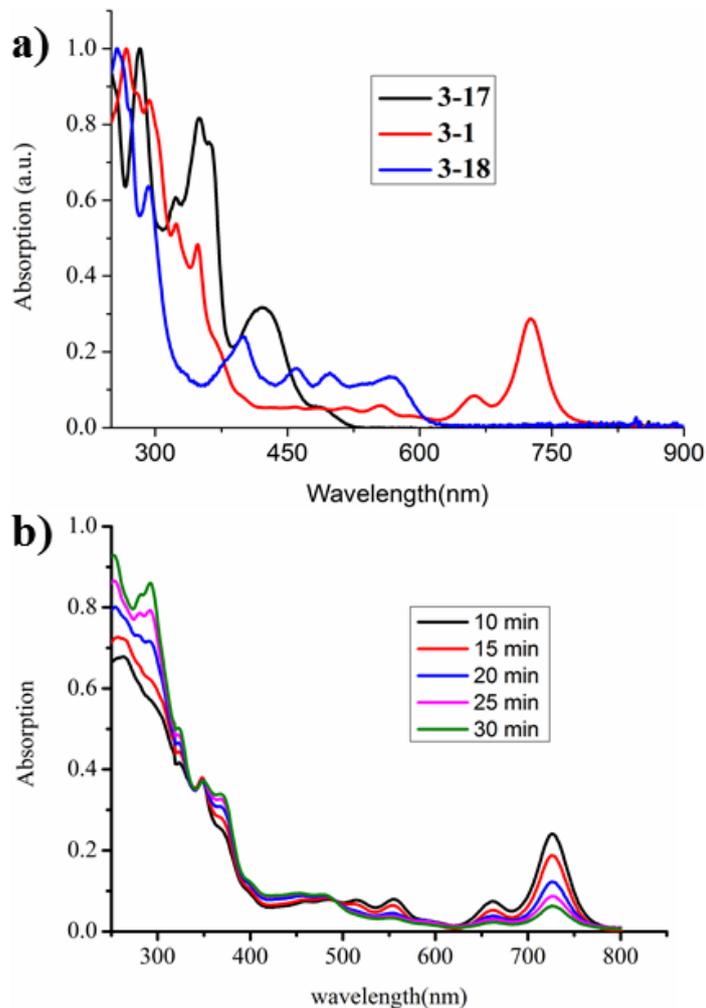
Figure **3-17**. a) UV-Vis spectra of the compounds **TBP 3-1**, **3-17** and **3-18**; b) time-dependent UV-Vis spectra of **TBP 3-1** at ambient condition.
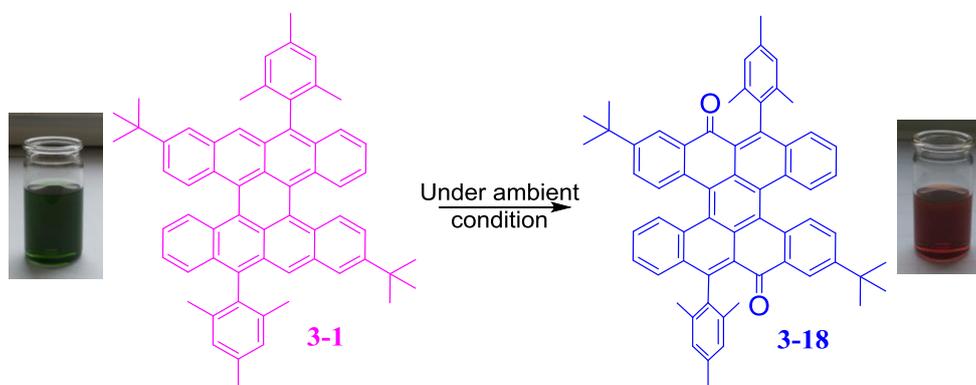
Figure **3-18**. Oxidation procedure from **TBP 3-1** to compound **3-18**.
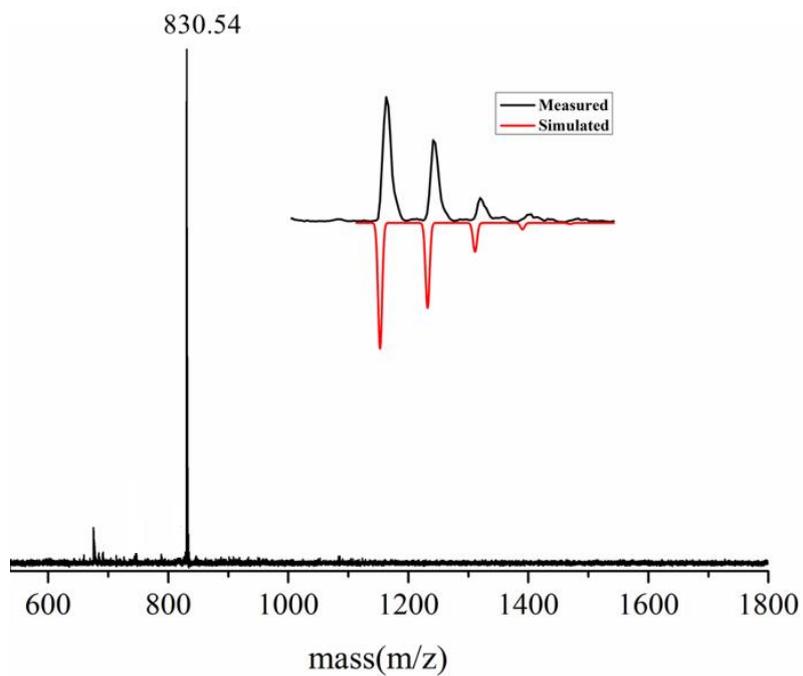
Figure **3-19**. MALDI-TOF spectra of compound **3-18**.
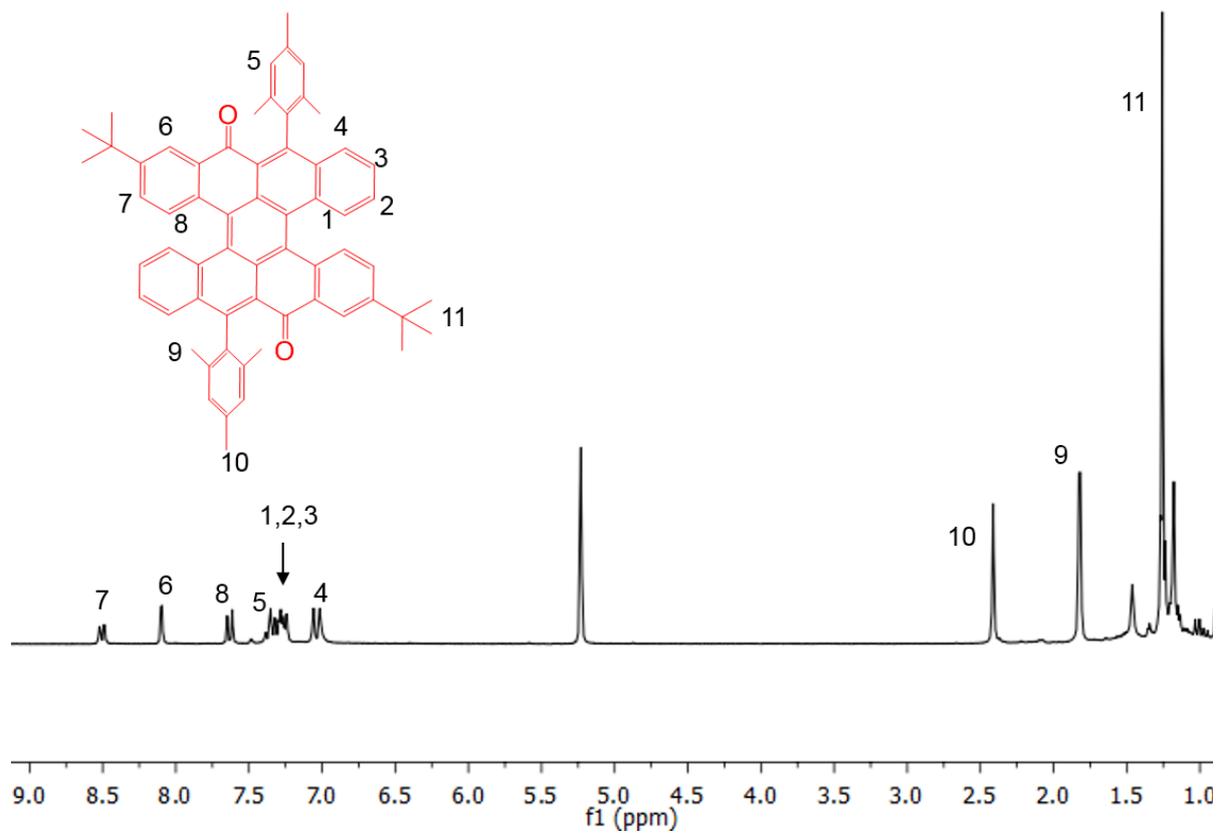
Figure **3-20**. ¹H-NMR spectra of compound **3-18** (300 MHz, CD$_2$Cl$_2$) at room temperature.
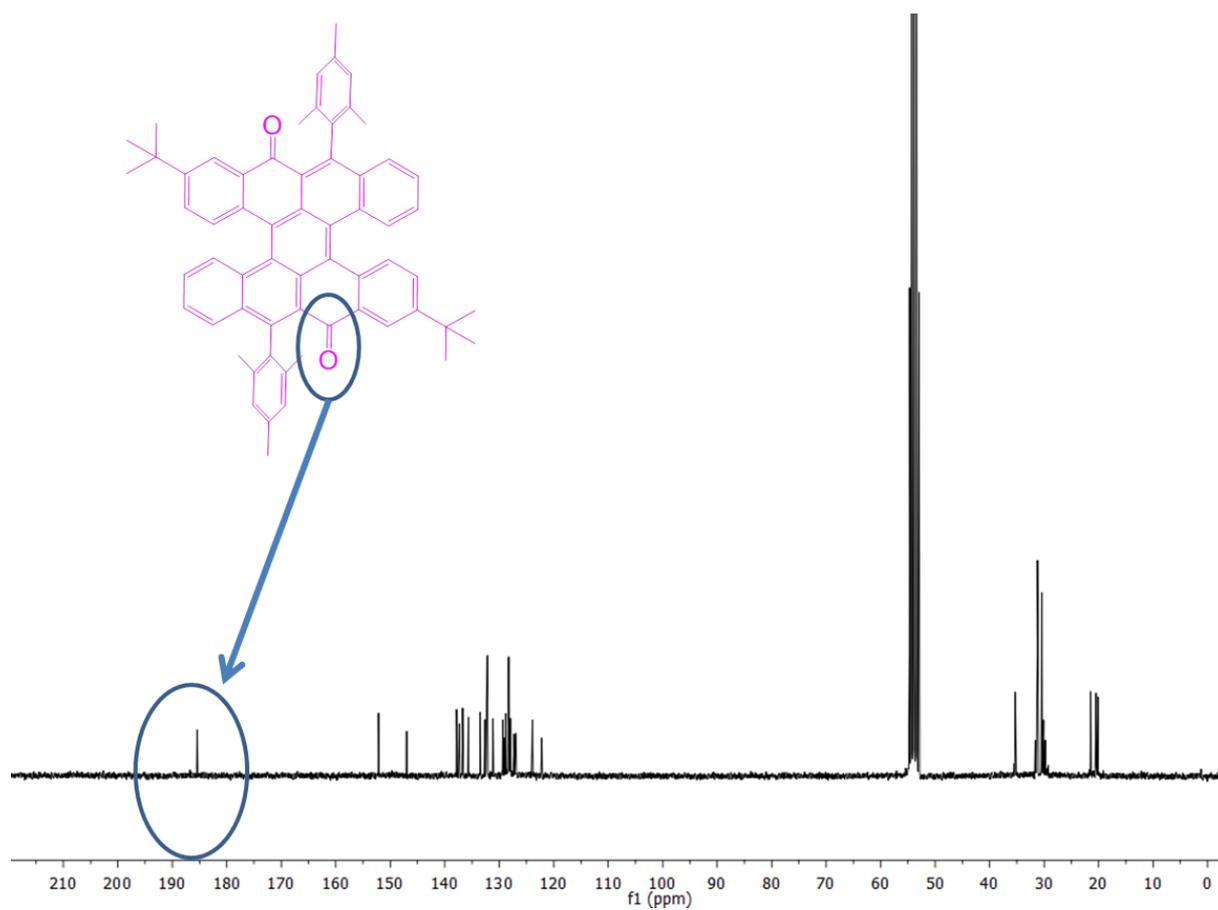
Figure **3-21**. ^{13}C-NMR spectra of compound **3-18** (300 MHz, CD$_2$Cl$_2$) at room temperature.
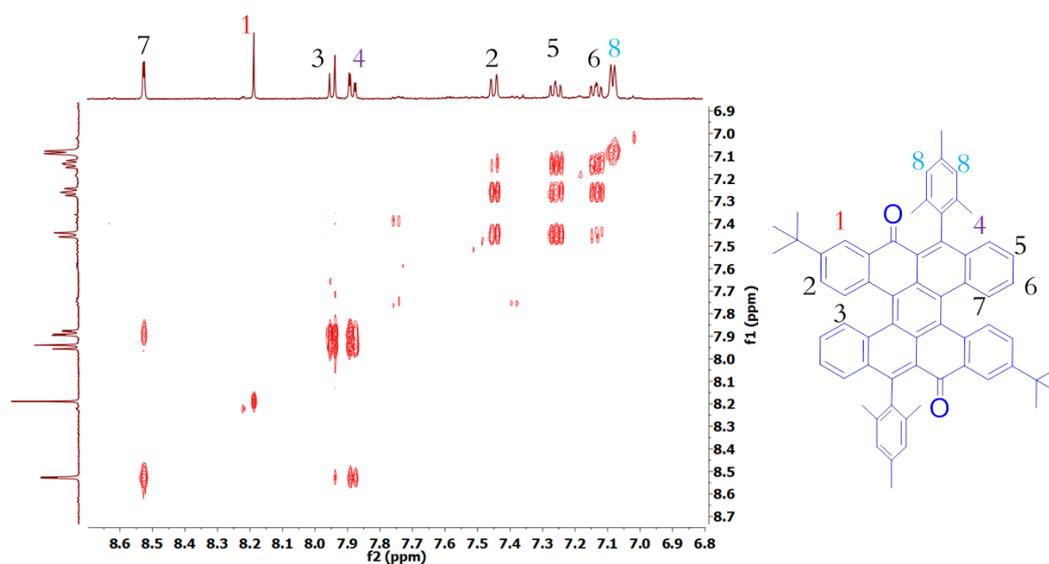
Figure **3-22**. 2D-COSY NMR spectrum of compound **3-18** (500 MHz, CD$_2$Cl$_2$) at room temperature.
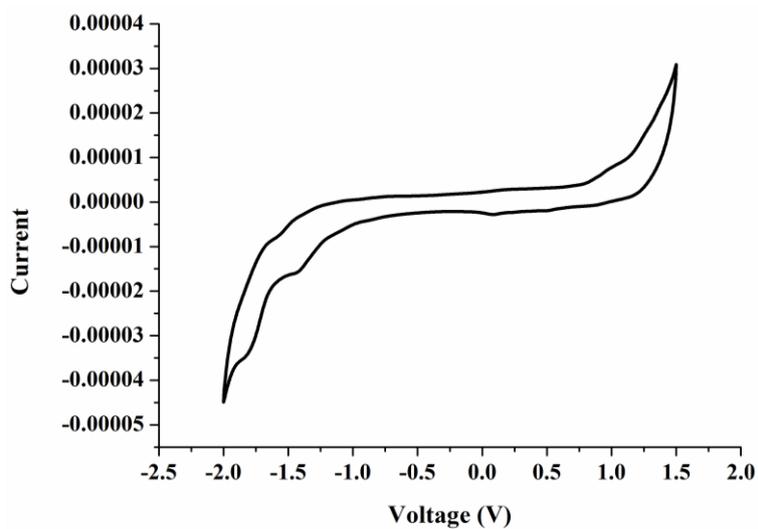
Figure **3-23**. Cyclic voltammetry of **TBP 3-1** in degassed and dry dichloromethane solution (scan rate 50 mV s^{-1}).
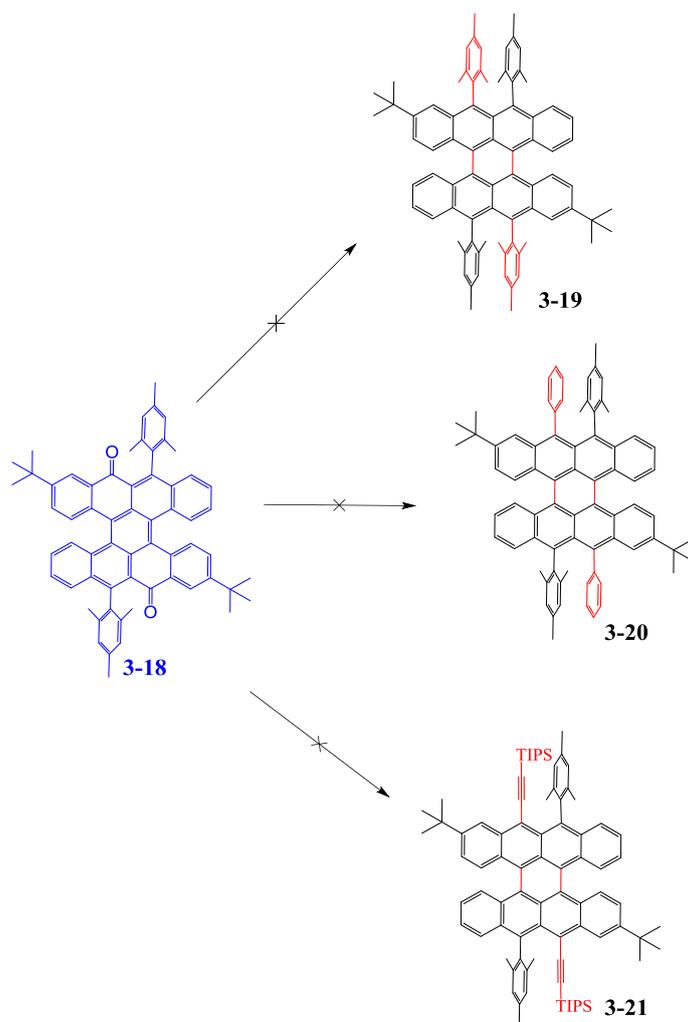
Scheme **3-4**. The strategy toward stable **TBP 3-1** with bulky groups.

3.5 Calculations

To gain an insight into the electronic structure of **TBP 3-1**, DFT calculations were conducted at the B3LYP/6-31G (d,p) level of theory using the Gaussian 09 program package. The DFT simulation geometry of **TBP 3-1** is depicted in Figure **3-24**. We can see that it adopts a non-planar π-conjugated carbon skeleton, due to the steric repulsion between the two C-H bonds. Thereby, there are two stereoisomers of **TBP 3-1**. From the calculation, we found that ***M*-TBP-1** is more stable than ***P*-TBP-1**. Furthermore, the calculated barrier for the interconversion of the isomers is about 284 kcal/mol. Similarly, ***M*-3-18** is more stable than ***P*-3-18** based on the calculation result. Moreover, UV-Vis spectroscopic calculations were performed at the AM1/CIS and TD-DFT levels of theory.[45,46] Both methods indicate one main absorption band in the low-energy (high wavelength) spectra domain (750-800 nm), as shows in Figure **3-25**.
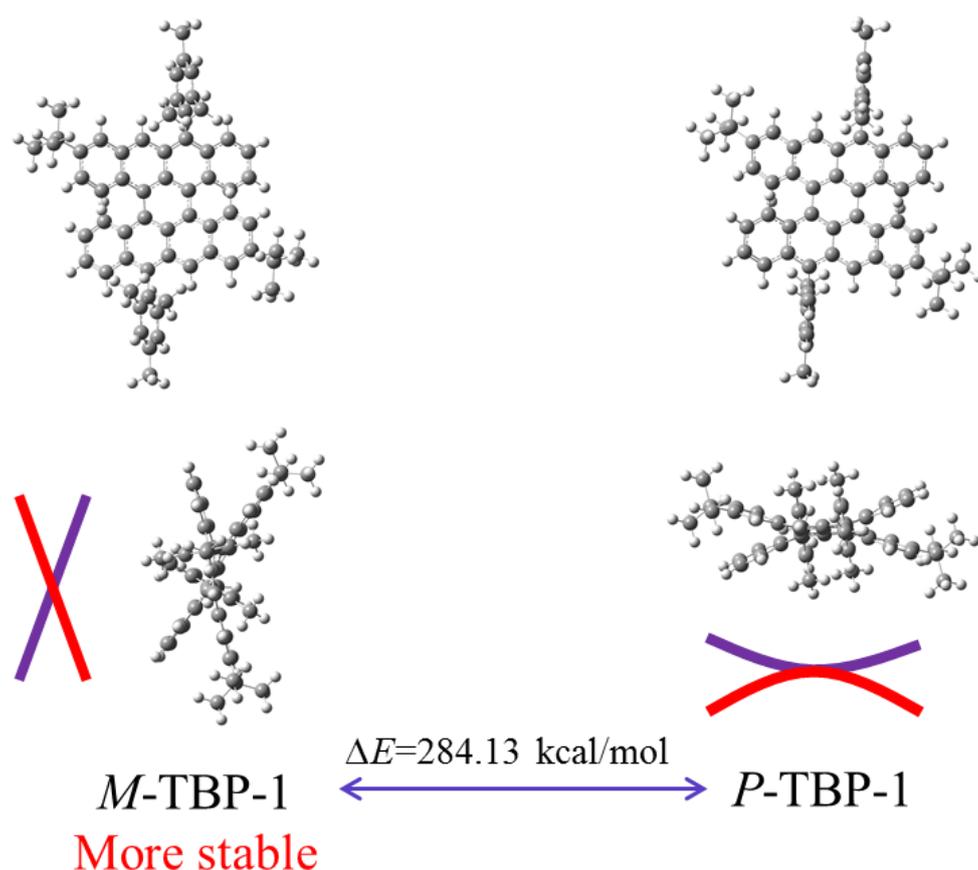
Figure **3-24**. DFT simulation geometry of **TBP 4-1**.
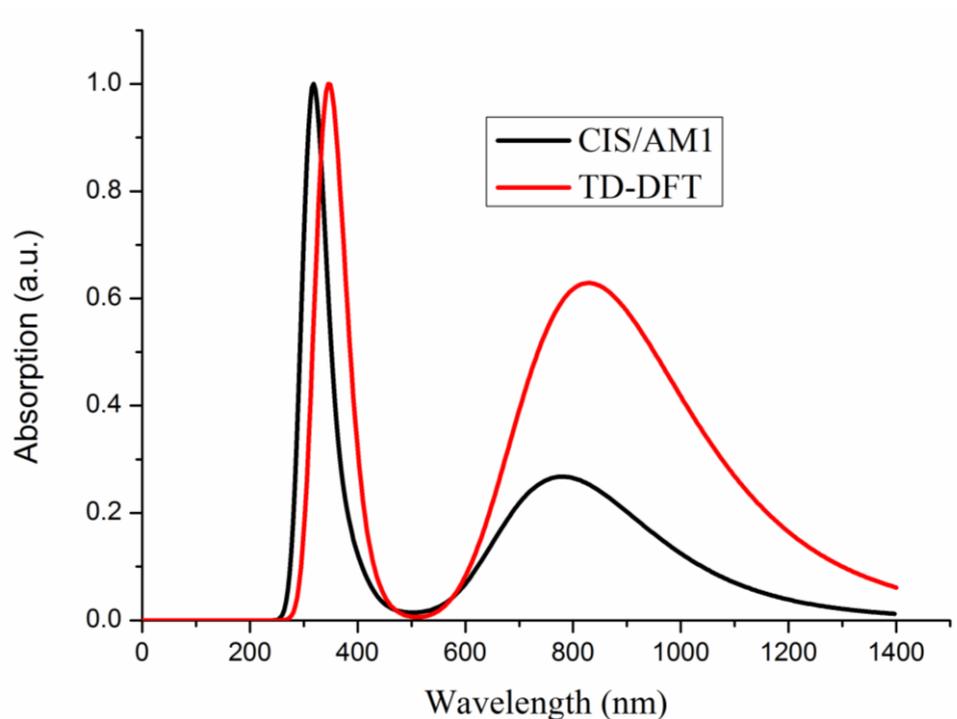
Figure **3-25**. UV-Vis spectra of **TBP 3-1** from the simulation.

Singlet biradical character index (y) was estimated using a symmetry-broken UB3LYP/6-31G (d, p) method along with geometry optimization.[47] The index y, related to the HOMO and LUMO for singlet states, is defined by the weight of the doubly-excited configuration in the multi-configurational MC-SCF theory, and is formally expressed in the case of the spin-projected UHF (PUHF) theory [48,49] as

$$y=1-2T/(1+T^2),$$

where T is the orbital overlap between the corresponding orbital pairs, and can be calculated using the occupation numbers of UHF natural orbitals:

$$T=(n_{HOMO}-n_{LUMO})/2$$

The calculations reveal that the bistetracene **TBP 3-1** has a moderate singlet biradical character index (y = 0.615). This result is in agreement with the above NMR and EPR analysis, which demonstrates the biradicaloid nature of **TBP 3-1**. The SOMO α and β orbitals and spin density are highly delocalized (Figure **3-26**). While the carbons C5 and C6 have the largest spin densities, the adjacent carbons C4 and C7 show much smaller spin densities (Figure **3-26b**). These results indicate that the **TBP 3-1** should be described as a resonance form between the Kekulé and biradical structure shown in Figure **3-1**. Furthermore, it was found that the energy of the singlet biradical state is lower than that of the triplet biradical and

closed shell state (**Table 3-1**). From the calculation, the singlet-triplet energy gap ($\Delta E_{\text{S-T}}$) is -6.7 kcal/mol, meaning that **TBP 3-1** features a singlet biradical ground state. In addition, the harmonic oscillator model of aromaticity (HOMA)[50,51] values, which are geometry based aromaticity indices, indicates more benzenoid character for the peripheral and central six-membered rings (Figure **3-27**). These findings strongly suggest that the formation of aromatic sextets overwhelms the penalty for breaking one π-bond and pushes the resulting unpaired electrons out to the zigzag edges.[37]
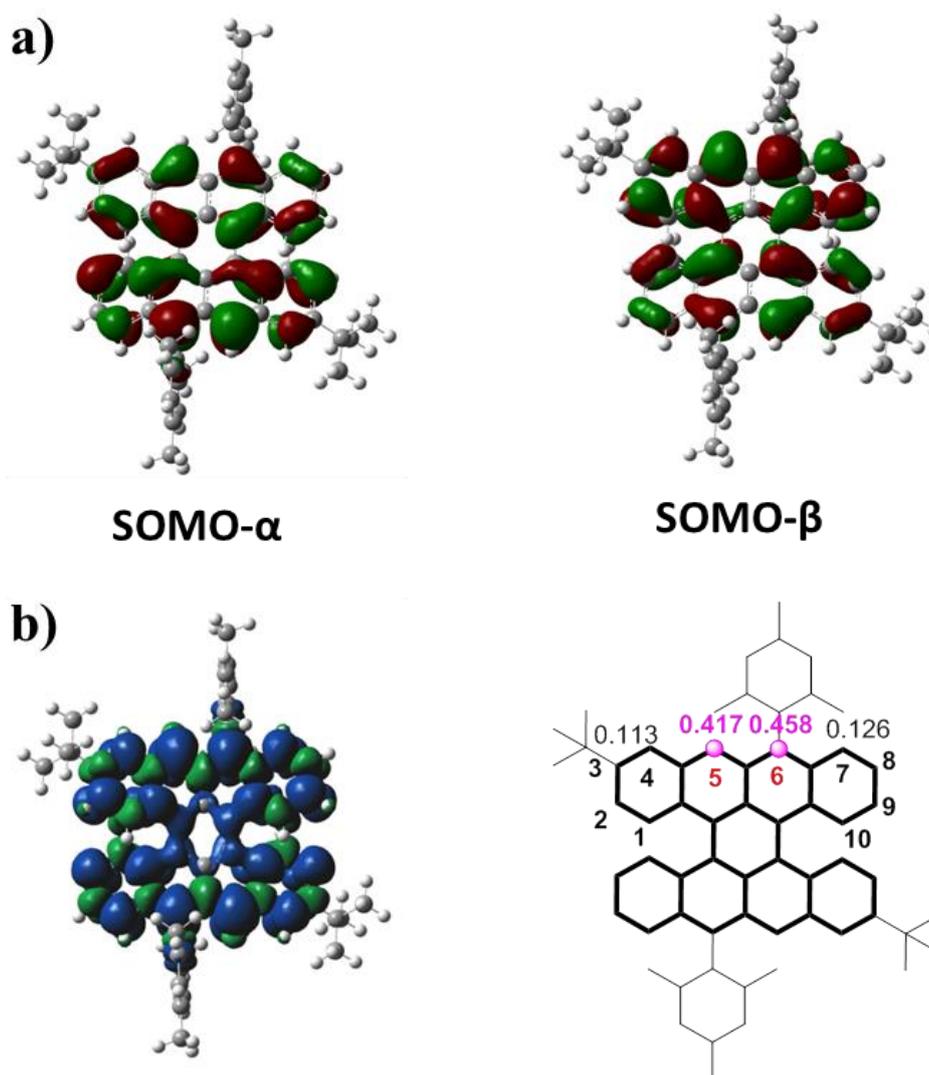
Figure **3-26**. a) Calculated SOMOs for the α and β electrons of the singlet biradical of **TBP 3-1**. b) The spin density distribution of the triplet ground state of the bistetracene **TBP 3-1** and the numbers given in pink denote the spin density of the specific carbon atoms.

Table **3-1**. The energy level of **TBP 3-1** from the theory calculation.

	Singlet close shell E, eV (CS)	Singlet open shell E, eV (BS)	S^2 (BS)	E, eV (triplet)	S^2 (triplet)	ΔE_{ST} eV	ΔE_{ST} kcal/mol
3-1	65211.254929	65211.264153	0.4125	65210.992389	2.058	0.27	6.27
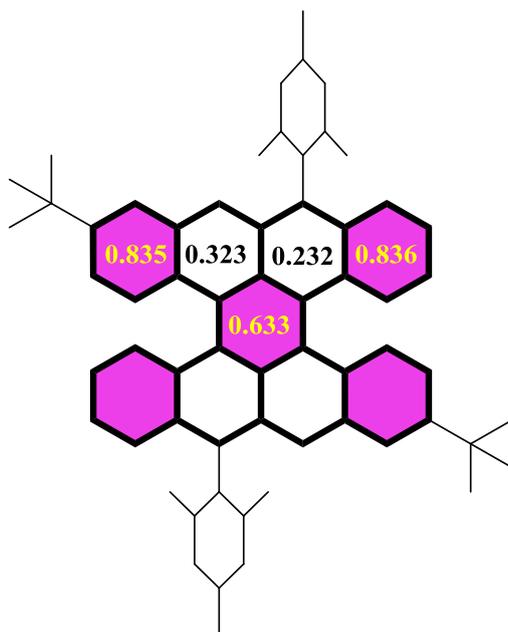
Figure **3-27**. Harmonic-Oscillator Model of Aromaticity (HOMA) values of **TBP 3-1**.

The HOMA values were obtained by using the following equations; [50]

$$\text{HOMA} = 1 - \alpha/n \sum (R_{opt} - R_{ij})^2$$

where n is the number of bonds taken into summation and α is an empirical constant fixed in a way to give HOMA = 0 for a Kekulé structure of the typical aromatic system and qual to 1 for the system with all bonds equal to the optimal value R_{opt}. To apply the HOMA index to study the aromatic character of a given π-electron system, the following data are needed: the precise geometry of the molecule in question, i.e., its bond lengths R_{ij}; the R_{opt} values for all types of bonds existing in the molecule in question; and the respective values of the constant α.

3.6 Conclusions

In summary, we have successfully synthesized the tetrabenzo[a,f,j,o]perylene, namely "bistetracene" with two tetracenes connected side by side with two bonds, for the first time. Such a zigzag-edged PAH exhibits a remarkable singlet biradical feature as proven by variable temperature ^{1}H-NMR and EPR spectroscopies, which is well supported by DFT calculations. Such zigzag-edged PAH can be considered as a short segment of infinite graphene nanoribbons with exceptionally long zigzag edges. Therefore, our studies contribute to an understanding of the edge states of expanded PAH homologues and graphene nanoribbons which may possess a localized nonbonding π-state around the zigzag edges. It is envisioned that these zigzag edged PAHs are promising candidates for the development of spintronics given that the edge localized spins can be polarized by applying external magnetic/electrical fields.

References:

[1] J. E. Anthony, *Chem. Rev.* **2006**, 106, 5028-5048.

[2] J. E. Anthony, *Angew. Chem. Int. Ed.* **2008**, 47, 452-483.

[3] Q. Ye, C. Chi, *Chem. Mater.* **2014**, 26, 4046-4056.

[4] A. Hepp, H. Heil, W. Weise, M. Ahles, R. Schmechel, H. Seggern, *Phys. Rev. Lett.* **2003**, 91, 157406.

[5] H. Moon, R. Zeis, E. J. Borkent, C. Besnard, A. J. Lovinger, T. Siegrist, C. Kloc, Z. Bao, *J. Am. Chem. Soc.* **2004**, 126, 15322-15323.

[6] J. E. Anthony, J. S. Brooks, D. L. Eaton, S. R. Parkin, *J. Am. Chem. Soc.* **2001**, 123, 9482-9483.

[7] Y. Diao, B. C. K. Tee, G. Giri, J. Xu, D. H. Kim, H. A. Becerril,R. M. Stoltenberg, T. H. Lee, G. Xue, S. C. B. Mannsfeld, Z. Bao, *Nat. Mater.* **2013**, 12, 665-671.

[8] G. Giri, E. Verploegen, S. C. B. Mannsfeld, S. Atahan-Evrenk, D. H. Kim, S. Y. Lee, H. A. Becerril, A. Aspuru-Guzik, M. F. Toney, Z. Bao, *Nature* **2011**, 480, 504-508.

[9] B. Purushothaman, M. Bruzek, S. R. Parkin, A. F. Miller, J. E. Anthony, *Angew. Chem. Int. Ed.* **2011**, 50, 7013-7017.

[10] C. Tçnshoff, H. F. Bettinger, *Angew. Chem. Int. Ed.* **2010**, 49, 4125-4128.

[11] D. E. Jiang, S. Dai, *Chem. Phys. Lett.* **2008**, 466, 72-75.

[12] F. Moscardó, E. San-Fabián, *Chem. Phys. Lett.* **2009**, 480, 26-30.

[13] L. B. Roberson, J. Kowalik, L. M. Tolbert, C. Kloc, R. Zeis, X. L. Chi, R. Fleming, C. Wilkins, *J. Am. Chem. Soc.* **2005**, 127, 3069-3075.

[14] B. H. Northrop, J. E. Norton, K. N. Houk, J. *Am. Chem. Soc.* **2007**, 129, 6536-6546.

[15] Z. Sun, J. Wu, *J. Mater. Chem.* **2012**, 22, 4151-4160.

[16] Z. Sun, Q. Ye, C. Chi, J. Wu, *Chem. Soc. Rev.* **2012**, 41, 7857-7889.

[17] J. Li, K. Zhang, X. Zhang, K. Huang, C. Chi, J. Wu, *J. Org. Chem.* **2010**, 75, 856-863.

[18] E. H. Fort, P. M. Donovan, L. T. Scott, *J. Am. Chem. Soc.* **2009**, 131, 16006-16007.

[19] Z. Sun, Z. Zeng, J. Wu, *Acc.Chem.Res.* **2014**, 47, 2582-2591.

[20] Z. Sun, Z. Zeng, J. Wu, *Chem. Asian J.* **2013**, 8, 2894-2904.

[21] A. Shimizua, M. Nakanob, Y. Hirao, T. Kubo, *J. Phys. Org. Chem.* **2011**, 24, 876-882.

[22] T. Kubo, *Chem. Rec.* **2014**, DOI: 10.1002/tcr.201402065.

[23] P. Ravat, M. Baumgarten, *Phys. Chem. Chem. Phys.* **2015**, 17, 983-991.

[24] K. Ohashi, T. Kubo, T. Masui, K. Yamamoto, K. Nakasuji, T. Takui, Y. Kai, I. Murata, I. *J. Am. Chem. Soc.* **1998**, 120, 2018-2027.

[25] T. Kubo, M. Sakamoto, M. Akabane, Y. Fujiwara, K. Yamamoto, M. Akita, K. Inoue, T. Takui, K. Nakasuji, *Angew. Chem. Int. Ed.* **2004**, 43, 7474-6479.

[26] T. Kubo, A. Shimizu, M. Sakamoto, M. Uruichi, K. Yakushi, M. Nakano, D. Shiomi, K. Sato, T. Takui, Y. Morita, K. Nakasuji, *Angew. Chem. Int. Ed.* **2005**, 44, 6564-6568.

[27] A. Shimizu, M. Uruichi, K. Yakushi, H. Matsuzaki, H. Okamoto, M.Nakano, Y. Hirao, K. Matsumoto, H. Kurata, T. Kubo, *Angew. Chem. Int. Ed.* **2009**, 48, 5482-5486.

[28] A. Shimizu,a Y. Hirao, K. Matsumoto, H. Kurata, T. Kubo, M. Uruichi, K. Yakushi, *Chem. Commun.* **2012**, 48, 5629-5631.

[29] K. Uchida, Y. Hirao, H. Kurata, T. Kubo, S, Hatano, K. Inoue, *Chem. Asian J.* **2014**, 9, 1823-1829.

[30] A. Le Berre, *Ann. Chim.* **1957**, 13, 371-425.

[31] D. T. Chase, A. G. Fix, B. D. Rose, C. D. Weber, S. Nobusue, C. E. Stockwell, L. N. Zakharov, M. C. Lonergan, M. M. Haley, *Angew. Chem. Int. Ed.* **2011**, 50, 11103-11106.

[32] D. T. Chase, B. D. Rose, S. P. McClintock, L. N. Zakharov, M. M. Haley, *Angew. Chem. Int. Ed.* **2011**, 50, 1127-1130.

[33] D. T. Chase, A. G. Fix, S. J. Kang, B. D. Rose, C. D. Weber, Y. Zhong, L. N. Zakharov, M. C. Lonergan, C. Nuckolls, M. M. Haley, *J. Am. Chem. Soc.* **2012**, 134, 10349-10352.

[34] A. Shimizu, Y. Tobe, *Angew. Chem. Int. Ed.* **2011**, 50, 6906-6910.

[35] A. Shimizu, R. Kishi, M. Nakano, D. Shiomi, K. Sato, T. Takui, I. Hisaki, M. Miyata, Y. Tobe, *Angew. Chem. Int. Ed.* **2013**, 52, 1-5.

[36] A. Konishi, Y. Hirao, M Nakano, A. Shimizu, E. Botek, B. Champagne, D. Shiomi, K. Sato, T. Takui, K. Matsumoto, H. Kurata, T. Kubo, *J. Am. Chem. Soc.* **2010**, 132, 11021-11023.

[37] A. Konishi, Y. Hirao, K. Matsumoto, H. Kurata, R. Kishi, Y. Shigeta, M. Nakano, K. Tokunaga, K. Kamada, T. Kubo, *J. Am. Chem. Soc.* **2013**, 135, 1430-1437.

[38] Z. Sun, K. W. Huang, J. Wu, *J. Am. Chem. Soc.* **2011**, 133, 11896-11899.

[39] Y. Li, W. K. Heng, B. S. Lee, N. Aratani, J. L. Zafra, N. Bao, R. Lee, Y. M. Sung, Z. Sun, K. W. Huang, R. D. Webster, J. T. L. Navarrete, D. Kim, A. Osuka, J. Casado, J. Ding, J. Wu, *J. Am. Chem. Soc.* **2012**, 134, 14913-14922.

[40] Z. Sun, S. Lee, K. H. Park, X. Zhu, W. Zhang, B. Zheng, P. Hu, Z. Zeng, S. Das, Y. Li, C. Chi, R. W. Li K. W. Huang J. Ding, D. Kim, J. Wu, *J. Am. Chem. Soc.* **2013**, 135, 18229-18236.

[41] S. Das, S. Lee, M. Son, X. Zhu, W. Zhang, B. Zheng, P. Hu, Z. Zeng, Z. Sun, W. Zeng, R. W. Li, K. W. Huang, J. Ding, D. Kim, J. Wu, *Chem. Eur. J.* **2014**, 20, 11410-11420.

[42] Y. Li, K. W. Huang, Z. Sun, R. D. Webster, Z. Zeng, W. Zeng, C. Chi, K. Furukawa, J. Wu, *Chem. Sci.* **2014**, 5, 1908-1914.

[43] E. Clar, The Aromatic Sextet; Wiley: London, 1972.

[44] Y. Kawanaka, A. Shimizu, T. Shinada, R. Tanaka, Y. Teki, *Angew. Chem. Int. Ed.* **2013**, 52, 6643-6647.

[45] R. Bauernschmitt, R. Ahlrichs, *Chem. Phys. Lett.* **1996**, 256, 454-464.

[46] J. B. Foresman, M. Head-Gordon, J. A. Pople, M. J. Frisch, *J. Phys. Chem.* **1992**, 96, 135-149.

[47] S. Markovi, S. Radenkovi, Z. Markovi, I. Gutman. *Russ. J. Phys. Chem. A*, **2011**, 85, 2368-2372.

[48] M. Nakano, R. Kishi, A. Takebe, M. Nate, H. Takahashi, T. Kubo, K. Kamada, K. Ohta, B. Champagne, E. Botek. *Co. Le.* **2007**, 3, 333.

[49] S. Yamanaka, M. Okumura, M. Nakano, and K. Yamaguchi, *J. Mol. Struct. (Theochem)* **1994**, 310, 205-218.

[50] J. Kruszewski, T. M. Krygowski, Tetrahedron Lett. 1972, 13, 3839-3842.

[51] T. M. Krygowski, *J. Chem. Inf. Comput. Sci.* **1993**, 33, 70-78.

Chapter 4. Dibenzo[*a,m*]rubicene: Pentagon-Embedded Bistetracene

In chapter 3, we have demonstrated the synthesis of a novel tetrabenzo[*a,f,j,o*]perylene, namely "bistetracene" in which two tetracenes are connected side by side with two bonds. Theoretical calculations and physical property investigations manifest that such bistetracene possesses a prominent biradical character in the ground state. However, the bistetracene can easily undergo oxidation into tetrabenzo[*a,f,j,o*]perylene-9,19-dione (diketone) under ambient conditions. Thereby, the stabilization is the critical issue for such PAHs. In this chapter, a novel dibenzo[*a,m*]rubicene, which can be considered as pentagon-embedded bistetracene, was synthesized, as a result of the phenyl migration of a key intermediate 6,7,13,14-tetraphenylbenzo[*k*]tetraphene during the Scholl reaction. Such pentagon-containing PAHs show higher stability than conventional bistetracene consisting only of six-membered rings. A possible mechanism for the phenyl ring migration during the cyclodehydrogenation is proposed, providing a unique and unprecedented entry to extend the stable *peri*-tetracene or *peri*-pentacene like molecules with five-membered rings, even eight-membered rings in the future.

4.1 Introduction

Polyacenes are prominent examples of semiconducting materials for device applications.[1-3] However, the longer acenes, such as hexacene, and higher homologues, are susceptible to oxidation and photolytic degradation under ambient conditions, which causes difficulties in their synthesis.[4,5] Great efforts have been dedicated to synthesize stable liner polyacene systems in the past decades.[6-10] In general, there are mainly two established strategies to prepare stable polyacenes: one avenue is exploration of compounds containing five or seven membered rings in acene-like structures, rather than the traditional acenes solely consisting of six-membered rings.[11-13] Another attractive strategy is the introduction of heteroatoms, such as sulfur, nitrogen, and oxygen atoms, into the acene frameworks to form stable heteroacenes.[14,15] On our way to pursue the synthesis of *peri*-fused acene molecules, we meet similar challenges. For example, in our previous work (in the chapter 3), the zigzag-edged bistetracene exhibits a remarkable singlet biradical feature, but can easily undergo oxidation

into tetrabenzo[a,f,j,o]perylene-9,19-dione (diketone) under ambient conditions. Up to now, the largest reported *peri*-fused acene with experimental evidence is *peri*-pentacene, which could only be detected by mass spectrometry in the residue after sublimation of pentacene.[16,17] Following the above-mentioned strategies for the stabilization of the higher homologue of acenes, we envisage the incorporation of five- or seven-membered rings in the *peri*-fused acene systems. In this chapter, a novel dibenzo[*a,m*]rubicene, namely pentagon-embedded bistetracene, was synthesized through the cyclodehydrogenation of a key intermediate 6,7,13,14-tetraphenylbenzo[*k*]tetraphene.
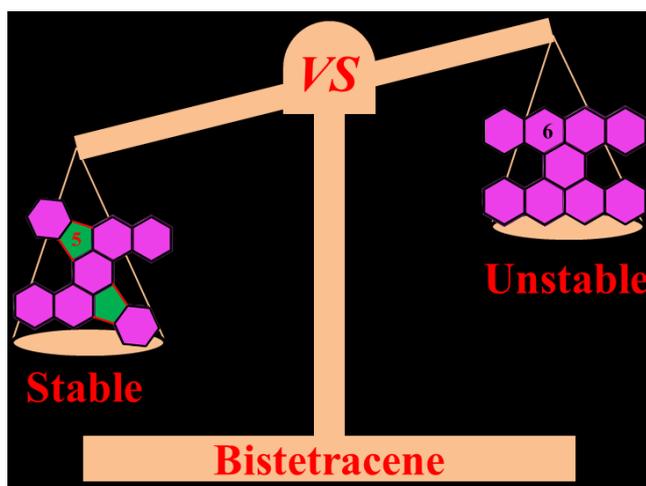

Figure **4-1**. Structure of pentagon-embedded bistetracene and bistetracene.

Dehydrogenation is a chemical reaction that involves the elimination of hydrogen from organic molecules, which, as a consequence, are oxidized. The formation of symmetrical C-C bonds by the oxidative homocoupling of benzene and its derivatives to yield poly(*p*-phenylene)s was achieved in the pioneering studies by Scholl et al during the early 1920s,[18, 19] by using various Lewis acid/oxidant combinations. Although the detailed mechanism of the Scholl reaction remains elusive, two principal reaction pathways have been proposed, namely, the radical cation and the arenium cation routes.[20] The intramolecular adaptations of these oxidative methods have been applied towards the synthesis of π-conjugated systems with extended aromatic frameworks, especially polycyclic aromatic hydrocarbons (PAHs), starting from oligophenylenes.[21, 22] As a typical representative among the all-benzenoid PAHs, hexa-*peri*-hexabenzocoronene (HBC), which is a disc-like molecule, and many of its derivatives have been successfully synthesized via the intramolecular Scholl reaction under mild conditions.[23, 24] Although the synthetic methods for HBCs are relatively simple and versatile, certain drawbacks and limitations have been encountered. In particular, the scope of the

substituent groups is limited by its compatibility with the final cyclodehydrogenation step. For instance, our group previously reported the cyclodehydrogenation of *p*-dimethoxy-hexaphenylbenzene (**4-1**), which gives two unexpected products, namely *m*-dimethoxy-HBC **4-2** and bisspirocyclic dienone **4-3** (Scheme **4-1**).[25] This result suggests that the course of the intramolecular Scholl reaction is to some extent subject to the judicious choice of substituents. Furthermore, the migration of alkyl groups under Friedel-Crafts conditions[26,27] and skeletal rearrangements leading to planar PAHs from "nonplanarizable" oligophenylenes[28] as well as the degenerate rearrangement of biphenyl[29] under Lewis acid catalysis have been observed previously. Here, we demonstrate the cyclodehydrogenation of 6,7,13,14-tetraphenylbenzo[*k*]tetraphene (**4-5**), which gives two unexpected products, namely 5,14-diphenyldibenzo[*a,m*]rubicene (**4-7**) and (*R*)-9b,14-diphenyldibenzo[*a,m*]rubicen-5(9b*H*)-one **4-8**, instead of the expected 5,14-diphenyltetrabenzo[*a,cd,j,lm*]perylene (**4-6**) (Scheme **4-2**). To the best of our knowledge, this is the first example showing migration of phenyl substituents that leads to the formation of five-membered rings during the cyclodehydrogenation process. Furthermore, the mechanism for the phenyl migration is proposed, providing a unique and unprecedented entry to extend the scope of stable *peri*-tetracenes and *peri*-pentacenes like molecules with five- and seven-membered rings.
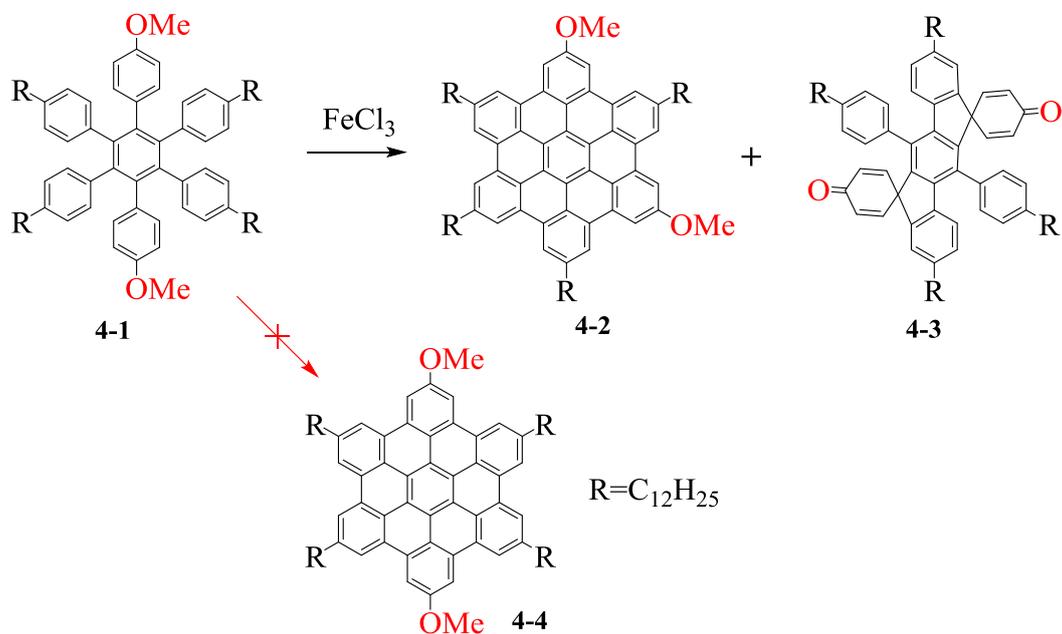

Scheme **4-1**.Cyclodehydrogenation of *p*-dimethoxy-substituted hexaphenylbenzene **4-1** to give unexpected *m*-dimethoxy-substituted **4-2** and bis-spirocyclic dienone **4-3**.
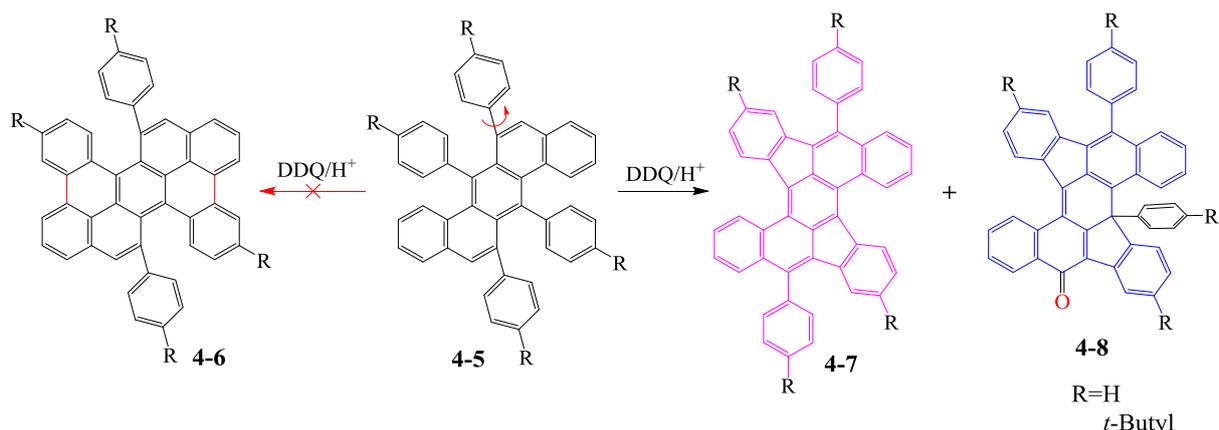
Scheme **4-2**. Cyclodehydrogenation of tetraphenylbenzo[*k*]tetraphene (**4-5**) to give unexpected diphenyldibenzo[*a,m*]rubicene (**4-7**) and diphenyldibenzo[*a,m*]rubicen-5(9b*H*)-one (**4-8**).

4.2 Synthesis and structure verification of 4-7 and 4-8

In this work, compounds **4-7** and **4-8** were synthesized as depicted in Scheme **4-3**. First, a selective Suzuki coupling between 1,4-dibromo-2,5-diiodobenzene (**4-9**) and commercially available (4-(*tert*-butyl)phenyl)boronic acid gave the 2',5'-dibromo-4,4''-di-*tert*-butyl-1,1':4',1''-terphenyl (**4-10**) in 72% yield. Afterwards, compound (2-((4-(*tert*-butyl)phenyl)ethynyl)phenyl)boronic acid (**4-13**) was obtained through Sonogashira coupling and boration. Then 4''-(*tert*-butyl)-5'-(4-(*tert*-butyl)phenyl)-2-((4-(*tert*-butyl)phenyl)ethynyl)-4'-(2-((4-(*tert*-butyl)phenyl)ethynyl)phenyl)-1,1':2',1''-terphenyl (**4-14**) was prepared by Suzuki coupling of **4-10** with **4-13** in 50% yield. ICl-induced cyclization was subsequently performed to afford 6,7,13,14-tetrakis(4-(*tert*-butyl)phenyl)-5,12-diiodobenzo[k]tetraphene (**4-15**) in 85% yield. Next, the iodine atom was removed by using *n*-BuLi to provide 6,7,13,14-tetrakis(4-(*tert*-butyl)phenyl)benzo[*k*]tetraphene (**4-5**) in 53% yield. Finally, the treatment of **4-5** with 2,3-dichloro-5,6-dicyano-1,4-benzoquinone (DDQ)/trifluoromethanesulfonic acid (CF$_3$SO$_3$H) as the oxidant/Lewis acid in dry DCM at 0 °C under argon, afforded compound **4-7** as reddish brown powder in 65% yield and **4-8** as red powder in 5% yield. The chemical identity of **4-7** and **4-8** was unambiguously confirmed by MALDI-TOF MS, NMR, and single-crystal X-ray analyses, as depicted in Figures **4-2** to **4-5**.
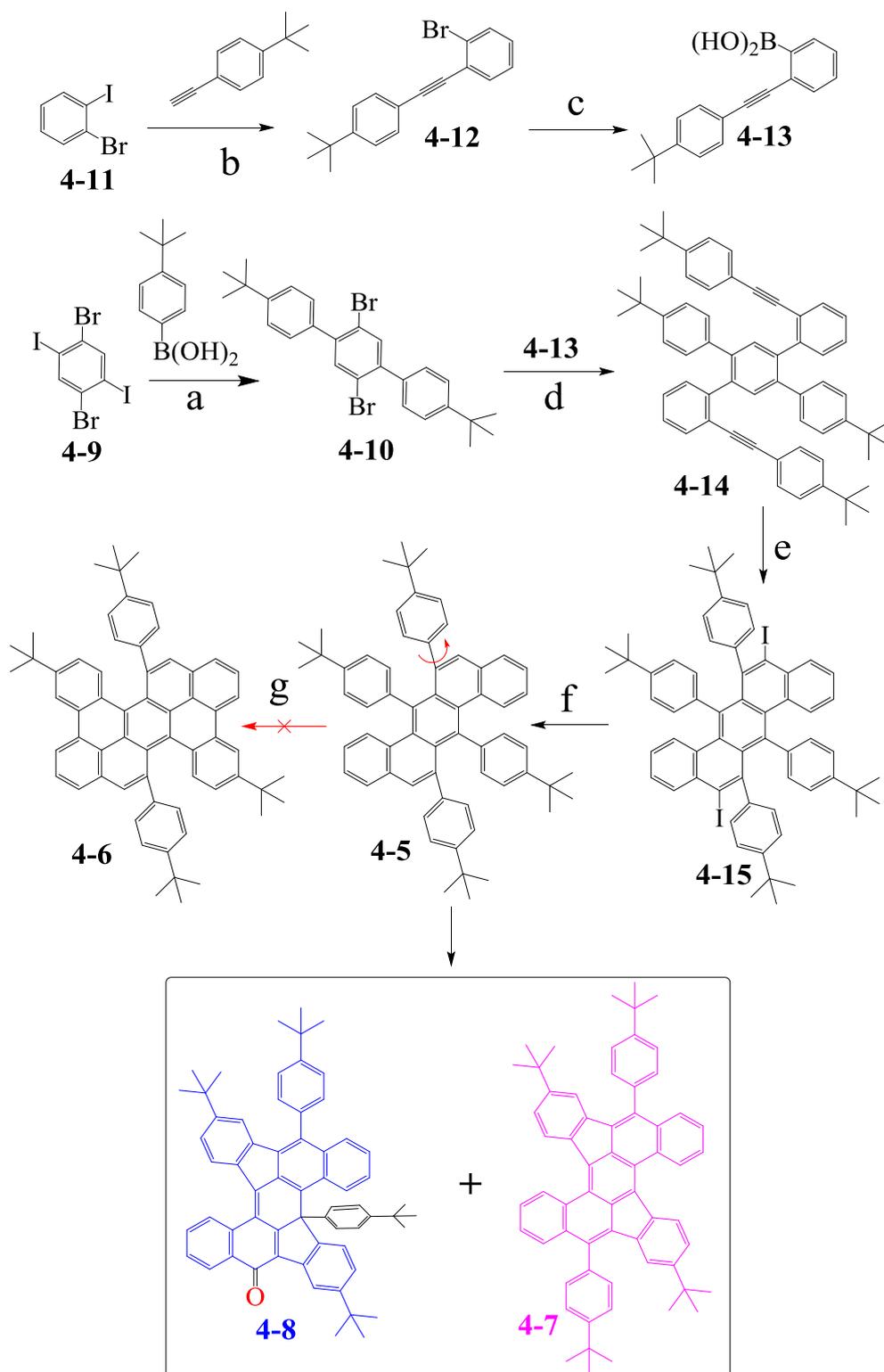
Scheme **4-3**. Synthesis of compounds **4-7** and **4-8**. (a) Pd(PPh₃)₄/K₂CO₃, dioxane/H₂O, 90 °C, 24 h, 71.8%. (b) PdCl₂(PPh₃)₂, CuI, Et₃N, THF, r.t, 92.4%. (c) *n*-BuLi, THF, B(OiPr)₃, −78 °C to r.t, direct for next step. (d) Pd(PPh₃)₄/K₂CO₃, dioxane/H₂O, 95 °C, 24 h, 49.7%. (e) ICl 1 M in DCM, DCM, −78 °C, 3 h, 85.4%. (f) *n*-BuLi, THF, MeOH, 1 h, 52.6%. (g) DDQ/ CF₃SO₃H, DCM, 0 °C, 1 h, **4-7**: 64.8%, **4-8**: 5%.
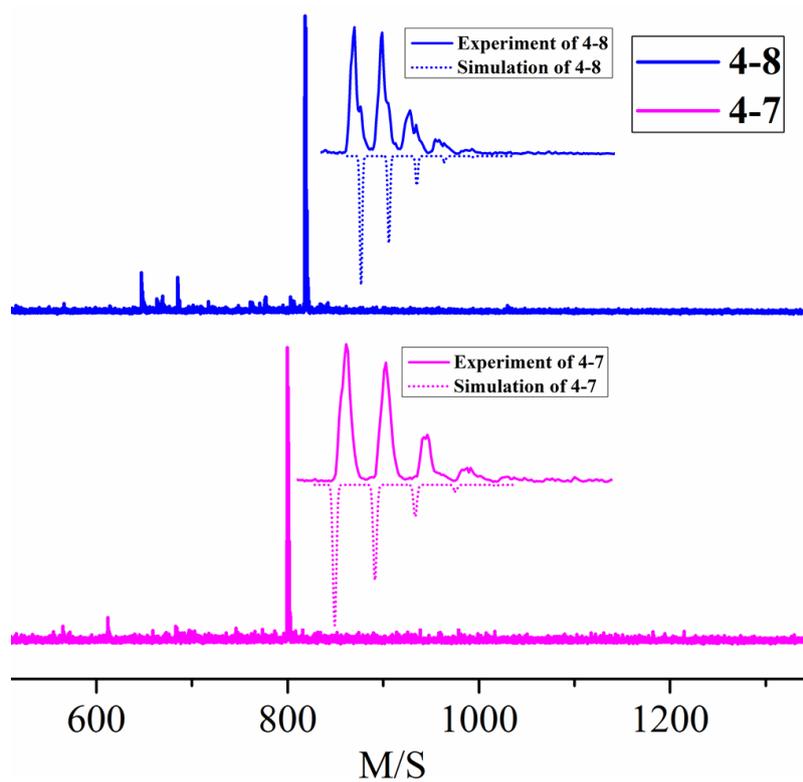
Figure **4-2**. MALDI-TOF MS spectra of **4-7** and **4-8**.
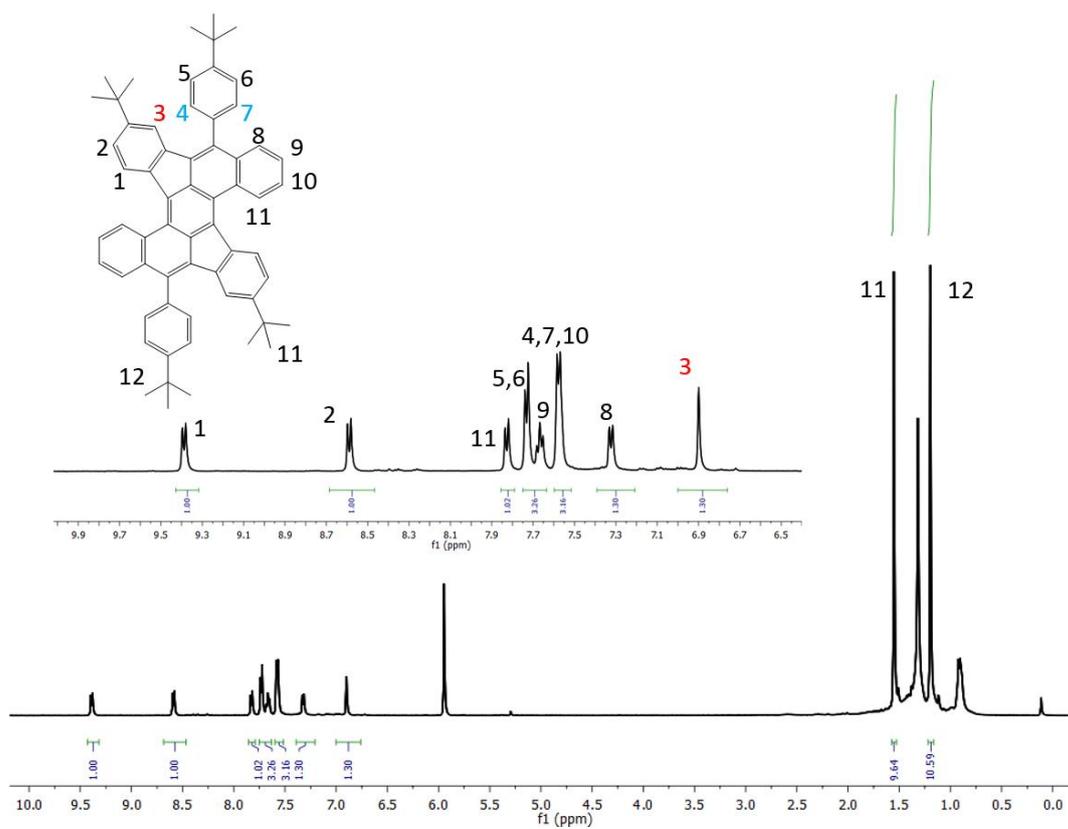
Figure **4-3**. ^{1}H-NMR spectrum of compound **4-7** in CD$_2$Cl$_2$ at 25 °C.
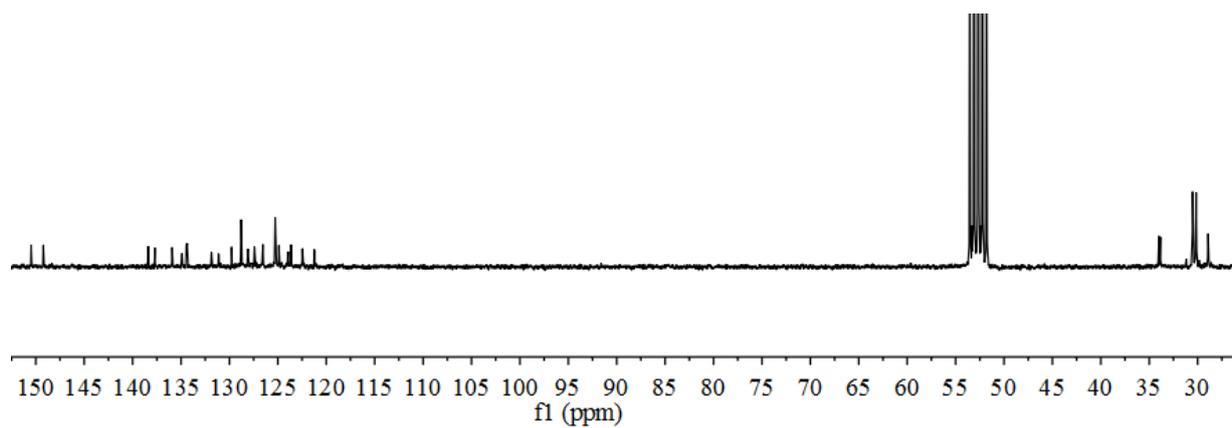
Figure **4-4**. ^{13}C-NMR spectrum of compound **4-7** in CD$_2$Cl$_2$ at 25 °C.
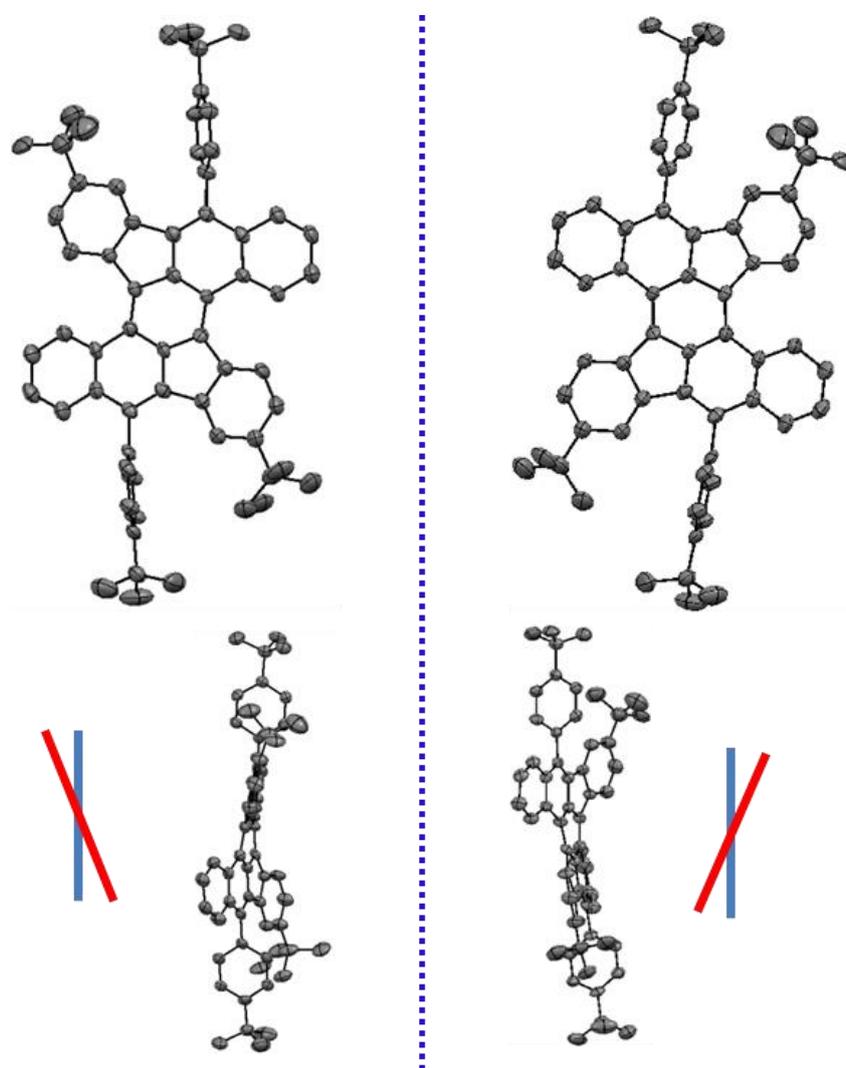
Figure **4-5**. Crystal structure of **4-7** (top and side views of enantiomer pair).

The reddish brown prisms shape crystals of compound **4-7** suitable for single-crystal X-ray analysis was grown from solutions in hexane/dichloromethane. The molecular structure is

shown in Figure **4-5**. Notably, compared to the planar structure of rubicene, the internal C-H steric repulsions cause the non-planarity of the skeleton of **4-7** with a mean torsional angle of 23.8°. Interestingly, the distorted carbon framework makes **4-7** chiral with *R* and *S* conformation in the stacked dimer, as demonstrated in Figure **4-5**. The π-π stacking distance within the dimer is 3.79 Å (Figure **4-6a**).
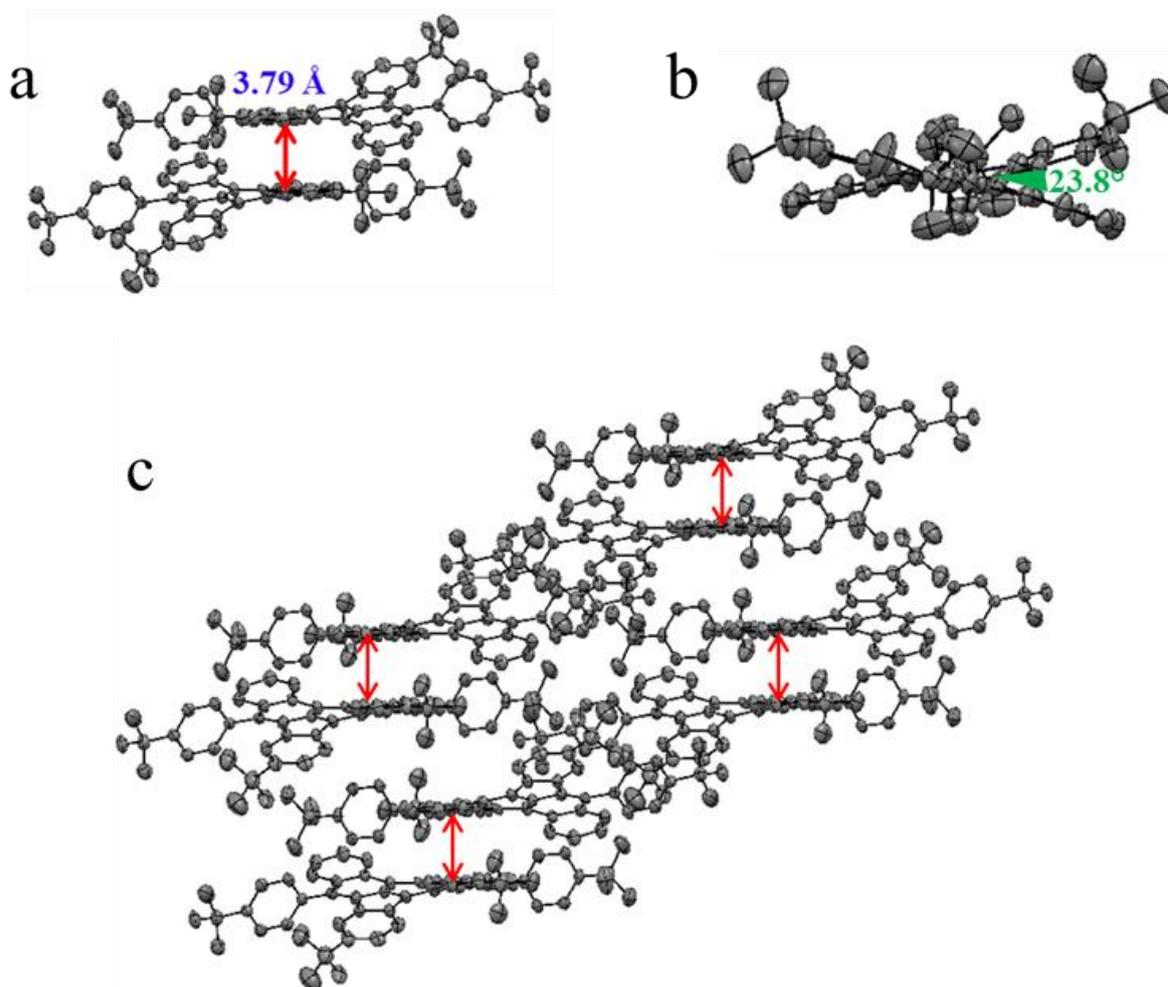
Figure **4-6**. (a) Crystal packing of dimer from side view; (b) Torsional angle of **4-7**; (c) Crystal packing of face-to-face (π-π).

The X-ray diffraction data further disclose the detailed bond parameters of **4-7** (Figure **4-7a**). The C-C bonds at the five-membered rings are obviously longer (1.47-1.49 Å) than other bonds. Thus it seems that the peripheral benzene rings are connected with the core dibenzoanthracene via two C-C single bonds. The Nucleus-independent chemical shift (NICS) calculation at the GIAO-B3LYP/6-31G (d,p) level of compound **4-7** was carried out to investigate the aromaticity of each ring, and the obtained NICS values are -17.34, -8.44, -

20.06, and -20.39 for the benzene rings, and 8.65 for the five-membered ring (Figure **4-7b**). These results suggest the aromatic and non-aromatic feature for the benzene ring and five-membered ring, respectively.
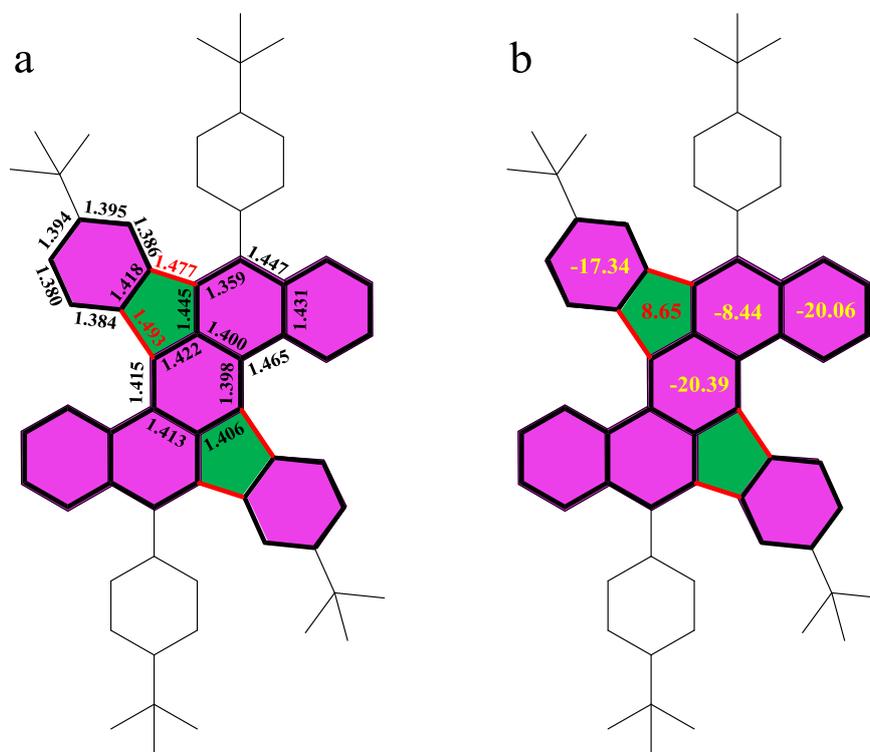

Figure **4-7**. (a) Bond lengths of **4-7**; (b) NICS values from calculation.

Here the critical question is why the migration occurred during the Scholl reaction, leading to the formation of **4-7** instead of **4-6**. At the beginning, we assumed that the five-membered rings were formed at the ICl-induced cyclization step. However, the chemical identities of **4-15** and **4-5** as confirmed by the single-crystal analyses (Figure **4-8** and **4-9**), excluded this conjecture. Although the detailed mechanism of the Scholl reaction remains elusive, mechanism involving either radical cations or arenium cations have been put forward.[30-33] Based on the theoretical insights discussed above, the proposed mechanisms with phenyl rearrangement, involving either type of radical cations intermediate,[34] can be drawn to account for the formation of **4-7**, as displayed in Scheme **4-4**. First, one-electron oxidation of **4-5** generates its radical cation **4-16**, which undergoes 1,2-shift of the 4-*tert*-butylphenyl group to afford the intermediate radical cation **4-18**, through radical cation **4-17** with a three-membered ring as part of an intermediate state. Then, removal of one more electron and intramolecular C-C bond formation of radical cation **4-18** yield dication **4-20**. The direct C-C bond formation in **4-18** to form radical cation **4-19** is unrealistic, because this structure is

estimated to be highly unstable by theoretical calculations (vide infra). Diradical **4-20** undergoes subsequent removal of two protons to form compound **4-21**. Repetition of the same sequence finally produces compound **4-7**.
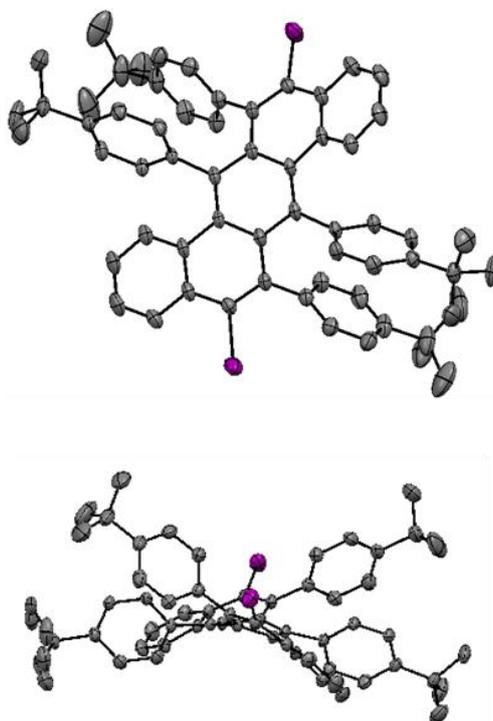

Figure **4-8**. Crystal structure of **4-15** (top and side views).
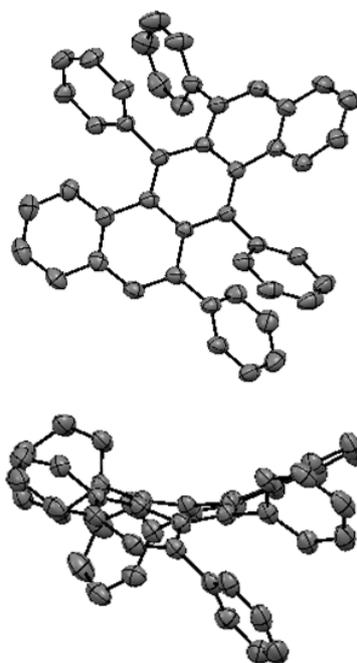
Figure **4-9**. Crystal structure of **4-5** (top and side views).
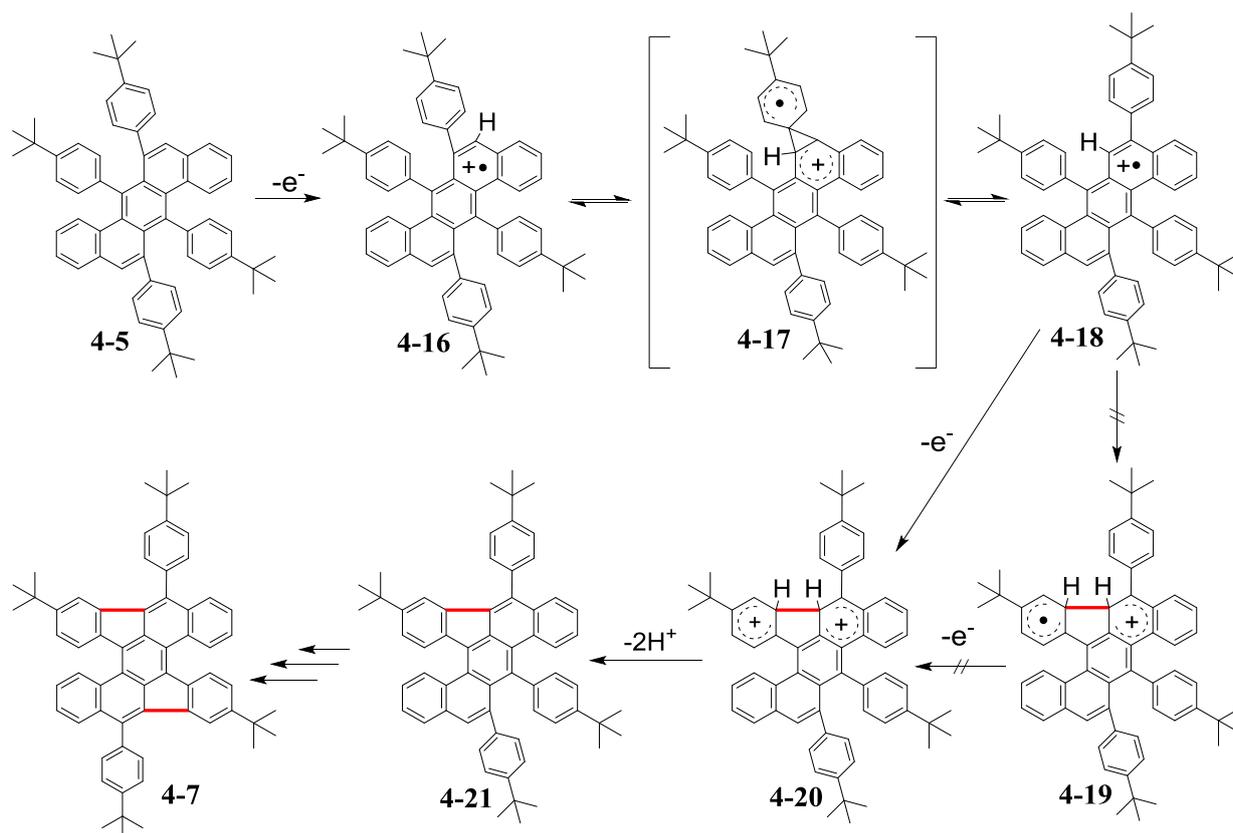
Scheme **4-4**. Proposed mechanism for the phenyl migration and the formation of compound **4-7**.

Theoretical studies were next carried out in order to examine the plausibility of this proposed reaction mechanism as well as to better understand the formation of compound **4-7** with five-membered rings instead of the "expected" product **4-6**. All structures have been optimized at the DFT level of theory with the B3LYP functional and 6-31G (d,p) Pople basis set, using the Gaussian 09 program package. A direct comparison of the energies of compounds **4-7** and **4-6** leads to a difference of 0.54 eV in favor of **4-6** with six-membered rings. Hence, we anticipate that the preferred formation of compound **4-7** is kinetically controlled. The selective 1,2-shift of the aryl groups during the Scholl reaction was then investigated by comparing the relative stability of intermediate radical cation **4-16** and its isomer **4-18**. The DFT calculations indicate that **4-18** is more stable than **4-16** by 0.32 eV, a difference likely associated with steric hindrance. This thus suggests that the 1,2-shift of the aryl group from position 6 to 5 is exergonic. Once radical cation **4-18** is formed, a ring closure reaction can in principle take place to yield either radical cation **4-19** with a five-membered ring or radical cation **4-22** with a six-membered ring (see Scheme 4-5). According to the DFT results, none of these scenarios

is realistic, as the conversion from **4-18** to **4-22** is highly endergonic (by 1.56 eV) while **4-19** is not even a stable structure (it spontaneously evolves back to **4-18**). We rather invoke another mechanism displayed in Schemes 4-5, according to which a second oxidation reaction gives rise to dication **4-23** prior to the ring closure. From **4-23**, again two possible scenarios can be envisioned, namely formation of either five- or six-membered ring, leading to dication **4-20** or **4-24**, respectively. Based on energetics, we expect **4-20** to be the major product, as this endergonic reaction requires an energy penalty (energy difference with respect to **4-23**) of 0.9 eV, which is smaller than that of 1.2 eV for **4-24**. These theoretical results rationalize the selective formation of compound **4-7** instead of **4-6**, and also suggest that the C-C bond formation occurs in a dication intermediate. Nevertheless, further computational analyses are needed to obtain deeper understanding of the mechanism of this Scholl reaction.
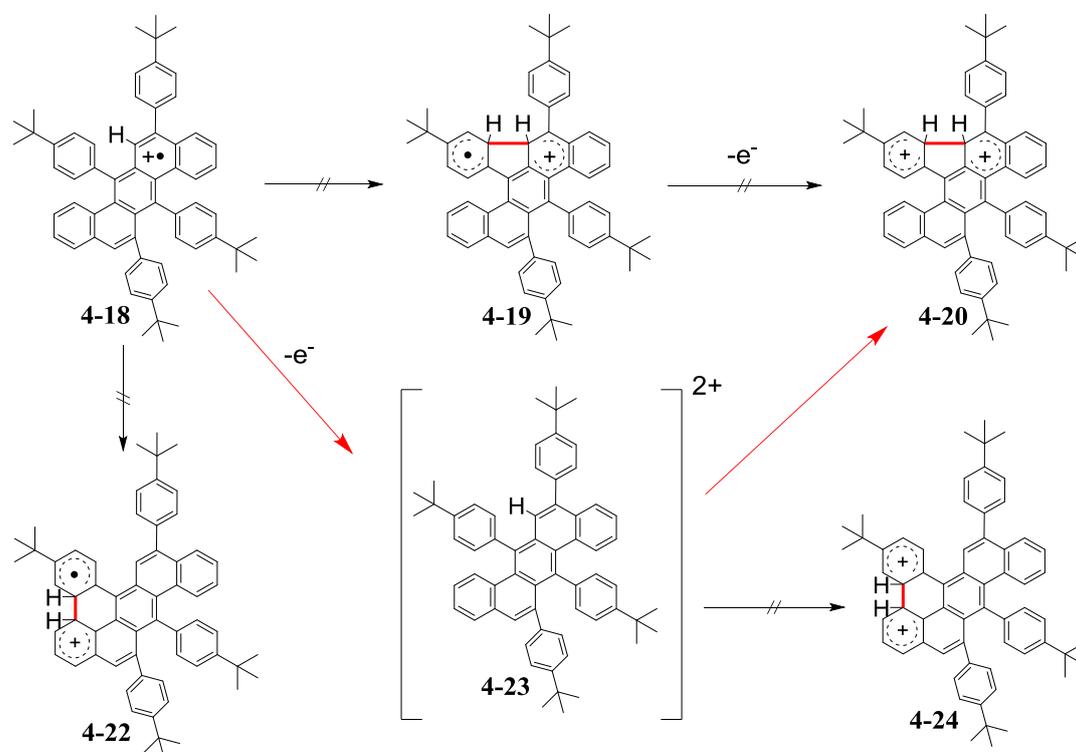
Scheme **4-5**. Possible pathways to formation of a five-membered ring from **4-18** to **4-20**.

Notably, another compound **4-8** was also formed during the Scholl reaction which was separated from the reaction mixture, and characterized by MALDI-TOF MS (Figure **2-2**), ^{1}H NMR (Figure **4-10**), and ^{13}C NMR (Figure **4-11**). Furthermore, red crystals of **4-8** suitable for single-crystal X-ray analysis was grown from solutions in hexane/dichloromethane. The crystal structure is shown in Figure **4-12**. The X-ray diffraction data elucidate the detailed bond parameters of **4-8** (Figure **4-13**). The C-C bonds at the five-membered rings are

obviously longer (1.46 Å) than other bonds, and the central six-membered rings have short (blue) and long (red) bonds, which are identified as double bonds and single bonds, respectively.
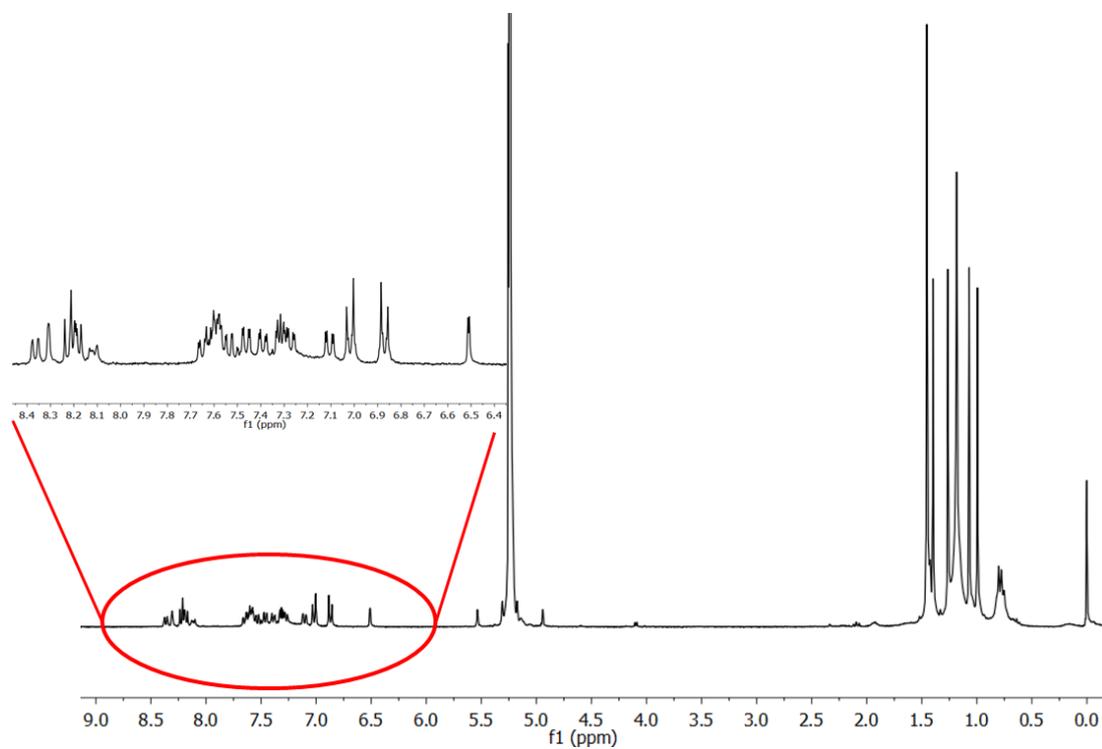
Figure **4-10**. ¹H-NMR spectrum of compound **4-8** in CD₂Cl₂ at 25 °C.
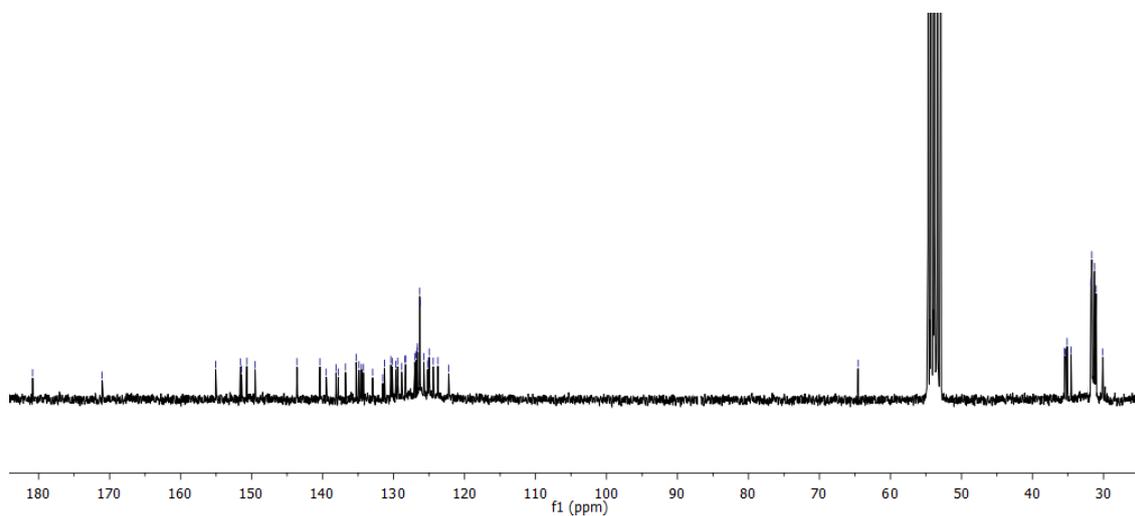
Figure **4-11**. ¹³C-NMR spectrum of compound **4-8** in CD₂Cl₂ at 25 °C.
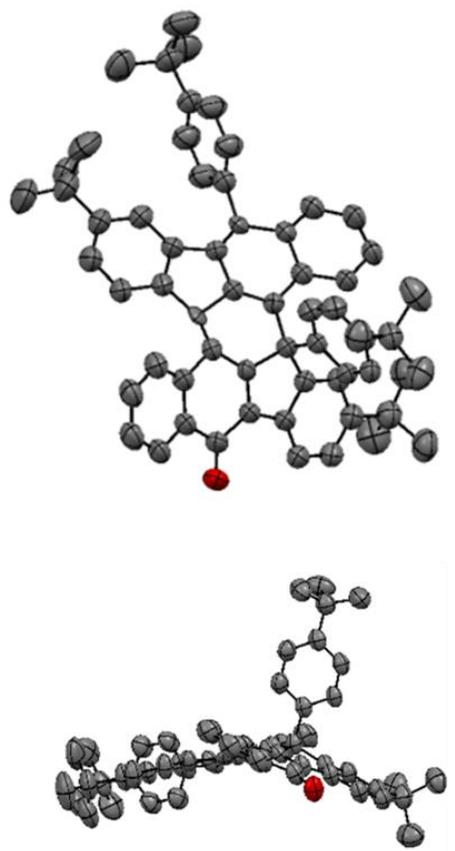
Figure **4-12**. Crystal structure of **4-8** (top and side views).
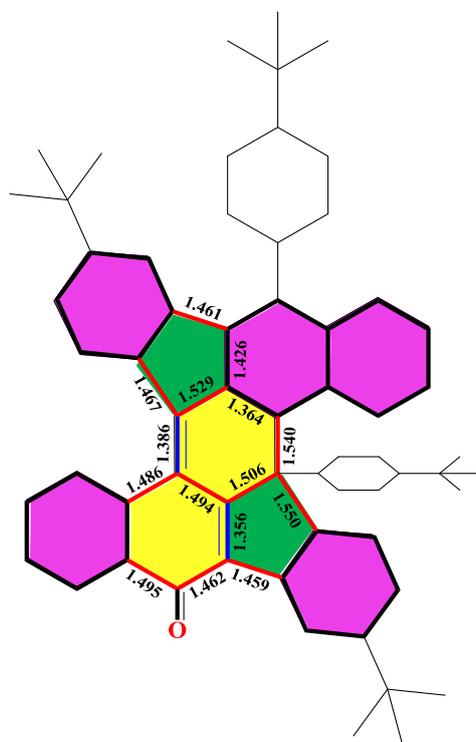
Figure **4-13**. Bond lengths of **4-8**.

In order to block the migrating position of phenyl group in compound **4-5**, we examined the cyclodehydrogenation of **4-15** substituted with iodine group. The Scholl reaction was performed using FeCl₃ as Lewis acid/oxidant in dichloromethane. However, a mixture was obtained which could not be clearly identified through NMR and MALDI-TOF MS analyses. Therefore, the cyclodehydrogenation using DDQ and CF₃SO₃H was attempted. Surprisingly, an unexpected compound **4-27** incorporated with eight member ring was obtained in 33% yield, rather than the prospective **4-25** or **4-26** with seven-membered rings (Scheme **4-6**). The chemical structure of **4-27** was further confirmed by NMR (Figure **14** and **15**) and single crystal structure analysis (Figure **16**).
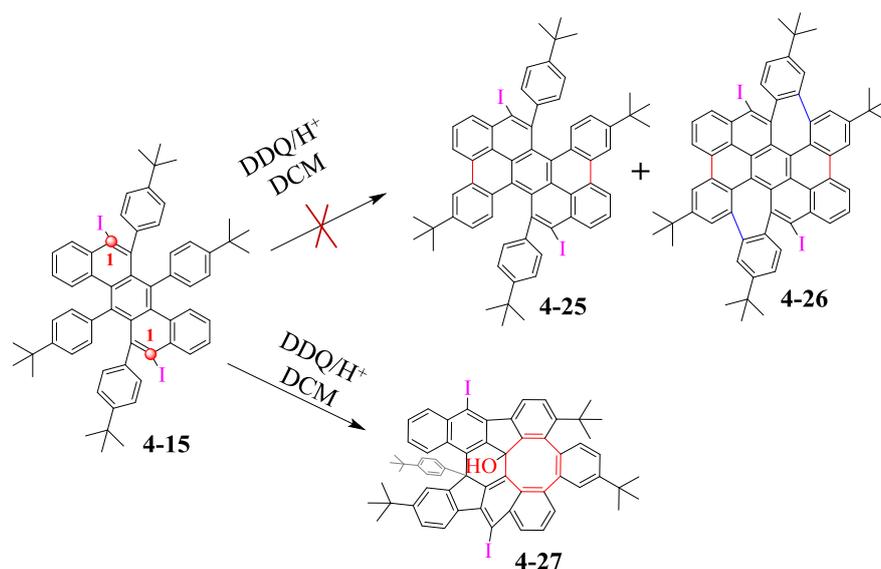
Scheme **4-6**. Cyclodehydrogenation of compound **4-15** by using DDQ and CF₃SO₃H.
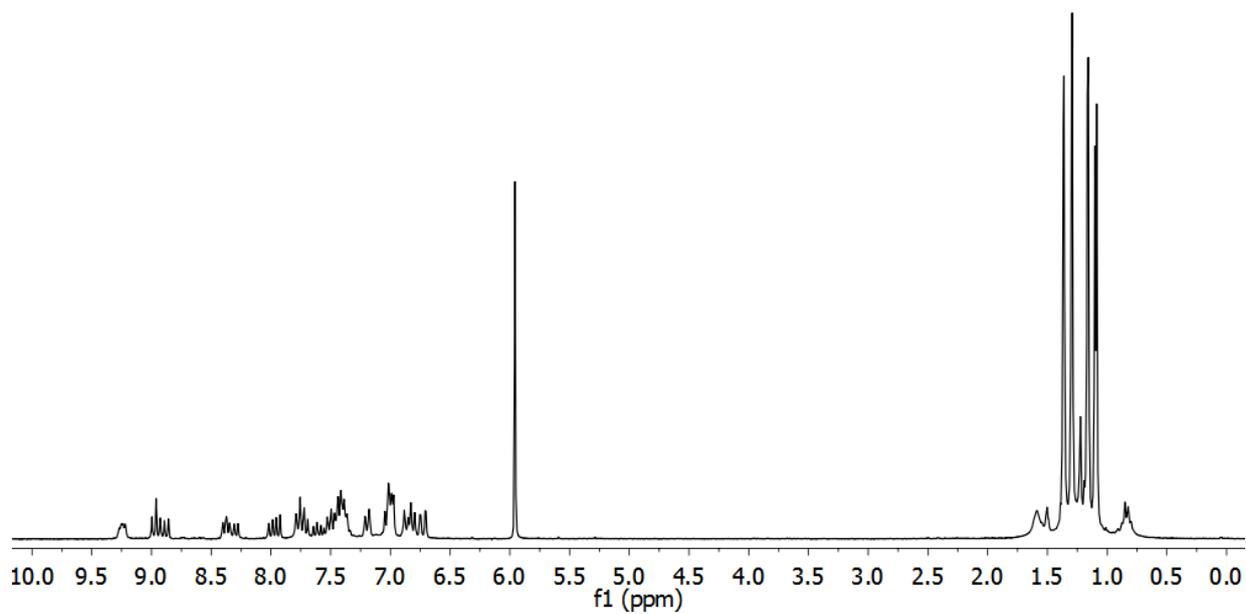
Figure **4-14**. ¹H-NMR spectrum of compound **4-27** in CD₂Cl₂ at 25 °C.
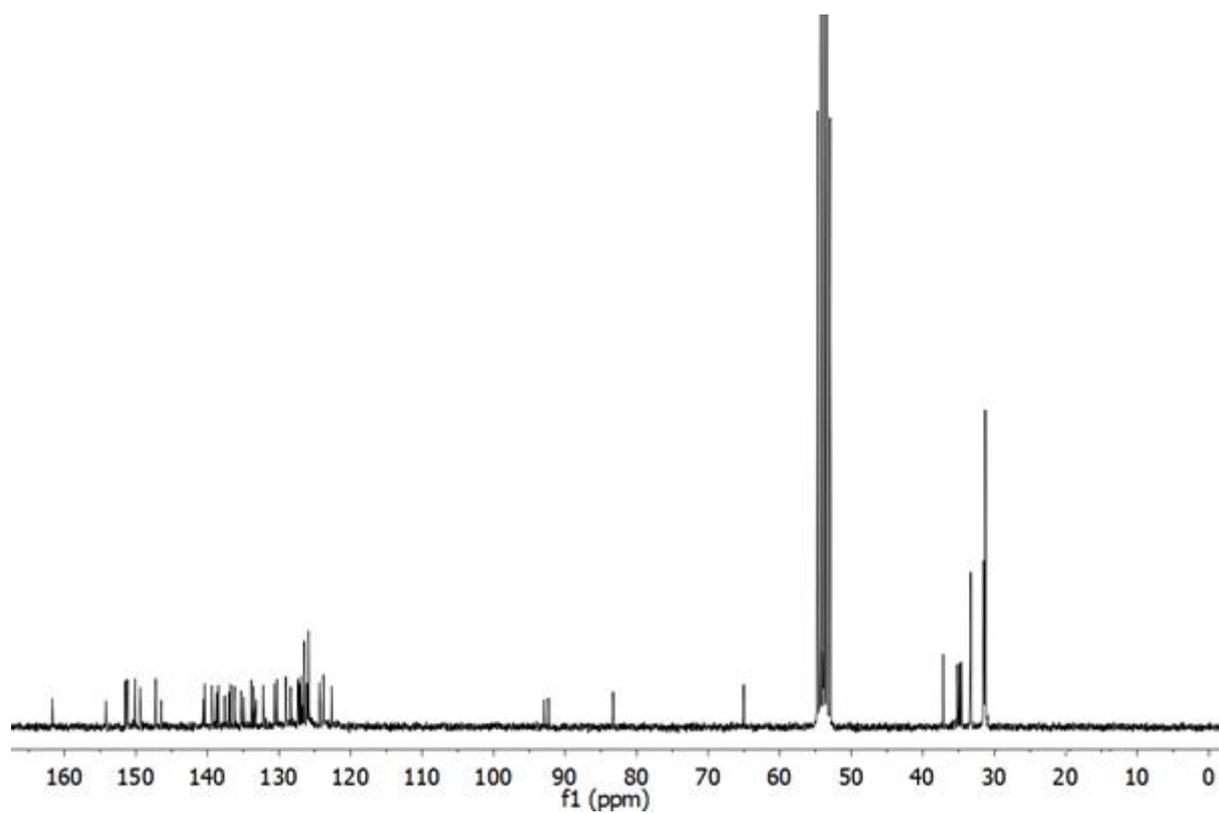
Figure **4-15**. ¹³C-NMR spectrum of compound **4-27** in CD₂Cl₂ at 25 °C.
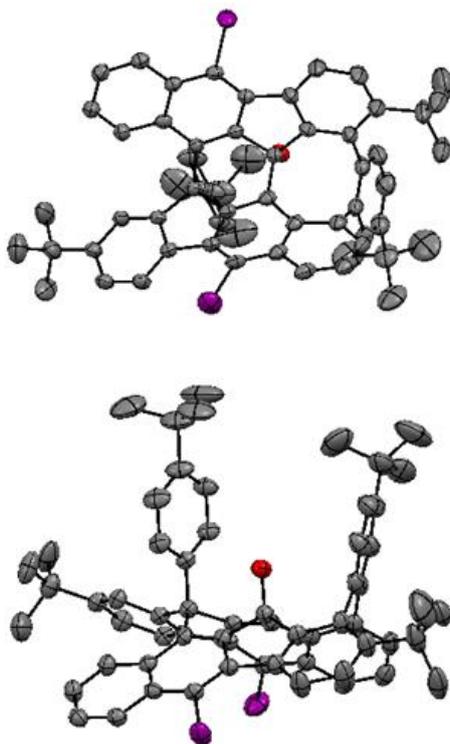
Figure **4-16**. Crystal structure of compound **4-27**.

We propose the possible mechanism for the formation of **4-27**, as shown in Scheme **4-7**. Firstly, radical cation **4-28** is formed, which further establishes a five-membered ring through the attack of the relatively nucleophilic carbon atom located at the central six-membered ring, and afforded a new radical cation **4-29**. Opening of radical cation **4-30** induces the migration of the phenyl group to afford the intermediate radical cation **4-31**. Thus, intermediate **4-32** was afforded undergoes a ready loss of proton and form a bond. Then, intermediate compound **4-33** was formed through the same oxidation Scholl sequence. Furthermore, radical cation **4-34** is afforded through the attack of the relatively nucleophilic carbon atom located at the central six-membered ring, and afforded a new radical cation **4-35**. Intermediate **4-37** was afforded undergoes a ready loss of one proton. Quenching the reaction with NaHCO3 solution finally provides **4-27**.
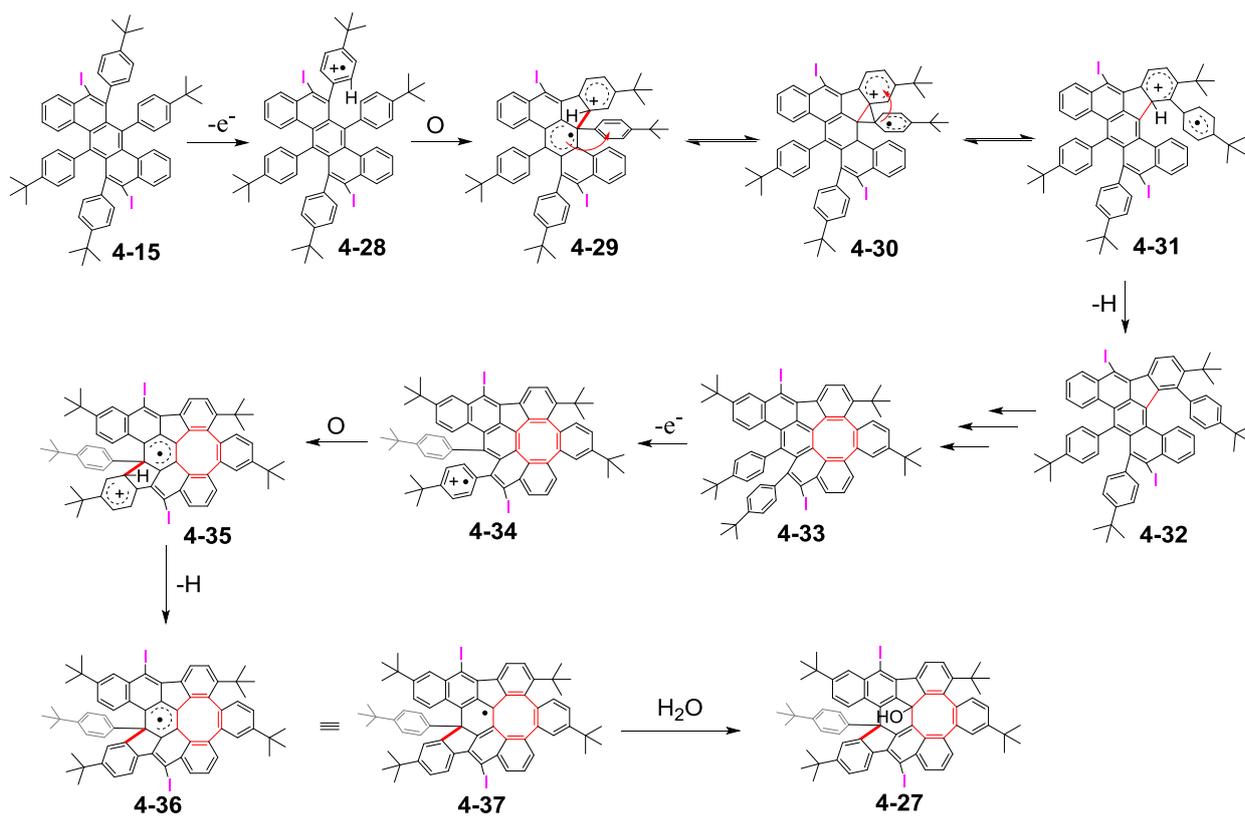
Scheme **4-7**. A possible mechanism for the formation of compound **4-24**.

4.3 Optical and Electrochemical Properties of 4-7, 4-8 and 4-27
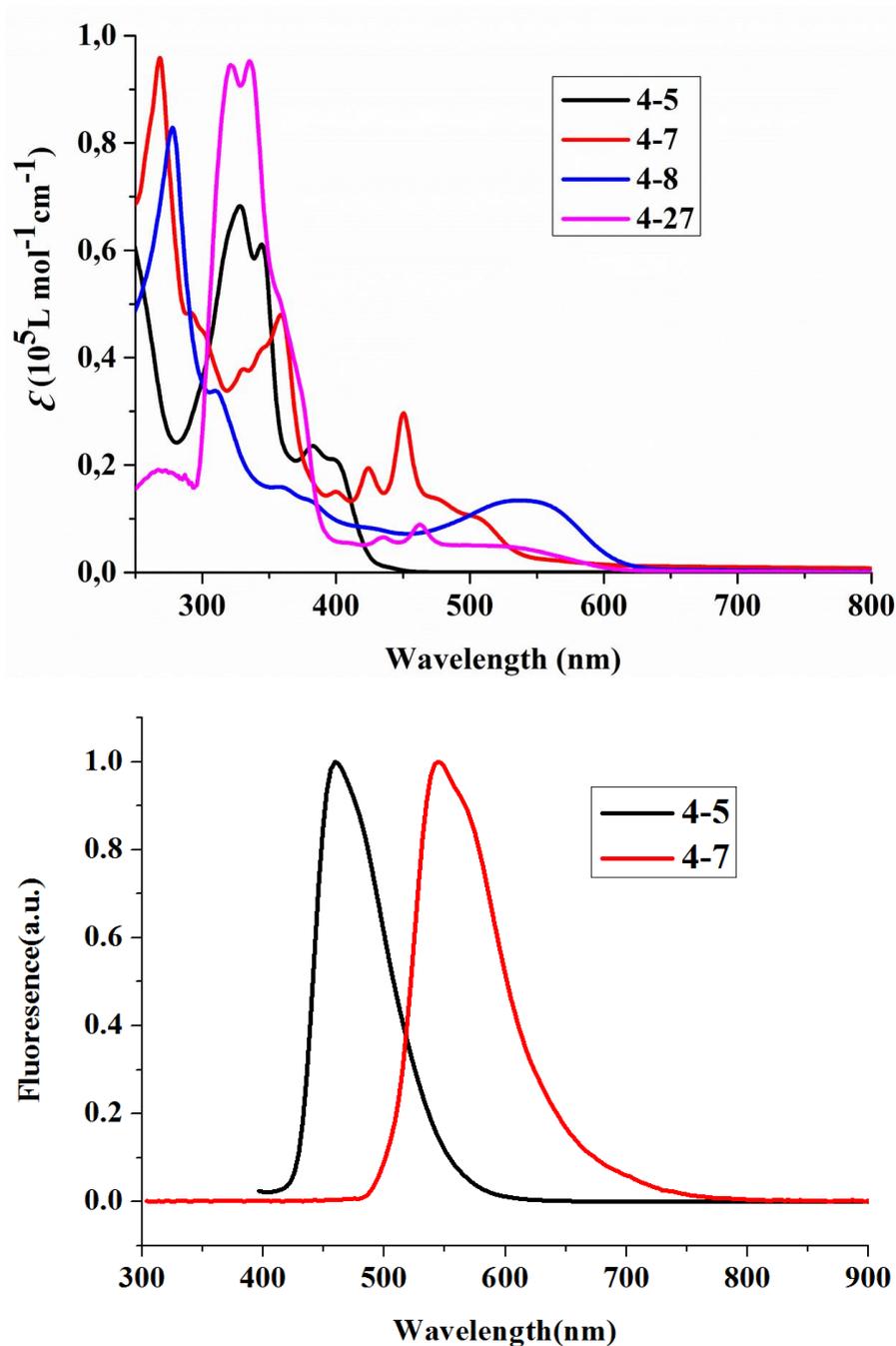
Figure **4-17**. (a) Normalized UV-vis absorption spectra of **4-5**, **4-7**, **4-8** and **4-27**. (b) Fluorescence spectra of **4-5** and **4-7** (for all spectra: 10^{-5} M in DCM).

The UV-vis absorption spectra of precursor **4-5** and the cyclodehydrogenation products **4-7**, **4-8** and **4-27** in DCM solutions are compared in Figure **4-17a**. The main absorption bands of **4-7**, **4-8** and **4-27** are significantly red shifted compared to the absorption of precursor **4-5**, suggesting the extended conjugation. Compound **4-7** shows an absorption maximum at 508

nm, while compound **4-8** exhibits a broad absorption band in the range of 465-618 nm, as a result of the ketone formation. Similar to **4-8**, compound **4-27** also presents a broad absorption band in 470-600 nm due to the n-π^* transition of the hydroxyl group. The optical energy gaps of **4-7**, **4-8** and **4-27** are determined from the onsets of their UV-vis absorption spectra, which are 2.26, 1.96 and 1.94 eV, respectively. Compounds **4-5** and **4-7** show moderate fluorescence in DCM solution with maxima at 460 and 544 nm respectively (Figure **4-17b**), while compounds **4-8** and **4-27** exhibit poor fluorescence.

The electrochemical properties of **4-7**, **4-8** and **4-27** were investigated by means of cyclic voltammetry (CV) in DCM solutions (Figure **4-18**). According to the CV analysis, compound **4-7** shows one reversible oxidation and one reversible reduction process, whereas there are one reversible oxidation and two reversible reductions for **4-8**. In contrast, there are only one reversible and one irreversible reduction for **4-27**. The HOMO energy levels estimated from the onsets of the reversible oxidation peaks are -5.77 and -5.69 eV for **4-7** and **4-8**, respectively. Thus, the LUMO energy levels of these compounds are calculated based on their HOMO levels and optical gaps, as listed in Table 1. The results are fully consistent with the DFT calculations (see below).
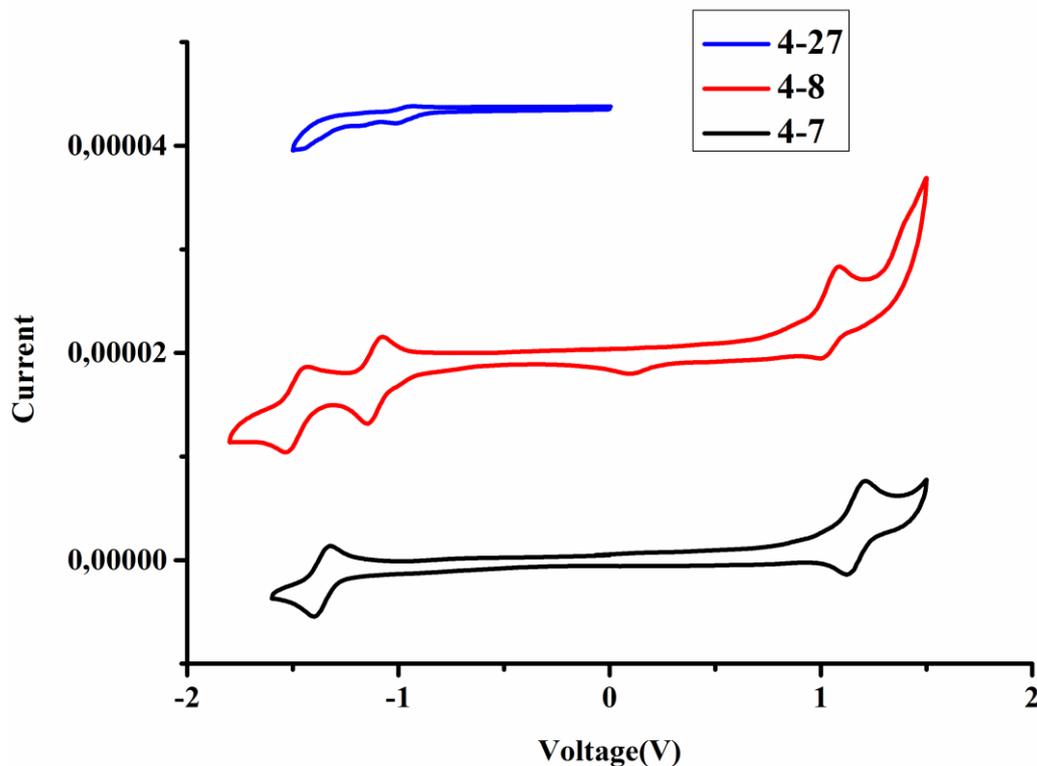
Figure **4-18**. Cyclic voltammograms of **4-7**, **4-8** and **4-24** vs Fc/Fc+ (0.1 M nBu$_4$NPF$_6$ in DCM), scan rate 50 mVs^{-1}.

	λ_{max}[a] [nm]	λ_{em}[b] [nm]	λ_{edge} [nm]	E_g (opt)[c] [eV]	E_{HOMO}[d] [ev]	E_{LUMO}[e] [ev]	E_{HOMO}[f] [ev]	E_{LUMO}[f] [ev]	E_g (cal)[f] [eV]
4-5	391	460	430	2.89	---	---	---	---	---
4-7	508	544	572	2.18	-5.77	-3.54	-5.05	-2.11	2.94
4-8	550	---	646	1.92	-5.69	-3.79	-5.29	-2.88	2.41
4-27	535	618	640	1.94	-5.92	-3.98	-5.78	-3.24	2.54

Table 4-1 Optical and electrochemical data: [a] λ_{max}: absorption maximum at the longest wavelength; [b] λ_{em}: emission wavelength; [c] Optical energy gaps were estimated from the wavelength of the onset values of the absorption; [d] HOMO values were derived from the first measured oxidation potential; [e] LUMO levels were calculated from the optical band gap E_g(opt) and the respective HOMO levels; [f] Estimated by DFT calculations at the B3LYP/6-31G (d,p) level.
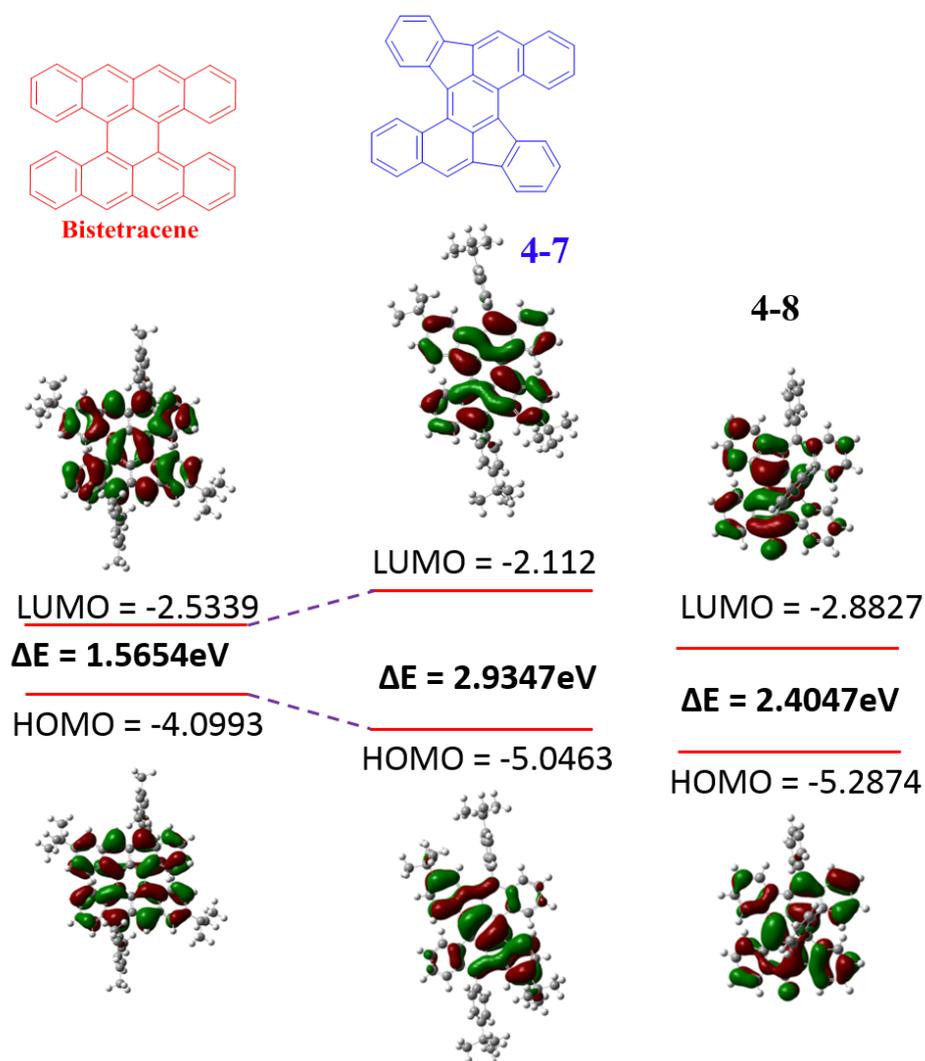
Figure **4-19**. HOMO-LUMO of **4-7** and **4-8** from the calculation.

To obtain deeper insight into the electronic and geometrical properties of the pentagon-embedded bistetracene and the conventional bistetracene consisting solely of six-membered rings, DFT calculations were conducted at the B3LYP/6-31G (d, p) level of theory using the Gaussian 09 program package. The graphical representations of the highest occupied molecular orbital (HOMO) and the lowest unoccupied molecular orbital (LUMO) are displayed in Figure 4-19. Obviously, the HOMO of traditional six-membered bistetracene is much higher than the pentagon-embedded bistetracene, while the corresponding LUMO value is much lower than the pentagon-embedded bistetracene. Accordingly, the pentagon-embedded bistetracene has a larger energy gap ($E_\mathrm{g}^\mathrm{cal}$=2.93 eV) compared to the bistetracene ($E_\mathrm{g}^\mathrm{cal}$=1.56 eV) consisting only of six-membered rings. Thus, the pentagon-embedded bistetracene 4-7 is stable enough during the synthesis and characterization, whereas the six-membered conventional bistetracene possesses a prominent biradical character in the ground state and can easily undergo oxidation under ambient conditions.[17]

4.4 Conclusion

In summary, we have synthesized a series of novel PAHs incorporated with five- or eight-membered rings from the precursor 6,7,13,14-tetraphenylbenzo[*k*]tetraphene, as a result of the phenyl migration during the Scholl reaction. These compounds are further investigated by UV-Vis absorption spectroscopy and single-crystal structure analysis, as well as assisted by the DFT calculation. We found that the pentagon-embedded bistetracene molecule is more stable compared to the conventional bistetracene consisting only of six-membered rings. Furthermore, the mechanism for the phenyl migration is proposed, providing a unique and unprecedented entry to extend the stable *peri*-tetracene or *peri*-pentacene like molecules with five- and eight-membered rings.

REFERENCES

[1] J. E. Anthony, *Chem. Rev.* **2006**, 106, 5028-5048.

[2] J. E. Anthony, *Angew. Chem. Int. Ed.* **2008**, 47, 452-483.

[3] Q. Ye, C. Chi, *Chem. Mater.* **2014**, 26, 4046-4056.

[4] B. Purushothaman, M. Bruzek, S. R. Parkin, A. F. Miller, J. E. Anthony, *Angew. Chem. Int. Ed.* **2011**, 50, 7013-7017.

[5] C. Tçnshoff, H. F. Bettinger, *Angew. Chem. Int. Ed.* **2010**, 49, 4125-4128.

[6] A. Hepp, H. Heil, W. Weise, M. Ahles, R. Schmechel, H. Seggern, *Phys. Rev. Lett.* **2003**, 91, 157406.

[7] H. Moon, R. Zeis, E. J. Borkent, C. Besnard, A. J. Lovinger, T. Siegrist, C. Kloc, Z. Bao, *J. Am. Chem. Soc.* **2004**, 126, 15322-15323.

[8] J. E. Anthony, J. S. Brooks, D. L. Eaton, S. R. Parkin, *J. Am. Chem. Soc.* **2001**, 123, 9482-9483.

[9] Y. Diao, B. C. K. Tee, G. Giri, J. Xu, D. H. Kim, H. A. Becerril, R. M. Stoltenberg, T. H. Lee, G. Xue, S. C. B. Mannsfeld, Z. Bao, *Nat. Mater.* **2013**, 12, 665-671.

[10] G. Giri, E. Verploegen, S. C. B. Mannsfeld, S. Atahan-Evrenk, D. H. Kim, S. Y. Lee, H. A. Becerril, A. Aspuru-Guzik, M. F. Toney, Z. Bao, *Nature* **2011**, 480, 504-508.

[11] D. T. Chase, A. G. Fix, B. D. Rose, C. D. Weber, S. Nobusue, C. E. Stockwell, L. N. Zakharov, M. C. Lonergan, M. M. Haley, *Angew. Chem. Int. Ed.* **2011**, 50, 11103-11106.

[12] D. T. Chase, B. D. Rose, S. P. McClintock, L. N. Zakharov, M. M. Haley, *Angew. Chem. Int. Ed.* **2011**, 50, 1127-1130.

[13] X. Yang, Da. Liu, Q. Miao, *Angew. Chem. Int. Ed.* **2014**, 53, 6786 -6790.

[14] Q. Miao, *Adv. Mater.* **2014**, 26, 5541-5549.

[15] M. Märken, B. D. Lindner, A. L. Appleton, F. Rominger, U. H. F. Bunz, *Pure. Appl. Chem.* **2014**, 86, 483-488.

[16] L. Zöphel, R. Berger, P. Gao, V. Enkelmann, M. Baumgarten, M. Wagner, K. Müllen, *Chem. Eur. J.* **2013**, 19, 17821-17826.

L. B. Roberson, J. Kowalik, L. M. Tolbert, C. Kloc, R. Zeis, X. L. Chi, R. Fleming, C. Wilkins, *J. Am. Chem. Soc.* **2005**, 127, 3069-3075.

[17] J. Liu, P. Ravat, M. Wagner, M. Baumgarten, X. Feng, K. Müllen, *Angew. Chem. Int. Ed.* DOI: 10.1002/anie.201502657 and 10.1002/ange.201502657.

B. H. Northrop, J. E. Norton, K. N. Houk, *J. Am. Chem. Soc.* **2007**, 129, 6536-6546.

[18] R. Scholl, C. Seer, *Justus Liebigs Ann. Chem.* **1912**, 394, 111.

[19] R. Scholl, C. Seer, *Chem. Ber.* **1922**, 55, 109.

[20] P. Kovacic, M. B. Jones, *Chem. Rev.***1987**, 87, 357.

[21] E. Clar, C. T. Ironside, M. Zander, *J. Chem. Soc.* 1959, 142-147.

[22] E. Clar, Polycyclic Hydrocarbons, vols I/II, 1964, Academic Press, New York.

[23] A. Stabel, P. Herwig, K. Müllen, J. P. Rabe, *Angew. Chem. Int. Ed.* **1995**, 34, 1609-1611.

[24] M. Müller, H. Mauermann-Düll, M. Wagner, V. Enkelmann, K. Müllen, *Angew. Chem. Int. Ed.* **1995**, 34, 1583-1586.

[25] X. Dou, X. Yang, G. J. Bodwell, M. Wagner, V. Enkelmann, V., K. Müllen, *Org. Lett.* **2007**, 9, 2485-2488.

[26] A. T. Balaban, C. D. Nenitzescu, Friedel-Crafts and Related Reaction, Olah, G. A., Ed.; Wiley & Sons: New York, **1964**, 2, 979-1047.

[27] V. S. Iyer, K. Yoshimura, V. Enkelmann, R. Epsch, J. P. Rabe, K. Müllen, *Angew. Chem. Int. Ed.* **1998**, *37*, 2696-2699.

[28] M. Müller V. S. Iyer, C. Kübel, V. Enkelmann, K. Müllen, *Angew. Chem. Int. Ed.* **1997**, 36, 1607-1610.

[29] A. Necula, A. Racoveanuschiketanz, M. D. Gheorghiu, L. T. Scott, *J. Org. Chem.* **1995**, 60, 3448-3451.

[30] M. DiStefano, F. Negri, P. Carbone, K. Müllen. *Chem. Phys.* **20005**, 314, 85-99.

[31] P. Rempala, J. Kroulík, B. T. King. *J. Org. Chem.* **2006**, 71, 5067-5081.

[32] A. Ronlan, O. Hammerich, V. D. Parker. *J. Am. Chem. Soc.* **1973**, 95, 7132-7138.

[33] R. Rathore, J. K. Kochi. *J. Org. Chem.* **1995**, 60, 7479-7490.

[34] L. Zhai, R. Shukla, S. H. Wadumethrige, R. Rathore. *J. Org. Chem.*, **2010**, 75, 4748-4760.

Chapter 5 Synthesis of New Stable Open-shell Odd-ring-embedded Nanographene

In chapter 4, we have demonstrated a series of novel Polycyclic aromatic hydrocarbons (PAHs) incorporating five- or eight-membered rings from the precursor 6,7,13,14-tetraphenylbenzo[*k*]tetraphene, as a result of the "unexpected" phenyl migration during the Scholl reaction. Thus, we consider whether such "unexpected" synthetic protocol can be extended to other systems. In this chapter, we will show that this "unexpected" migration protocol can serve as a universal approach to prepare structurally well-defined five- and seven-membered-ring embedding nanographene. As a typical example, azuene-embedding nanographene, with five- and seven-membered rings, can be synthesized rapidly from our previous phenyl migration of the precursor 6,7,13,14-tetraphenylbenzo[*k*]tetraphene during the cyclodehydrogenation process. Remarkably, this odd-ring-embedded graphene subunit has a low optical energy gap (1.24 eV) and exhibits a remarkable singlet biradical character in the ground state.

5.1 Introduction

Graphene is a two-dimensional, atomically thick sheet composed of a hexagonal network of sp2-hybridized carbon atoms, which can be viewed as fused benzene structure. PAHs can be regarded as finite graphene segments composed of all-sp^2 carbons that are termed as nanographenes with an average diameter from 1 to 100 nm in size.[1-3] Pi-conjugated open-shell molecules, such as phenalenyl[4,5] and triangulene[6,7] (Figure 5-1), have long attracted the attention of experimental and theoretical organic chemists due to its delocalized spin structure, which can be viewed as triangular units of a graphene sheet. Thereby, by extension, open-shell PAHs can be viewed as open-sell graphene subunit to a certain extent.
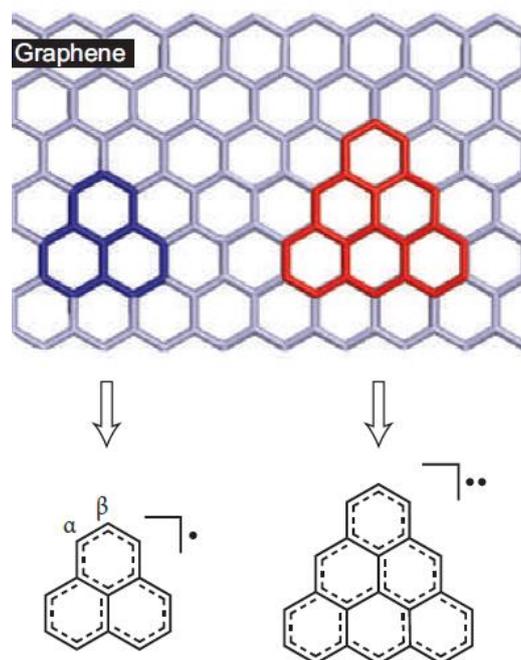
Figure 5-1. Structure of phenalenyl-based neutral radicals.[4]

Recently, nanographene with stable radicals have been intensively explored as new functional molecular materials, because the open-shell graphene structure exhibits unique electronic, magnetic and optical properties.[8,9] The stability of radicals is the precondition not only in the synthesis, but also for their future applications in materials science.[10] Generally, there are two established methods for the stabilization of radicals, including kinetic stabilization via protecting the spin bearing center with steric hindrance and thermodynamic stabilization through spin delocalization. To date, several representative types of stable open-shell nanographene have been reported, including bisphenalenyls,[11-16] indenofluorenes,[17-22] anthenes,[23,24] and zethrenes,[25-29] which allow a glimpse of their peculiar properties arising from the singlet biradical character. The fundamental reason for their instability can be attributed to their intrinsic biradical character, which is induced by the topology of their π-electron array, even if they have an even number of carbon atoms. Accordingly, the development of new nanographene with radical features is crucial for promising novel and diverse applications in high-spin materials. In addition, exploring the relationships between structure and property of nanographenes will provide valuable information about the molecular design. However, most recent works have been focussed on the traditional six-membered nanographene with biradical feature,[5,8] other carbon nanostructures, such as those with heptagon-membered-rings, are still not explored. Recent approaches to carbon

nanostructures with saddle-shaped PAHs including two heptagons[30] and a grossly warped nanographene containing five heptagons ($C_{80}H_{30}$)[31] (Figure 5-2) have been reported, however, until now, all of the reported nanographene with heptagon-membered-rings show a typical close-shell electronic structure in the ground state.
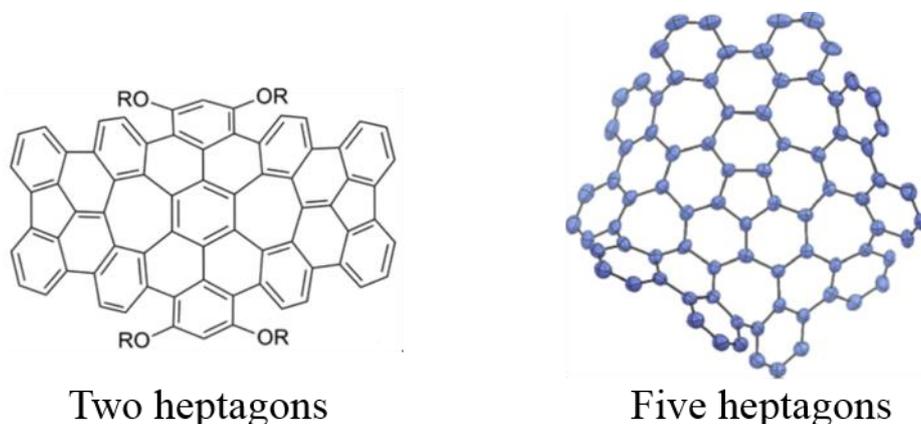
Figure 5-2. Heptagon-embeded graphene segments.
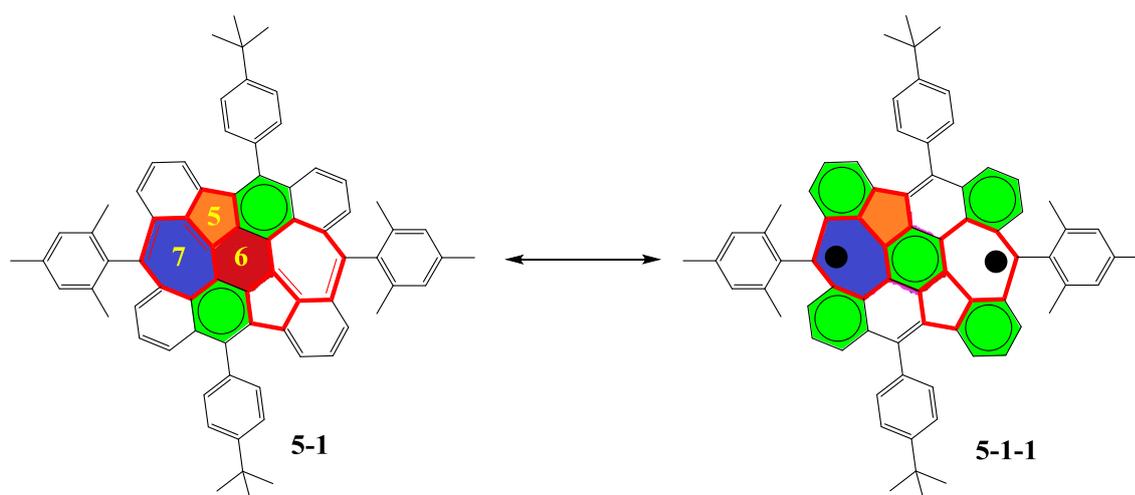
Figure 5-3. Resonance structures of **5-1**.

Herein, we report a structurally well-defined azulene-embedding nanographene dipleiadeno[2,1,12,11-*cdefg*:2',1',12',11'-*ijkla*]-*s*-indacene (**5-1**), the first member of a new family of nanocarbons with fused five- and seven- membered rings (Figure 5-3). This warped nanographene, with five- and seven-membered rings, can be synthesized utilizing our previous "unexpected" phenyl migration of the precursor 6,7,13,14-tetraphenylbenzo[*k*]tetraphene during the cyclodehydrogenation processs (chapter 4). Remarkably, the achieved odd-ring-embedding nanographene has a low optical energy gap

(1.24 eV) and exhibits a remarkable singlet biradical character in the ground state. From the resonance structures, there are two aromatic sextets in the closed shell form and a maximum of five aromatic sextets in the biradical form (Figure 5-3). According to the Clar sextet rule, the alternative form with more aromatic sextets, **5-1-1**, will help to stabilize the biradical resonance borderline structure as a result of gaining the aromatic stabilization energies, and thus it is expected to show more biradical character in the ground state. Furthermore, to obtain stable and soluble materials, our design is to kinetically block the reactive sites with bulky mesityl groups. To the best of our knowledge, this is the first example that a stable biradical feature has been observed in five- and seven- membered rings embedding nanographene.

5.2 Synthesis and structure verification

The synthesis towards compound **5-1** is described in Scheme 5-1. First, selective Suzuki coupling between 1,4-dibromo-2,5-diiodobenzene (**5-2**) and commercially available *o*-tolylboronic acid gave the 2',5'-dibromo-2,2''-dimethyl-1,1':4',1''-terphenyl (**5-3**) in 75% yield. Then compound 2-((4-(*tert*-butyl)phenyl)ethynyl)-4'-(2-((4-(*tert*-butyl)phenyl)ethynyl)phenyl)-2''-methyl-5'-(*o*-tolyl)-1,1':2',1''-terphenyl (**5-5**) was prepared by Suzuki coupling of **5-3** with (2-((4-(*tert*-butyl)phenyl)ethynyl)phenyl)boronic acid (**5-4**) in 69% yield. Afterwards, utilizing ICl-induced cyclization of **5-5** afforded compound 6,13-bis(4-(*tert*-butyl)phenyl)-5,12-diiodo-7,14-di-*o*-tolylbenzo[*k*]tetraphene (**5-6**) in 85% yield. Next, removing the iodine group of 5-6 by *n*-BuLi to furnish compound 6,13-bis(4-(*tert*-butyl)phenyl)-7,14-di-*o*-tolylbenzo[*k*]tetraphene (**5-7**) in 53% yield. The cyclodehydrogenation of **5-7** was performed with 2,3-dichloro-5,6-dicyano-1,4-benzoquinone (DDQ)/ trifluoromethanesulfonic acid (CF$_3$SO$_3$H) as the Lewis oxidant/acid in dry DCM at 0 ^{o}C under argon, leading to compound 5,14-bis(4-(*tert*-butyl)phenyl)-9,18-dimethyldibenzo[*a,m*]rubicene (**5-8**) as reddish brown powder in 65% yield. Subsequently, the dimethyl groups of **5-8** were transformed into dialdehyde functions to provide 5,14-bis(4-(*tert*-butyl)phenyl)dibenzo[*a,m*]rubicene-9,18-dicarbaldehyde (**5-9**) via a bromination-esterification-hydrolysis-oxidation sequence in a yield of 32%. Then compound 5-9 was treated with mesitylmagnesium bromide to give diol compound, which was subjected to Friedel-Crafts alkylation promoted by BF$_3$•OEt$_2$ to afford 4,12-bis(4-(*tert*-butyl)phenyl)-8,16-dimesityl-8,16-dihydropleiadeno[2',1',12',11':3,4,5,6]-*s*-indaceno[2,1,8,7-*nopqa*]pleiadene (**5-10**) in 40% yield in two steps, and 5% of compound **5-11** as byproduct. Finally, oxidation of

5-10 with *p*-chloranil in dry toluene at room temperature under argon produced the target compound **5-1** as purple powder in 25% yield.
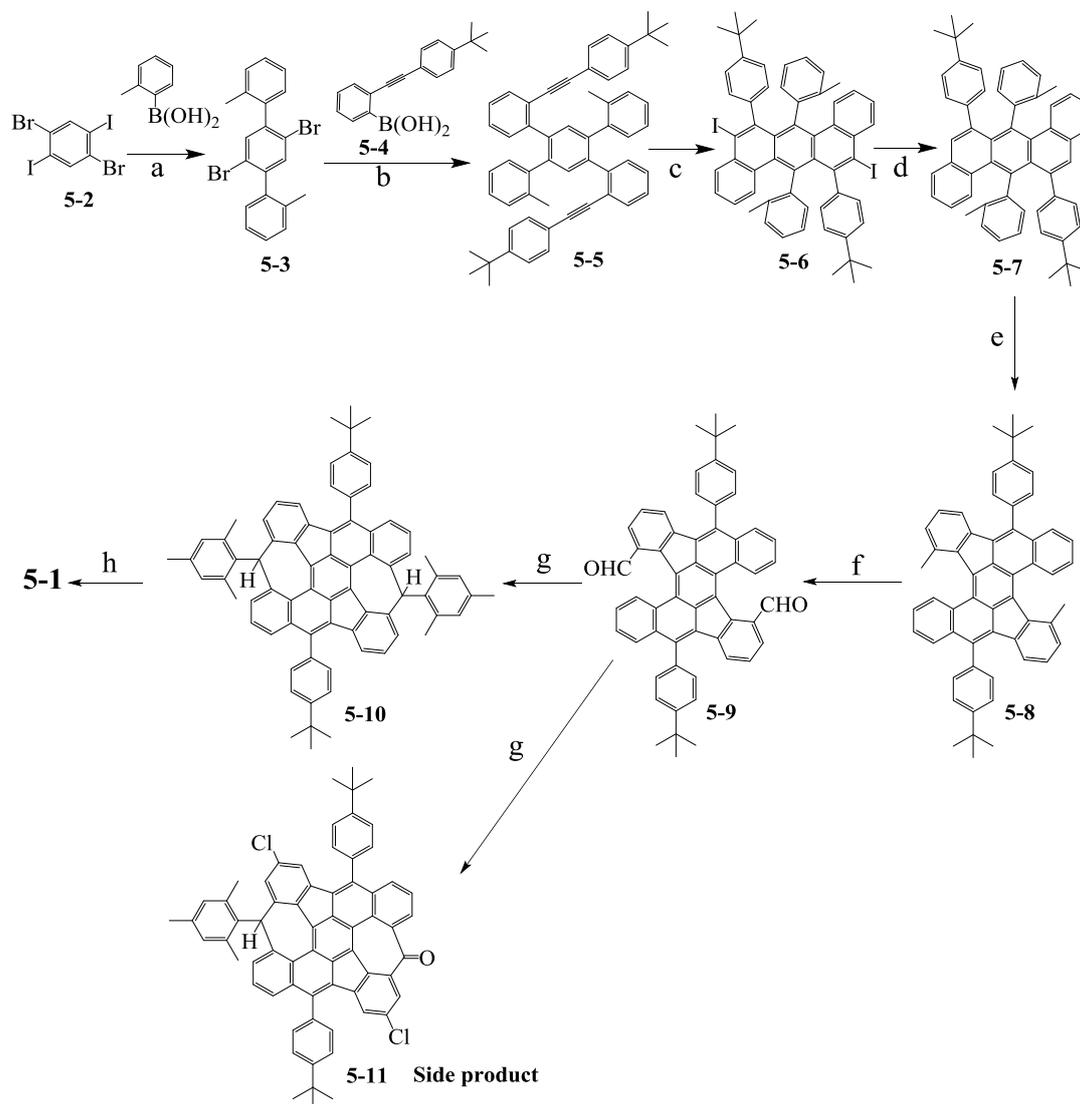
Scheme 5-1. Synthetic route toward **5-1**. Reagents and conditions: (a) Pd(PPh$_3$)$_4$/K$_2$CO$_3$, dioxane/H$_2$O, 90 ℃, 24h, 75%. (b) Pd(PPh$_3$)$_4$/K$_2$CO$_3$, dioxane/H$_2$O, 90 ℃, 24h, 69%. (c) ICl 1 M in DCM, DCM, -78 ℃, 3h, 85.4%. (d) *n*-BuLi, THF, MeOH, 1h, 52.6%. (e) DDQ/ CF$_3$SO$_3$H, DCM, 0 ℃, 1h, 65%. (f) (1) NBS, BPO, CCl$_4$, reflux. (2) KOAc, Bu$_4$NBr, DMF, 100 ℃. (3) KOH (aq), THF/ethanol, reflux. (4) PCC, DCM, room temperature, 32% in four steps. (g) (1) mesitylmagnesium bromide, THF, room temperature. (2) BF$_3$•OEt$_2$, CH$_2$Cl$_2$, room temperature, **5-10**: 40 % yield and **5-11**: 5 % yield in two steps. (h) *p*-chloranil, toluene, room temperature, 12 h, 25%.
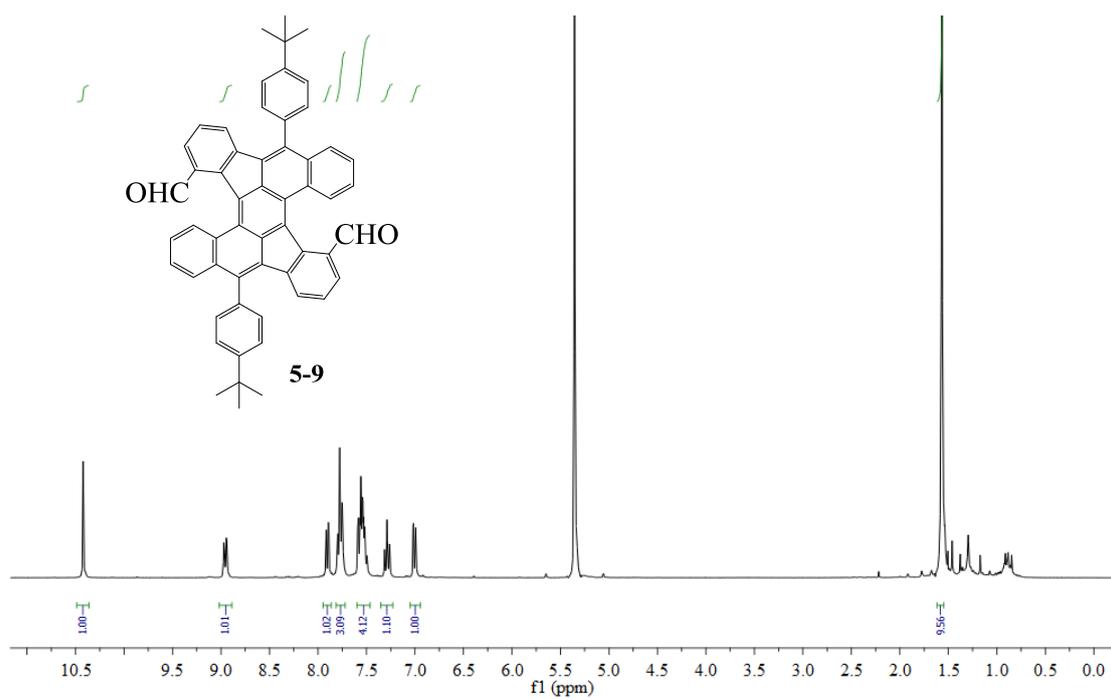
Figure 5-4. ^{1}H-NMR spectra of compounds **5-9** in CD$_2$Cl$_2$ at r.t.
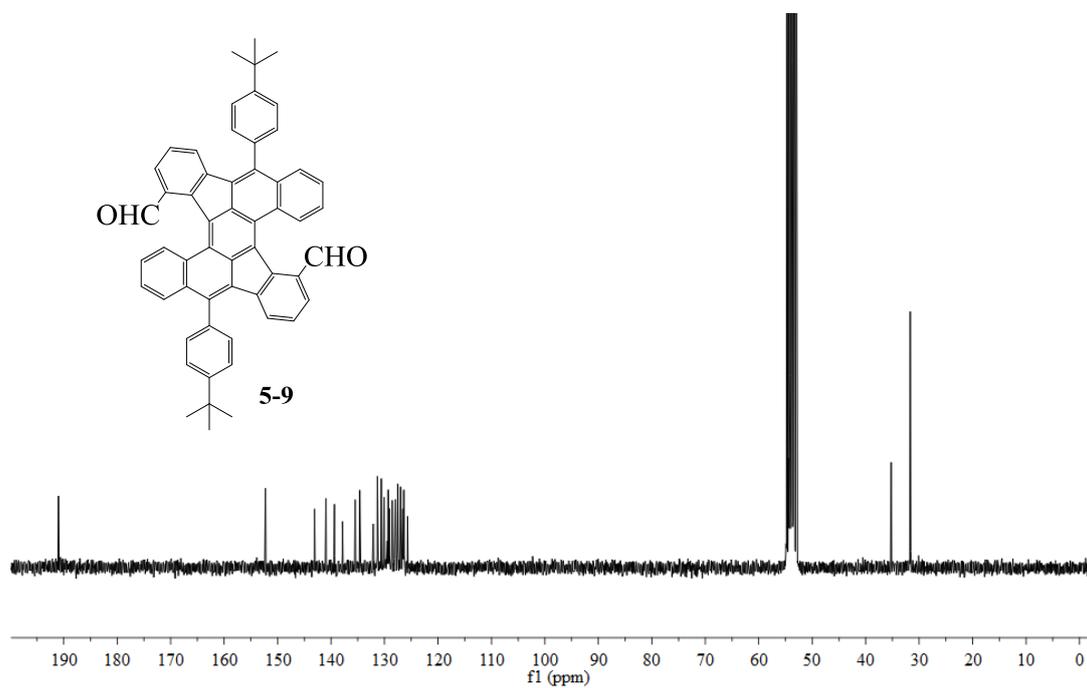
Figure 5-5. ^{13}C-NMR spectra of compounds **5-9** in CD$_2$Cl$_2$ at r.t.
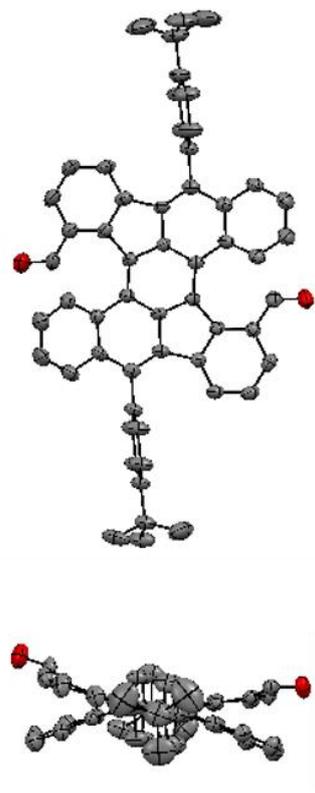
Figure 5-6. Crystal structure (ORTEP drawing) of **5-9** (Top and side view).

The key intermediate compound **5-9** was unambiguously characterized by nuclear magnetic resonance (NMR) (Figure 5-4 and 5-5) and single crystal X-ray analysis (Figure 5-6), from which one can confirm the aldehyde formation. The precursor compound **5-10** was also identified by MALDI-TOF MS analysis (Figure 5-7) and Nspectroscopy (Figure 5-8). Interestingly, the side product **5-11** also formed during the Friedel-Crafts alkylation step, which can be isolated from the mixture and identified by the single crystal X-ray analysis (Figure 5-9). From the crystal structure of **5-11**, it appears clearly that the Friedel-Crafts reaction leads to the formation of two seven-membered rings.
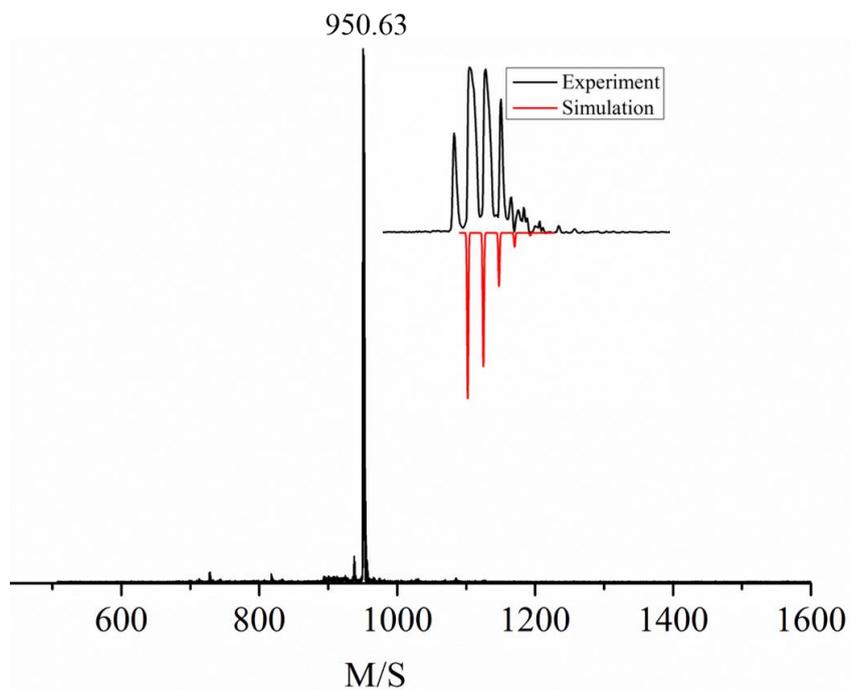
Figure 5-7. MALDI-TOF MS results of **5-10**.
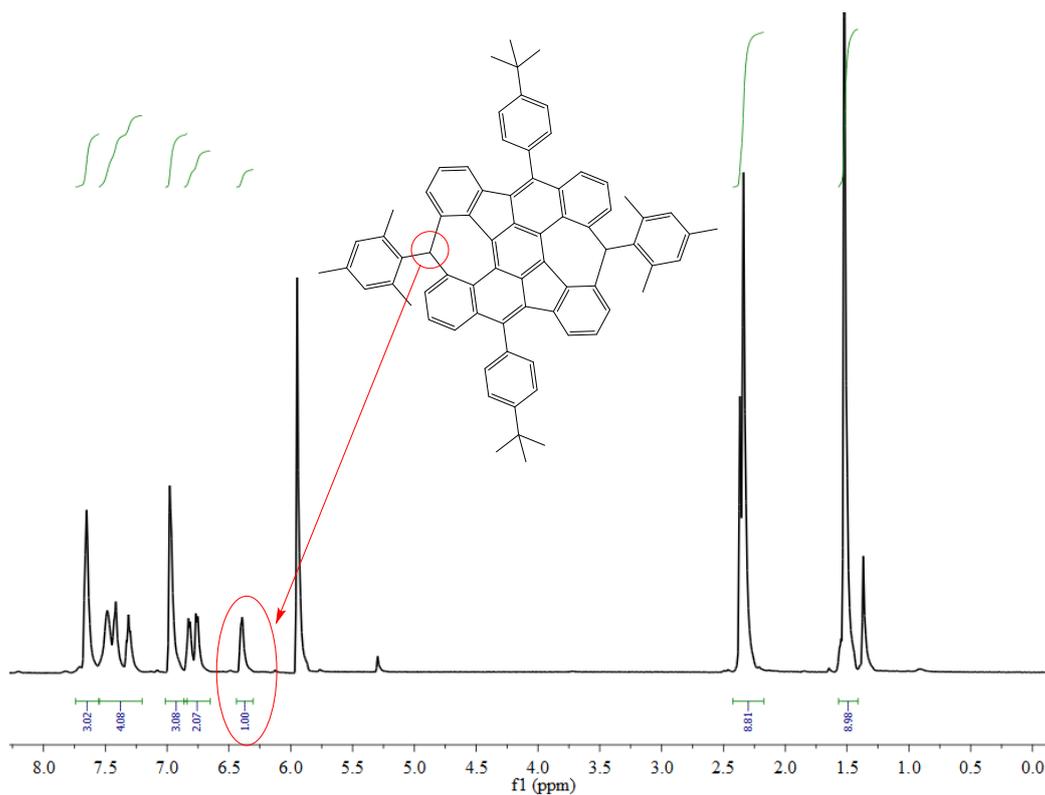
Figure 5-8. ^{1}H-NMR spectra of compounds **5-10** in C$_2$D$_2$Cl$_4$ at 403K.
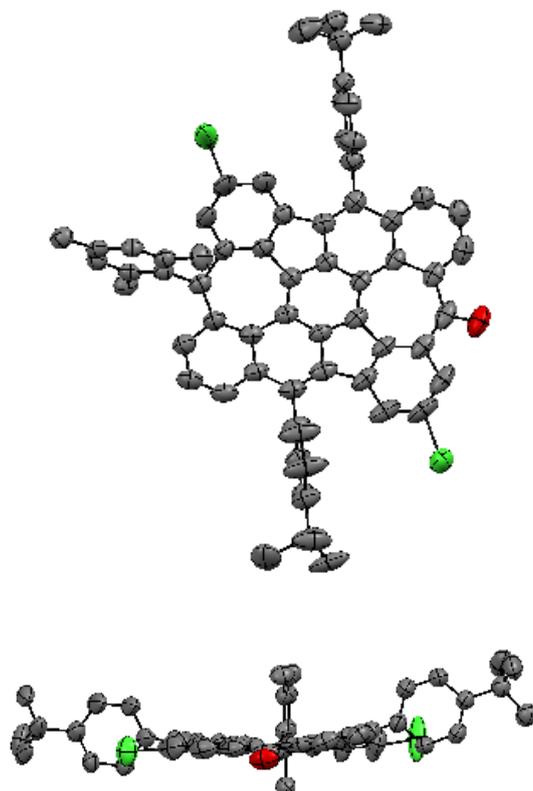
Figure 5-9. Crystal structure (ORTEP drawing) of by-product **5-11** (Top and side view).
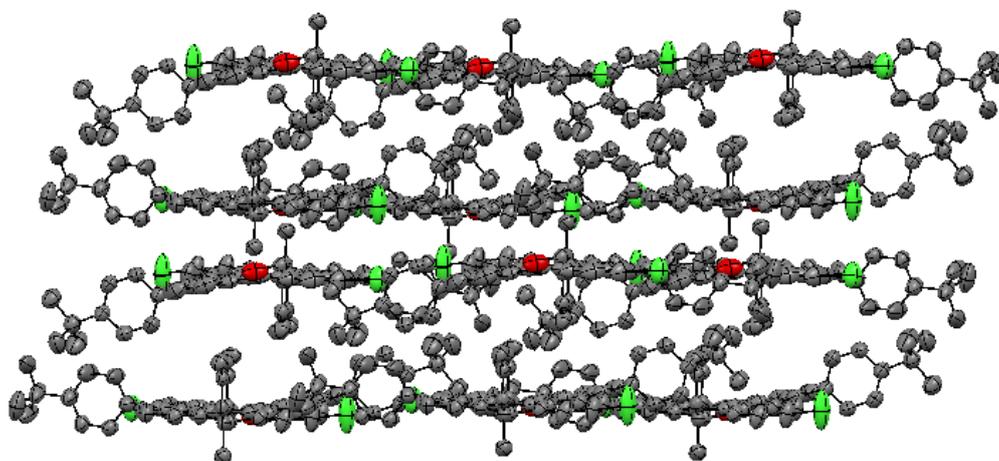
Figure 5-10. Crystal packing of by-product **5-11** (ORTEP drawing).

5.3 EPR analysis of 5-1

An electron paramagnetic resonance (EPR) measurement was carried out both in solution and in the solid state to confirm the biradical nature of **5-1**. Compound **5-1** in toluene at room temperature gave a well-resolved EPR spectrum with five lines due to the two electron spins with four adjacent hydrogen atoms. Furthermore, The EPR spectra can be reproduced by spectral simulation (Figure 5-11) (Collaboration with Prof. ███████████). The freshly prepared **5-1** in the solid state gave unresolved EPR spectra for a biradical with a broad peak at g-value 2.0003, as a result of both the inter- and intra-molecular interactions (Figure 5-12). Upon increasing the temperature, the EPR signal intensity increased resulting from a thermally excited triplet species which is slightly higher in energy than the singlet biradical state. Remarkably, the biradical feature was observed in toluene solution when it was frozen at 140 K, and the distance of the 2D/2 is approximately 62.8 mT (Figure 5-13). Interestingly, upon increasing temperature, the peak of the biradical feature became much broader, as a result of the melting of the toluene (Figure 5-14). Based on these EPR results we can safely conclude as to the biradical feature of compound **5-1**.
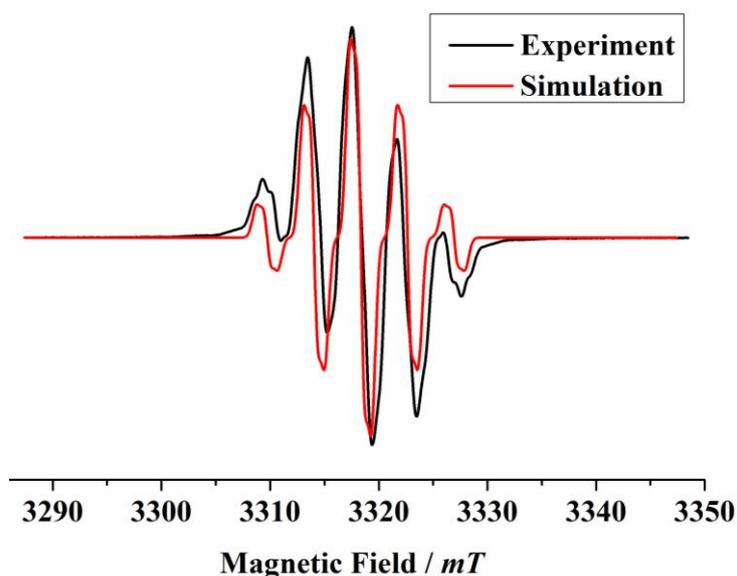
Figure 5-11. EPR spectra of 5-1 in toluene solution at room temperature (black line) and the simulation (red line).
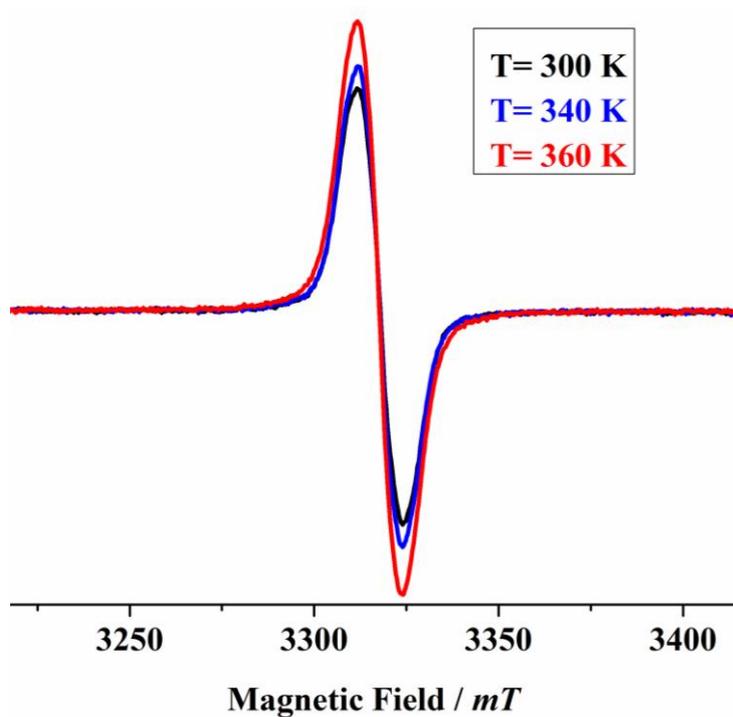
Figure 5-12. EPR spectra of **5-1** in solid state at different temperatures.
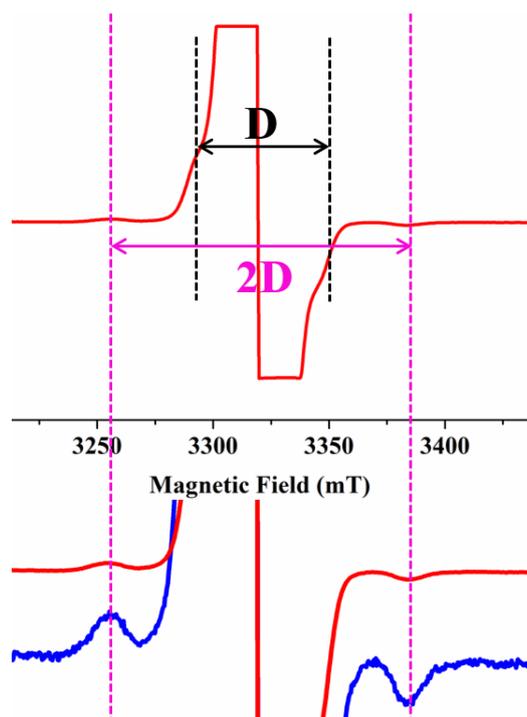
Figure 5-13. EPR spectra of **5-1** when frozen at 140 K.
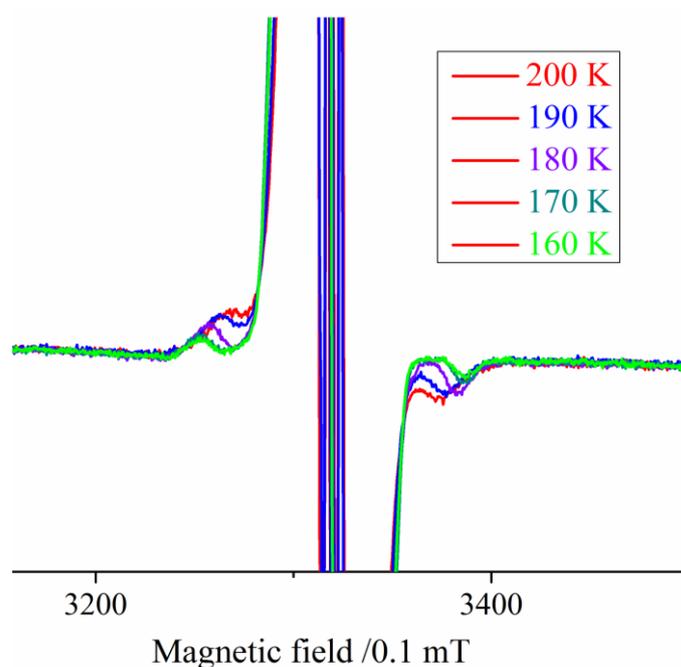
Figure 5-14. EPR spectra of **5-1** in the frozen state at different temperatures.

5.4 Optical Properties of 5-1
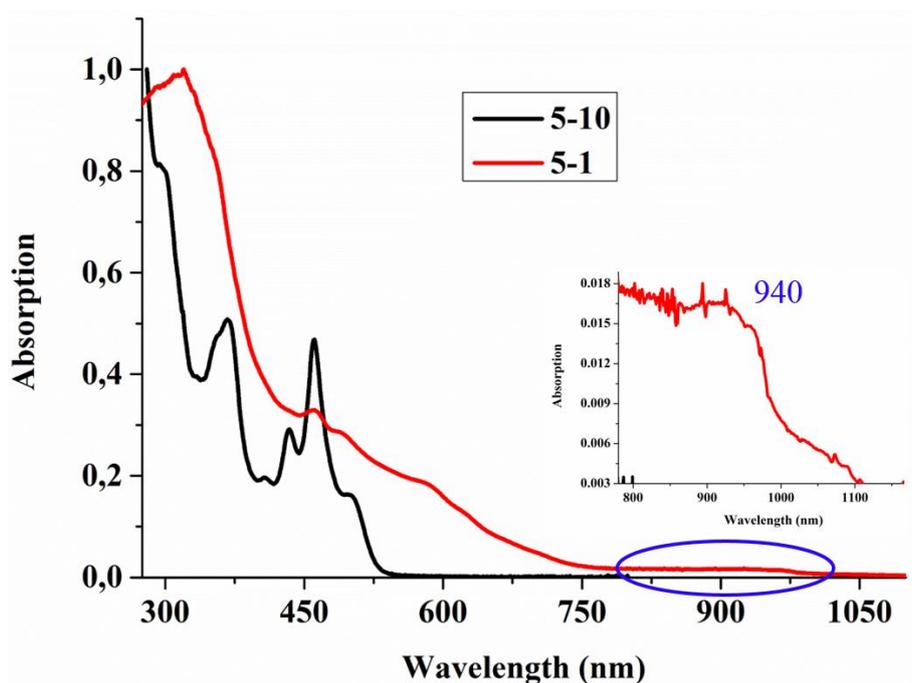
Figure 5-15. UV-vis absorption spectra of **5-1**.

Next, the UV-Vis absorption of precursor **5-10** and **5-1** were recorded in degassed and dry dichloromethane (DCM) solution and shown in Figure 5-15. The precursor **5-10** shows a

well-resolved *p*-band at 501 nm, which is typical for closed-shell PAHs. On the other hand, the absorption spectrum of deprotonated **5-10** displays a broad band in the near-infrared region with a maxima at 940 nm. Thus, from the onsets of the UV-vis absorption spectra, a low optical energy gap of 1.24 eV is derived for **5-1**. Importantly, the signature of the biradicaloid character is the presence of a low-lying excited singlet state dominated by the doubly excited configuration,[32] which suggested a singlet biradical nature of molecules **5-1**.

5.5 DFT calculations at the B3LYP/6-31G (d, p) level
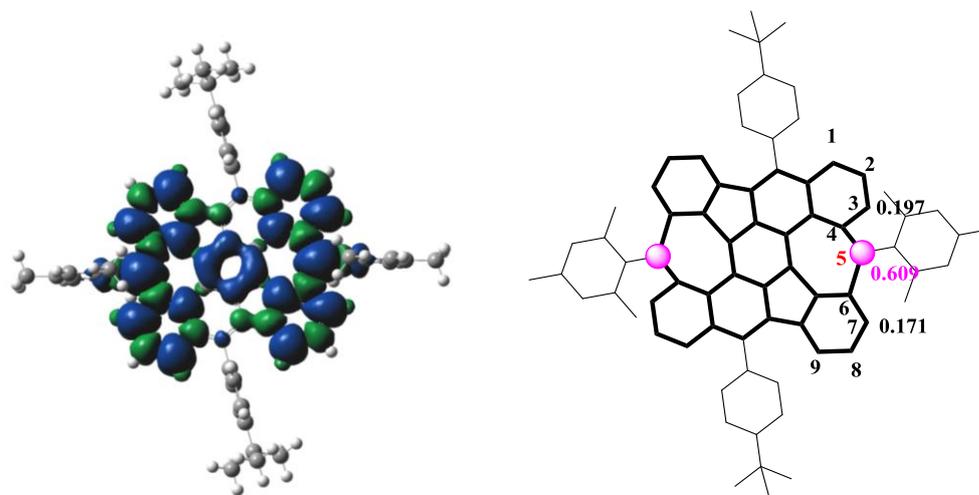
Figure 5-16. The spin density distribution of the triplet ground state of **5-1** and the numbers given in pink denote the spin density of the specific carbon atoms.

To gain an insight into the electronic structure of **5-1**, DFT calculations were conducted at the B3LYP/6-31G (d, p) level of theory using the Gaussian 09 program package. It appears that **5-1** has a moderate singlet biradical character index (y=0.66), as calculated by using the occupation numbers of the spin-unrestricted Hartree-Fock natural orbitals. This result is in agreement with the above EPR and UV-Vis analysis. Furthermore, the spin density of **5-1** is highly delocalized (Figure 5-16), while the carbons C5 has the largest spin densities, and the adjacent carbons C3 and C7 show much lower spin densities (Figure 5-16). These results suggest that **5-1** should be described as a resonance form between the Kekulé and biradical structure displayed in Figure 5-3. Furthermore, it was found that the energy of the singlet biradical state is lower than that of the triplet biradical and closed shell state (Table 1). From the calculation, the singlet-triplet energy gap ($\Delta E_{\text{S-T}}$) is 1.14 kcal/mol, meaning that **5-1** features a singlet biradical ground state.

Table 5-1. The energy level of 5-1 from the theory broken symmetry DFT calculation.

molecule	E, eV (triplet)	S^2 (triplet)	Singlet open shell E, eV (BS)	Singlet close shell E, eV (CS)	ΔE_{ST}, eV	ΔE_{ST}, kcal/mol
5-1	-7720.117093	2.056	-77720.166369	-77719.789332	-0,049276	-1,1443

5.6 Conclusions

In summary, we have successfully synthesized a five- and seven-membered rings embedding nanographene from an unexpected ring migration of 6,7,13,14-tetraphenylbenzo[k]tetraphene during the cyclodehydrogenation processs. Remarkably, the obtained odd-ring-embeding graphene subunit has a low optical energy gap (1.24 eV) and exhibits a singlet biradical character in the ground state, which is confirmed by EPR and UV-vis spectroscopies and also supported by DFT calculations. The outstanding method providing a unique and unprecedented entry to extend the new stable nanographene with biradicals feature. Furthermore, this pentagon- and heptagon-embedded compound can be considered as a short segment of an infinite graphene with defined defects. Therefore, our studies contribute to an understanding of the defect engineering in expanded PAH homologues or graphene.

References:

[1] L. Zhi, K. Müllen. J. Mater. Chem. 2008, 18, 1472-1484.

[2] J. Wu, W. Pisula, K. Müllen. Chem. Rev. 2007, 107, 718-747.

[3] L. Chen, Y. Hernandez, X. Feng, K. Müllen. Angew. Chem. Int. Ed. 2012, 51, 7640-7654.

[4] Y. Morita, S. Suzuki, K. Sato, T. Takui, Nature chem. 2011, 3, 197-203.

[5] T. Kubo, Chem. Rec. 2015, 15, 218-232.

[6] J. Inoue, K. Fukui, T. Kubo, S. Nakazawa, K. Sato, D. Shiomi, Y. Morita, K. Yamamoto, T. Takui, K. Nakasuji. J. Am. Chem. Soc. 2001, 123, 12702-12703.

[7] K. Fukui, J. Inoue, T. Kubo, S. Nakazawa, T. Aoki, Y. Morita. Synth. Metals. 2001, 121, 1824-1825.

[8] Z. Sun, Z. Zeng, J. Wu, Acc.Chem.Res. 2014, 47, 2582-2591.

[9] Z. Zeng, X. Shi, C. Chi, J. T. L. Navarrete, J. Casado, J. Wu. Chem. Soc. Rev. 2015, DOI: 10.1039/C5CS00051C.

[10] Y. Morita, S. Nishida, T. Murata, M. Moriguchi, A. Ueda, M. Satoh, K. Arifuku, K. Sato, T. Takui. Nature nano. 2011, 10, 947-951.

[11] K. Ohashi, T. Kubo, T. Masui, K. Yamamoto, K. Nakasuji, T. Takui, Y. Kai, I. Murata, I. J. Am. Chem. Soc. 1998, 120, 2018-2027.

[12] T. Kubo, M. Sakamoto, M. Akabane, Y. Fujiwara, K. Yamamoto, M. Akita, K. Inoue, T. Takui, K. Nakasuji, Angew. Chem. Int. Ed. 2004, 43, 7474-6479.

[13] T. Kubo, A. Shimizu, M. Sakamoto, M. Uruichi, K. Yakushi, M. Nakano, D. Shiomi, K. Sato, T. Takui, Y. Morita, K. Nakasuji, Angew. Chem. Int. Ed. 2005, 44, 6564-6568.

[14] A. Shimizu, M. Uruichi, K. Yakushi, H. Matsuzaki, H. Okamoto, M.Nakano, Y. Hirao, K. Matsumoto, H. Kurata, T. Kubo, Angew. Chem. Int. Ed. 2009, 48, 5482-5486.

[15] A. Shimizu,a Y. Hirao, K. Matsumoto, H. Kurata, T. Kubo, M. Uruichi, K. Yakushi, Chem. Commun. 2012, 48, 5629-5631.

[16] K. Uchida, Y. Hirao, H. Kurata, T. Kubo, S, Hatano, K. Inoue, Chem. Asian J. 2014, 9, 1823-1829.

[17] A. Le Berre, Ann. Chim. 1957, 13, 371-425.

[18] D. T. Chase, A. G. Fix, B. D. Rose, C. D. Weber, S. Nobusue, C. E. Stockwell, L. N. Zakharov, M. C. Lonergan, M. M. Haley, Angew. Chem. Int. Ed. 2011, 50, 11103-11106.

[19] D. T. Chase, B. D. Rose, S. P. McClintock, L. N. Zakharov, M. M. Haley, Angew. Chem. Int. Ed. 2011, 50, 1127-1130.

[20] D. T. Chase, A. G. Fix, S. J. Kang, B. D. Rose, C. D. Weber, Y. Zhong, L. N. Zakharov, M. C. Lonergan, C. Nuckolls, M. M. Haley, J. Am. Chem. Soc. 2012, 134, 10349-10352.

[21] A. Shimizu, Y. Tobe, Angew. Chem. Int. Ed. 2011, 50, 6906-6910.

[22] A. Shimizu, R. Kishi, M. Nakano, D. Shiomi, K. Sato, T. Takui, I. Hisaki, M. Miyata, Y. Tobe, Angew. Chem. Int. Ed. 2013, 52, 1-5.

[23] A. Konishi, Y. Hirao, M Nakano, A. Shimizu, E. Botek, B. Champagne, D. Shiomi, K. Sato, T. Takui, K. Matsumoto, H. Kurata, T. Kubo, J. Am. Chem. Soc. 2010, 132, 11021-11023.

[24] A. Konishi, Y. Hirao, K. Matsumoto, H. Kurata, R. Kishi, Y. Shigeta, M. Nakano, K. Tokunaga, K. Kamada, T. Kubo, J. Am. Chem. Soc. 2013, 135, 1430-1437.

[25] Z. Sun, K. W. Huang, J. Wu, J. Am. Chem. Soc. 2011, 133, 11896-11899.

[26] Y. Li, W. K. Heng, B. S. Lee, N. Aratani, J. L. Zafra, N. Bao, R. Lee, Y. M. Sung, Z. Sun, K. W. Huang, R. D. Webster, J. T. L. Navarrete, D. Kim, A. Osuka, J. Casado, J. Ding, J. Wu, J. Am. Chem. Soc. 2012, 134, 14913-14922.

[27] Z. Sun, S. Lee, K. H. Park, X. Zhu, W. Zhang, B. Zheng, P. Hu, Z. Zeng, S. Das, Y. Li, C. Chi, R. W. Li K. W. Huang J. Ding, D. Kim, J. Wu, J. Am. Chem. Soc. 2013, 135, 18229-18236.

[28] S. Das, S. Lee, M. Son, X. Zhu, W. Zhang, B. Zheng, P. Hu, Z. Zeng, Z. Sun, W. Zeng, R. W. Li, K. W. Huang, J. Ding, D. Kim, J. Wu, Chem. Eur. J. 2014, 20, 11410-11420.

[29] Y. Li, K. W. Huang, Z. Sun, R. D. Webster, Z. Zeng, W. Zeng, C. Chi, K. Furukawa, J. Wu, Chem. Sci. 2014, 5, 1908-1914.

[30] K. Y. Cheung, X. Xu, Q. Miao. J. Am. Chem. Soc. 2015, 137, 3910-3914.

[31] K. Kawasumi1, Q. Zhang, Y. Segawa, L. T. Scott, K. Itami. Nature chem. 2013, 5, 739-744.

[32] S. D. Motta, F. Negri, D. Fazzi, C. Castiglioni, E. V. Canesi. J. Phys. Chem. Lett. 2010, 1, 3334-3339.

Chapter 6. Stable Antiaromatic Acene Analogue:
Cyclopenta[*pqr*]indeno[2,1,7-*ijk*]tetraphene

To date, it remains highly challenging to synthesize antiaromatic polycyclic aromatic hydrocarbons due to their high highest occupied molecular orbital (HOMO) levels and low lowest unoccupied molecular orbital (LUMO) levels leading to reactive and unstable nature. In chapter 3, a novel tetrabenzo[*a,f,j,o*]perylene, namely "bistetracene" that consists of two tetracenes connected side by side with two bonds, was synthesized and characterized. At the beginning of the synthetic attempts toward this bistetracene, another synthetic route was employed, which unexpectedly led to the formation of an antiaromatic acene analogue, dibenzo-indeno[1,2-*b*]fluorene: cyclopenta[*pqr*]indeno[2,1,7-*ijk*]tetraphene (**CPIT**). In this work, the detail synthetic procedure towards **CPIT** will be described. Moreover, **CPIT** shows stable 24-π-electron antiaromatic feature. The synthetic strategy to construct five-membered ring in this work provides a unique entry to develop pentagon-embedded or antiaromatic polycyclic aromatic hydrocarbons (PAHs).

6.1 Introduction
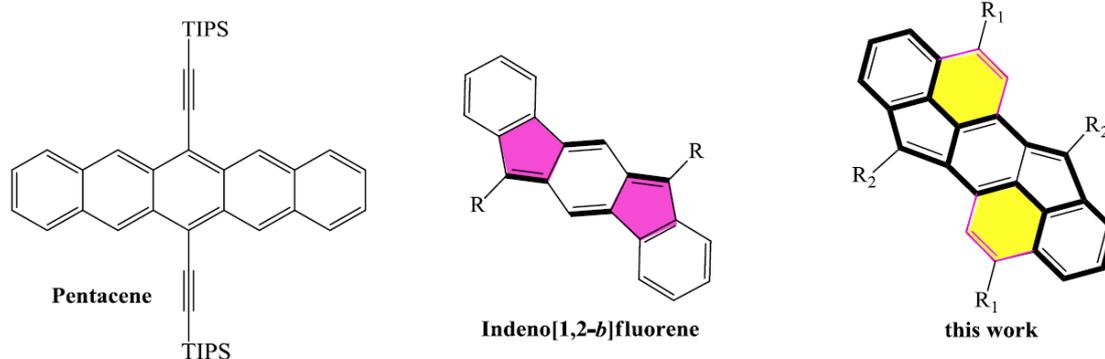
Scheme **6-1**. Structure of the indeno[1,2-*b*]fluorene and its derivatives.

PAHs have attracted considerable attention over the last two decades for the potential use in a variety of materials applications, for example, in field-effect transistors, photovoltaics, and light-emitting diodes.[1-7] Among various PAHs, acenes such as pentacene and its derivatives

are remarkable candidates for electronic devices due to their high intrinsic charge carrier mobilities.[8] These acene-systems are, however, susceptible to oxidation under ambient conditions and photolytic degradation when further extended to higher acence homologues.[9-11]

indeno[1,2-b]fluorene

indeno[2,1-b]fluorene

indeno[2,1-a]fluorene

indeno[2,1-c]fluorine
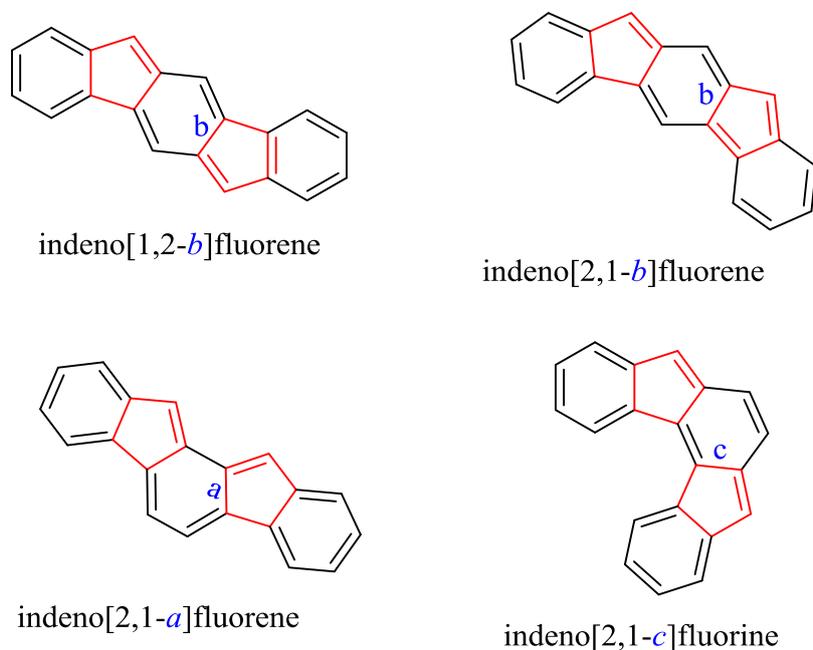
Scheme **6-2**. The isomers structure of indenofluorene molecules.

As discussed in the chapter 3, the zigzag-edged bistetracene possesses a prominent biradical character in the ground state due to the formation of aromatic sextets that overwhelms the penalty for breaking the π-bond and pushes the resulting unpaired electrons out to the zigzag edges. These molecules generally belong to the Kekulé diradicals with *pro*-aromatic structures.[12] In the *pro*-aromatic concept for the formation of diradicals, the driving force is the aromaticity gaining from aromatic stabilization energy, i.e., a net energy minimization that can eventually surpass the energy required to break a double bond, thus giving a way to the generation of a diradical. In addition, some other Kekulé diradicals have antiaromatic cores instead of the *pro*-aromatic structures. Antiaromatic molecules are defined in terms of the existence of 4n π-electrons disposed in a planar cyclic arrangement. As a typical representative among the antiaromatic system, indenofluorenes, which is a prominent 20-π-electron, fully conjugated antiaromatic analogue of acenes with 6-5-6-5-6 fused ring (Scheme **6-2**). Compared to the acene-type aromatic compounds, the fused polycyclic antiaromatic systems are considered to have high HOMO levels and low LUMO levels, leading to

narrower HOMO-LUMO energy gaps. Although antiaromatic systems are generally reactive and unstable, the introduction of bulky groups at the reactive sites would enhance the kinetic and thermodynamic stability and even allow for their solution processing for device studies.[13, 14] Thus, alternative acene-like stable topology is of great demand for further application of such materials. Recently, indenofluorene skeleton with a 6-5-6-5-6 fused ring system in its fully conjugated state like the pentacene geometry, has been introduced by the Haley and Tobe groups.[15-26] However, only a few examples of the synthesis of *o*- and *p*-quino-dimethane derivatives containing indeno[1,2-*b*]fluorene or indeno[2,1-*b*]fluorene have been reported until now (Scheme **6-2**).[27-30] It remains a great challenge to develop expanded indenofluorene systems, because of the high reactivity of such antiaromatic compounds. In order to elucidate more details about the physical and chemical properties of the antiaromatic systems, new or much larger π-conjugated antiaromatic analogues need to be systematically investigated. In pursing the synthesis of larger and stable conjugated antiaromatic molecules, we unexpectedly achieved the synthesis of an 24-π-electron antiaromatic acene analogue in the solution, namely dibenzo-Indeno[1,2-*b*]fluorene: cyclopenta[*pqr*]indeno[2,1,7-*ijk*]tetraphene (**CPIT**) from the key precursor 5,12-diphenylbenzo[*k*]tetraphene, which is associated with the Friedel-Crafts reaction during the UV-irradiation.

6.2 Synthesis and structure verification

In chapter 3, a novel tetrabenzo[*a,f,j,o*]perylene (**3-1**), namely "bistetracene", in which two tetracenes are connected side by side with two bonds, was synthesized and characterized. At the beginning, we conceived another strategy to prepare bistetracene **3-1** from the key precursor 7,14-diphenylbenzo[*k*]tetraphene (**6-5**), as depicted in Scheme **6-3**. Interestingly, the results were not what we expected. We found that the key intermediate 2',5'-di((*Z*)-styryl)-1,1':4',1''-terphenyl (**6-4**) was transformed into 5,12-diphenylbenzo[*k*]tetraphene (**6-12**) instead of **6-5** upon the photocyclization (Scheme **6-4**), which is associated with the Friedel-Crafts reaction during the UV-irradiation, most likely due to the steric hindrance of the phenyl group which prevented the photocyclization of stilbenes. Thus, the final compound 4,10-dimesityl-6,12-diphenylcyclopenta[*pqr*]indeno[2,1,7-*ijk*]tetraphene (**6-1**) was obtained instead of **3-1** (Scheme **6-4**). The chemical identity of **6-1b** was firstly confirmed by MALDI-TOF MS analysis with solid-state sample preparation, as depicted in Figure **6-1**. There is only one dominant peak in the respective mass spectrum of **6-1b**, revealing its defined molecular composition. The isotopic distribution pattern of the mass peak is in good agreement with the

calculated one. Moreover, the structure of **6-1** was also unambiguously confirmed by the single crystal analysis (Figure **6-2**).
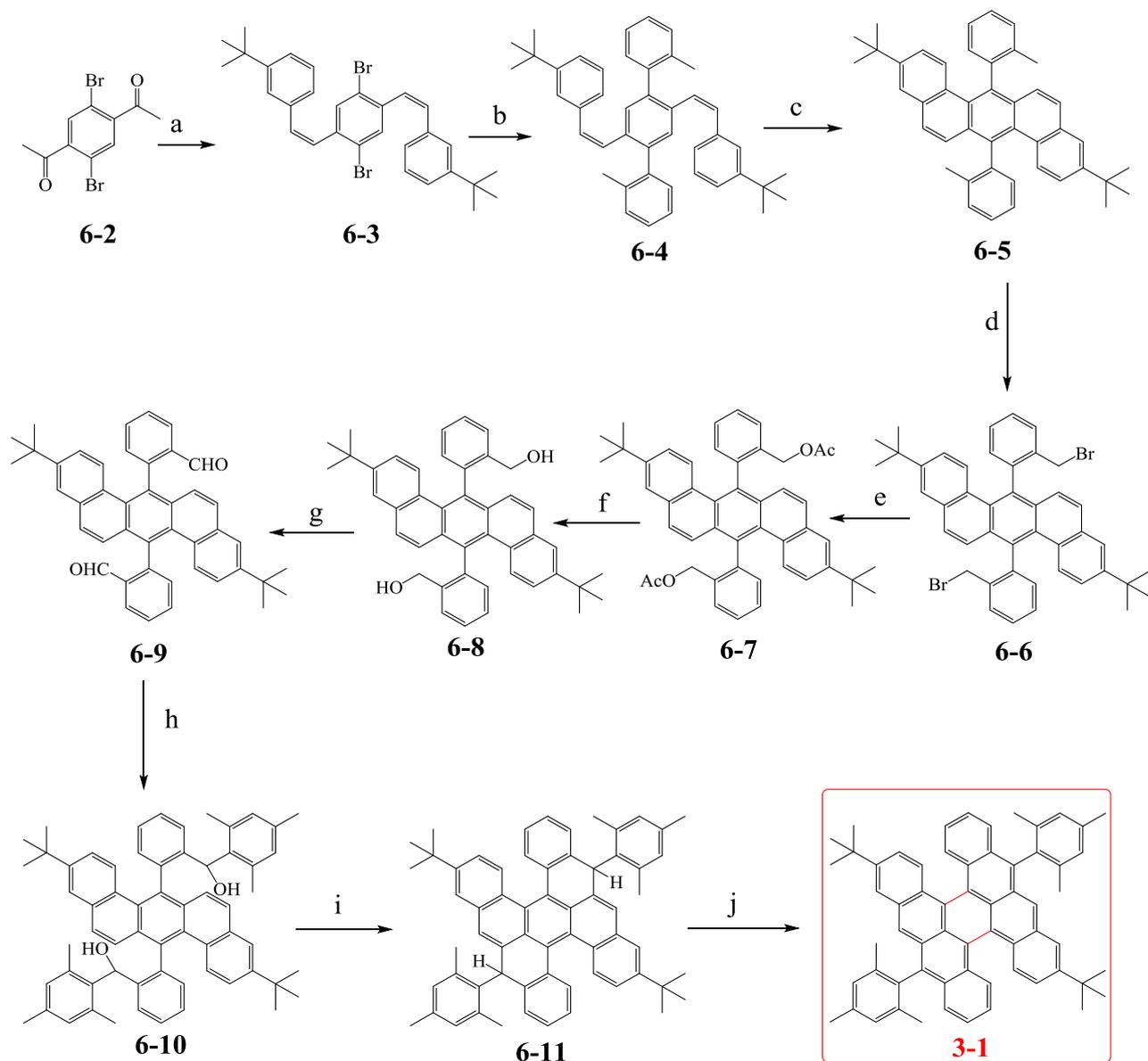
Scheme **6-3**. Synthetic route toward the bistetracene **3-1**.
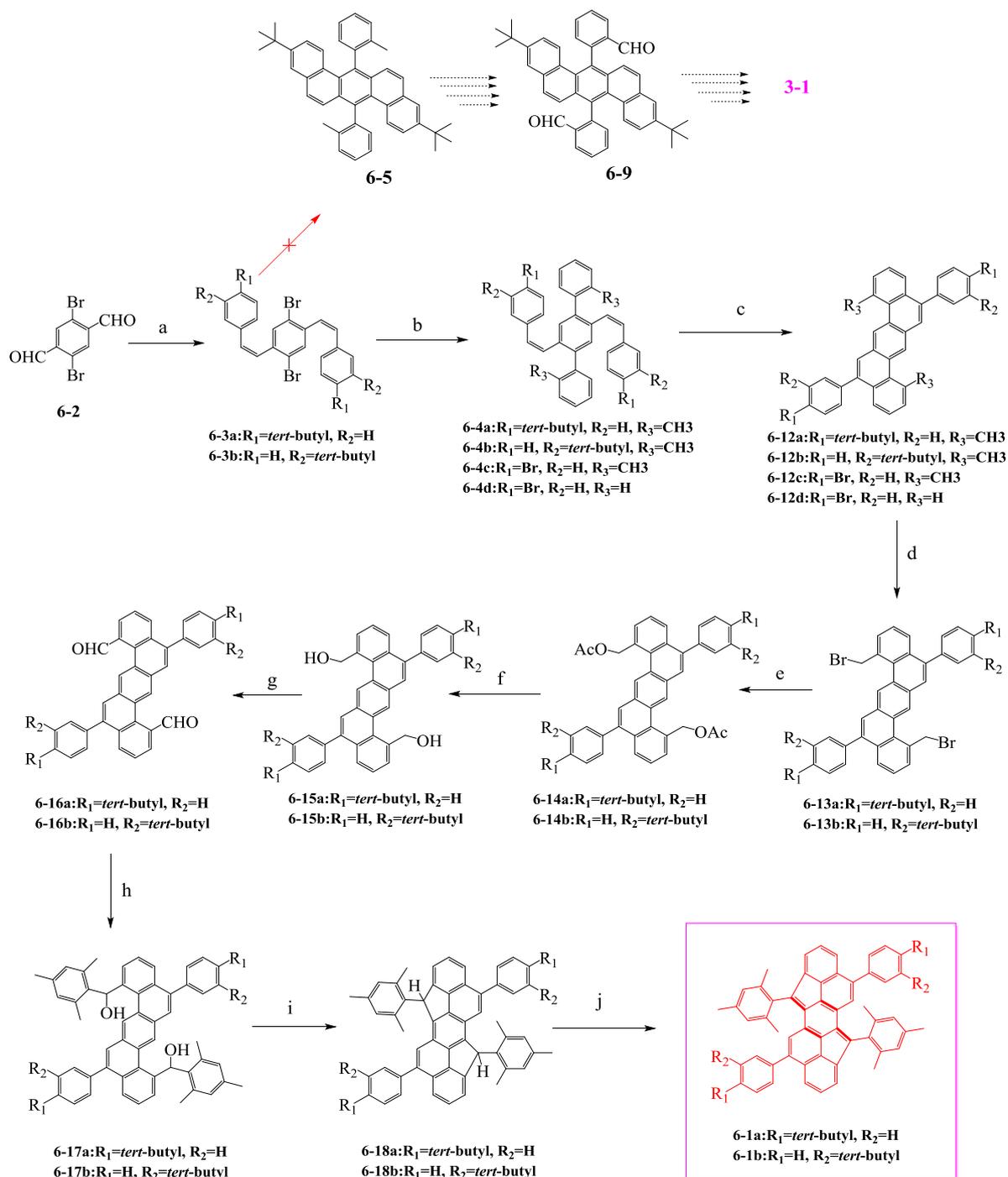
Scheme **6-4**. Synthetic route toward **6-1**. (a) *t*-BuOK, THF, 12 h, 76.8%. (b) Pd(PPh$_3$)$_4$/Na$_2$CO$_3$, toluene/H$_2$O/ethanol, 85 °C , 24 h, 80.6%. (c) *hv*, I$_2$, propylene oxide, toluene, 8 h, 60.5%. (d) NBS, BPO, CCl$_4$, reflux. (e) KOAc, Bu$_4$NBr, DMF, 100 °C, 57% in two steps from **6-12**. (f) KOH (aq), THF/ethanol, reflux. (g) PCC, DCM, room temperature, 50% in two steps from **6-14**. (h) mesitylmagnesium bromide, THF, room temperature. (i) BF$_3$·OEt$_2$, CH$_2$Cl$_2$, room temperature. (j) DDQ, toluene, room temperature, 40% in three steps from **6-16**.
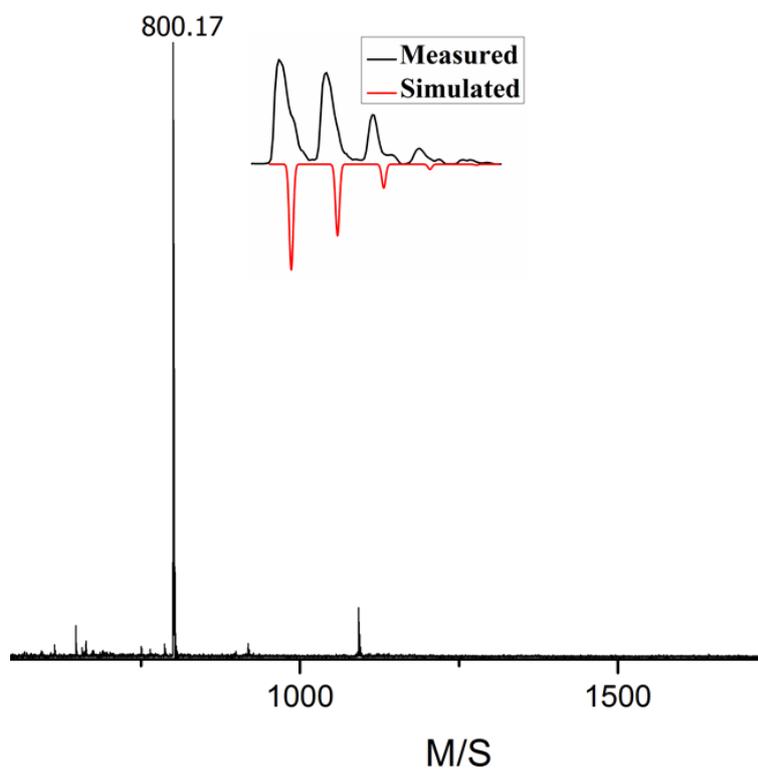
Figure **6-1**. MALDI-TOF spectrum of **6-1b**.
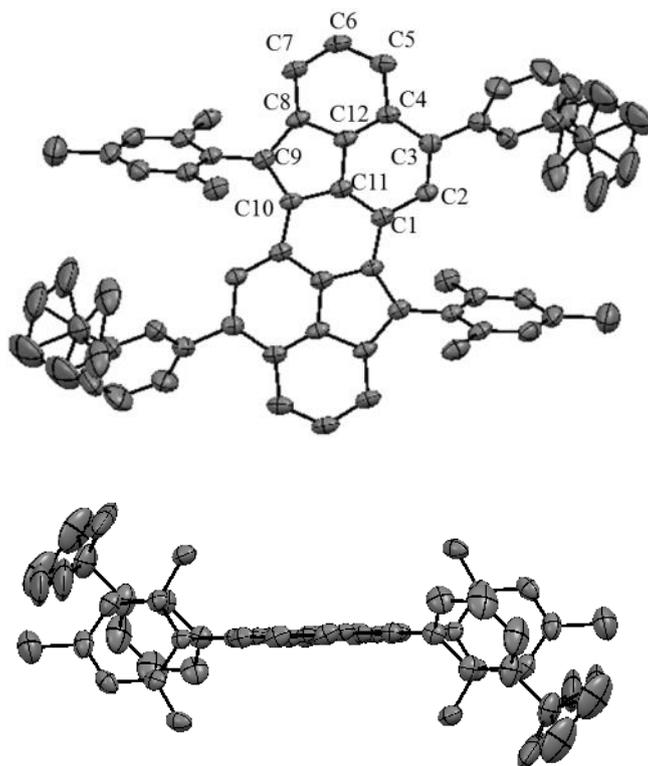
Figure **6-2**. X-ray crystal structure of compound **6-1b** (top and side views).
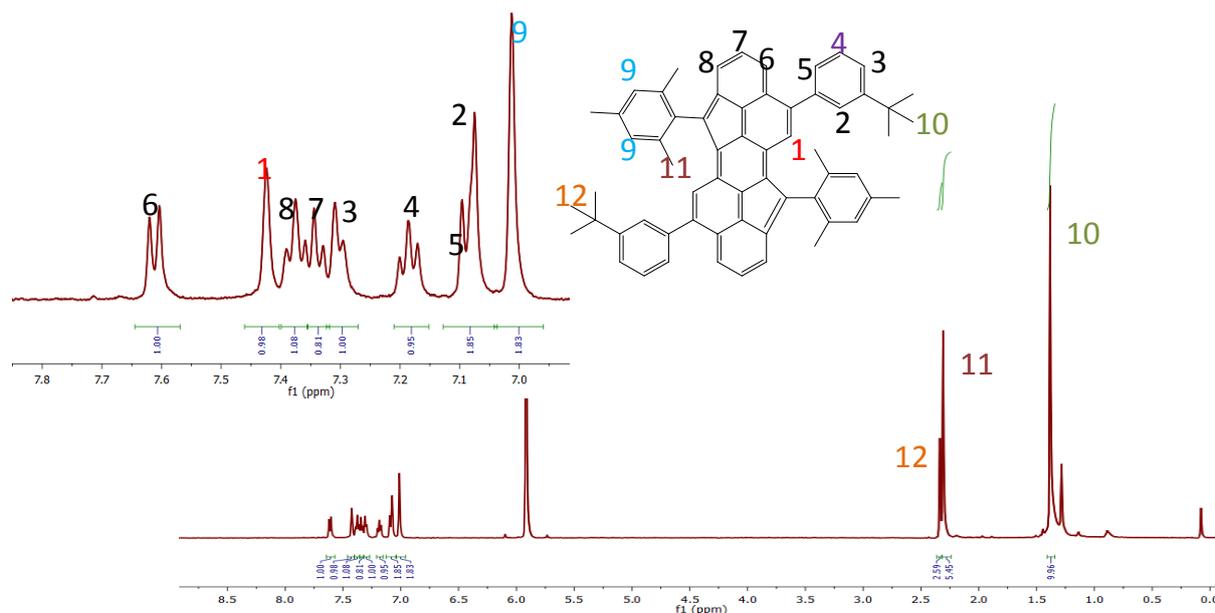
Figure **6-3**. ^{1}H-NMR spectrum of compound **6-1b** in CD$_2$Cl$_2$.
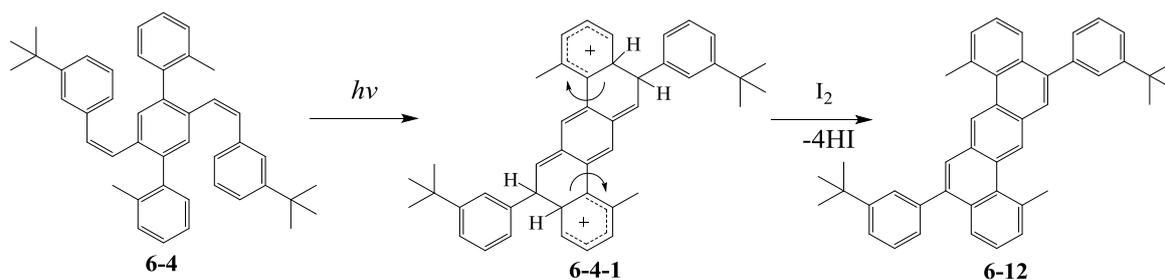
Figure **6-4**. A possible formation mechanism of the compound **6-12**.

Firstly, we need to know why the unexpected compound **6-1** was obtained during the synthesis of bistetracene **3-1**. We found that **6-4** was transformed into **6-12** instead of **6-5** upon the photocyclization. In such case, compound **6-4** underwent the Friedel-Crafts reaction during the UV irradiation, rather than the photocyclization of stilbenes, most likely due to the steric hindrance of the phenyl group. A possible formation mechanism of **6-12** is depicted in Figure **6-4**. First, the arenium cation **6-4-1** was formed under the UV-irradiation. Then, dehydrogenation was preformed via oxidation by using the iodine which afforded compound **6-12**. The structure of the photocyclization product **6-12d** was confirmed by the single crystal analysis, as show in Figure **6-5**.
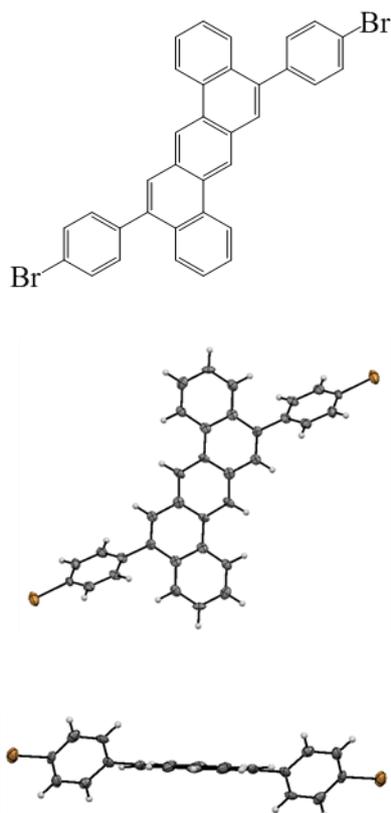
Figure **6-5**. X-ray crystal structure of compound **6-12d** (top and side views).

Thus, compound **6-1** was synthesized through eight steps starting from 2,5-dibromoterephthalaldehyde by following the efficient synthetic route, as shown in Scheme **6-4**. First, **6-4** was obtained by Wittig reaction and Suzuki coupling in 75% yield. Then **6-12** was furnished from **6-4** through the photocyclization in 60% yield. The two methyl groups of **6-12** were then transformed into aldehydes to afford 5,12-diphenylbenzo[*k*]tetraphene-1,8-dicarbaldehyde (**6-16**), via a bromination, esterification, hydrolysis and oxidation sequence in 40% yield in four steps. Afterwards, dialdehyde **6-16** was treated with mesitylmagnesium bromide to provide (5,12-diphenylbenzo[*k*]tetraphene-1,8-diyl)bis(mesitylmethanol) (**6-17**), which was further subjected to a Friedel-Crafts alkylation reaction promoted by $BF_3 \cdot OEt_2$ to afford 4,10-dimesityl-6,12-diphenyl-4,10-dihydrocyclopenta[*pqr*]indeno[2,1,7-*ijk*]tetraphene (**6-18**) in 78% yield in two steps. The final product **6-1** was obtained as a purple-red solid by oxidation of **6-18** with DDQ in toluene in 81% yield.
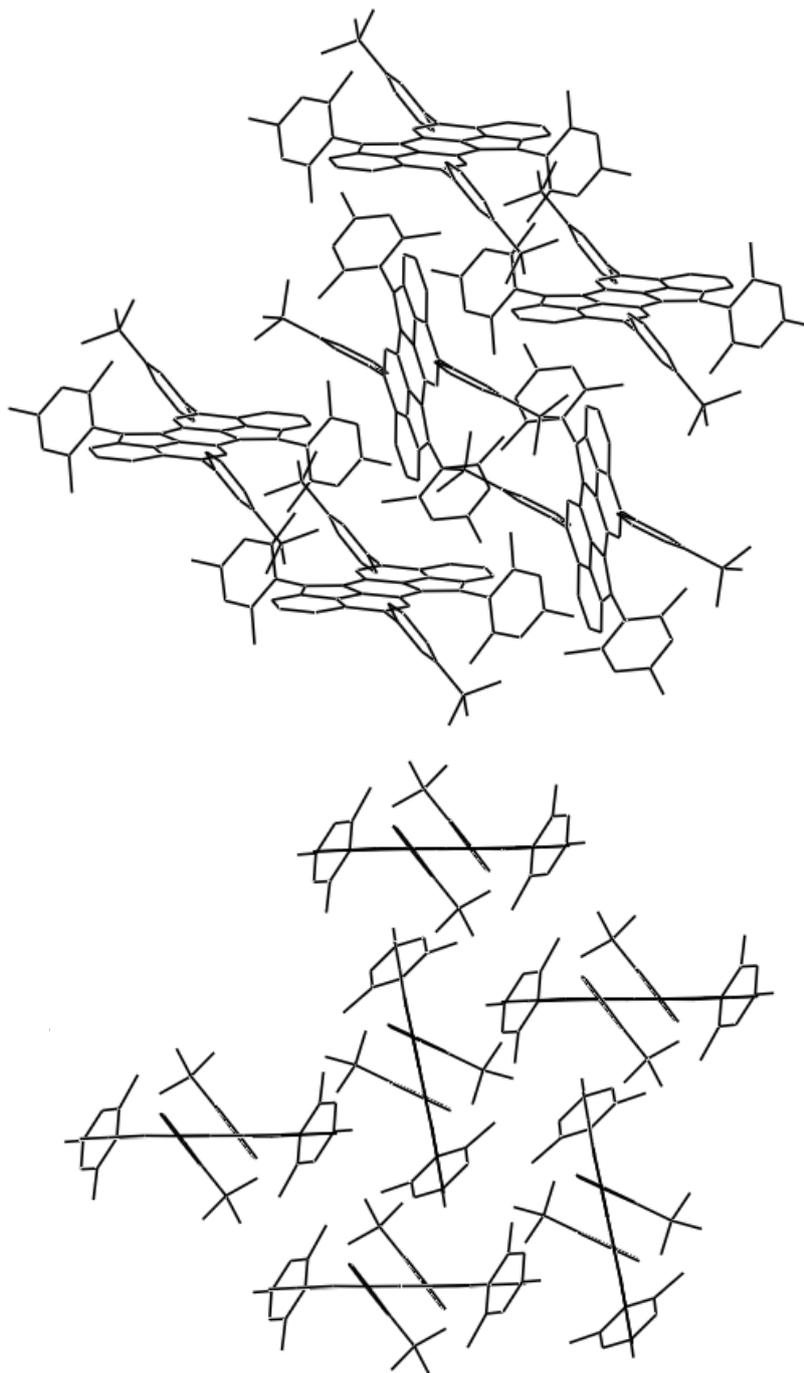
Figure **6-6**. Crystal packing of the **6-1b**.

The purple prism shaped crystals of **6-1b** suitable for single-crystal X-ray analysis was grown from solutions in hexane/dichloromethane. The crystal structure of **6-1b** is shown in Figure **6-2**, and relevant bond lengths are given in Table **6-1**. Notably, the planarity of the skeleton of **6-1** has not been affected by the extension of the indenofluorene core with two additional annulene rings at the bay positions. The observed bond lengths indicate that the central six-membered ring has two short $C(sp^2)$-$C(sp^2)$ bonds (C1-C11: 1.389Å) and four long $C(sp^3)$-

$C(sp^3)$ bonds (C1-C10: 1.460 Å and C10-C11: 1.455 Å). These core bond lengths are in agreement with a *p*-quinodimethane structure (Figure **6-7**). Furthermore, we found that the opposite ring of the five-membered ring contains a C-C double bond (C2-C3), which is 1.388 Å, and in comparison, the lengths displayed for C1-C2 and C3-C4 are 1.421 Å and 1.438 Å, respectively. The bonds of the outside peripheral benzene are relatively homogeneous and around 1.388-1.400 Å. The Nucleus-independent chemical shift (NICS) calculations were performed at the GIAO-B3LYP/6-31G(d,p) level of **6-1b** to investigate the aromaticity of each ring, and the obtained NICS values were -12.64 and -16.85 for the peripheral benzene rings, and 20.23 and 15.51 for the five-membered and the central rings, respectively (Figure **6-8**). This result suggests that the central *p*-xylylene core has alternating long and short bonds as shown in Figure **6-7**, and the outer benzene rings stay π-electron delocalized. All these characters agree with the antiaromatic nature of **6-1b**.
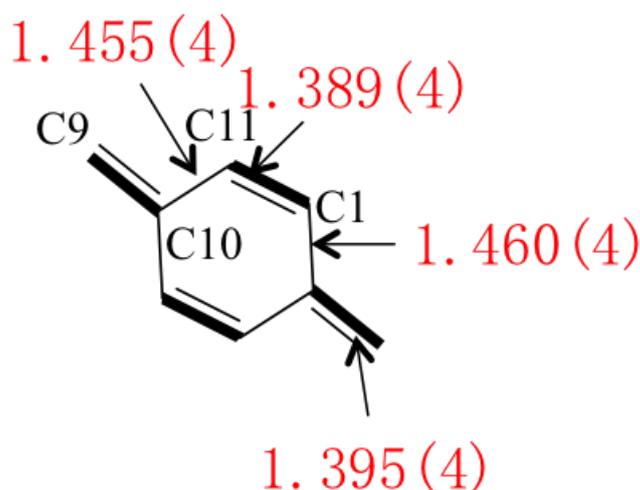
Figure **6-7**. Bond length in the central benzene ring of **6-1b**.

Next, DFT calculations were performed to gain theoretical insight into the structure of compound **6-1**. The geometry optimization was performed at B3LYP/6-31G(d,p) level of theory using Gaussian 09 program package, which provided bond length of 1.389Å, 1.457Å and 1.387Å for C1-C11, C1-C10 and C9-C10, respectively (Table **6-1**). And the bond lengths of the peripheral ring are 1.396Å, 1.388Å and 1.425Å for C2-C3, C5-C6 and C6-C7, respectively. These results are consistent with those obtained from the X-ray analysis.

Table **6-1**. Experimental and calculated bond lengths of **6-1b** and a structurally related *p*-xylylene molecule.

bond	X-ray structure	Optimized geometry
C(1)----C(10)	1.460(4)	1.457
C(1)----C(11)	1.389(4)	1.389
C(1)----C(2)	1.421(4)	1.431
C(4)----C(5)	1.440(4)	1.428
C(5)----C(6)	1.389(5)	1.388
C(6)----C(7)	1.400(5)	1.425
C(7)----C(8)	1.388(4)	1.382
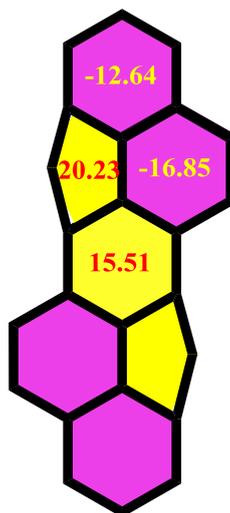
Figure **6-8**. Nucleus-independent chemical shift (NICS) values of the **6-1b**.
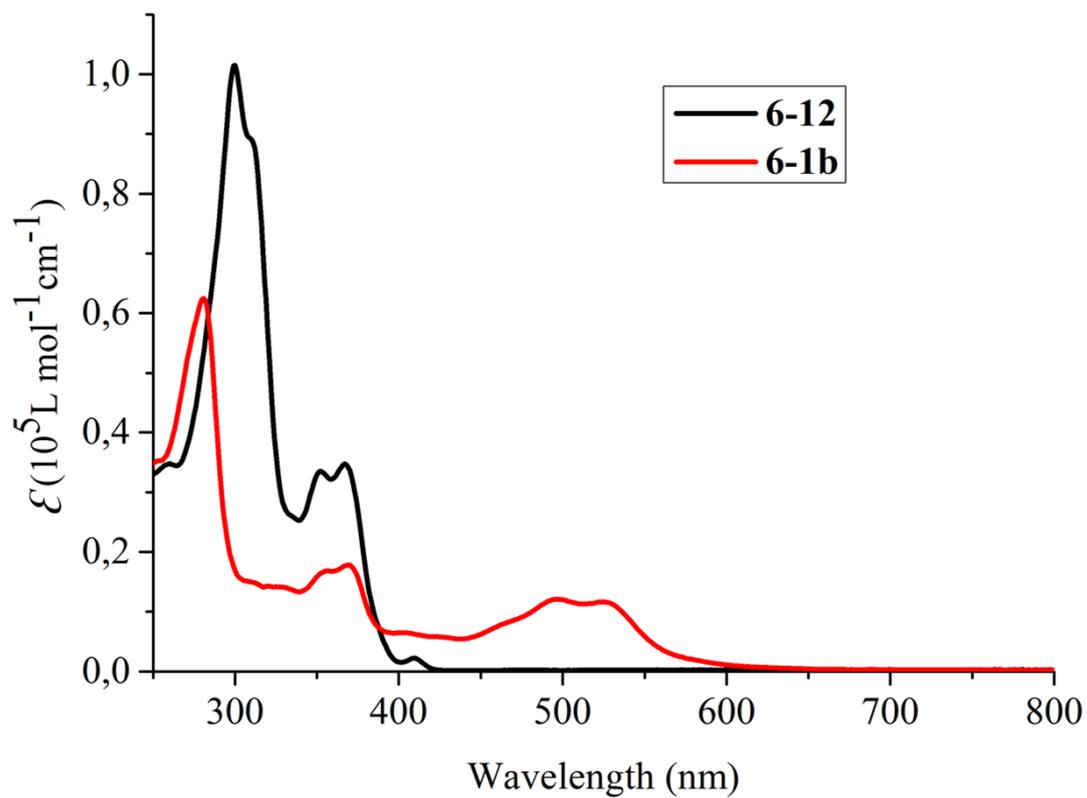
Figure **6-9**. UV-Vis absorption spectra of compound **6-1** (10^{-5} M in DCM).
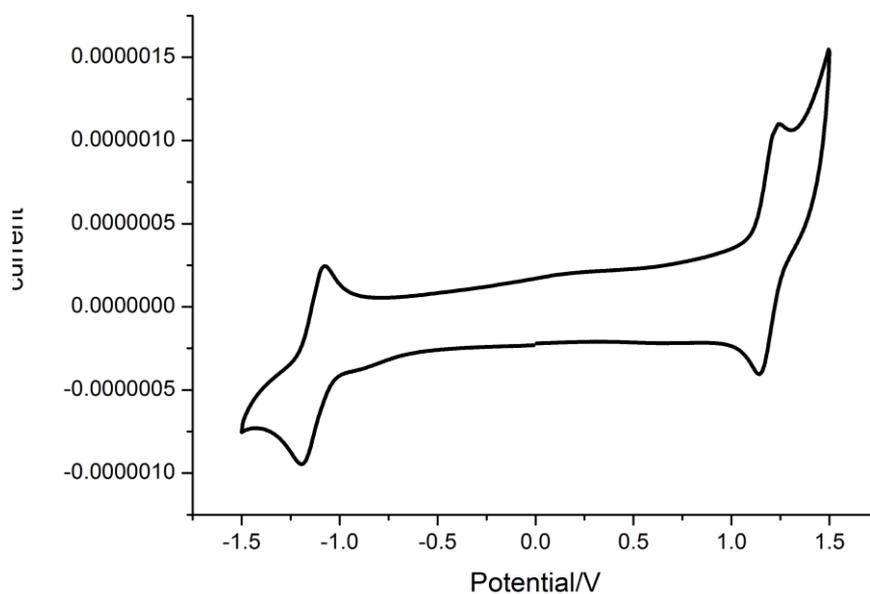
Figure **6-10**. Cyclic voltammogram of **6-1b** in degassed and dry dichloromethane solution (scan rate 50 mVs^{-1}).

The deep purple solution of compound **6-1b** was non-emissive when excited with UV-light, which agrees with the case of [4n]-π-electrons antiaromatic system. The UV-Vis absorption spectrum of **6-1** is shown in Figure **6-9**. The longest wavelength absorption maximum (526 nm) of **6-1b** was approximately 20 nm blue-shifted in comparison to that of indenofluorene.[15] From the onsets of its UV-vis absorption spectra, a low optical energy gap of 2.01 eV is derived for **6-1b**. The electrochemical properties of **6-1b** were investigated by cyclic voltammetry (CV) measurements (Figure **6-10**). Compound **6-1b** exhibited reversible reduction and oxidation peak at -1.18 and 1.21 eV, respectively. On this basis, the LUMO and HOMO energy levels of **6-1b** were estimated to be -3.46 and -5.57 eV, respectively. This corresponds to an electrochemical energy gap of 2.11 eV, which is in good agreement with optical energy gap (E_g^{op}=2.17 eV) derived from the onset of the UV-vis absorption. The derived energy gap is further supported by the calculation (E_g^{cal}=2.40 eV).

The stability of **6-1b** under ambient condition was further examined with NMR, EPR and UV-Vis analysis. There was no broadening in the proton NMR spectrum even at high temperature (up to 110 °C) (Figure **6-11**), and it was EPR silent both at room temperature and high temperature. Furthermore, no significant difference was observed in the variable-temperature UV-Vis measurements (Figure **6-12**). All these results suggest that compound **6-1** is highly stable even at high temperature. Furthermore, the DFT calculation was carried out at the broken-symmetry UB3LYP/6-31G(d,p) level of theory using Gaussian 09 program package. It was found that the singlet closed-shell and the singlet open-shall biradical states are at the same energy level, implying that **6-1** possesses a closed-shell feature in the ground state (Table **6-2**).
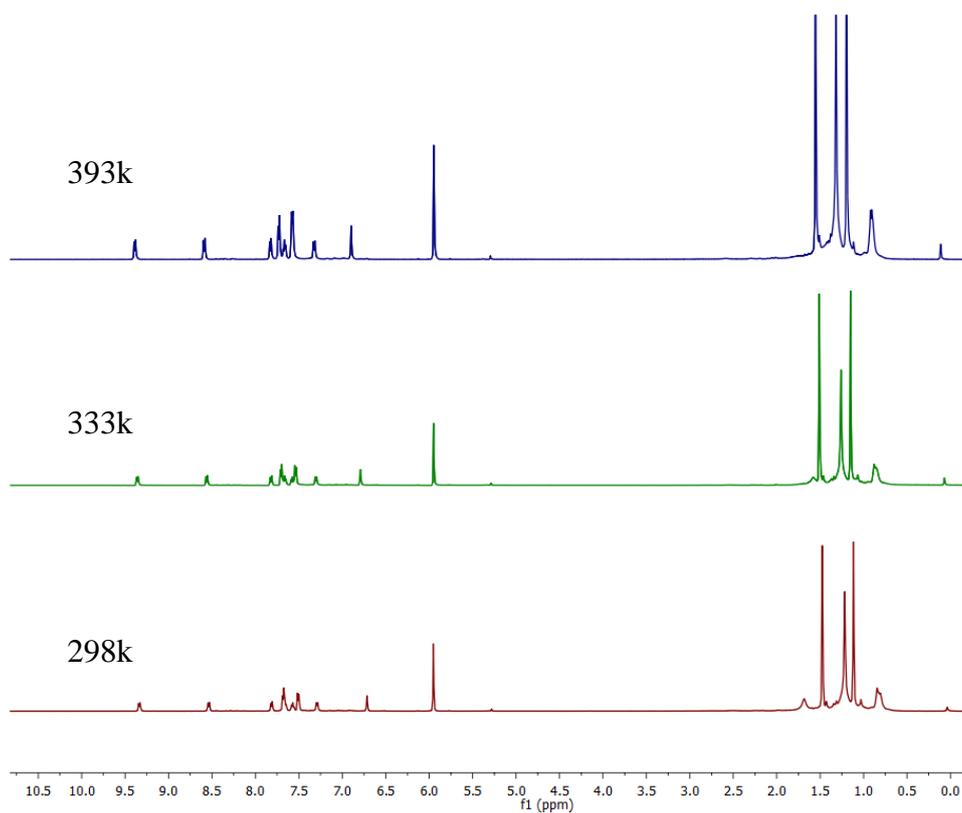
Figure **6-11**. Variable-temperature ^{1}H NMR spectra of **6-1b** in $C_2D_2Cl_4$.
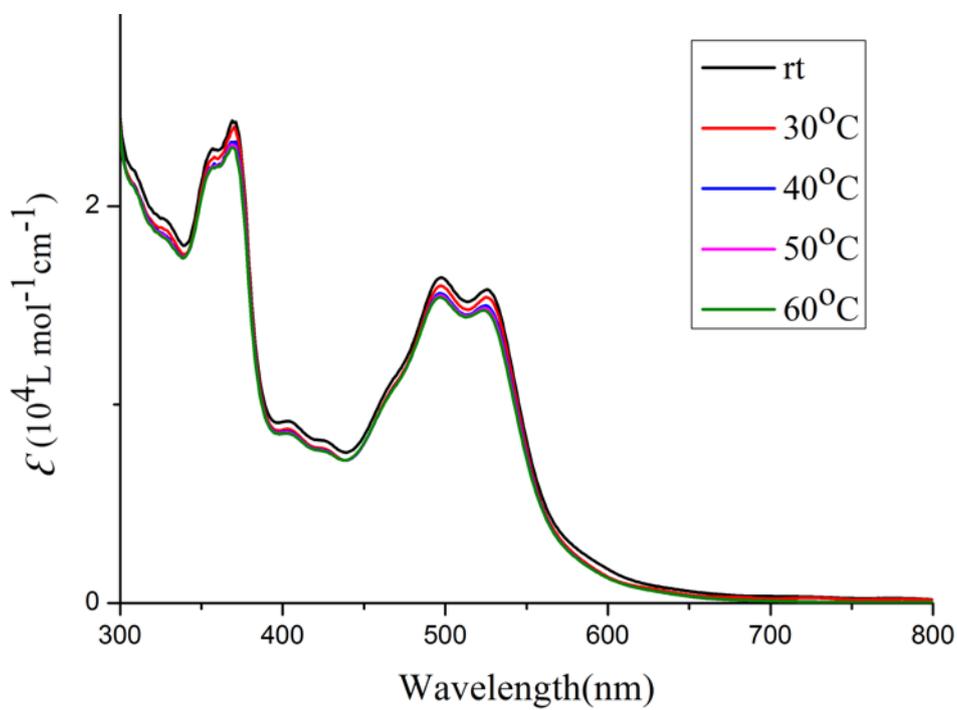
Figure **6-12**. Variable-temperature UV-Vis absorption spectra of compound **6-1b**.
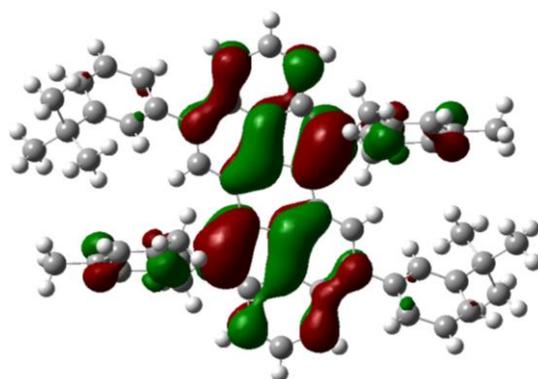
HOMO = -4.91
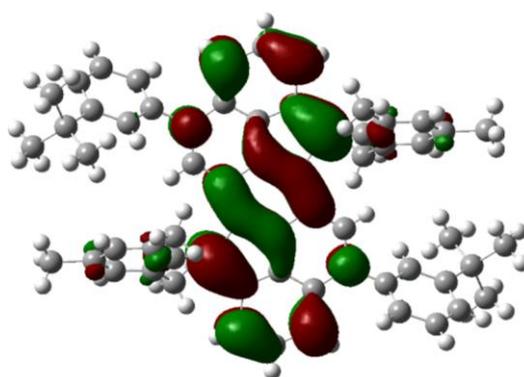
LUMO = -2.51

Figure **6-13**. HOMO-LUMO of **6-1b**.

Table **6-2**. The energy levels of **6-1b** from the DFT calculations.

molecule	E, eV (triplet)	S^2 (triplet)	Singlet open shell E, eV (BS)	Singlet close shell E, eV (CS)	S^2 (BS)	ΔE_{ST}, eV
6-1b	65184.69683	2.003	65185.95357	65185.95357	0.0	1.256741437

5.3 Conclusion

In summary, we have presented a novel efficient synthetic route toward an unprecedented antiaromatic PAHs, namely dibenzo-indeno[1,2-*b*]fluorene: cyclopenta[*pqr*]indeno[2,1,7-*ijk*]tetraphene. The physical and chemical properties of the dibenzo-indeno[1,2-*b*]fluorene were systematically studied by UV-vis, CV, X-ray single crystal analysis and DFT calculations. The results unambiguously demonstrated the dibenzo-indeno[1,2-*b*]fluorene was a new type of air stable and fully conjugated 24-π-electron antiaromatic systems. The design concept and the synthetic strategy starting from the corresponding *ortho*-methyl group to construct the five-membered ring can be applied to the synthesis of other stable antiaromatic PAHs. With this powerful synthetic strategy in our hand, one can envisage that the future work can be designed to integrate pentagon-embedded PAHs and graphene nanoribbons (Scheme 6-5).
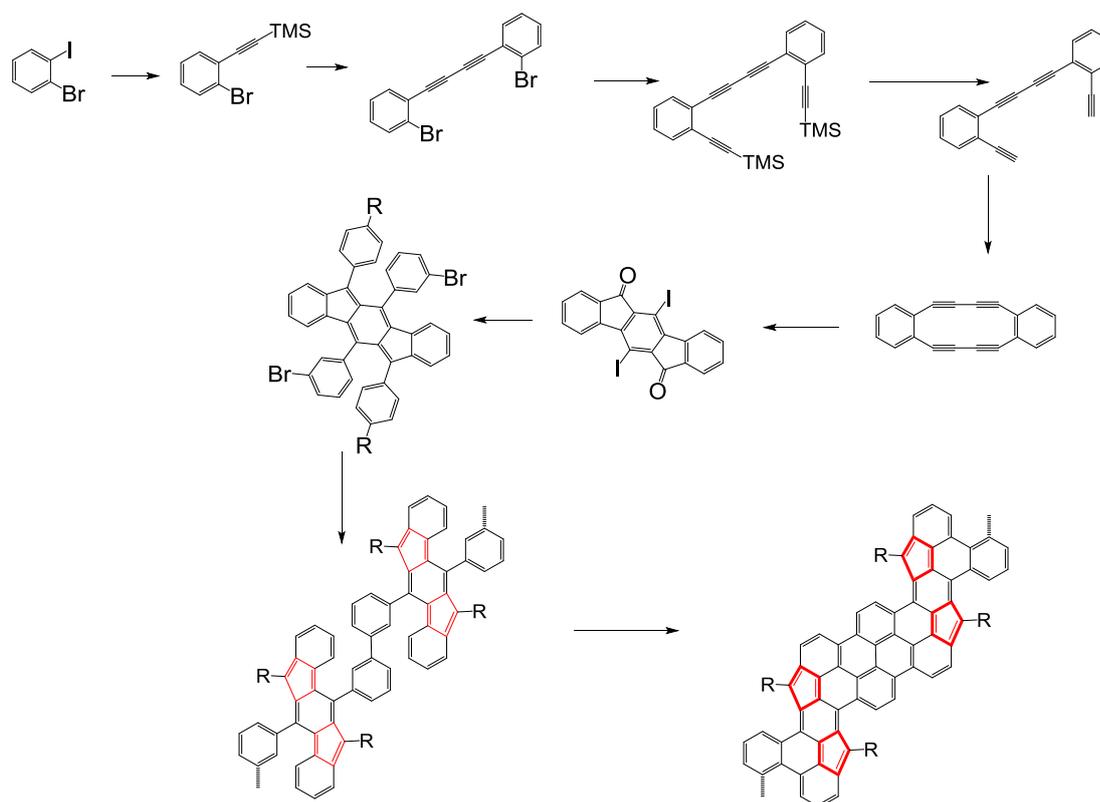
Scheme **6-5**. Synthetic route toward to the pentagon-embedded graphene nanoribbons.

Reference:

[1] E. Clar. Polycyclic Hydrocarbons; Academic Press: New York, **1964**; Vol. 1.

[2] M. Bendikov, F. Wudl, D. F. Perepichka. *Chem. Rev.* **2004**, 104, 4891-4945.

[3] J. Wu, W. Pisula, K. Müllen. *Chem. Rev.* **2007**, 107, 718-747.

[4] J. E. Anthony. *Angew. Chem., Int. Ed*. **2008**, 47, 452-483.

[5] J. E. Anthony. *Chem. Rev.* **2006**, 106, 5028-5048.

[6] S. Zade, M. Bendikov. *Angew. Chem. Int. Ed.* **2010**, 49, 4012-4015.

[7] M. Winkler, K. N. Houk. *J. Am. Chem. Soc.* **2007**, 129, 1805-1815.

[8] I. Kaur, W. Jia, R. P. Kopreski, S. Selvarasah, M. R. Dokmeci, C. Pramanik, N. E. McGruer, G. P. Miller. *J. Am. Chem. Soc.* **2008**, 130, 16274-16286.

[9] J. E. Anthony, J. S. Brooks, D. L. Eaton, S. R. Parkin, *J. Am. Chem. Soc.* **2001**, 123, 9482-9483.

[10]   J. E. Anthony, D. L. Eaton, S. R. Parkin, *Org. Lett.* **2002**, 4, 15-18.

[11]   M. M. Payne, S. R. Parkin, and J. E. Anthony. *J. Am. Chem. Soc.* **2005**, 127, 8028-8029.

[12]   Z. Zeng, X Shi, C Chi, J. T. L. Navarrete, J Casado, J Wu. *Chem. Soc. Rev.* **2015**, DOI: 10.1039/C5CS00051C.

[13]   T. Ohmae, T. Nishinaga, M. Wu, M. Iyoda. *J. Am. Chem. Soc.* **2010**, 132, 1066-1074.

[14]   Q. Zhou, P. J. Carroll, T. M. Swager. *J. Org. Chem.* **1994**, 59, 1294-1301.

[15]   D. T. Chase, B. D. Rose, S. P. McClintock, L. N. Zakharov, M. M. Haley. *Angew. Chem., Int. Ed.* **2011**, 50, 1127-1130.

[16]   D. T. Chase, A. G. Fix, B. D. Rose, C. D. Weber, S. Nobusue, C. E. Stockwell, L. N. Zakharov, M. C. Lonergan, M. M. Haley. *Angew. Chem. Int. Ed.* **2011**, 50, 11103-11106.

[17]   D. T. Chase, A.G. Fix, S. J. Kang, B. D. Rose, C. D. Weber, Y. Zhong, L. N. Zakharov, M. C. Lonergan, C. Nuckolls, M. M. Haley. *J. Am. Chem. Soc.* **2012**, 134, 10349-10352.

[18]   A. G. Fix, D. T. Chase, M. M. Haley. *Top. Curr. Chem.* **2012**, DOI: 10.1007/128_2012_376.

[19]   A. G. Fix, P. E. Deal, C. L. Vonnegut, B. D. Rose, L. N. Zakharov and M. M. Haley, *Org. Lett.* **2013**, 15, 1362-1365.

[20]   A. Shimizu, Y. Tobe. *Angew. Chem. Int. Ed.* **2011**, 50, 6906-6910.

[21]   J. Nishida, S. Tsukaguchi, Y. Yamashita, *Chem.–Eur. J.* **2012**, 18, 8964-8970.

[22]   A. Shimizu, R. Kishi, M. Nakano, D. Shiomi, K. Sato, T. Takui, I. Hisaki, M. Miyata and Y. Tobe. *Angew. Chem., Int. Ed.* **2013**, 52, 6076-6079.

[23]   H. Miyoshi, S. Nobusue, A. Shimizu, I. Hisaki, M. Miyata and Y. Tobe, *Chem. Sci.* **2014**, 5, 163-168.

[24]   See also: D. K. Frantz, J. J. Walish and T. M. Swager, *Org. Lett.* **2013**, 15, 4782-4785.

[25]   Nishida, J.; Tsukaguchi, S.; Yamashita, Y. *Chem.-Eur. J.* **2012**, 18, 8964-8970.

[26]   A. Shimizu, Y. Tobe. *Angew. Chem. Int. Ed.* **2011**, 50, 6906-6910.

[27]

[28]   A. Shimizu, M. Uruichi, K. Yakushi, H. Matsuzaki, H. Okamoto, M. Nakano, Y. Hirao, K. Matsumoto, H. Kurata. T. Kubo. *Angew. Chem.* **2009**, 121, 5590 –5594.

[29]   A. Shimizu,Y. Hirao, K. Matsumoto, H. Kurata, T. Kubo, M. Uruichi, K. Yakushi. *Chem. Commun.* **2012**, 48, 5629–5631.

[30]   D. K. Frantz, J. J. Walish, T. M. Swager. *Org. Lett.* **2013**, 15, 4782-4785.

Chapter 7. Summary and outlook

Up to now, "bottom-up" synthesis has mainly focused on armchair-edged PAHs, whereas PAHs with cove-type or zigzag edges have remained elusive. However, depending on the size and periphery structure, dramatically different optical and chemical properties are observed. For this reason, we have developed a series of different edge structure of nanographenes in this thesis to investigate the electronic and optoelectronic properties. The results can be summarized as follows:

1. A series of new cove-type PAHs, even towards cove-edged graphene nanoribbons, are presented in the second chapters to investigate the electronic and optoelectronic properties. As model subunits of the infinite cove-edged GNRs, fused chrysene-based oligomers or PAHs, namely the dimer (two units of chrysene) and tetramer (four units of chrysene), can be synthesized via the Ullmann coupling reaction of 11,11'-dibromo-5,5'-bischrysene followed by intramolecularly oxidative cyclodehydrogenation in solution, and much higher GNR homologues via on-surface synthesis. The unambiguous crystallographic characterization of the tetramer reveals that the cove-edge structure causes it to twist away from planarity due to the steric repulsion, and shows alternative "up-down" geometry. DFT calculation further reveals that the "up-down" geometry of the tetramer has the lowest energy compared to the "mix" and "helix" conformers, which is in agreement with the experiment crystal result. One would safely conclude that the corresponding infinite GNRs also adopt the alternating "up-down" rolling hill. Moreover, the calculation predicts that these type GNRs turn to low band gap (E_g=1.70 eV) and high mobility with the cove edge at the periphery. From our surface synthesis, the length of the ribbons is around 20 nm. The unique optical electronics properties of such oligomers and GNRs suggest that they are promising candidates for the OFET, OLED and photovoltaic applications.

By using the same "bottom-up" method, we can extend our system with different width and doped PAHs and GNRs, such as:
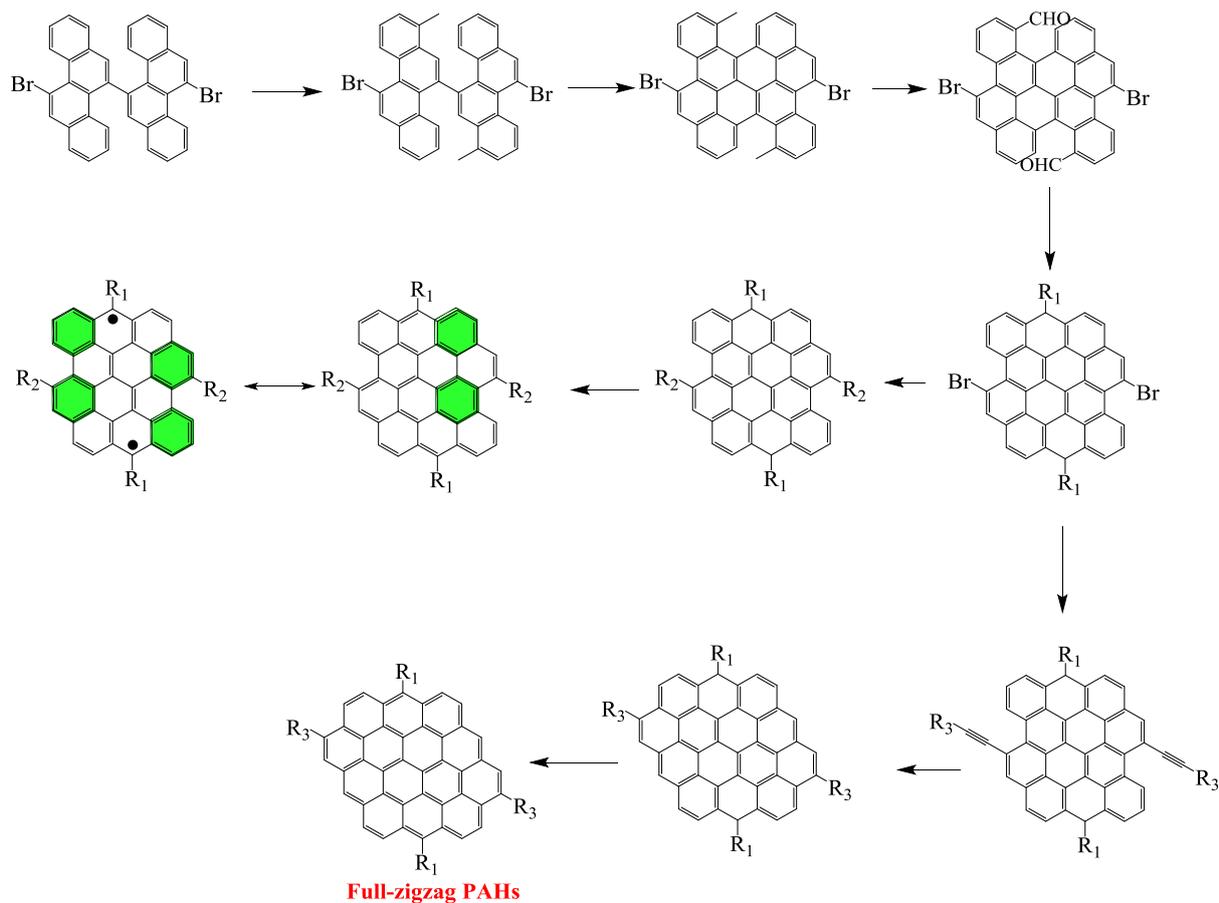
Figure 7-1. Structure of full zigzag-edged PAHs.
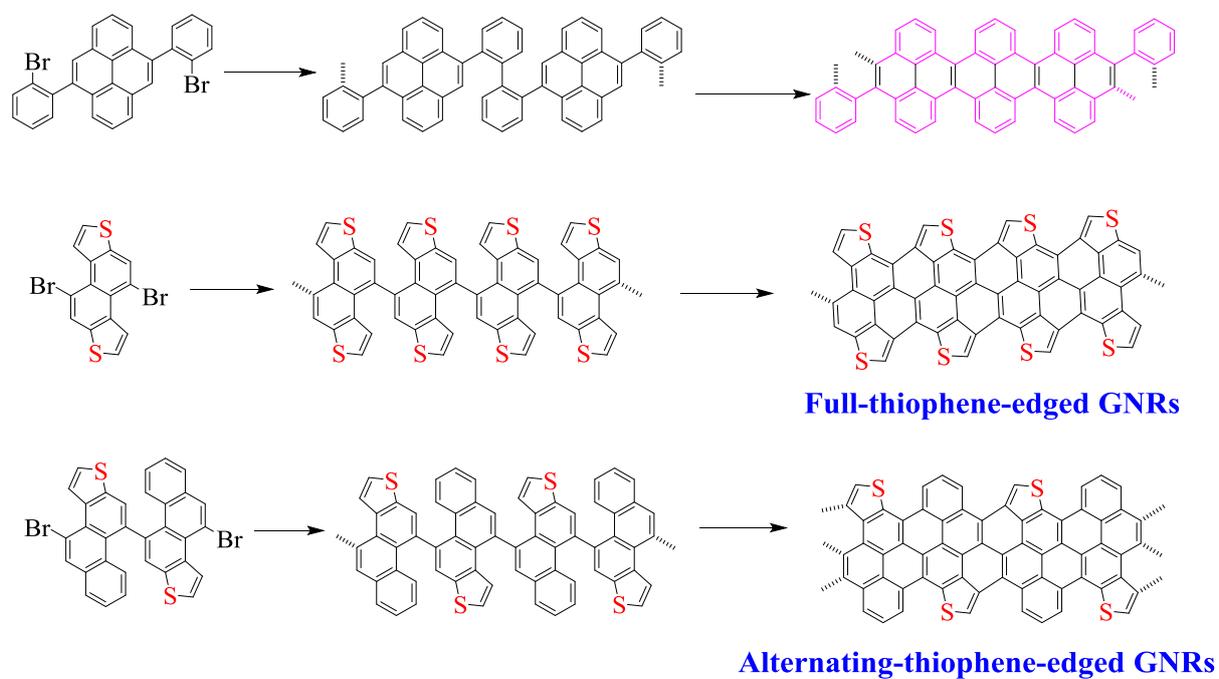
Figure 7-2. Different edge structure of GNRs.

2. PAHs with zigzag periphery display fascinating electronic and optoelectronic properties resulting from the spin-polarized state at the zigzag edges. We demonstrated a PAHs with zigzag periphery in chapter 3. A novel tetrabenzo[*a,f,j,o*]perylene, namely "bistetracene" in which two tetracenes are connected side by side with two bonds, was synthesized and characterized. An optical energy gap of about 1.56 eV is derived from the UV-vis absorption spectrum, showing the low optical gap feature of such zigzag-edged type polycyclic aromatic hydrocarbons (PAHs). Theoretical calculations and physical property investigations manifest that such a PAH possesses a prominent biradical character in the ground state, which is the first example among bistetracene derivatives. However, the bistetracene can easily undergo oxidation into tetrabenzo[*a,f,j,o*]perylene-9,19-dione (diketone) under ambient conditions. Such zigzag-edged PAH can be considered as a short segment of infinite graphene nanoribbons with exceptional zigzag edges. Therefore, our studies contribute to an understanding of the edge states of expanded PAH homologues (such as *peri*-tetracenes or *peri*-pentacenes) and graphene nanoribbons which may possess a localized nonbonding π-electron around the zigzag edges. It is envisioned that these zigzag edged PAHs are promising candidates for the development of spintronics given that the edge localized spins can be polarized by applying external magnetic/electrical fields.


Bispentacene 1

Bistetracene 2

Bispentacene 2
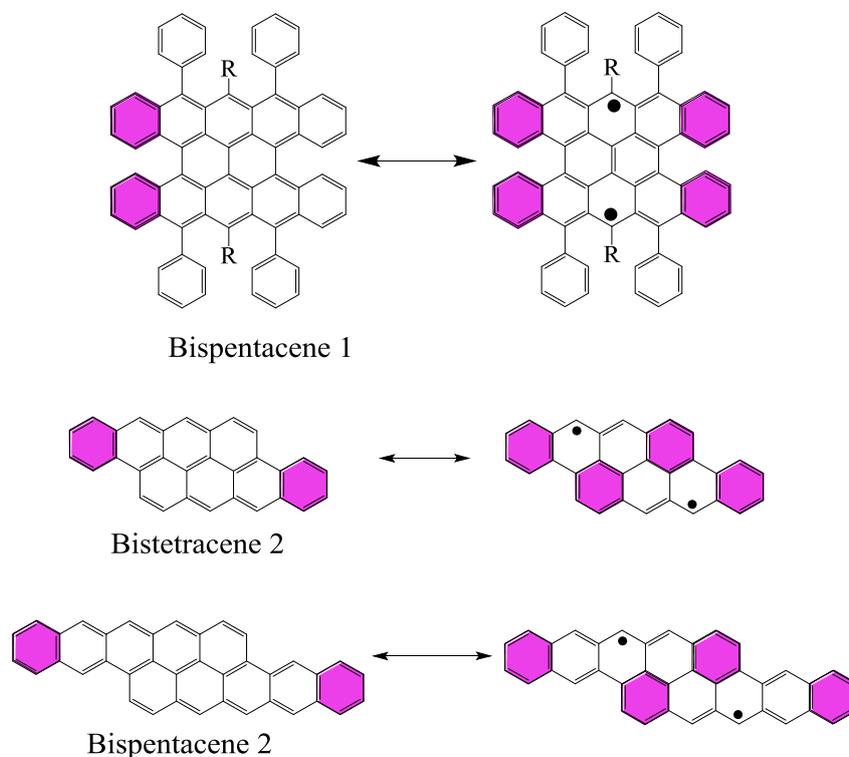
Figure 7-3. Structure of PAHs with biradical feature.

3. In chapter 3, we have demonstrated the synthesis of a novel tetrabenzo[*a*,*f*,*j*,*o*]perylene, namely "bistetracene" in which two tetracenes are connected side by side with two bonds. However, theoretical calculations and physical property investigations manifest that such bistetracene possesses a prominent biradical character in the ground state. Accordingly, this bistetracene can easily undergo oxidation into tetrabenzo[*a*,*f*,*j*,*o*]perylene-9,19-dione (diketone) under ambient conditions. Thereby, the stabilization is the critical issue for such PAHs. In chapter 4, a novel dibenzo[*a*,*m*]rubicene, pentagon-embendded bistetracene, was synthesized and characterized. This pentagon-embendded molecular is more stable compared to the traditional six-membered bistetracene. In chapter 4, we report the cyclodehydrogenation reaction of compound 6,7,13,14-tetraphenylbenzo[*k*]tetraphene (**4-5**), which gives two unexpected products, namely 5,14-diphenyldibenzo[a,m]rubicene (**4-7**) and the (*R*)-9*b*,14-diphenyldibenzo[*a*,*m*]rubicen-5(9*bH*)-one (**4-8**), instead of 5,14-diphenyltetrabenzo[*a*,*cd*,*j*,*lm*]perylene (**4-6**) (Scheme 4-2), during the Scholl reaction. Nevertheless, to the best of our knowledge, this is the first example that a position exchange of substituents has been observed and formation the five-membered rings during the cyclodehydrogenation process. More importantly, this pentagon-embedded molecular is more stable than the traditional six-membered bistetracene.
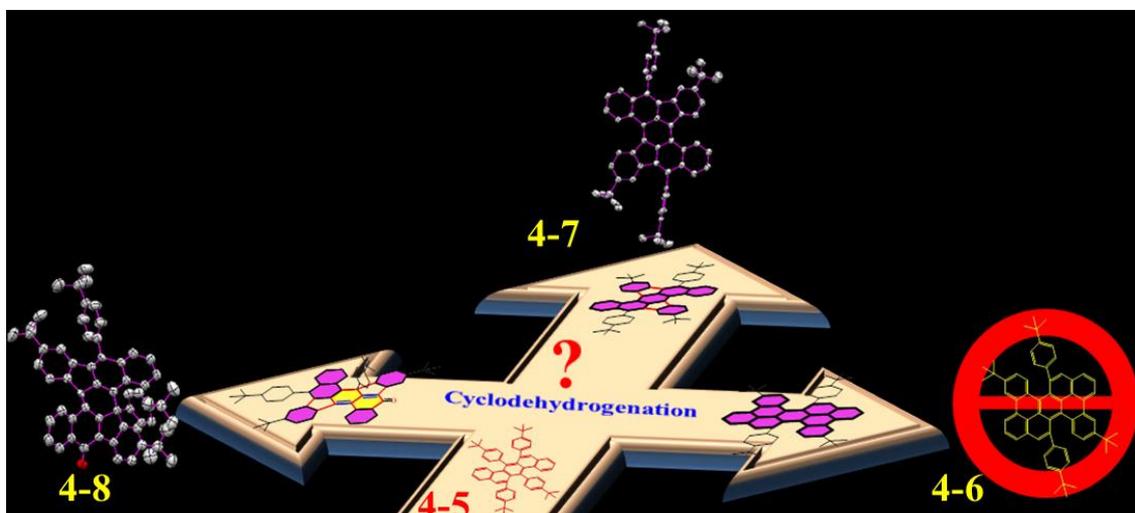
So following this unexpected cyclodehydrogenation, we can purposefully design some very interesting PAHs with five-membered rings, as well as seven-membered rings.
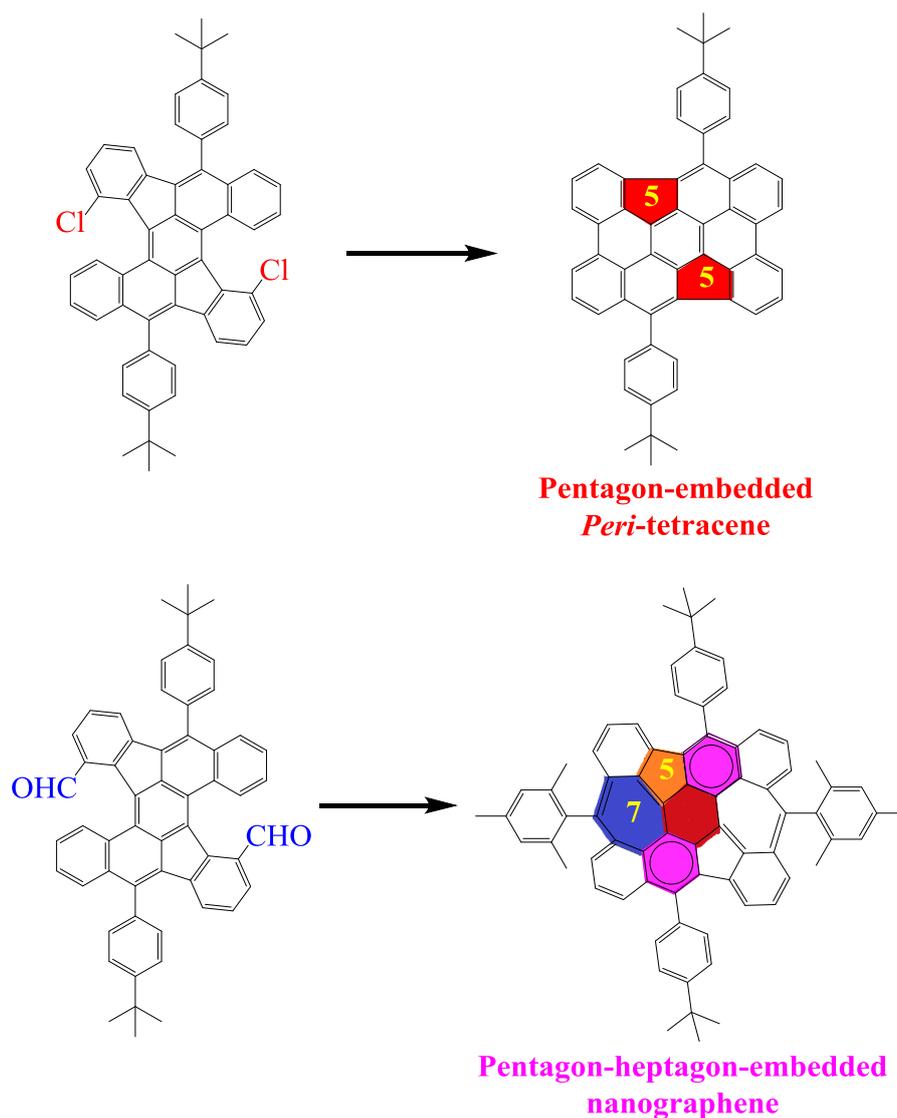
Figure 7-4. Structure of PAHs with odd-rings.

4. Indenofluorene is a prominent 20-π-electrons fully conjugated antiaromatic analogues of acenes with a 6-5-6-5-6 skeleton. In chapter 6, we have developed a new efficient synthetic method toward an unknown antiaromatic dibenzene indeno[1,2-*b*]fluorene and its derivatives. The physical and chemical properties were systematically studied by various experimental methods and DFT calculations. The results unambiguously demonstrated that compounds were new type air stable and fully conjugated antiaromatic system. The design concept and the new synthetic strategy starting from the corresponding methyl group to construct the five-member ring can be applied to synthesis of other stable antiaromatic polycyclic hydrocarbons or even hybrid structures.
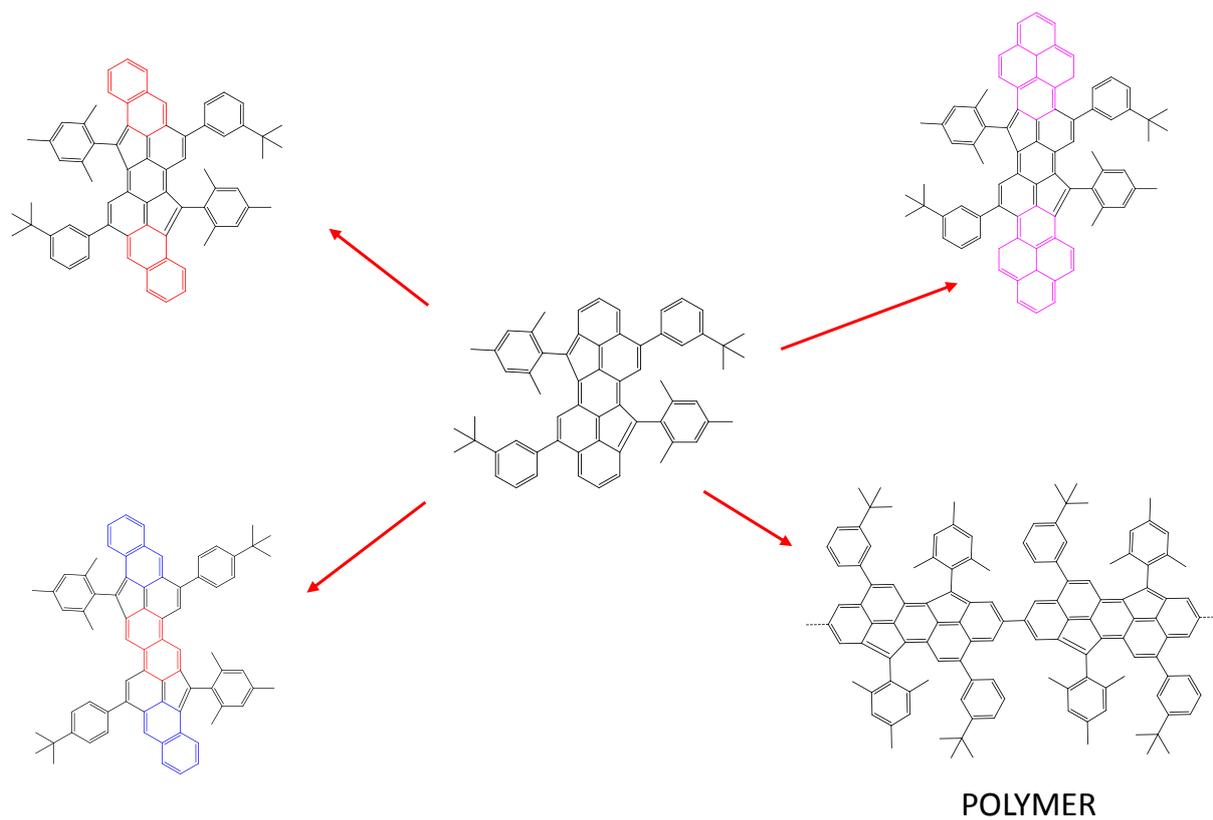
Figure 7-5. Structure of antiaromatic PAHs by extend dibenzene indeno[1,2-*b*]fluorene.

Chapter 8. Experimental Section

General Methods:

^{1}H NMR and ^{13}C NMR spectra were recorded in deuterated solvents on a Bruker DPX 250, Bruker DPX 300 and Bruker DRX 500. UV-visible spectra were measured on a Perkin-Elmer Lambda 9 spectrophotometer at room temperature using a 10 mm quartz cell. FD mass measurements were carried out on a VG instruments ZAB 2-SE-FPD. MALDI-TOF mass spectra were recorded on a Bruker Reflex II-TOF Spectrometer using a 337 nm nitrogen laser with TCNQ as matrix. CV measurements were carried out on a computer-controlled GSTAT12 in a three-electrode cell in a dichloromethane solution of Bu_4NPF_6 (0.1 M) with a scan rate of 100 mV/s at room temperature. A Pt wire, a silver wire, and a glassy carbon electrode were used as the counter electrode, the reference electrode, and the working electrode, respectively. EPR spectra were recorded in diluted and oxygen-free solutions of toluene by using a Bruker Xband spectrometer ESP300 E, equipped with an NMR gauss meter (Bruker ER035), a frequency counter (Bruker ER 041 XK) and a variable temperature control continuous flow N_2 cryostat (Bruker B-VT 2000). The melting points were performed at Büchi Melting Point B-545. DFT calculations were performed on Gaussian 09 program package using B3LYP functional and 6-31G (d,p) basis set. Unless otherwise noted, all starting materials were purchased from Aldrich, Acros, TCI and Alfa Aesar, use as received without further purification.

Synthetic details:

1-Bromo-4-*tert*-butyl-2-nitrobenzene (2-16):
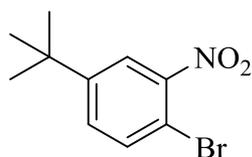
2-16

Concentrated sulfuric acid (31.6 mL, 594 mmol) was added slowly to nitric acid (27.4 mL, 396 mmol) at 0 °C. This cold mixture was added carefully to 4-bromo-*tert*-butylbenzene (56.2

g, 264 mmol). The temperature was kept below 10 °C, and the mixture was stirred for an additional 20 h at ambient temperature, then poured into water (750 mL). The organic layer was separated, and the water layer was washed with Et_2O (200 mL). The combined organic phases were dried over $MgSO_4$. Removal of the solvents under reduced pressure and distillation (bp 190 °C, at 40 mbar) gave 62.7 g of the title compound (243 mmol, 92%): ^{1}H-NMR (250 MHz, $CDCl_3$): 7.83 (d, 1H), 7.63 (d, 1H), 7.44 (dd, 1H), 1.33 (s, 9H); ^{13}C-NMR (250MHz, $CDCl_3$): 157.2, 152.5, 134.5, 130.6, 122.7, 111.1, 34.9, 30.9,.

2-Bromo-5-*tert*-butylaniline (2-17):

2-17
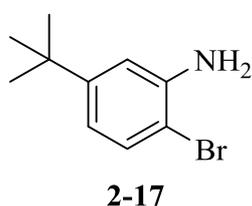
A mixture of 1-bromo-4-*tert*-butyl-2-nitrobenzene (**2-16**) (59.1 g, 229 mmol) and $Na_2S_2O_4$ (146.4 g, 841 mmol) in glycol monomethyl ether (350 mL) and water (350 mL) was heated under reflux for 6 h. Water (300 mL) and concentrated hydrochloric acid (300 mL) were added to the warm solution; then the mixture was heated under reflux for 15 min and poured into ice water (500 mL). Solid Na_2CO_3 was added until the mixture was basic. The organic layer was separated and the water layer extracted with Et_2O (200 mL). The combined organic phases were dried over $MgSO_4$. Removal of the solvents under reduced pressure and distillation of the residue (bp 153 °C, at 35 mbar) gave 42.3 g (185 mmol, 81%) of the title compound **2-17**: ^{1}H-NMR (250 MHz, $CDCl_3$): 7.33 (d, 1H), 6.80 (d, 1H), 6.48 (dd, 1H), 3.96 (s, 2H), 1.29 (s, 9H); ^{13}C-NMR (250MHz, $CDCl_3$): 151.8, 143.5, 132.0, 117.0, 113.1, 106.3, 34.4, 31.2.

1-Bromo-2-iodo-4-*tert*-butylbenzene (2-18):

2-18
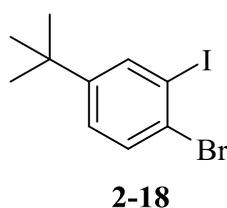
A solution of NaNO$_2$ (13.3 g, 193 mmol) in water (40 mL) was added dropwise to a mixture of 2-bromo-5-*tert*-butylaniline (**2-17**) (40.0 g, 175 mmol) in water (275 mL) and concentrated hydrochloric acid (66.2 mL) below 5 °C, and the mixture was stirred for 10 min. Then a solution of potassium iodide (43.7 g, 263 mmol) in water (67 mL) was added. The mixture was stirred for 15 min without cooling, then at 50 °C for 15 min and at 80 °C for 15 min. After that the mixture was cooled to 0 °C, and a solution of 5% aqueous sodium sulfite (50 mL) was added. The organic layer was separated, and the water layer extracted with Et$_2$O (200 mL, 3 times). The combined organic phases were dried over MgSO$_4$. After removal of the solvents under reduced pressure the crude product was purified by column chromatography (silica gel, hexane) to yield 47.6 g of the title compound **2-18** (141 mmol, 80%): ^{1}H-NMR (250 MHz, CDCl$_3$): 7.83 (d, 1H), 7.50 (d, 1H), 7.22 (dd, 1H), 1.28 (s, 9H); ^{13}C-NMR (250 MHz, CDCl$_3$): 152.0, 137.4, 132.1, 126.9, 126.3, 101.1, 34.4, 31.0.

((2-Bromophenyl)ethynyl)trimethylsilane (2-7) and
((2-bromo-5-(*tert*-butyl)phenyl)ethynyl)trimethylsilane (2-19):
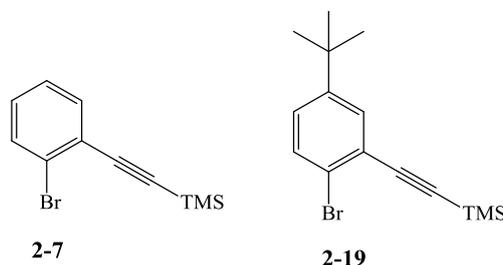
A 50mL round bottomflask equipped with a magnetic stir bar was charged with compound 2-**6** (35 mmol), THF (100 mL), triethylamine (20 mL, 150mmol), PdCl$_2$(PPh$_3$)$_2$ (500 mg, 0.7mmol), CuI (150mg, 0.754 mmol) and trimethylsilylacetylene (5.25 mL, 37.1mmol) under argon atmosphere. The reaction mixture was stirred overnight at room temperature, diluted in CH$_2$Cl$_2$, washed with NH$_4$Cl and dried over Mg$_2$SO$_4$. The solvent was removed under reduced pressure and the crude productwas purified by flash chromatography on silica gel with hexanes as eluent to afford the desired compound 2-**7** (yield, **2-7**: 82%, **2-19**: 85%) as yellow orange oil.

2-7: ^{1}H-NMR (CD$_2$Cl$_2$, 250 MHz): 7.58 (d, 1H), 7.49 (dd,1H), 7.24 (t, 1H), 7.16 (t, 1H), 0.28 (s, 9H); ^{13}C-NMR (CD$_2$Cl$_2$, 250 MHz): 137.9, 134.2, 132.6, 131.3, 128.1, 126.8, 108.4, 104.3, 12.4. FD-MS (8 KV): m/z 251.8.

2-19: ^{1}H-NMR (CD$_2$Cl$_2$, 250 MHz): 7.48 (s, 1H), 7.32 (dd, 1H), 7.18 (dd, 1H), 1.6 (s, 9H), 0.28 (s, 9H); ^{13}C-NMR (CD$_2$Cl$_2$, 250 MHz): 148.9, 134.2, 132.5, 131.4, 125.1, 123.8, 106.3, 100.3, 33.6, 31.3,12.7. FD-MS (8 KV): m/z 308.4.

1,4-Bis(2-iodophenyl)buta-1,3-diyne (2-12) and
### 1,4-bis(5-(*tert*-butyl)-2-iodophenyl)buta-1,3-diyne (2-21):

2-12   **2-21**
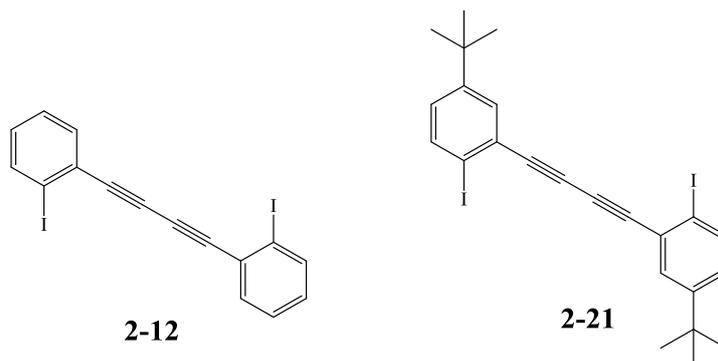
A 250 mL round bottom flask equipped with a magnetic stir bar was charged with compound **2-8** (11.9 mmol), THF (100 mL). The temperature was cooled to -78 ^{o}C and *n*-BuLi (1.4 mL, 23.7 mmol) was added slowly. The reaction mixturewas stirred for one hour and 1,2-diiodoethane was added (17.8 mmol). The reaction mixture was stirred overnight at room temperature, diluted in CH$_2$Cl$_2$, washed with H$_2$O and dried over Mg$_2$SO$_4$. The solvent was removed under reduced pressure and the crude product was purified by flash chromatography on silica gel with hexanes as eluent to afford the desired compound **2-12** (yield, **2-12**:88%, **2-21**:90%) as yellow solid.

2-12: ^{1}H-NMR (CD$_2$Cl$_2$, 250 MHz): 7.82 (d, 1H), 7.55 (d,1H), 7.28 (t, 1H), 7.12 (t, 1H); ^{13}C-NMR (CD$_2$Cl$_2$, 250 MHz): 144.78, 138.74, 134.19, 133.49, 132.35, 131.45, 130.59, 130.45, 129.29, 128.34, 128.22, 127.51, 127.16, 127.07, 122.09, 121.32, 81.14, 76.81. FD-MS (8 KV): m/z 453.9.

2-21: ^{1}H-NMR (CD$_2$Cl$_2$, 250 MHz): 7.86 (s, 1H), 7.66 (d,1H), 7.23 (d, 1H), 1.45 (s, 9H); ^{13}C-NMR (CD$_2$Cl$_2$, 250 MHz): 144.78, 138.74, 134.19, 133.49, 132.35, 131.45, 130.59, 130.45, 129.29, 128.34, 128.22, 127.51, 127.16, 127.07, 122.09, 121.32, 81.14, 76.81. FD-MS (8 KV): m/z 565.8.

(3-Bromonaphthalen-2-yl)boronic acid (2-13):
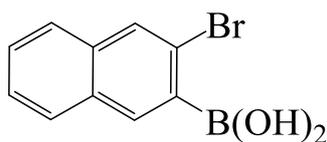
2-13

2,2,6,6-Tetramethylpiperidine (17.6 g, 96.8 mmol, 0.83 g/ml, 16.4 ml) in dry THF (200 mL) was degassed and *n*-BuLi (60.5 mL, 96.8 mmol) was added dropwise at 0 °C under Ar. After stirring for 30 min the solution was cooled to –78 °C and triisopropyl borate (36.4 g, 193.6 mmol, 45 ml, 0.815 g/ml) was added through a septum. After another 10 min 2-bromonaphthalene (10 g, 48.4 mmol) in degassed THF (20 mL) was added dropwise *via* a Teflon canula. The solution was stirred for 4 h while slowly warming to about –45 °C. The reaction was again cooled to –78 °C and a second crop of triisopropyl borate (9.2 g, 48.8 mmol) was added. The solution was then allowed to warm to r.t. over 6-8 h. The reaction was quenched with dil. HCl (1 M, 60 mL). The phases were separated and the aqueous layer was extracted with ethyl acetate (3 × 40 mL). The combined organic phases were then extracted with NaOH (1 M, 3 × 70 mL) and the combined basic extracts were acidified with 2 M HCl aq. and extracted with ethyl acetate (3 × 60 mL). The combined organic extracts were dried over MgSO$_4$ and the solvent was evaporated to provide the boronic acid as an off-white to pale brown crystalline solid. It was directly used for the next step.

1,4-Bis(2-(3-bromonaphthalen-2-yl)phenyl)buta-1,3-diyne (2-14) and

2-bromo-3-(2-((3-bromo-5-(*tert*-butyl)-2-(naphthalen-2-yl)phenyl)buta-1,3-diyn-1-yl)-4-(*tert*-butyl)phenyl)naphthalene (2-22):
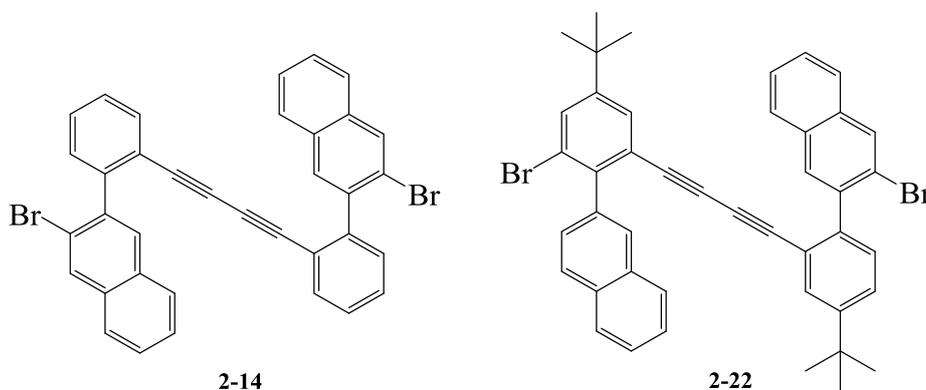
2-14

2-22

Nitrogen was bubbled through a mixing solution of THF (100 mL), EtOH (20 mL) and water (20 mL) for 30 min, and to this solution was added compound **2-12** (4.96 mmol), Pd(PPh$_3$)$_4$ (0.5 mmol), K$_2$CO$_3$ (29.76 mmol) and compound 2-**13** (9.95 mmol). The mixture was heated at 60°C for 36h. The solution was extracted three times with ethyl acetate. After removal of the solvent in vacuo, the crude material was purified by column chromatography (dichloromethane/hexane = 1/10) to afford compound **2-14** (yield, **2-14**:50%, **2-22**:56%) as a yellow solid.

2-14: ^{1}H-NMR (CD$_2$Cl$_2$, 250 MHz): 8.01(s, 1H), 7.76 (d, 1H), 7.68 (d,1H), 7.54 (s, 1H), 7.45 (m, 2H), 7.3 (m, 4H); ^{13}C-NMR (CD$_2$Cl$_2$, 250 MHz): 144.78, 138.74, 134.19, 133.49, 132.35, 131.45, 130.59, 130.45, 129.29, 128.34, 128.22, 127.51, 127.16, 127.07, 122.09, 121.32, 81.14, 76.81 FD-MS (8 KV): 611.8m/z.

2-22: ^{1}H-NMR (CD$_2$Cl$_2$, 250 MHz): 8.28(s, 1H), 8.23 (s, 1H), 8.14 (s,1H), 8.01 (dd, 1H), 7.88 (dd, 1H), 7.64 (m, 2H), 7.36 (m, 2H); ^{13}C-NMR (CD$_2$Cl$_2$, 250 MHz): 145.58, 136.47, 134.14, 130.81, 129.55, 127.63, 126.82, 124.88, 124.65, 124.13, 124.08, 123.96, 123.54, 122.76, 117.85, 115.64, 77.38, 74.31, 33.68, 31.34. FD-MS (8 KV): 723.8m/z.

11,11'-Dibromo-5,5'-bichrysene (2-5a) and

11,11'-dibromo-8,8'-di-*tert*-butyl-5,5'-bichrysene (2-5b):

2-5a   2-5b
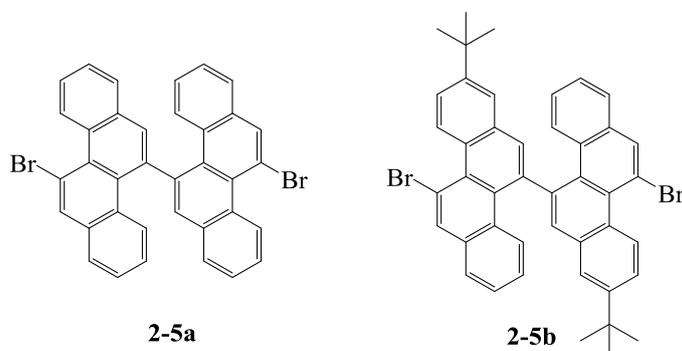
A reaction tube containing PtCl$_2$ (0.07 mmol) was dried in vacuo for 1 h, and vacuum was filled with nitrogen using a nitrogen balloon. To this round bottom flask was added compound **2-14** (0.74 mmol) and toluene (74 mL), and the mixture was stirred at 25°C for 5 min before it was heated at 90°C for 24 h. After removal of the solvent in vacuo, the crude material was purified by column chromatography (dichloromethane/hexane = 1/5) to afford compound **2-5a** (yield, **2-5a**:70%, **2-5b**: 78%) as a yellow solid.

2-5a: ^{1}H-NMR (CD$_2$Cl$_2$, 250 MHz): 9.55(dd, 1H), 8.28 (s, 1H), 7.78 (d,1H), 7.68 (m, 3H), 7.69 (t, 1H), 7.54 (t, 1H), 7.25 (t, 1H), 6.74 (t, 1H); ^{13}C-NMR (CD$_2$Cl$_2$, 250 MHz): 138.82, 133.26, 131.84, 131.64, 130.38, 130.01, 128.59, 128.47, 126.82, 126.74, 126.39, 126.09, 125.81, 124.53, 124.04, 120.65, 116.11, 115.72. FD-MS (8 KV): 611.7m/z. MALDI-TOF (TCNQ as matrix): m/z 612.58, cacld.: 612.36; Elemental analysis: Calculated: C 70.61, H 3.29, Br 26.10; Found: C 71.21, H 3.39.

2-5b: ^{1}H-NMR (CD$_2$Cl$_2$, 250 MHz): 9.54(dd, 1H), 8.28 (s, 1H), 7.81 (d,1H), 7.65 (m, 4H), 7.24(t, 1H), 6.75 (t, 1H), 1.34 (s, 9H); ^{13}C-NMR (CD$_2$Cl$_2$, 250 MHz):150.55, 140.11, 134.29, 132.95, 132.82, 131.84, 130.76, 129.76, 129.29, 127.87, 127.75, 127.61, 127.19, 126.75, 125.67, 123.83, 123.48, 117.36, 35.09, 31.28. FD-MS (8 KV): 723.9m/z. MALDI-TOF (TCNQ as matrix): m/z 724.88, cacld.: 724.58; Elemental analysis: Calculated: C 72.94, H 5.01, Br 22.06; Found: C 73.01, H 5.82.

8,8'-Di-*tert*-butyl-5,5'-bichrysene (2-23) and
2'',8,8',8'''-tetra-*tert*-butyl-5,5':11',5'':11'',5'''-quaterchrysene (2-24):

2-23   **2-24**
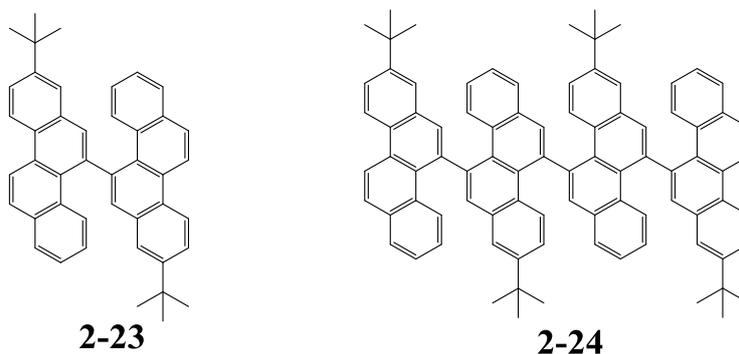
A reaction tube containing **2-5b** (100.00 mg, 0.1380 mmol), activated Cu (1.76 mg, 0.0276 mmol) and Pd(PPh$_3$)$_4$ (7.97 mg, 0.0069 mmol) was dried in vacuo for 1 h, and vacuum was filled with argon with a argon balloon. To this flask was added degassed dry DMSO (5 mL), and the mixture was stirred at 150°C for 48 hours under argon condition. After cooling down the room temperature, pour it into water, extracted it with CHCl$_3$ by three times, and washed with H$_2$O and dried over with Mg$_2$SO$_4$. The solvent was removed under reduced pressure. Firstly, the crude product was purified by flash chromatography on silica gel with DCM/hexane(1/3) as eluent, then afforded the desired compound **2-23** and **2-24** by recycle GPC with CHCl$_3$ as eluent (yield, **2-23**:30%, **2-24**: 12%) as a yellow solid.

2-23: ^{1}H-NMR (CD$_2$Cl$_2$, 250 MHz): 8.83(dd, 1H), 8.74 (s, 1H), 8.05 (d,1H), 7.88 (d, 1H), 7.81 (s, 1H), 7.78 (d, 1H), 7.61 (t, 1H), 7.58 (t, 1H), 7.53 (d, 1H), 1.52(s, 9H); ^{13}C-NMR (CD$_2$Cl$_2$, 250 MHz): 147.45, 133.68, 130.84, 130.64, 130.38, 130.01, 128.59, 128.47, 128.42, 128.14, 126.89, 126.59, 126.31, 125.93, 124.24, 121.85, 121.61, 121.32, 35.67, 31.32. FD-MS (8 KV): 566.3m/z. MALDI-TOF (TCNQ as matrix): m/z 566.88, cacld.: 566.79; Elemental analysis: Calculated: C 93.24, H 6.76; Found: C 93.31, H 6.82.

2-24: ^{1}H-NMR (C$_2$D$_2$Cl$_4$, 500 MHz): 9.14(dd, 2H), 8.95 (dd, 2H), 8.56 (dd,2H), 8.35 (m, 2H), 8.22(d, 1H), 7.98-7.99 (m, 5H), 7.81-7.83 (m, 5H), 1.55 (s, 18H); ^{13}C-NMR (C$_2$D$_2$Cl$_4$, 500 MHz): 143.10. 142.43, 142.21, 142.09, 141.99, 141.95, 141.85, 141.78, 141.74, 141.70, 141.68, 141.61, 141.53, 141.37, 141.11, 141.02, 140.61, 140.26, 139.44, 139.40, 139.13, 138.70, 134.64, 133.11, 132.96, 132.87, 132.70, 132.52, 131.30, 130.43, 128.80, 128.49, 128.21, 128.12, 128.99, 127.97,35.09, 31.28. FD-MS (8 KV): 1130.8m/z. MALDI-TOF (TCNQ as matrix): m/z 1131.87, cacld.: 1131.56. Elemental analysis: Calculated: C 93.41, H 6.59; Found: C 93.35, H 6.62.

3,12-Di-*tert*-butylbenzo[a]dinaphtho[2,1,8-cde:1',2',3',4'-ghi]perylene (2-1):
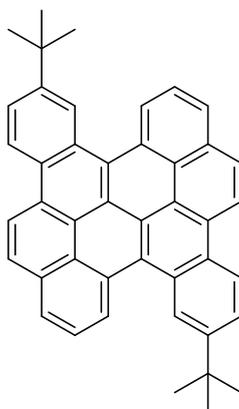
Dimer 2-1

To a mixture of **2-23** (20 mg, 0.035 mmol) and DDQ (32 mg, 0.14 mmol) in dry CH$_2$Cl$_2$ (9.5 mL) at 0 °C was added trifluoromethanesulfonic acid (0.5 mL). After 3 hours, the resulting mixture was quenched with saturated NaHCO$_3$ solution (20 mL), and then extracted with CH$_2$Cl$_2$ twice. The combined extracts were washed with brine and dried over MgSO$_4$. After removal of the solvent in vacuo, the crude material was purified by column chromatography (dichloromethane/hexane=1:5) to afford **dimer 2-1** (16 mg, 80.8%) as an orange solid.

^{1}H-NMR (C$_2$D$_2$Cl$_4$, 300 MHz): 9.32(S, 1H), 9.05 (dd, 1H), 9.02 (t,1H), 8.99 (d, 1H), 8.34 (d, 1H), 8.24 (d, 1H), 8.04 (d, 1H), 7.97 (d, 1H); ^{13}C-NMR (C$_2$D$_2$Cl$_4$, 300 MHz): 149.17, 128.12, 128.07, 127.85, 127.75, 127.54, 126.44, 126.39, 126.31, 126.26, 126.19, 125.79, 125.72, 124.91, 124.73, 123.92, 123.28, 121.92, 35.33, 31.55. MALDI-TOF (TCNQ as matrix): m/z 562.87, cacld.: 562.76; Elemental analysis: Calculated: C 93.91, H 6.09; Found: C 93.83, H 6.07. MP: >300 °C.

Tetramer (2-2):
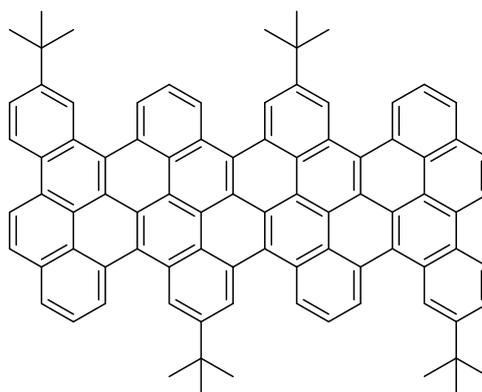
Tetramer 2-2

To a mixture of **2-24** (10 mg, 0.0088 mmol) and DDQ (18 mg, 0.077 mmol) in dry CH$_2$Cl$_2$ (9.5 mL) at 0 °C was added trifluoromethanesulfonic acid (0.5 mL). After 6 hours, the resulting mixture was quenched by saturated NaHCO$_3$ solution (20 mL), and then extracted with CH$_3$Cl twice. The combined extracts were washed with brine and dried over MgSO$_4$. After removal of the solvent in vacuo, the crude material was purified by column chromatography (dichloromethane/hexane=1:1) to afford **tetramer 2-2** (7 mg, 70.8%) as a red solid.

^{1}H-NMR (C$_2$D$_2$Cl$_4$, 500 MHz): 9.08-9.27(m, 3H), 8.28-8.54 (m, 3H), 8.07-8.14 (m, 2H), 6.78-7.12 (m, 5H), 1.58 (s, 18H); ^{13}C-NMR (C$_2$D$_2$Cl$_4$, 500 MHz): 145.18. 143.43, 143.21, 143.09, 142.99, 142.95, 142.85, 142.78, 142.74, 142.70, 142.68, 142.61, 142.53, 142.37, 142.11, 142.02, 140.61, 140.26, 139.44, 139.40, 139.13, 138.70, 134.64, 133.11, 132.96, 132.87, 132.70, 131.52, 128.30, 128.43, 123.80, 123.49, 121.21, 121.12, 121.99, 127.97,35.89, 33.28. MALDI-TOF (TCNQ as matrix): m/z 1117.17, cacld.: 1118.48; Elemental analysis: Calculated: C 94.42, H 5.58; Found: C 94.52, H 5.46. MP: >300 °C.

1-Bromo-2-iodo-3,5-dimethylbenzene (2-28):
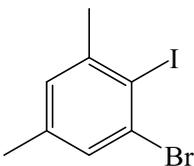
2-28

A mixture of compound **2-27** (0.05 mol), H_2O(100mL), and 37% aq.HCl(100mL) was heated to 80°C while stirring. The mixture was stirred 30 min followed by cooling to 0°C on an ice/water bath.$NaNO_2$(0.055 mol) was added maintaining the internal temperature below 10°C. The resulting clear, orange solution was stirred at 0°C for 30 min followed by addition of KI(0.055mol) as a solution in H_2O (50 mL) keeping the internal temperature below 10°C. The black suspension was allowed to reach room temperature and stirred for 12h. The suspension was extracted with DCM, washed with water and brine, dried over with Mg_2SO_4, cncentration of the solution in vacuo gave a brown residue that was purified by column chromatography (hexane) to afford compound **9** (60%) as a yellow orange oil.

2-28:^{1}H-NMR (CD_2Cl_2, 250 MHz): 7.34 (s, 1H), 7.03 (s, 1H), 2.54 (s, 3H), 2.28 (s, 3H).

((2-Bromo-4,6-dimethylphenyl)ethynyl)trimethylsilane (2-29):
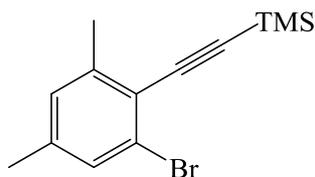
2-29

A 50mL round bottomflask equipped with a magnetic stir bar was charged with compound **2-28** (35 mmol),THF (100 mL), triethylamine (20 mL, 150mmol), $PdCl_2(PPh_3)_2$ (500 mg, 0.7mmol), CuI (150mg, 0.754 mmol) and trimethylsilylacetylene (5.25 mL, 37.1mmol) under argon atmosphere. The reaction mixture was stirred overnight at room temperature, diluted in CH_2Cl_2, washed with NH_4Cl and dried over Mg_2SO_4. The solvent was removed under reduced pressure and the crude productwas purified by flash chromatography on silica gel with hexanes as eluent to afford the desired compound **2-29** (82%) as yellow solid.

2-29: ^{1}H-NMR (CD$_2$Cl$_2$, 250 MHz): 7.43 (s, 1H), 7.13 (s, 1H), 2.58 (s, 3H), 2.32 (s, 3H), 0.28 (s, 9H);

1,4-Dis(2-bromo-4,6-dimethylphenyl)buta-1,3-diyne (2-30):

2-30
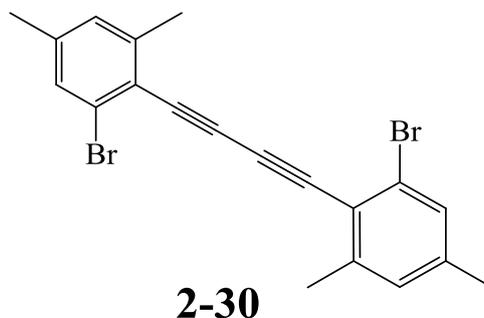
To a dimethylformamide (DMF) (100 mL) solution of compound **2-29** (32.3 mmole) placed in round bottom flask was added CuCl (32.3 mmol) equipped with a magnetic stirring bar. The reaction mixture was stirred for 6 h at 80°C and quenched with 1.0 M HCl(aq). The aqueous layer was separated and extracted with 100 mL of diethyl ether. The combined ethereal layer was washed with brine and dried over Mg$_2$SO$_4$, cncentration of the solution in vacuo gave a brown residue that was purified by column chromatography (dichloromethane/hexane = 1/8) to afford compound **2-30** (78%) as a yellow solid.

2-30:^{1}H-NMR (CD$_2$Cl$_2$, 250 MHz): 7.23 (s, 1H), 6.95 (s, 1H), 2.39 (s, 3H), 2.23 (s, 3H). FD-MS (8 KV): 415.7m/z.

1,4-Bis(2-iodo-4,6-dimethylphenyl)buta-1,3-diyne (2-31):

2-31
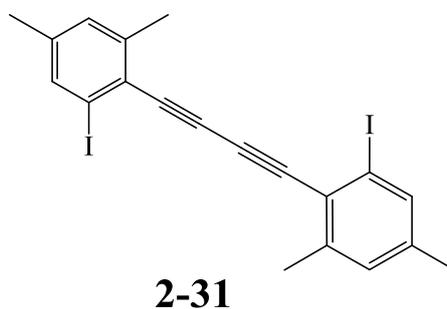
A 250 mL round bottom flask equipped with a magnetic stir bar was charged with compound **2-30** (11.9 mmol), THF (100 mL). The temperature was cooled to -78 °C and n-BuLi (1.4 mL, 47.4 mmol) was added slowly. The reaction mixturewas stirred for one hour and 1,2-

diiodoethane was added (35.6 mmol). The reaction mixture was stirred overnight at room temperature, diluted in CH_2Cl_2, washed with H_2O and dried over Mg_2SO_4. The solvent was removed under reduced pressure and the crude product was purified by column chromatography (dichloromethane/hexane = 1/8) to afford the desired compound **2-31** (80%) as yellow solid.

**2-31:**^{1}H-NMR (CD_2Cl_2, 250 MHz): 7.48 (s, 1H), 6.97 (s, 1H), 2.41 (s, 3H), 2.20 (s, 3H). FD-MS (8 KV): 509.8m/z.

1,4-Bis(2-(3-bromonaphthalen-2-yl)-4,6-dimethylphenyl)buta-1,3-diyne (2-32):
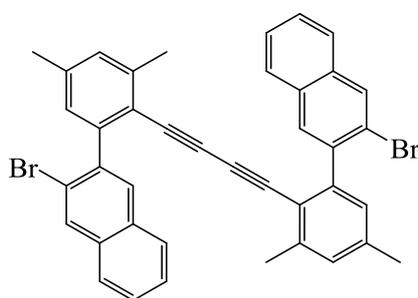
2-32

Nitrogen was bubbled through a mixing solution of THF (100 mL), EtOH (20 mL) and water (20 mL) for 30 min, and to this solution was added compound **2-31** (4.96 mmol), Pd(PPh$_3$)$_4$ (0.5 mmol), K_2CO_3 (29.76 mmol) and compound **2-13** (9.95 mmol). The mixture was heated at 60°C for 36h. The solution was extracted three times with ethyl acetate. After removal of the solvent in vacuo, the crude material was purified by column chromatography (dichloromethane/hexane = 1/8) to afford compound **2-32** (56%) as a yellow solid.

2-32: ^{1}H-NMR (CD_2Cl_2, 250 MHz): 8.13(s, 1H), 7.98 (s, 1H), 8.00 (s,1H), 7.83 (t, 1H), 7.72 (d, 3H), 7.61 (t, 1H), 7.37 (t, 1H), 7.11(s, 1H), 6.98 (s, 1H), 2.39 (s, 3H), 2.35 (s, 3H). FD-MS (8 KV): 667.9m/z.

11,11'-Dibromo-6,6'-diiodo-7,7',9,9'-tetramethyl-5,5'-bichrysene (2-33):
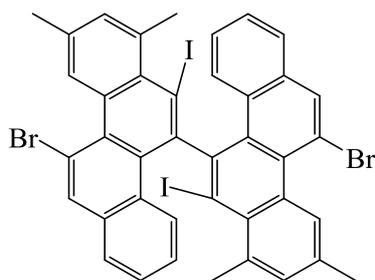
2-33

A solution of compound **2-32** (1.55 mmol) in dry CH$_2$Cl$_2$ (100 mL) was maintained at -78°C with an acetone-liquid N$_2$ bath. To this solution was added ICl (3.41 mL, 1 M solution in CH$_2$Cl$_2$), using a standard syringe. The reaction was stirred for 3 h. Quenched with a saturated sodium sulfite solution and warmed to RT. Extracted with CH$_2$Cl$_2$ (2×30 mL) and dried over MgSO$_4$. After removal of solvent in vacuo, the crude material was purified by column chromatography (dichloromethane/hexane = 1/8) to afford compound **2-33** (87%) as a yellow solid.

2-33: ^{1}H-NMR (CD$_2$Cl$_2$, 250 MHz): 8.91(s, 1H), 7.89 (s, 1H), 7.47 (d,1H), 7.26 (s, 1H), 7.22 (dd, 1H), 7.17 (dd, 1H), 6.70 (t, 1H), 2.70 (s, 3H), 2.48 (s, 3H); ^{13}C-NMR (CD$_2$Cl$_2$, 250 MHz):149.46, 134.66, 134.37, 132.61, 132.34, 131.41, 131.36, 131.05, 130.75, 130.09, 127.41, 126.54, 125.43, 125.15, 123.75, 122.86, 114.75, 100.49, 24.56, 20.40. FD-MS (8 KV): 919.9m/z.

11,11'-Dibromo-7,7',9,9'-tetramethyl-5,5'-bichrysene (2-5c):
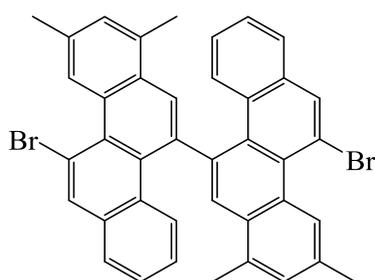

2-5c

A solution of **2-33** (0.108mmol) in dry THF (100 mL) was irradiated in a standard immersion well photoreactor with 360nm high pressure mercury vapor lamp (4*360nm) for 2 h. The reaction mixture was then washed with aqueous sodium thiosulfate, water, brine and dried

over anhydrous MgSO4. The solvent was removed under vacuum and recrystallization from chloroform to afford compound **2-5c** (50%) as a yellow solid.

2-5c: ^{1}H-NMR (CD$_2$Cl$_2$, 250 MHz): 9.21(s, 1H), 8.30 (s, 1H), 8.00 (s,1H), 7.73 (dd, 1H), 7.32 (m, 3H), 6.79 (t, 1H), 2.64 (s, 3H), 2.56 (s, 3H); ^{13}C-NMR (CD$_2$Cl$_2$, 250 MHz):139.12, 134.39, 134.24, 133.91, 132.78, 131.13, 130.42, 130.09, 129.85, 129.65, 129.58, 128.00, 127.86, 126.97, 126.72, 125.78, 125.39, 117.47, 22.34, 19.91. FD-MS (8 KV): 667.8m/z.

2',5'-Dibromo-2,2''-dimethyl-1,1':4',1''-terphenyl (3-8):

3-8
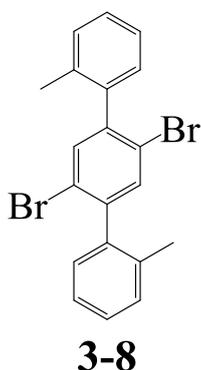
A mixture of 1,4-dibromo-2,5-diiodobenzene (5.00 g, 10.27 mmol), 2-methylbenzeneboronic acid (3.35 g, 24.64 mmol), 1,2-dioxane/H$_2$O (100/30 mL), K$_2$CO$_3$ (5.71g, 41.08 mmol) was degassed by bubbling through nitrogen stream for 30 min. Catalyst Pd(PPh$_3$)$_4$ (593 mg, 0.51 mmol) was added and the mixture was further degassed by three freeze-pump-thaw cycles. The reaction was heated at 90 ^{o}C for 24 h under nitrogen atmosphere. After cooling to the room temperature, the mixture was poured into water and extracted with dichloromethane (DCM). The organic layer was washed by water and dried over anhydrous MgSO$_4$. The solvent was removed under vacuum and the residue was purified by silica gel column chromatography using DCM/hexane (1/10, v/v) as eluent to give compound **3-8** as a white solid (3.20 g, yield: 75 %). ^{1}H-NMR (CD$_2$Cl$_2$, 300 MHz): 8.12 (d, 1H), 7.37 (t, 1H), 7.09-7.37 (m,3H), 2.73 (s, 3H); ^{13}C-NMR (CD$_2$Cl$_2$, 300 MHz): 146.69, 143.58, 140.09, 137.53, 132.49, 130.87, 128.71, 125.96, 125.49, 23.24 FD-MS (8 KV): m/z 415.8, cacld.:416.16. Melting point: 155.8-156.5 ^{o}C.

4-(*tert*-Butyl)-4'-(4-(*tert*-butyl)-2-ethynylphenyl)-2-ethynyl-2''-methyl-5'-(*o*-tolyl)-1,1':2',1''-terphenyl (3-10):

3-9   **3-10**
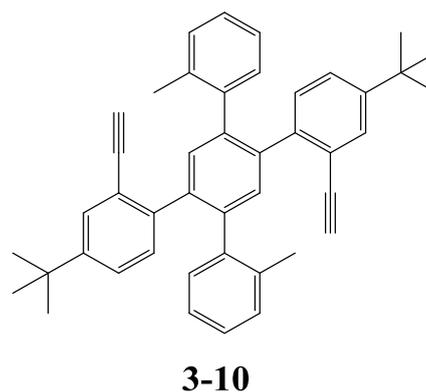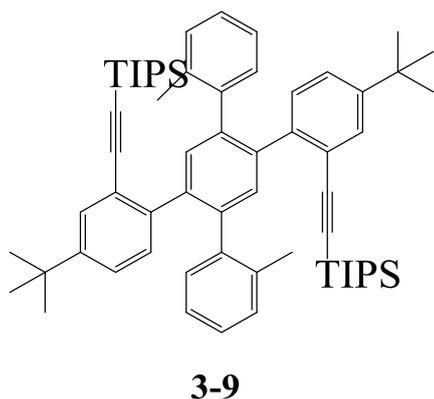
A mixture of **3-8** (3.00 g, 7.21 mmol), (4-(tert-butyl)-2-((triisopropylsilyl)ethynyl)phenyl)boronic acid **3-7** (7.75 g, 21.63 mmol), 1,2-dioxane/H_2O (100/30 mL), K_2CO_3 (5.01 g, 36.05 mmol) was degassed by bubbling through nitrogen stream for 30 min. Catalyst $Pd(PPh_3)_4$ (416 mg, 0.36 mmol) was added and the mixture was further degassed by three freeze-pump-thaw cycles. The reaction was heated at 95 ºC for 24 h under nitrogen atmosphere. After cooling to room temperature, the mixture was poured into water and extracted with DCM. The organic layer was washed with water and dried over anhydrous $MgSO_4$. The solvent was removed under vacuum and the residue was purified by silica gel column chromatography using DCM/hexane (1/5, v/v) as eluent to give compound **3-9** as a white solid (5.10 g, yield: 69 %). Then the compound **3-9** (5.10 g, 5.77 mmol) was dissolved in 50 mL THF, and added the 5.8 mL TBAF (1 M in the THF) in the solution via dropwise. After 30 min, the reaction was quenched with methanol. Most THF was removed under vacuum and the residue was purified by recrystallization from chloroform affording the target white solid **3-10** (2.80 g, yield: 85 %).

3-9: ^{1}H-NMR (CD_2Cl_2, 300 MHz): 7.41 (d, 1H), 7.33 (s, 1H), 7.24 (d, 1H), 6.95-7.02 (m, 4H), 6.80 (d, 1H), 2.02 (s, 3H), 1.18 (s, 9H), 0.92 (s, 18H); ^{13}C-NMR (CD_2Cl_2, 300 MHz): 149.79, 142.36, 141.22, 139.23, 139.06, 136.62, 133.77, 132.31, 131.36, 129.80, 127.02, 125.22, 124.99, 122.56, 114.75, 107.74, 100.36, 34.42, 30.98, 20.84, 18.74, 11.51. FD-MS (8 KV): m/z 882.9, cacld.: 883.51. Melting point: 258.2-259.1 ºC. HR-MS (MALDI): m/z = 882.5940, calcd. for C62H82Si2: m/z = 882.5955, error = -1.7 ppm.

3,10-Di-*tert*-butyl-7,14-di-*o*-tolylbenzo[k]tetraphene (3-11):
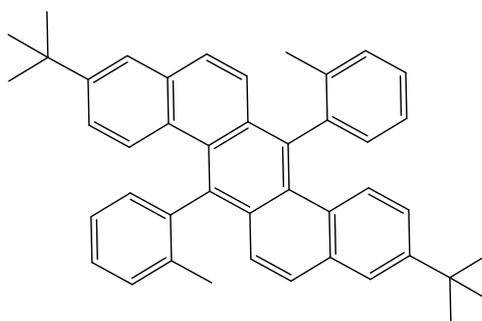
3-11

A reaction flask containing PtCl$_2$ (466 mg, 1.75 mmol) was dried in vacuo for 1 h, and vacuum was filled with nitrogen using a nitrogen balloon. To this round bottom flask was added compound **3-10** (2.00 g, 3.50 mmol) and toluene (50 mL), and the mixture was stirred at 25 °C for 5 min before it was heated at 110 °C for 24 h. After removal of solvent in vacuo, the crude material was purified by column chromatography (dichloromethane/hexane = 1/5) to afford compound **3-11** (540 mg, yield: 27 %) as a yellow solid. ^{1}H-NMR (CD$_2$Cl$_2$, 300 MHz): 7.79 (s, 1H), 7.59 (m, 2H), 7.52 (d, 2H), 7.44 (t, 1H), 7.42 (t, 1H), 7.24 (s, 2H), 1.96-2.07 (d, 3H), 1.40 (s, 9H); ^{13}C-NMR (THF-d, 300 MHz): 150.16, 138.91, 138.28, 133.43, 130.97, 130.57, 129.59, 129.55, 129.36, 127.97, 127.93, 127.30, 126.27, 126.20, 126.08, 125.41, 125.22, 34.21, 30.76, 25.80. FD-MS (8 KV): m/z 570.1, cacld.: 570.82. Melting point: 310.3-311.1 ^{o}C. Elemental analysis: Calculated: C 92.58, H 7.42; Found: C 92.49, H 7.46.

((3,10-Di-*tert*-butylbenzo[k]tetraphene-7,14-diyl)bis(2,1-phenylene))bis(methylene) diacetate (3-13):
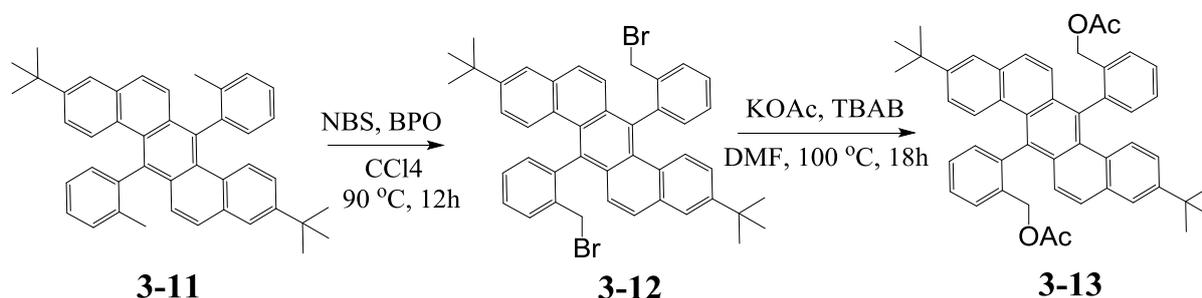
Compound **3-11** (300 mg, 0.53 mmol), *N*-bromosuccinimide (NBS, 207 mg, 1.12 mmol) and benzoyl peroxide (BPO, 52 mg, 0.21 mmol) were dissolved in 100 mL of CCl$_4$ and heated to reflux (95 ^{o}C) under argon atmosphere. After 24 hours, the mixture was cooled to room temperature and the solvent was removed under reduced pressure. The residue was passed

through a short silica gel column using hexane/chloroform (2/1, v/v) as eluent and the first fraction was collected containing a majority of compound **3-12**, together with a mixture of starting material **3-11** and mono-bromide byproduct. The polarity of the byproducts is slightly smaller than **3-11** and they cannot be separated. Therefore, the crude product was used directly for the next step. The crude product, KOAc (517 mg, 5.26 mmol) and tetrabutylammonium bromide (170 mg, 0.53 mmol) were dissolved in 15 mL of DMF and heated to 100 °C under argon atmosphere. The mixture was stirred for 18 hours and poured into 200 mL of ice water. The solvent was then filtered off and the brown solid was collected and washed with water and methanol for several times. And the yellow solid **3-13** was used directly for the next step.

2,2'-(3,10-Di-*tert*-butylbenzo[k]tetraphene-7,14-diyl)dibenzaldehyde (3-15):

3-13   **3-14**   **3-15**
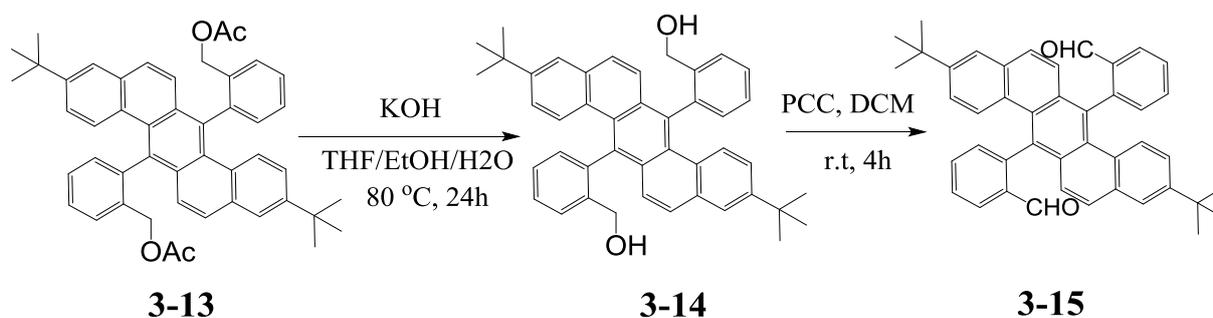
Compound **3-13** (200 mg, 0.29 mmol) was dissolved in mixed solvent of THF (60 mL), ethanol (60 mL) and 10% aqueous KOH solution (20 mL) under argon atmosphere. The mixture was heated to reflux (80 °C) and stirred for 24 hours. The solvent was removed under reduced pressure and the residue was redissolved in 50 mL chloroform, washed with water and brine and dried over $MgSO_4$. The solvent was evaporated and the residue was redissolved in 50 mL of dry DCM. To the solution was added pyridinium chlorochromate (PCC, 126 mg, 0.58 mmol) and the mixture was stirred at room temperature for 2 hours. Afterwards, the solvent was removed and the residue was purified by column chromatography (silica gel, hexane/chloroform (3/1, v/v)) to give compound **3-15** (100 mg, 32 % in four steps) as a yellow solid. ^{1}H-NMR (THF-d, 300 MHz): 10.66 (s, 1H), 8.65 (s, 1H), 8.06 (t, 3H), 7.66 (t, 1H), 7.55 (t, 1H), 7.44 (d, 1H), 7.38 (t, 3H), 7.32 (d, 1H), 1.31 (s, 9H); ^{13}C-NMR (THF-d, 300 MHz): 191.24, 151.24, 139.77, 139.66, 136.09, 133.05, 131.10, 131.04, 130.77, 129.36, 128.59, 128.05, 127.71, 127.44, 127.08, 126.90, 126.71, 124.59, 34.29, 30.49. FD-MS (8

KV): m/z 597.9, cacld.: 598.79. Elemental analysis: Calculated: C 88.26, H 6.40, O 5.34; Found: C 88.21, H 6.48.

## 2,12-Di-*tert*-butyl-9,19-dimesityl-9,19-dihydrotetrabenzo[a,f,j,o]perylene (3-17):
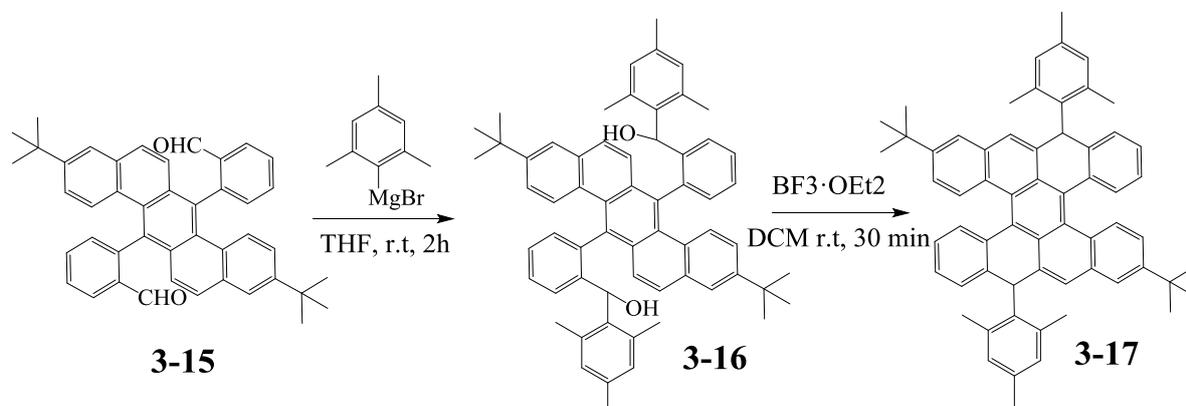
Compound **3-15** (50 mg, 0.084 mmol) was dissolved in 20 mL of dry THF under argon atmosphere. To the solution was added 0.84 mL mesitylmagnesium bromide solution (1M in ether, 0.84 mmol) and the mixture was stirred at room temperature for 2 hours. The reaction mixture was then poured into 50 mL water and extracted by chloroform. The organic layer was dried over MgSO$_4$ and the solvent was removed under reduced pressure. The residue (compound **9**) was then redissolved in 40 mL dry DCM under argon atmosphere and 4 mL of BF$_3$·OEt$_2$ was added. The mixture was stirred for 30 minutes and then washed with NaHCO$_3$ solution (3x20 mL) and water (3x20 mL). The organic layer was dried over MgSO$_4$ and the solvent was removed under reduced pressure. The residue was purified by column chromatography (silica gel, hexane/DCM (5/1, v/v)) to give compound **3-17** (45 mg, 67 % in two steps) as a yellow solid. Two isomers exist in this compound and they were used directly for the next step. ^{1}H-NMR (CD$_2$Cl$_2$, 500 MHz): 8.28, 8.07, 7.80, 7.57, 7.31-7.6.76 (m, 3H), 7.44-7.42 (m, 2H), 7.22-7.19 (m, 2H), 6.95-6.78 (m, 4H), 6.59, 6.26, 6.07 (three single peaks, 2H), 5.86, 5.84, 5.74 (three single peaks, 2H), 2.58-1.19 (nine groups of single peaks due to the isomers, 36H).; ^{13}C-NMR (CD$_2$Cl$_2$, 500 MHz): 157.70, 154.00, 138.29, 138.18, 137.91, 137.84, 137.67, 137.46, 137.39, 137.19, 136.96, 136.85, 136.37, 136.26, 135.66, 135.11, 133.77, 131.53, 131.12, 130.23, 129.82, 128.70, 128.67, 128.49, 128.32, 127.97, 126.73, 126.42, 125.62, 125.39, 124.45, 124.15, 123.73, 41.46, 34.59, 32.07, 31.21, 31.11, 30.95, 30.77, 29.83, 22.83, 21.19, 21.11, 20.85, 20.65, 14.00. FD-MS (8 KV): m/z 802.8. MALDI-

TOF (TCNQ as matrix): m/z 803.11, cacld.: 803.15. Elemental analysis: Calculated: C 92.72, H 7.28; Found: C 92.63, H 7.37.

2,12-Di-*tert*-butyl-9,19-dimesityltetrabenzo[*a,f,j,o*]perylene (3-1):

3-1
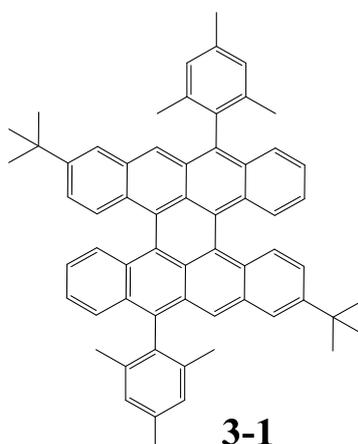
Compound **3-17** (24 mg, 0.037 mmol) was redissolved in 2 mL dry toluene under argon atmosphere and *p*-chloranil (20.2 mg, 0.082 mmol dissolved in 1 mL dry toluene) was added dropwise. The mixture was stirred at room temperature for 12 hours. The residue was purified by column chromatography (silica gel was degased and protected it with argon, hexane/DCM (5/1, v/v), the eluent was also degased) to give compound **3-1** (20 mg, 85 %) as a green solid. This compound was stored under argon. ^{1}H-NMR (CD$_2$Cl$_2$, 500 MHz): 8.11 (s, 1H), 7.79 (d, 2H), 7.67 (d, 1H), 7.52 (d, 1H), 7.34-7.31 (m, 2H), 7.2 (d, 2H), 7.23 (t, 1H), 2.55 (s, 3H), 1.94 (s, 3H), 1.91 (s, 3H), 1.38 (s, 9H). MALDI-TOF (TCNQ as matrix): m/z 800.18, cacld.: 800.44. HR-MS (MALDI): m/z = 800.4374, calcd. for C62H56: m/z = 800.4382, error = -1.0 ppm.

Tetrabenzo[*a,f,j,o*]perylene-9,19-dione (3-18):
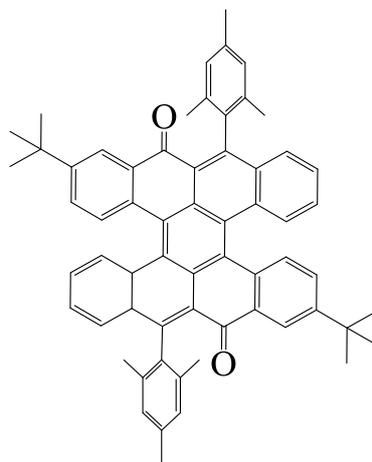
3-18

The green solution of compound **3-1** (10 mg, 0.012 mmol) in dichloromethane was exposed to air condition overnight. Finally, a red color was achieved due to the oxidation of compound **3-1**. The residue was purified by column chromatography (hexane/DCM (2/1, v/v)) to give compound **3-18** (6.75 mg, 65 %) as a red solid. ^{1}H-NMR (CD$_2$Cl$_2$, 250 MHz): 8.49 (d, 1H), 8.09 (s, 1H), 7.61 (d, 1H), 7.38-7.24 (m, 4H), 7.06 (d, 2H), 2.41 (s, 3H), 1.82 (s, 3H), 1.26 (s, 9H); ^{13}C-NMR (CD$_2$Cl$_2$, 250 MHz): 185.43, 152.17, 146.99, 137.85, 137.33, 136.70, 135.66, 133.49, 132.65, 132.38, 132.19, 131.15, 129.35, 129.03, 128.77, 128.25, 127.97, 127.30, 126.93, 123.90, 122.19, 35.29, 31.22, 30.42, 21.45, 20.46, 20.11. FD-MS (8 KV): m/z 831.6. MALDI-TOF (TCNQ as matrix): m/z 830.54, cacld.: 830.43. Elemental analysis: Calculated: C 89.60, H 6.55, O 3.85; Found: C 89.71, H 6.63.

1-Bromo-2-((4-(*tert*-butyl)phenyl)ethynyl)benzene (4-12):
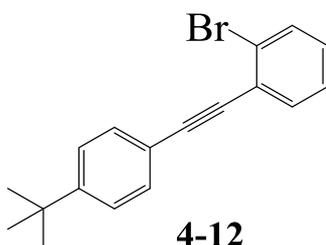
4-12

A 250 mL round-bottom schlenk flask was charged under an atmosphere of argon with 2-bromoiodobenzene (15.42 g, 54.0 mmol), 4-tert-butylphenylacetylene (11.23 g, 71.0 mmol) and Et$_3$N (25 mL) in anhydrous THF (100 ml). The solution was degassed with argon for 30 minutes. The mixture was freezed with liquid nitrogen and Bis(triphenylphosphine)palladium(II) dichloride (4.7 g, 5.4 mmol, 10 mol %), and copper(I)

iodide (1.03 g, 5.4 mmol, 10 mol %)) was added. After deoxygenation by three "freeze-pump-thaw" cycles the reaction mixture was stirred at room temperature for 24 h. The reaction mixture was diluted in 200 ml DCM and washed with saturated ammonium chloride solution (3×100 mL) and dried over magnesium sulfate. The solvent was removed under reduced pressure and the residue was purified by column chromatography on silica (hexane) to afford the title compound **4-12** as a yellow solid (20.81 g, 66.4 mmol, 92.4 %). ^{1}H-NMR (CD$_2$Cl$_2$, 300 MHz): 7.72(dd, 1H), 7.66 (dd, 1H), 7.63 (d, 2H), 7.51 (d, 2H), 7.37 (td, 1H), 7.25 (td, 1H), 1.42 (s, 9H); ^{13}C-NMR (CD$_2$Cl$_2$, 300 MHz): 152.65, 133.60, 132.87, 131.80, 129.79, 127.59, 120.20, 94.58, 87.85, 35.19, 31.39. FD-MS (8 KV): m/z 312.7, cacld.: 313.23.

(2-((4-(*tert*-Butyl)phenyl)ethynyl)phenyl)boronic acid (4-13):

4-13
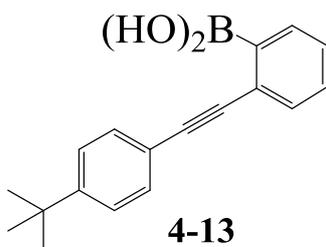
A solution of compound **4-12** (5.00 g, 15.96 mmol) in anhydrous THF (100 ml) was degassed with argon for 30 minutes. After the solution was cooled to -78 °C, a 1.6 M solution of BuLi in hexanes (12 ml, 19.15 mmol, 1.2 eq.) was added dropwise to the solution under argon atmosphere. After 1 hour, B(O*i*Pr)3 (7.3 mL, 31.92 mmol, 2.0 eq) was added and the reaction mixture was left to stir at −78 °C overnight gradually warming up to room temperature. The reaction was quenched with1 M HCl aq solution (100 mL) and then extracted with Et2O (3×100 mL), dried over MgSO4, filtered and concentrated. The residue was used directly for the next step.

2',5'-Dibromo-4,4''-di-*tert*-butyl-1,1':4',1''-terphenyl (4-10):

4-10
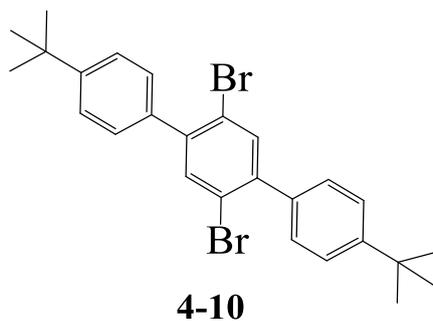
In a two-necked round-bottom flask equipped with a condenser, a mixture of commercially available 1,4-dibromo-2,5-diiodobenzene (5.00 g, 10.25 mmol), 4-*tert*-butylbenzoboronic acid (4.10 g, 22.56 mmol) and potassium carbonate (14.10 g, 102 mmol) in dioxane (100 ml) and water (40 ml) was added and degassed with agron for 30 minutes and tetrakis(triphenylphosphine)palladium(0) (592 mg, 0.51 mmol) was added. After deoxygenated by three "freeze-pump-thaw" cycles the reaction mixture was heated to 90°C for 24 h. After cooling, the reaction mixture was diluted in 200 ml dichloromethane (DCM) and washed with water (3×100 mL) and dried over magnesium sulfate. The solvent was removed under reduced pressure and the residue was purified by column chromatography on silica (hexane) to give white solid of 1,4-dibromo-2,5-di(4´-*tert*-butylphenyl)benzene **4-10** (3.7 g, 7.39 mmol, 71.8 %). ^{1}H-NMR (CD$_2$Cl$_2$, 300 MHz): 7.56(s, 1H), 7.40 (d, 2H), 7.33 (d,2H), 1.29 (s, 9H); ^{13}C-NMR (CD$_2$Cl$_2$, 300 MHz): 151.62, 142.96, 136.90, 135.69, 129.31, 125.48, 121.63, 34.96, 31.44. FD-MS (8 KV): m/z 499.6, cacld.: 500.32. Melting point: 264.4 ºC

4''-(*tert*-Butyl)-5'-(4-(*tert*-butyl)phenyl)-2-((4-(*tert*-butyl)phenyl)ethynyl)-4'-(2-((4-(*tert*-butyl)phenyl)ethynyl)phenyl)-1,1':2',1''-terphenyl (4-14):

4-14
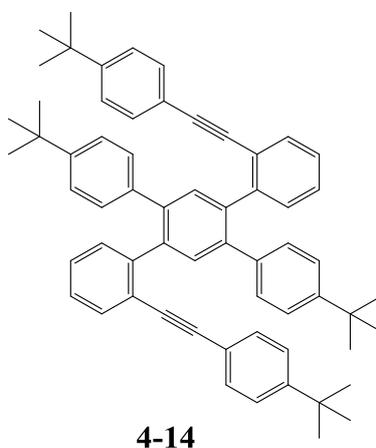
In a two-necked round-bottom flask equipped with a condenser, a mixture of 1,4-dibromo-2,5-di(4´-*tert*-butylphenyl)benzene (1.50 g, 3.00 mmol), compound **4-13** (5.00 g, 18.00 mmol)) and potassium carbonate (3.30 g, 24.00 mmol) in dioxane (100 ml) and water (40 ml) was added and degassed with agron for 30 minutes and tetrakis(triphenylphosphine)palladium(0) (350 mg, 0.30 mmol) was added. After deoxygenated by three "freeze-pump-thaw" cycles the reaction mixture was heated to 90°C for 72 h. After cooling, the reaction mixture was diluted in 200 ml DCM and washed with water (3×100 mL) and dried over magnesium sulfate. The solvent was removed under reduced pressure and the residue was purified by column chromatography first (hexane), later (hexane/DCM; 10/1) to obtain the title compound **4-14** (1.2 g, 1.49 mmol, 49.7 %) as a yellow solid. ^{1}H-NMR (CD$_2$Cl$_2$, 300 MHz): 7.71 (s, 1H), 7.62 (dd, 1H), 7.32 (m, 1H), 7.28 (m, 3H), 7.23 (m, 4H), 7.08 (broad, 3H), 1.30 (s, 9H), 1.25 (s, 9H); 13C-NMR (CD$_2$Cl$_2$, 300 MHz): 149.76, 144.53, 139.67, 139.02, 138.41, 133.61, 132.08, 131.45, 131.15, 129.66, 127.94, 127.22, 125.46, 125.03, 123.79, 120.43, 93.64, 89.04, 34.90, 34.66, 31.44, 31.22. FD-MS (8 KV): m/z=805.9. HR-MS (MALDI): m/z = 806.4824, calcd. for C$_{62}$H$_{62}$: m/z = 806.4852, error = -3.5 ppm.

6,7,13,14-Tetrakis(4-(*tert*-butyl)phenyl)-5,12-diiodobenzo[*k*]tetraphene (4-15):

4-15
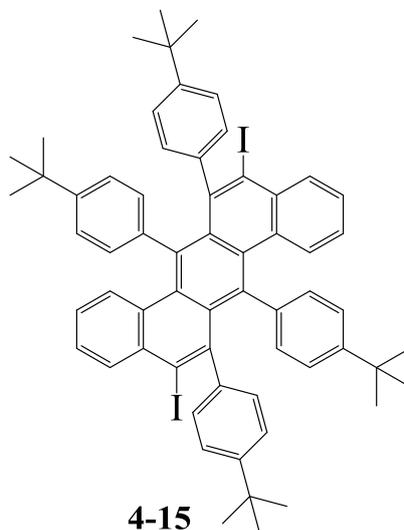
A solution of compound **4-14** (500 mg, 0.62 mmol) in anhydrous DCM (50 ml) was degassed with argon for 30 minutes. After the solution was cooled to -78 °C, a 1 M solution of iodine monochloride (1.48 ml, 2.4 eq) in DCM was added dropwise to the solution under argon atmosphere. The reaction was stirred for 3 h and quenched with saturated sodium sulfite solution. The reaction mixture was diluted in 200 ml DCM and washed saturated sodium sulfite solution (3×100 mL) and dried over magnesium sulfate. The solvent was removed

under reduced pressure and the residue was dissolved in hexane and precipitated in methanol (30 mL). The precipitate was filtered off and washed with methanol to obtain the title compound **4-15** (575 mg, 85.4%) as a yellow solid. ^{1}H-NMR (CD$_2$Cl$_2$, 300 MHz): 8.17 (d, 2H), 7.28 (dd, 1H), 7.25 (dd, 1H), 7.02 (dd, 1H), 6.98 (dd, 1H), 6.76-6.60 (m, 5H), 6.24 (dd, 1H), 6.16 (dd, 1H), 1.30 (s, 9H), 1.19 (s, 9H); 13C-NMR (CD$_2$Cl$_2$, 300 MHz): 150.37, 149.00, 145.53, 144.47, 139.56, 136.06, 135.70, 135.47, 134.54, 133.29, 132.28, 130.64, 129.87, 138.66, 128.20, 126.61, 125.79, 125.43, 124.57, 123.48, 122.48, 34.81, 34.63, 31.67, 31.53. FD-MS (8 KV): m/z=1058.1. HR-MS (MALDI): m/z = 1058.2821, calcd. for C$_{62}$H$_{60}$I$_2$: m/z = 1058.2784, error = 3.5 ppm.

6,7,13,14-Tetrakis(4-(*tert*-butyl)phenyl)benzo[*k*]tetraphene (4-5):

4-5
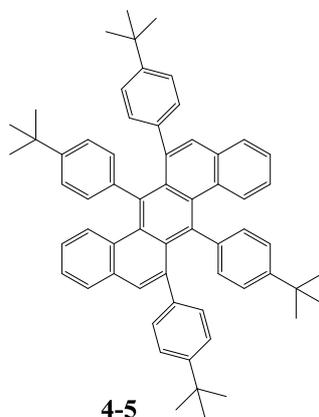
A solution of compound **4-15** (200 mg, 0.19 mmol) in anhydrous THF (30 ml) was degassed with argon for 30 minutes. After the solution was cooled to -78 °C, a 1.6 M solution of BuLi (0.73 ml, 2.4 eq) was added dropwise to the solution under argon atmosphere. The reaction was stirred for 2 h and quenched with methanol (10 ml). The reaction mixture was diluted in 200 ml DCM and washed with water (3×100 mL) and dried over magnesium sulfate. The solvent was removed under reduced pressure and the residue was purified by column flash chromatography on silica (hexane/DCM; 10/1) to obtain the title comound **4-5** (80 mg, 0.1 mmol, 52.6%) as a yellow solid. ^{1}H-NMR (CD$_2$Cl$_2$, 300 MHz): 7.64 (dd, 1H), 7.27 (s, 1H), 7.21 (m, 2H), 6.90 (d, 4H), 6.78 (dd, 2H), 6.74-6.68 (m, 3H), 1.23 (s, 9H), 1.16 (s, 9H); 13C-NMR (CD$_2$Cl$_2$, 300 MHz): 150.13, 148.45, 141.72, 140.37, 139.95, 135.99, 133.35, 133.22, 131.38, 130.46, 129.73, 129.39, 128.63, 127.58, 126.33, 125.46, 124.44, 124.40, 34.72, 34.52, 31.58, 31.52. FD-MS (8 KV): m/z=805.6. HR-MS (MALDI): m/z = 806.4878, calcd. for C$_{62}$H$_{62}$: m/z = 806.4852, error = 3.2 ppm.

7,16-Di-*tert*-butyl-5,14-bis(4-(*tert*-butyl)phenyl)dibenzo[*a,m*]rubicene (4-7) and

(*R*)-7,16-di-*tert*-butyl-9b,14-bis(4-(*tert*-butyl)phenyl)dibenzo[*a,m*]rubicen-5(9*bH*)-one   (4-8):
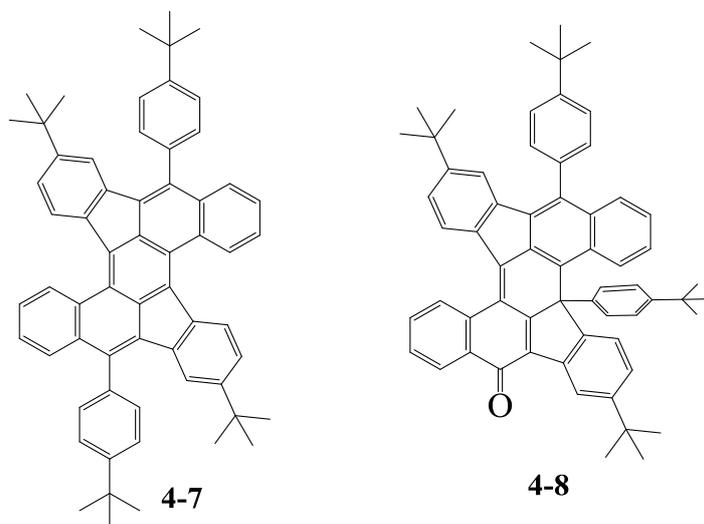

After a solution of compound **4-5** (40 mg, 0.049 mmol) in anhydrous DCM (20 ml) was degassed with argon for 30 minutes, it was added dropwise to 2,3-dichloro-5,6-dicyanobenzoquinone (DDQ: 51 mg, 0.223 mmol, 5 equiv) in a 50 ml round-bottom schlenk flask at 0 ℃ under argon atmosphere. After stirring for 15 min, trifluoromethanesulfonic acid (0.5 mL) was added to the mixture. The reaction mixture was left to stir for further 30 minutes and quenched with saturated NaHCO$_3$ solution. The reaction mixture was diluted in 200 ml DCM and washed with saturated NaHCO$_3$ solution (3×100 mL) and water (3×100 mL) and dried over magnesium sulfate. The solvent was removed under reduced pressure and the residue was purified by column flash chromatography on silica (first: hexane:DCM; 10:1) to obtain the title compound **4-7** (51.6 mg, 64.8%) as a yellow solid. Then change the eluent as hexane/DCM=3:1, afforded the compound **4-8** (4 mg, 5%) as a red solid.

Compound **4-7**: ^{1}H-NMR (CD$_2$Cl$_2$, 500 MHz): 9.40 (d, 1H), 8.60 (d, 1H), 7.84 (d, 1H), 7.74 (d, 2H), 7.67(t, 1H), 7.58 (d, 3H), 7.33 (d, 1H), 6.90 (s, 1H), 1.55 (s, 9H), 1.20 (s, 9H); 13C-NMR (CD$_2$Cl$_2$, 300 MHz): 150.49, 149.22, 138.38, 137.69, 135.92, 134.91, 134.46, 134.37, 131.86, 131.13, 129.77, 128.78, 128.09, 127.42, 126.54, 125.28, 124.89, 123.93, 123.64, 122.46, 121.23, 34.04, 33.85, 30.52, 30.16, 28.93. FD-MS (8 KV): m/z=802.8. HR-MS (MALDI): m/z = 802.4543, calcd. for C$_{62}$H$_{58}$: m/z = 802.4539, error = 0.5 ppm.

Compound **4-8**: ^{1}H-NMR (CD$_2$Cl$_2$, 250 MHz): 8.38-8.09 (m, 5H), 7.76-7.25 (m, 11H), 7.12 (dd, 1H), 7.04 (dd, 2H), 6.89(dd, 2H), 6.51 (d, 1H), 1.40 (s, 9H), 1.26 (s, 9H), 1.07 (s, 9H), 0.99 (s, 9H); 13C-NMR (CD$_2$Cl$_2$, 250 MHz): 180.84, 171.05, 155.05, 151.57, 151.41, 150.67,

149.50, 143.59, 140.37, 139.48, 138.11, 137.79, 136.77, 135.27, 134.87, 134.54, 134.24, 132.94, 131.51, 131.28, 130.38, 130.19, 129.70, 129.41, 128.85, 128.38, 128.30, 127.01, 126.81, 126.67, 126.63, 126.31, 126.29, 125.74, 125.17, 125.02, 124.98, 124.40, 123.75, 122.22, 64.57, 35.49, 35.33, 35.12, 34.56, 31.75, 31.64, 31.27, 31.02, 30.09. FD-MS (8 KV): m/z=817.6. HR-MS (MALDI): m/z = 818.4487, calcd. for $C_{62}H_{58}O$: m/z = 818.4488, error = -0.1 ppm.

(12bR,12c2R)-3,11,20-Tri-*tert*-butyl-12b-(4-(*tert*-butyl)phenyl)-8,17-diiodobenzo[5,6]indeno[1,2,3,4-*vwxa*]fluoreno[9,1,2,3-*cdef*]tetraphenylen-12c2(12bH)-ol (4-26):


4-26
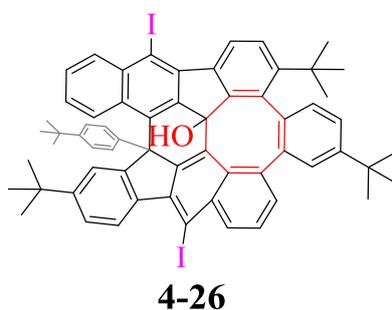
After a solution of compound **4-15** (50 mg, 0.047 mmol) in anhydrous DCM (9.5 ml) was degassed with argon for 30 minutes, it was added dropwise to 2,3-dichloro-5,6-dicyanobenzoquinone (DDQ: 53 mg, 0.235 mmol, 5 equiv) in a 50 ml round-bottom Schlenk flask at 0 ºC under argon atmosphere. After stirring for 15 min, trifluoromethanesulfonic acid (0.5 mL) was added to the mixture. The reaction mixture was left to stir for further 30 minutes and quenched with saturated $NaHCO_3$ solution. The reaction mixture was diluted in 200 ml DCM and washed with saturated $NaHCO_3$ solution (3×50 mL) and water (3×50 mL) and dried over magnesium sulfate. The solvent was removed under reduced pressure and the residue was purified by column flash chromatography on silica (hexane:DCM; 1:1) to obtain the title compound **4-26** (32.7 mg, 65%) as a red solid.

^{1}H-NMR (CD$_2$Cl$_2$, 250 MHz): 9.27-9.22 (m, 1H), 9.00-8.86 (m, 1.5H), 8.40-8.27 (m, 1.5H), 8.02-7.92 (dd, 1H), 7.79-7.69 (dd, 2H), 7.64-7.36 (m, 5H), 7.21 (d, 1H), 7.05-6.97 (m, 3H), 6.88-6.80 (dd, 2H), 6.75 (dd, 1H), 1.36 (s, 9H), 1.29 (s, 9H), 1.16 (d, 9H), 1.09 (d, 9H); ^{13}C-NMR (CD$_2$Cl$_2$, 250 MHz): 161.70, 154.17, 151.53, 151.23, 151.11, 150.13, 149.43, 147.24, 146.45, 140.54, 140.40, 139.40, 139.35, 138.72, 138.46, 137.57, 137.00, 136.73, 136.21, 135.30, 134.93, 133.84, 133.53, 133.18, 132.20, 130.65, 130.26, 129.04, 128.97, 128.37, 127.33, 127.16, 126.90, 126.46, 126.09, 125.86, 124.35, 123.84, 123.77, 122.63, 92.91, 92.34,

83.30, 65.05, 37.13, 35.19, 34.82, 34.59, 33.32, 31.50, 31.27, 17.88. FD-MS (8 KV): m/z=1071.4. HR-MS (MALDI): m/z = 1070.2455, calcd. for $C_{62}H_{58}$: m/z = 1070.2421, error = 3.2 ppm.

2-((4-(*tert*-Butyl)phenyl)ethynyl)-4'-(2-((4-(*tert*-butyl)phenyl)ethynyl)phenyl)-2''-methyl-5'-(*o*-tolyl)-1,1':2',1''-terphenyl (5-5):


5-5
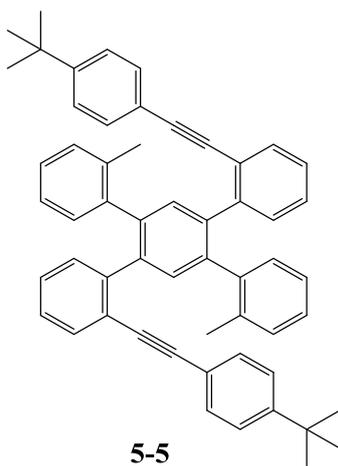
In a two-necked round-bottom flask equipped with a condenser, a mixture of **5-3** (2.0 g, 4.8 mmol), compound **5-4** (5.4 g, 19.2 mmol)) and potassium carbonate (3.3 g, 24.0 mmol) in dioxane (100 ml) and water (40 ml) was added and degassed with agron for 30 minutes and tetrakis(triphenylphosphine)palladium(0) (554 mg, 0.48 mmol) was added. After deoxygenated by three "freeze-pump-thaw" cycles the reaction mixture was heated to 90°C for 72 h. After cooling, the reaction mixture was diluted in 200 ml DCM and washed with water (3×100 mL) and dried over magnesium sulfate. The solvent was removed under reduced pressure and the residue was purified by column chromatography first (hexane), later (hexane/DCM; 7/1) to obtain the title compound **5-5** (2.4 g, 69 %) as a yellow solid. ^{1}H-NMR (CD$_2$Cl$_2$, 300 MHz): 7.49-7.43 (t, 2H), 7.14-7.05 (m, 6H), 7.00-6.91 (m, 5H), 1.99 (s, 3H), 1.15 (s, 9H); ^{13}C-NMR (CD$_2$Cl$_2$, 300 MHz): 151.90, 141.08, 139.45, 139.25, 136.68, 131.56, 130.00, 127.47, 127.32, 127.12, 125.59, 125.31, 123.37, 120.54, 93.47, 89.17, 77.97, 35.01, 31.29, 20.52. FD-MS (8 KV): m/z=723.8. HR-MS (MALDI): m/z = 722.3888, calcd. for $C_{56}H_{50}$: m/z = 722.3913, error = -2.5 ppm.

**6,13-Bis(4-(*tert*-butyl)phenyl)-5,12-diiodo-7,14-di-*o*-tolylbenzo[*k*]tetraphene (5-6):**

5-6
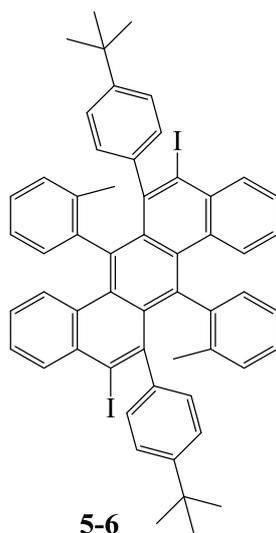
A solution of compound **5-5** (1.0 g, 1.38 mmol) in anhydrous DCM (50 ml) was degassed with argon for 30 minutes. After the solution was cooled to -78 °C, a 1 M solution of iodine monochloride (3.46 ml, 2.5 eq) in DCM was added dropwise to the solution under argon atmosphere. The reaction was stirred for 3 h and quenched with saturated sodium sulfite solution. The reaction mixture was diluted in 200 ml DCM and washed saturated sodium sulfite solution (3×100 mL) and dried over magnesium sulfate. The solvent was removed under reduced pressure and the residue was dissolved in hexane and precipitated in methanol (30 mL). The precipitate was filtered off and washed with methanol to obtain the title compound **5-6** (1.15 g, 85.4%) as a yellow solid. ^{1}H-NMR (C$_2$D$_2$Cl$_4$, 300 MHz): 8.23 (d, 1H), 7.35-7.26 (m, 1H), 7.23-7.00 (m, 3H), 6.97-6.89 (m, 2H), 6.83-6.77 (m, 2H), 6.71-6.66 (t, 1H), 6.52 (d, 1H), 6.18-6.10 (t, 1H), 1.84 (s, 1H), 1.22 (s, 9H), 1.11 (s, 2H); ^{13}C-NMR (C$_2$D$_2$Cl$_4$, 300 MHz): 151.93, 151.30, 151.19, 148.29, 148.01, 146.69, 146.45, 146.36, 144.13, 144.08, 144.03, 141.11, 139.27, 139.22, 137.43, 137.04, 136.56, 136.49, 136.40, 136.30, 136.15, 136.05, 135.34, 135.25, 134.54, 134.03, 133.81, 133.27, 132.78, 132.48, 131.17, 130.92, 130.84, 130.45, 130.41, 130.29, 130.22, 130.03, 129.68, 129.23, 129.12, 129.04, 128.66, 128.51, 126.97, 126.81, 126.70, 126.38, 111.45, 111.00, 110.49, 37.37, 37.30, 34.42, 34.37, 23.79, 23.67, 23.62. FD-MS (8 KV): m/z=975.2. HR-MS (MALDI): m/z = 974.1877, calcd. for C$_{56}$H$_{48}$I$_2$: m/z = 974.1845, error = 3.2 ppm.

6,13-Bis(4-(*tert*-butyl)phenyl)-7,14-di-*o*-tolylbenzo[*k*]tetraphene (5-7):


5-7
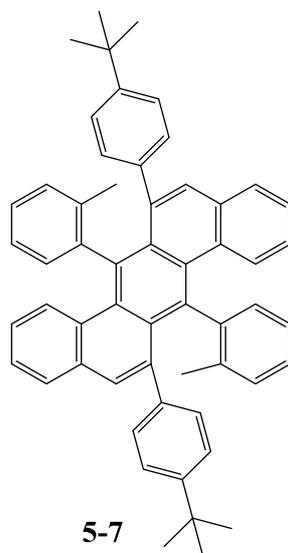
A solution of compound **5-6** (500 mg, 0.52 mmol) in anhydrous THF (30 ml) was degassed with argon for 30 minutes. After the solution was cooled to -78 °C, a 1.6 M solution of BuLi (0.77 ml, 2.4 eq) was added dropwise to the solution under argon atmosphere. The reaction was stirred for 1 h and quenched with methanol (10 ml). The reaction mixture was diluted in 200 ml DCM and washed with water (3×100 mL) and dried over magnesium sulfate. The solvent was removed under reduced pressure and the residue was purified by column flash chromatography on silica (hexane/DCM; 5/1) to obtain the title compound **5-7** (187 mg, 52.6%) as a yellow solid. ^{1}H-NMR ($C_2D_2Cl_4$, 300 MHz): 7.69 (d, 1H), 7.39 (d, 1H), 7.32 (t, 1H), 7.10-6.50 (broad, 10H), 1.62-1.47(3H), 1.23(s, 9H); ^{13}C-NMR ($C_2D_2Cl_4$, 300 MHz): 150.96, 150.86, 144.64, 144.57, 143.90, 143.75, 142.99, 142.76, 140.03, 137.49, 137.28, 137.13, 136.98, 135.31, 135.10, 133.80, 133.68, 133.59, 133.38, 133.23, 132.59, 132.46, 132.42, 130.85, 130.69, 130.33, 129.80, 129.34, 129.09, 127.68, 127.56, 77.37, 77.26, 77.00, 76.64, 71.01, 37.26, 37.24, 34.36, 28.76, 23.57, 23.52. FD-MS (8 KV): m/z=723.1. HR-MS (MALDI): m/z = 722.3898, calcd. for $C_{56}H_{50}$: m/z = 722.3913, error = -1.5 ppm.

5,14-Bis(4-(*tert*-butyl)phenyl)-9,18-dimethyldibenzo[*a,m*]rubicene (5-8):

5-8
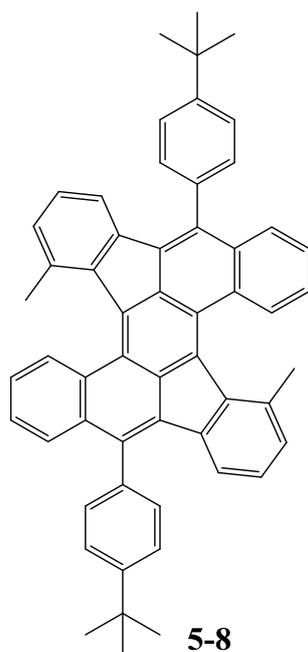
After a solution of compound **5-7** (200 mg, 0.277 mmol) in anhydrous DCM (20 ml) was degassed with argon for 30 minutes, it was added dropwise to 2,3-dichloro-5,6-dicyanobenzoquinone (DDQ: 314 mg, 1.38 mmol, 5 equiv) in a 50 ml round-bottom schlenk flask at 0 ºC under argon atmosphere. After stirring for 15 min, trifluoromethanesulfonic acid (0.5 mL) was added to the mixture. The reaction mixture was left to stir for further 30 minutes and quenched with saturated NaHCO$_3$ solution. The reaction mixture was diluted in 200 ml DCM and washed with saturated NaHCO$_3$ solution (3×100 mL) and water (3×100 mL) and dried over magnesium sulfate. The solvent was removed under reduced pressure and the residue was purified by column flash chromatography on silica (first: hexane:DCM; 5:1) to obtain the title compound **5-8** (129 mg, 64.8%) as a red solid. ^{1}H-NMR (THF-d8, 250 MHz): 8.36 (dd, 1H), 7.70-7.63 (m, 2H), 7.56 (dd, 1H), 7.4-7.37 (m, 4H), 7.08 (d, 1H), 6.89 (t, 1H), 6.58 (d, 1H), 2.28 (s, 3H), 1.42 (s, 9H); ^{13}C-NMR (THF-d8, 250 MHz): 151.06, 141.64, 139.98, 137.28, 136.50, 135.45, 134.90, 133.74, 132.88, 131.86, 130.60, 130.46, 130.01, 129.93, 128.91, 127.61, 126.82, 126.57, 125.88, 125.84, 125.27, 123.20, 121.09, 34.59, 30.77, 22.68. FD-MS (8 KV): m/z=717.8. HR-MS (MALDI): m/z = 718.3618, calcd. for C$_{56}$H$_{46}$: m/z = 718.3600, error = 1.8 ppm.

5,14-Bis(4-(*tert*-butyl)phenyl)dibenzo[*a,m*]rubicene-9,18-dicarbaldehyde (5-9):
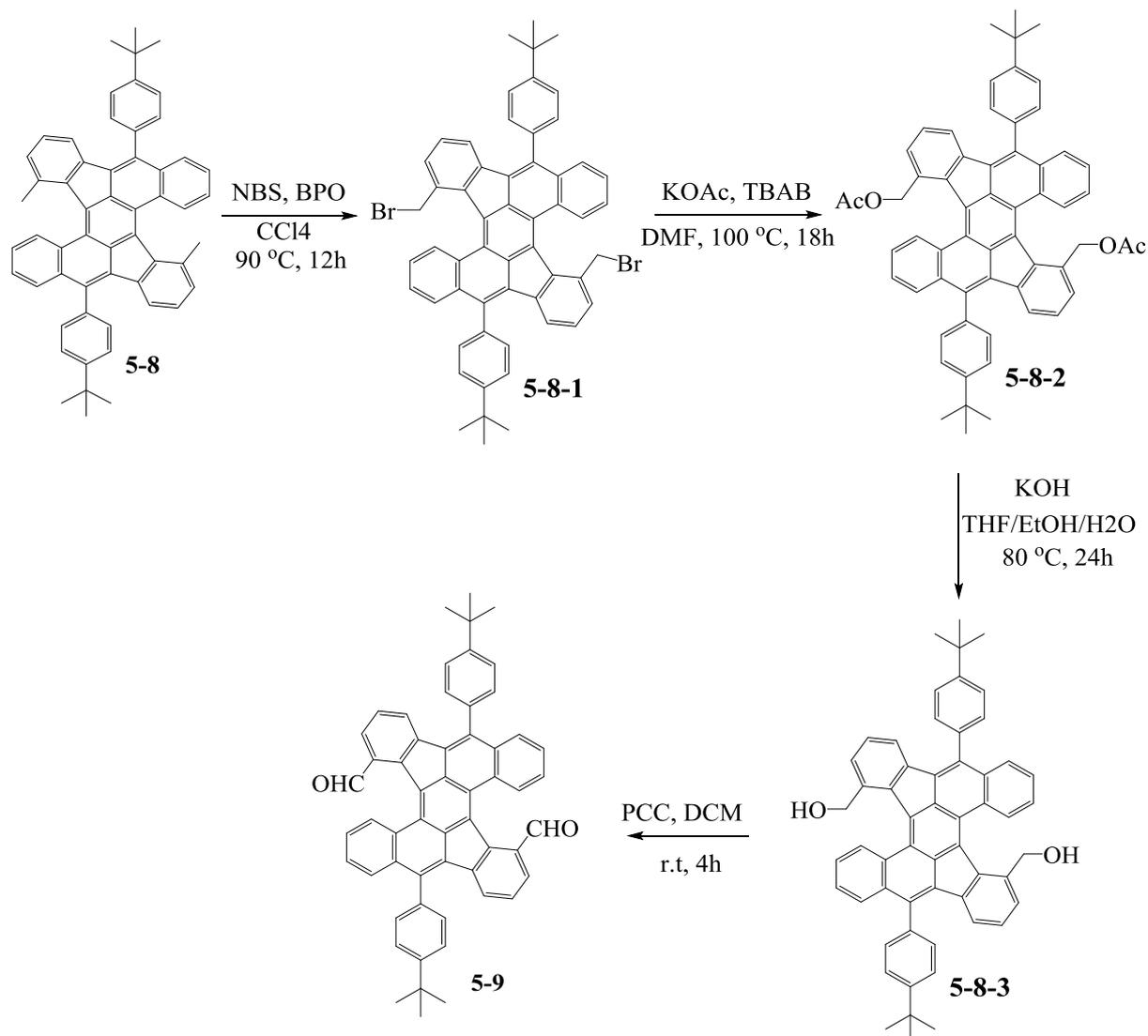
Compound **5-8** (300 mg, 0.42 mmol), *N*-bromosuccinimide (NBS, 207 mg, 1.12 mmol) and benzoyl peroxide (BPO, 52 mg, 0.21 mmol) were dissolved in 100 mL of CCl4 and heated to reflux (95 ^{o}C) under argon atmosphere. After 24 hours, the mixture was cooled to room temperature and the solvent was removed under reduced pressure. The residue was passed through a short silica gel column using hexane/chloroform (2/1, v/v) as eluent and the first fraction was collected containing a majority of compound **5-8-1**, together with a mixture of starting material **5-8** and mono-bromide byproduct. The polarity of the byproducts is slightly smaller than **5-8** and they cannot be separated. Therefore, the crude product was used directly for the next step. The crude product, KOAc (517 mg, 5.26 mmol) and tetrabutylammonium bromide (170 mg, 0.53 mmol) were dissolved in 15 mL of DMF and heated to 100 ^{o}C under argon atmosphere. The mixture was stirred for 18 hours and poured into 200 mL of ice water. The solvent was then filtered off and the brown solid was collected and washed with water

and methanol for several times. And the yellow solid **5-8-2** was used directly for the next step. The crude product **5-8-2** was dissolved in mixed solvent of THF (60 mL), ethanol (60 mL) and 10% aqueous KOH solution (20 mL) under argon atmosphere. The mixture was heated to reflux (80 °C) and stirred for 24 hours. The solvent was removed under reduced pressure and the residue was redissolved in 50 mL chloroform, washed with water and brine and dried over MgSO$_4$. The solvent was evaporated and the residue was redissolved in 50 mL of dry DCM. To the solution was added pyridinium chlorochromate (PCC, 126 mg, 0.58 mmol) and the mixture was stirred at room temperature for 4 hours. Afterwards, the solvent was removed and the residue was purified by column chromatography (silica gel, hexane/DCM (2/1, v/v)) to give compound **5-9** (100 mg, 32 % in four steps) as a red solid. ^{1}H-NMR (CD$_2$Cl$_2$, 250 MHz): 10.42 (s, 1H), 8.97 (dd, 1H), 7.92 (dd, 1H), 7.80-7.75 (m, 3H), 7.59-7.51 (m, 4H), 7.29 (t, 1H), 7.02 (dd, 1H), 1.57 (s, 9H); ^{13}C-NMR (CD$_2$Cl$_2$, 250 MHz): 190.98, 152.27, 143.09, 140.95, 139.36, 137.86, 135.48, 134.63, 132.51, 131.34, 130.60, 130.06, 129.46, 129.31, 129.11, 128.54, 127.96, 127.56, 127.52, 126.98, 126.54, 126.38, 125.68, 35.23, 31.67. FD-MS (8 KV): m/z=746.9. HR-MS (MALDI): m/z = 746.3218, calcd. for C$_{56}$H$_{42}$O$_2$: m/z = 746.3185, error = 3.3 ppm.

4,12-Bis(4-(*tert*-butyl)phenyl)-8,16-dimesityl-8,16-dihydrodipleiadeno[2,1,12,11-*cdefg*:2',1',12',11'-*ijkla*]-*s*-indacene (5-10):


5-10   **5-11**
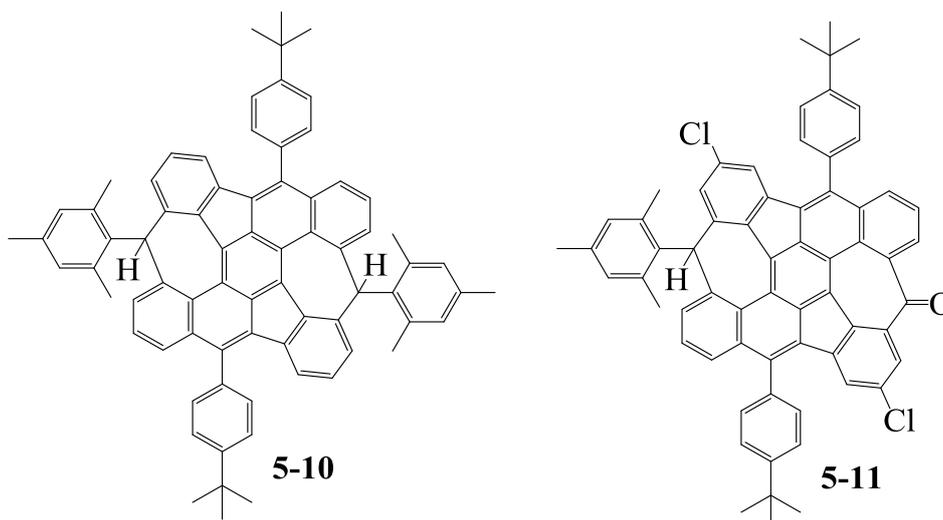
Compound **5-9** (50 mg, 0.067 mmol) was dissolved in 20 mL of dry THF under argon atmosphere. To the solution was added 0.84 mL mesitylmagnesium bromide solution (1M in ether, 0.84 mmol) and the mixture was stirred at room temperature for 2 hours. The reaction mixture was then poured into 50 mL water and extracted by chloroform. The organic layer

was dried over MgSO$_4$ and the solvent was removed under reduced pressure. The residue was then redissolved in 40 mL dry DCM under argon atmosphere and 4 mL of BF$_3$·OEt$_2$ was added. The mixture was stirred for 30 minutes and then washed with NaHCO$_3$ solution (3x20 mL) and water (3x20 mL). The organic layer was dried over MgSO$_4$ and the solvent was removed under reduced pressure. The residue was purified by column chromatography (silica gel, hexane/DCM (5/1, v/v)) to give compound **5-10** (45 mg, 40 % in two steps) as a red solid and **5-11** in 5% yield.

Compound **5-10**: ^{1}H-NMR (CD$_2$Cl$_2$, 500 MHz): 7.65 (s, 3H), 7.49-7.42 (m, 3H), 7.31 (t, 1H), 6.98 (s, 3H), 6.84 (dd, 2H), 6.39 (s, 1H), 2.37 (s, 3H), 2.34 (s, 6H), 1.52 (s, 9H). FD-MS (8 KV): m/z 952.6. MALDI-TOF (TCNQ as matrix): m/z 950.63, cacld.: 950.49.

4,12-Bis(4-(*tert*-butyl)phenyl)-8,16-dimesityldipleiadeno[2,1,12,11-*cdefg*:2',1',12',11'-*ijkla*]-*s*-indacene (5-1):

5-1
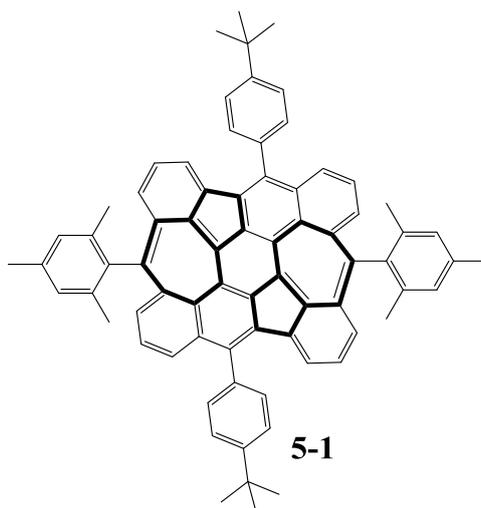
Compound **5-10** (20 mg, 0.021 mmol) was redissolved in 5 mL dry toluene under argon atmosphere and *p*-chloranil (11.4 mg, 0.046 mmol dissolved in 1 mL dry toluene) was added dropwise. The mixture was stirred at room temperature for 12 hours. The residue was purified by column chromatography (silica gel was degased and protected it with argon, hexane/DCM (2/1, v/v), the eluent was also degased) to give compound **5-1** (5 mg, 25.4 %) as a purple solid. This compound was stored under argon.

2,5-Dibromobenzene-1,4-dicarbaldehyde (6-2):
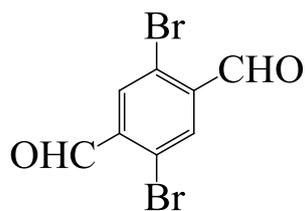
Sulfuric acid (28.0 ml) was added dropwise to a suspension containing 1,4-dibromo-2,5-dimethylbenzene (8.0 g), acetic acid (40.0 ml) and acetic anhydride (80.0 ml) at 0 °C. CrO_3 (12.0 g) was then added to the mixture in portions. The resulting mixture was stirred vigorously at this temperature for a further 5 h until the reaction was completed. The greenish slurry was poured into ice-water and filtered. The white solid was washed with water and cold methanol. The diacetate was then hydrolyzed by refluxing with a mixture of water (40.0 ml), ethanol (40.0 ml) and sulfuric acid (4.0 ml) for 5 h. After the mixture had cooled, the pale yellow product was separated by filtration. The crude product was purified by recrystallization from chloroform (4.5 g, yield 49%). ^{1}H NMR (250 MHz, 25 °C, CD_2Cl_2, ppm), 10.35 (s, 2H; CHO), 8.16 (s, 2H; benzo H).

2',5'-Dibromo-1,1':4',1''-terphenyl:
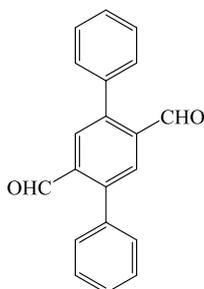
A mixture of **6-2** (1.0 g), phenylboronic acid (1.1 g), Pd(PPh$_3$)$_4$ (0.2 g), toluene (12.5 ml) and 2 M Na$_2$CO$_3$ solution (2.5 ml) was refluxed at 85 °C for 36 h under nitrogen, then poured into water and extracted with dichloromethane. The organic layer was washed with brine and water and dried over MgSO$_4$. The crude product was first purified by flash column chromatography (dichloromethane as eluent) and then recrystallized form chloroform. A 0.79 g amount of product (yield 81%) was obtained as pale yellow crystals, m.p. 197–200 °C. ^{1}H NMR (500 MHz, 25 °C, CDCl3, TMS, ppm), 10.09 (s, 2H; CHO), 8.12 (s, 2H; benzo H), 7.53–7.44 (m, 10H; benzo H); FT-IR (KBr pellet, cm^{-1}), 3024(w), 2889(w), 1678(vs),

1469(m), 1446(m), 1390(m), 1267(w), 1242 (w), 1149(m), 1076(w), 1022(w), 904(w), 837(s), 766 (m), 706(s).

2',5'-Bis((*Z*)-4-bromostyryl)-1,1':4',1''-terphenyl (6-4d):

6-4d
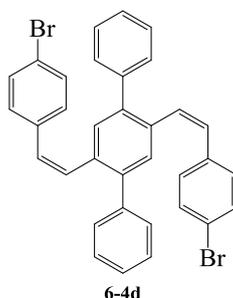
The bromo(4-(*tert*-butyl)benzyl)triphenylphosphorane (14.8g, 30 mmol) and **6-2** (4g, 13.7 mmol) were placed in a dry flask, which was wrapped with tinfoil, and the flask was flushed with nitrogen. Dry, cooled THF (150 ml) was added to the flask via an injector and then *t*-BuOK (3.36g, 30 mmol) in dry THF was added slowly to allow the colored ylide formed to react with aldehyde groups between successive additions. When no color was observed upon addition of base, the mixture was stirred for a further 12 h at room temperature. After the reaction was completed, filtered and most of the solvent was removed under reduced pressure and then the residue was purified by silica gel column chromatography using DCM/hexane (1/10, v/v) as eluent to give compound **6-4d** (5.8 g) as a white solid in 76.8% yield.

^{1}H-NMR (THF-d, 300 MHz): 7.46 (t, 1H), 7.45 (t, 1H), 7.31-7.29 (tt, 2H), 7.27-7.25 (m, 4H), 7.19 (t, 1H), 7.18 (t, 1H), 6.53 (d, 1H), 6.48 (d, 1H); ^{13}C-NMR (THF-d, 300 MHz): 141.03, 140.79, 137.44, 135.37, 132.67, 132.28, 131.62, 131.55, 130.19, 130.08, 128.84, 128.01, 121.72. FD-MS (8 KV): m/z=592.4. HR-MS (MALDI): m/z = 592.0215, calcd. for $C_{34}H_{24}Br_2$: m/z = 592.0224, error = 0.9 ppm.

5,12-Bis(4-bromophenyl)benzo[*k*]tetraphene (6-12d):

6-12d
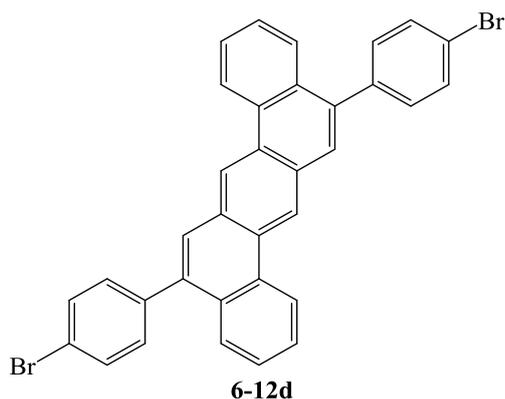
A solution of **6-4d** (500mg, 0.87 mmol) and iodine (500mg, 2 mmol) in toluene (400 mL) and propylene oxide (100 mL) was irradiated in a standard immersion well photoreactor with 360nm high pressure mercury vapor lamp(8*360nm) for 8 h. The reaction mixture was then washed with aqueous sodium thiosulfate, water, brine and dried over anhydrous $MgSO_4$. The solvent was removed under vacuum and the residue was purified by silica gel column chromatography using DCM /hexane (1/5, v/v) as eluent to give compound **6-12d** (300mg) as a white solid in 60.5% yield.

^{1}H-NMR (THF-d, 250 MHz): 9.27 (s, 1H), 8.97 (d, 1H), 7.88 (s, 1H), 7.76 (d, 1H), 7.64-7.62 (m, 3H), 7.52-7.43 (m, 3H); ^{13}C-NMR (THF-d, 250 MHz): 140.95, 138.77, 132.70, 132.46, 131.95, 131.72, 131.56, 130.24, 129.00, 127.90, 127.79, 127.46, 124.32, 123.31, 122.39. FD-MS (8 KV): m/z=588.9. HR-MS (MALDI): m/z = 587.9890, calcd. for $C_{34}H_{20}Br_2$: m/z = 587.9911, error = 2.1 ppm.

5,12-Bis(3-(*tert*-butyl)phenyl)-1,8-dimethylbenzo[*k*]tetraphene (6-12b):

6-12b

213
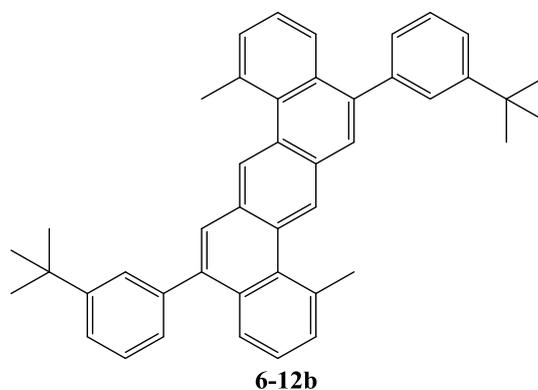
A solution of **6-4b** (500mg, 0.87 mmol) and iodine (500mg, 2 mmol) in toluene (400 mL) and propylene oxide (100 mL) was irradiated in a standard immersion well photoreactor with 360nm high pressure mercury vapor lamp(8*360nm) for 8 h. The reaction mixture was then washed with aqueous sodium thiosulfate, water, brine and dried over anhydrous MgSO₄. The solvent was removed under vacuum and the residue was purified by silica gel column chromatography using DCM /hexane (1/5, v/v) as eluent to give compound **6-12b** (300mg) as a white solid in 60% yield.

^{1}H-NMR (CD2Cl2, 250 MHz): 9.30 (s, 1H), 7.81 (s, 1H), 7.75 (d, 1H), 7.55-7.30 (m, 6H), 3.24 (s, 3H), 1.33 (s, 9H); ^{13}C-NMR (CD$_2$Cl$_2$, 250 MHz): 150.16, 138.91, 138.28, 133.43, 130.97, 130.57, 129.59, 129.55, 129.36, 127.97, 127.93, 127.30, 126.27, 126.20, 126.08, 125.41, 125.22, 34.21, 30.76, 25.80. FD-MS (8 KV): m/z 570.1, cacld.: 570.82. Melting point: 310.3-311.1 ºC. Elemental analysis: Calculated: C 92.58, H 7.42; Found: C 92.49, H 7.46.

5,12-Bis(3-(*tert*-butyl)phenyl)benzo[*k*]tetraphene-1,8-diyl diacetate (6-14b):

6-14b
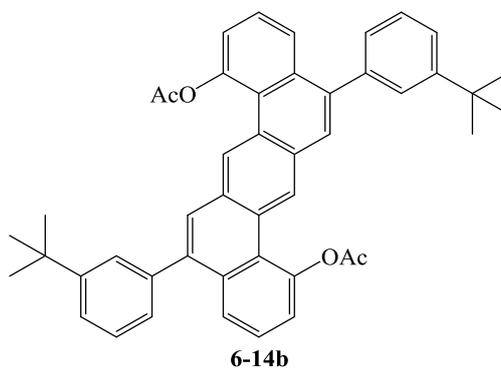
Compound **6-12b** (300 mg, 0.53 mmol), *N*-bromosuccinimide (NBS, 207 mg, 1.12 mmol) and benzoyl peroxide (BPO, 52 mg, 0.21 mmol) were dissolved in 100 mL of CCl₄ and heated to reflux (95 ºC) under argon atmosphere. After 24 hours, the mixture was cooled to room temperature and the solvent was removed under reduced pressure. The residue was passed through a short silica gel column using hexane/chloroform (2/1, v/v) as eluent, together with a mixture of starting material **7** and mono-bromide byproduct. The polarity of the byproducts is slightly smaller than **6-12b** and they can not be separated. Therefore, the crude product was used directly for the next step. The crude product, KOAc (517 mg, 5.26 mmol) and tetrabutylammonium bromide (170 mg, 0.53 mmol) were dissolved in 15 mL of DMF and heated to 100 ºC under argon atmosphere. The mixture was stirred for 18 hours and poured

into 200 mL of ice water. The solvent was then filtered off and the brown solid was collected and washed with water and methanol for several times. And the yellow solid **6-14b** was used directly for the next step.

5,12-Bis(3-(*tert*-butyl)phenyl)benzo[*k*]tetraphene-1,8-dicarbaldehyde (6-16b):

6-16b
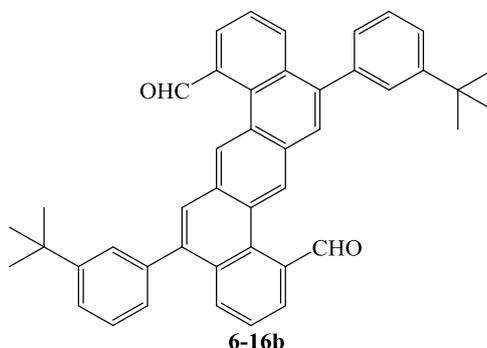
Compound **6-14b** (200 mg, 0.29 mmol) was dissolved in mixed solvent of THF (60 mL), ethanol (60 mL) and 10% aqueous KOH solution (20 mL) under argon atmosphere. The mixture was then heated to reflux (80 ^{o}C) and stirred for 24 hours. The solvent was then removed under reduced pressure and the residue was redissolved in 50 mL chloroform, washed with water and brine and dried over $MgSO_4$. The solvent was then evaporated and the residue was redissolved in 50 mL of dry DCM. To the solution was added pyridinium chlorochromate (PCC, 126 mg, 0.58 mmol) and the mixture was stirred at room temperature for 2 hours. Afterwards, the solvent was removed and the residue was purified by column chromatography (silica gel, hexane/chloroform (3/1, v/v)) to give compound **6-16b** (100 mg, 32 % in four steps) as a yellow solid.

^{1}H-NMR (THF-d, 300 MHz): 10.66 (s, 1H), 8.65 (s, 1H), 8.09-8.03 (t, 3H), 7.69-7.63 (t, 1H), 7.56 (s, 1H), 7.48-7.28 (m, 3H), 1.31 (s, 9H); ^{13}C-NMR (THF-d, 300 MHz): 191.27, 151.29, 139.77, 139.71, 136.15, 133.10, 131.13, 131.01, 130.77, 129.37, 128.59, 128.05, 127.71, 127.43, 127.08, 126.90, 126.72, 124.59, 34.52, 30.76. FD-MS (8 KV): m/z 597.9, cacld.: 598.79. Elemental analysis: Calculated: C 88.26, H 6.40, O 5.34; Found: C 88.21, H 6.48.

6,12-Bis(3-(*tert*-butyl)phenyl)-4,10-dimesitylcyclopenta[*pqr*]indeno[2,1,7-*ijk*]tetraphene (6-1b):

6-1b
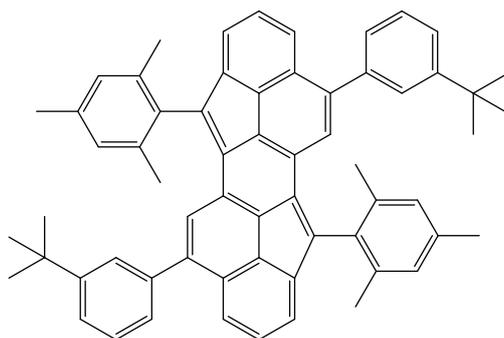
Compound **6-16b** (50 mg, 0.0836 mmol) was dissolved in 20 mL of dry THF under argon atmosphere, to the solution was added 0.836 mL mesitylmagnesium bromide solution (1M in ether, 0.836 mmol) and the mixture was stirred at room temperature for 2 hours. The reaction mixture was then poured into 50 mL water and extracted by chloroform. The organic layer was dried over $MgSO_4$ and the solvent was removed under reduced pressure. The residue was then redissolved in 20 mL dry DCM under argon atmosphere and 4 mL of $BF_3 \cdot OEt_2$ was added. The mixture was stirred for 15 minutes and then washed with $NaHCO_3$ solution (3x20 mL) and water (3x20 mL). The organic layer was dried over $MgSO_4$ and the solvent was removed under reduced pressure. The residue (compound 10) was redissolved in 20 mL dry toluene under argon atmosphere and DDQ (18mg, 0.0836 mmol dissolved in 10 mL dry toluene) was added dropwise. Upon addition of DDQ solution, the color of the reaction mixture changed slowly from light green to dark blue, and the reaction was monitored by TLC until completion. After evaporation of the solvent, the residue was purified by column chromatography (silica gel, hexane/chloroform (3/1, v/v)) to give compound **6-1b** (35 mg, 40% in three steps) as a red solid.

^{1}H-NMR (CD_2Cl_2, 500 MHz): 7.62 (d, 1H), 7.42 (s, 1H), 7.34 (t, 1H), 7.33 (t, 1H), 7.31 (d, 1H), 7.19 (t, 1H), 7.07 (d, 2H), 7.01 (s, 2H), 2.34 (s, 3H), 2.31 (s, 6H), 1.38 (s, 9H); ^{13}C-NMR (CD_2Cl_2, 250 MHz): 152.11, 139.59, 139.04, 138.03, 137.32, 132.35, 131.64, 130.93, 129.06, 128.81, 128.53, 128.26, 127.69, 127.51, 127.04, 124.89, 124.76, 123.70, 35.02, 31.47, 30.08, 21.30, 20.77. FD-MS (8 KV): m/z 802.1, cacld.: 801.13. HR-MS (MALDI): m/z = 800.4374, calcd. for C62H56: m/z = 800.4382, error = -1.0 ppm.

Acknowledgements

I feel overjoyed to acknowledge all the people who have been explicitly and implicitly involved in my life during my PhD studies.

First and foremost, I would like to express my gratitude to Prof. Dr. ███████ for being such a great Guide. Prof. ██████ is a wealth of knowledge. He always encouraged and inspired me with his intensive research capability. Prof. ██████ has contributed immensely in fostering my scientific point of view and enriching my research orientation. His constant direction has been significantly influential during my entire term of PhD. As an individual, he is a role model.

I would like to thank Prof. Dr. ███████ as my project leader, with whom I discussed synthetic as well as preparative challenges frequently. His synthetic experiences and his knowledge about nanographene and graphene nanoribbons were very valuable for the progress of my work. Apart from the academic unreserved professional guidance and continuous inspiration. He is also a valuable mentor in my life.

All the members in the department of synthetic chemistry group have held high esteem and always been encouraging to me. I am very thankful to Prof. Dr. ████████████ who helped me readily whenever I had synthetic chemistry related radicals and Dr. ████████ ████████ with NMR.

Furthermore, I am truly grateful to all the past and present members in Prof. ██████ group:

In addition, I would also thank all our partners, including Prof. Dr. ██████ Prof. Dr. ████████ , Prof. Dr. ██████ Dr. █████████████ Dr. ██████ ██████ without the efforts of them, accomplishment this thesis would not have been possible.

Last but not the least, I would like to thank my loved ones, my parents and sister. Especially, I acknowledge the loving support of my wife ████████ she was nice enough to keep up with my erratic time schedules and patiently waited for me till I reached home every day. And

thank my lovely daughter ▮▮▮▮▮▮ who born during my PhD studying. I will be grateful forever their love. Their unconditional love support are the motive force for me throughout the entire process.

Many thanks also to everybody I might have unintentionally forgotten to mention here.

Curriculum Vitae

Personal Details

Name: Junzhi Liu

Place of birth: Sichuan, China

Nationality: Chinese

Marital status: Married

University Education

07.2011-07.2015 **PhD** studies, Max Planck Institute for Polymer Research, Mainz,

Germany.

Research adviser: Prof. Dr. ▮▮▮▮▮▮▮

09.2008-06.2011 **M.Sc.** Materials Science, State Key Laboratory of Polymer Materials

Engineering, College of Polymer Science and Engineering,

Sichuan University, Chengdu, China.

Research adviser: Prof. Dr ▮▮▮▮ Prof. Dr. ▮▮▮▮▮

Thesis title*: Preparation of Hierarchical Porous Materials Based on*

High Performance Polymers

10.2004-06.2008 **B.A.** Chemistry of Materials, College of Chemical Engineering,

Hebei University of Technology, Tianjin, China.

School Education

09 2001 – 06 2004   The Third Senior High School of Panzhihua, Panzhihua,

Sichuan, China

09 1998 – 06 2004   The Second Junior High School of Panzhihua, Panzhihua,

Sichuan, China

09 1992 – 06 1998   Dashuijing Primary School of Panzhihua, Panzhihua,

Sichuan, China

<u>Awards and Fellowships</u>

Marie-Curie Fellowship	2011-2014
Best Poster Award, EUROMAT2013, Spain	2013
"Outstanding Graduate" scholarship, Sichuan University	2011
Royal DSM N.V. (DSM) scholarship	2009
Second-class scholarship, National, China	2008